

DISSERTATION ZUR ERLANGUNG DES DOKTORGRADES
DER FAKULTÄT FÜR CHEMIE UND PHARMAZIE
DER LUDWIG-MAXIMILIANS-UNIVERSITÄT MÜNCHEN

Analysis of Aging by Quantitative Proteomics
and
Mitochondrial Organellar Proteomics

Dirk Martin Walther

aus
Heidelberg

2012

Erklärung

Diese Dissertation wurde im Sinne von §7 der Promotionsordnung vom 28. November 2011 von Herrn Prof. Dr. Matthias Mann betreut.

Eidesstattliche Versicherung

Diese Dissertation wurde eigenständig und ohne unerlaubte Hilfe von mir erbracht.

München, 17. September 2012

Dirk Martin Walther

Dissertation eingereicht am 18.09.2013

1. Gutachter: Prof. Dr. Matthias Mann
2. Gutachter: Prof. Dr. Franz-Ulrich Hartl

Mündliche Prüfung am 04.10.2012

Summary

Aging, a hallmark of metazoan organisms, leads to a gradual decline of important biological functions and, ultimately, death. In humans age is the most important risk factor for numerous diseases, such as neurodegenerative disorders, most prominently Alzheimer's and Parkinson's disease, as well as metabolic disorders such as type II diabetes. Recent advances in the biomedical sciences have dramatically changed our understanding of aging. It is now generally accepted that senescence is not merely a stochastic process but that its rate is regulated by various molecular signaling pathways. Nonetheless, both the mechanisms by which this regulation is achieved and the nature of aging itself remain mostly obscure. Discovery-based experimental approaches are best suited to address such questions, in particular the emerging field of mass spectrometry-based proteomics, which now allows identification and quantification of thousands of proteins in tissue samples. The focus of this thesis was to establish workflows and assess proteome remodeling during aging in two commonly used model organisms.

The first project was aimed at studying the effect of aging on mouse tissue. While until recently, quantitative proteomic analysis of tissue samples posed a major challenge an internal standard derived from SILAC mice allowed us to accurately quantify protein abundance in several tissues. Surprisingly, proteome differences even in postmitotic tissues were very low between young and aged animals, suggesting that proteostasis is efficiently maintained during aging.

In the second project, aging in the nematode *C. elegans* was addressed. Of particular interest in this model organism is the conserved insulin/insulin-like growth factor 1 (IIS) signalling pathway. Mutations in the DAF-2 receptor result in constitutive activation of the DAF-16/FOXO transcription factor and more than doubles the organism's lifespan. To elucidate the mechanism of this lifespan extension, SILAC labeling of *C. elegans* was established and employed to quantify protein expression changes of wild type and IIS mutant strains throughout their lifespan. Furthermore, insoluble protein aggregates were biochemically isolated and quantified. In contrast to mice, *C. elegans* undergoes extensive proteome remodeling during senescence. Moreover, a large proportion the proteins that accumulate with age in the proteome have a tendency to form

aggregates. This process was markedly delayed in the long-lived *daf-2*-mutant strain. The data indicate that in worms, aging is associated with deleterious proteome remodeling, results in protein aggregation and proteostasis collapse.

Collectively, the work presented here generated the most comprehensive proteomics datasets addressing aging to date. A comparison between the two analyzed organism suggests that the proteostasis system during aging is more efficiently preserved in mammals than in nematodes.

In a further part of this thesis, different methods were explored to identify novel mitochondrial membrane protein complexes in yeast. SILAC-based immunoprecipitation experiments with GFP-tagged variants of the mitochondrial outer membrane protein Mim1 were performed after mild detergent lysis. This lead to the discovery of a Mim1 interactor, named Mim2. Both proteins form the MIM complex, a central component in the biogenesis of outer membran proteins.

In a different study, protein correlation profiling was applied to identify a complex responsible for the formation of mitochondrial contact sites, the attachment points between the inner and the outer mitochondrial membrane. To that end, vesicles from isolated yeast mitochondria were generated by ultrasonication, separated by density gradient centrifugation and highly accurate abundance profiles were determined via an internal SILAC standard. By this means, the mitochondrial contact sites (MICOS) complex was discovered, consisting of Fcj1 and five novel proteins. Biochemical assays and electron microscopy confirmed that these subunits were required for contact site formation. Furthermore, their deletion resulted in impaired growth on non-fermentable carbon sources.

Contents

Summary	v
Contents	vii
1 Introduction	1
1.1 Biology of Aging	1
1.1.1 Paradigms of Aging Research	1
1.1.2 Invertebrate Model Systems	6
1.1.3 Insulin/Insulin-like Growth Factor 1 Signaling	11
1.1.4 Proteostasis and Protein Aggregation during Aging	18
1.2 Mass Spectrometry-based Quantitative Proteomics	22
1.2.1 Mass Analyzers for MS-Based Proteomics	22
1.2.2 Fragmentation Methods in Tandem Mass Spectrometry	26
1.2.3 Instruments for High Resolution MS-Based Shotgun Proteomics .	27
1.2.4 Quantification Strategies	29
1.2.5 Computational Proteomics and Bioinformatics	33
1.2.6 Mitochondrial Organellar Proteomics	35
2 Results	39
2.1 Accurate Quantification of More Than 4000 Mouse Tissue Proteins Re-	
veals Minimal Proteome Changes during Aging.	39
2.1.1 Aim and Summary	39
2.1.2 Contribution	40
2.1.3 Publication	40
2.2 Extensive Proteome Remodeling during Aging in <i>C. elegans</i> Revealed by	
Quantitative Proteomics	48
2.2.1 Aim and Summary	48
2.2.2 Contribution	49
2.2.3 Manuscript	49

2.3	The Mitochondrial Contact Site Complex, a Determinant of Mitochondrial Architecture.	120
2.3.1	Aim and Summary	120
2.3.2	Contribution	120
2.3.3	Publication	121
2.4	A Crucial Role of Mim2 in the Biogenesis of Mitochondrial Outer Membrane Proteins.	137
2.4.1	Aim and Summary	137
2.4.2	Contribution	137
2.4.3	Publication	138
3	Discussion and Outlook	149
3.1	The Proteome of Aging	149
3.1.1	Studying Aging by Quantitative Proteomics	149
3.1.2	The Proteome of Mice, but Not of Worms Is Conserved during Aging	150
3.1.3	Outlook and Future Directions	152
3.2	Mitochondrial Organellar Proteomics	154
	Abbreviations	157
	References	159
	Curriculum Vitae	191

1 Introduction

1.1 Biology of Aging

A hallmark of multicellular organisms is their restricted lifespan, ultimately leading to an individual's death. From an evolutionary perspective, this limitation is necessary to assure a species' genetic adaptation and progression. Studies on animal populations in the wild demonstrated that the majority of individuals die prematurely, for example because of predation or diseases, before a significant onset of intrinsic cellular deterioration. Long term population studies of wild mouse populations showed a decline by at least 40% in each of several consecutive two month intervals [17]. In contrast, commonly used laboratory mouse strains kept in captivity have median lifespans in the range of two years [290]. Similarly, the aging process of humans in developed countries differs considerably from that of our ancestors before the establishment of modern civilization. Accompanying improvements in nutrition and medicine, life expectancies of humans worldwide have more than doubled in the past two centuries and are still increasing [223]. Accompanying these significant demographic changes, humanity is faced with an altered occurrence of medical conditions, resulting in rising healthcare costs of up to 7% yearly in the western world [32]. Age-related pathologies include a decline in cognitive and sensory functions of the brain and a progressive immunodeficiency. Furthermore, aging is associated with a higher incidence of particular diseases, including dementia, Alzheimer's disease or type II diabetes, explaining the great interest in the field of aging research [70].

1.1.1 Paradigms of Aging Research

Advances in the biomedical sciences have provided researchers with new tools to investigate the biological basis underlying aging at the molecular level, and considerable advances have been made in the past decades. In spite of a general consensus that aging results from accumulation of cellular damage, several conflicting models have been proposed to explain the nature and the origin of these deteriorations.

Mitotic Clock, Cellular Senescence and Organismal Aging

The previously prevailing assumption that cells can proliferate indefinitely was first challenged in 1961 when Hayflick and Moorehead demonstrated that cultured human fibroblast can only undergo a limited number of cell divisions and enter a state of growth arrest [122]. Later, the molecular mechanisms were identified which restrict the proliferative capacity of cells and result in a permanent cell cycle arrest. The most prominent example is the successive shortening of telomeres, protective structures at the termini of chromosomes [116, 121]. Moreover, an accumulation of point mutations and chromosomal rearrangements has been observed [15]. This natural restriction of somatic cells by this *mitotic clock* to proliferate is referred to as *cellular senescence* [46]. Preventing telomere shortening by constitutive expression of telomerase alone is often sufficient to reverse this effect and allows an indefinite number of divisions [20].

In multicellular organisms, however, the situation is considerably more complex and the relevance of the above mentioned cellular senescence to organismal aging is still controversial [227]. The notion that cellular senescence represents a safeguard against cancer, a condition that results from uncontrolled cell proliferation, is widely accepted [34]. However, it is currently unclear which role growth arrested senescent cells play *in vivo*. A range of biomarkers have been reported that are associated with cellular senescence, for example DNA replication or the expression of senescence-associated β galactosidase or p16. None of these, however, is characteristic for all organisms and tissue types [35]. Based on such markers, some studies have found an accumulation of senescent cells with age in renewable tissues of several mammalian species [66, 137, 162]. The proportion of senescent cells across studies varies widely between less than 1% and more than 15 %. Similarly, a greater proportion of senescent cells was also found in tissues affected with various age-related pathologies, including osteoarthritis and atherosclerosis [37, 247, 297].

Although many pieces of evidence point towards an accumulation of cell cycle arrested senescent cells in mammalian tissues during aging *in vivo*, their role in organismal aging is poorly understood. Some reports suggest that tissue stem and progenitor cells are significantly affected and thereby limit the tissue self renewal capacity [136, 161, 208]. It has further been suggested that senescent cells may cause tissue damage due to the release of matrix degrading enzymes and cytokines and growth factors [35].

Further evidence for the hypothesis that organismal aging is closely related to cellular senescence was provided by the finding that counteracting telomere deterioration by constitutive expression of the telomerase reverse transcriptase subunit in somatic

cells delayed aging in mice [284]. However, since systemic activation of telomerase is known to induce malignancies [36, 103] this had to be compensated by the simultaneous overproduction of tumor suppressor proteins, underscoring the notion that cellular senescence represents a defense mechanism against cancer.

Free Radical Hypothesis

The *free-radical theory of aging* was originally founded by D. Harman in 1956 [117] and was later substantiated by experimental evidence for the occurrence of highly reactive molecules termed reactive oxygen species (ROS) in tissues. These include the superoxide anion ($O_2^{\cdot-}$) which can further yield other molecules like the relatively stable hydrogen peroxide (H_2O_2) or the highly reactive hydroxyl radical ($\cdot OH$) by dismutation or Fenton chemistry, respectively. The vast majority of ROS are generated as a consequence of normal aerobic metabolism. Besides minor contributions by NADPH dependent oxidases in the plasma membrane, cytosolic cyclooxygenases or enzymes of the lipid metabolism, the mitochondrial respiratory chain is their primary source, generating up to 90% of the overall oxidating burden (reviewed in [10]). Recent data indicate that *in vivo*, ROS are mainly formed at complexes I and III of the respiratory chain, involving flavin mononucleotide iron sulfur cluster electron transfer intermediates and ubisemiquinone radicals [96, 182, 289]. ROS are known to spontaneously react with nucleic acids, lipids and proteins and thus cause cellular damage.

Being highly controversial at first, the discovery of enzymes with the purpose of clearing highly reactive radicals provided experimental support for the free-radical theory [201]. Particularly isoforms of superoxide dismutase and catalase serve as a natural scavenging system for ROS. Experimental data showing that the lifespan of flies can be prolonged by overexpressing these enzymes were seen as a proof for the life shortening impact of free radicals [235]. However, after a critical re-evaluation of the study the data turned out to be biased due to the use of short-lived control strains. In a revised experimental setting, no significant impact on longevity was observed upon overexpression of superoxide dismutase or catalase [234].

A variety of oxidative modifications of amino acid side chains have been reported in proteins. Examples of these modifications are oxidations of the sulfur atom in cysteine and methionine, hydroxylations and carbonylations on aliphatic residues as well as substitutions at the aromatic systems of phenylalanine, tyrosine or tryptophane (reviewed in [252]). Using biochemical assays, immunodetection or mass spectrometry (MS), some studies have demonstrated an increase in oxidative protein modifications with age [4, 286]. However, no conclusive data has been presented as to the extent of

such oxidative damage, i. e. the ratios between modified and unmodified proteins, and their impact on biological function *in vivo*. Therefore it is still a matter of debate whether oxidative damage to proteins is the main cause or simply correlated with aging.

Rate of Living

Related to the free radical theory is the *rate of living* concept. It is based on the observation that the metabolic rate of an organism is often inversely related to its longevity. This not only holds true for a comparison between different species but also to individuals of the same species under different metabolic conditions. Reducing the metabolism by means of caloric restriction, lowering of the body temperature or the oxygen concentration was shown to prolong lifespan in a variety of organisms, including worm, fly and rodents. Similar effects were further shown for primary human cell lines [199, 206, 237]. Notably, increased longevity upon caloric restriction was also observed in yeast but in contrast to the examples mentioned above, this shift was accompanied by an increased rate of oxygen consumption [179].

Vicious Cycle Hypothesis

Oxidative modification of DNA is one of the most extensively studied cellular damages induced by ROS. The formation of oxidized bases, so-called oxidative lesions, leads to an increased rate of point mutations or deletions in the nuclear and, even more pronounced, in the mitochondrial DNA (mtDNA) [255]. Since mtDNA mainly encodes for components of the respiratory chain, the *vicious cycle* concept has been established, stating that mutant proteins promote radical formation in mitochondria and in return further increase mutation rates. In support of this model, multiple studies have provided evidence that aging is associated with a decline in cytochrome c oxidase activity and other mitochondrial functions as well as increased ROS production [48, 217, 270]. However, the technical quality of these studies has been challenged because of unsuitable sample preparation techniques and lacking controls [195]. Hence, it is not yet clearly decided whether aging indeed affects the integrity of the electron transport chain.

As further evidence for the vicious cycle theory, a mouse model was presented in which proofreading capacity of the mitochondrial DNA polymerase was abolished, resulting in an increased mutational burden in the mtDNA. These animals had a significantly decreased lifespan, reduced rates of mitochondrial ATP generation and showed various signs of premature tissue aging [288]. However, using a more sensitive assay to

measure mtDNA mutation rates, a recent study concluded that the mutational burden posed on the mitochondrial mutator mouse model was unnaturally high. Strikingly, heterozygous animals for the mutator allele had a 500 fold higher mutation rate compared to wt but displayed neither a shortened lifespan nor signs of the pathologies observed in homozygous mice. Moreover, although a marked increase of mtDNA mutations with age was observed, the new data suggested that previous studies had overestimated their extent due to technical limitations. The authors therefore concluded that mtDNA mutations are associated with but not causative of aging [298].

Antagonistic Pleiotropy Hypothesis

It has been proposed that the influence of genes on an organism's fitness is dependent on its age. While some genes provide an advantage during early life and would therefore be selected for by evolution, they may have harmful effects during later stages of life. At this post-reproductive phase, the selective pressure no longer applies. This idea was formed by G. C. Williams in 1957 and was later named *antagonistic pleiotropy* theory [305].

The number of identified genes with the postulated characteristics, however, remains low [156]. The observation that mutations which cause longevity in worms, flies or mice are often associated with reduced fecundity is often brought up as evidence for the existence of antagonistic pleiotropy [175]. Another commonly cited example is a gain-of-function allele of the tumor suppressor p53 in mice. Heterozygous mutant animals were better protected against spontaneous tumor formation than wt animals. However, they displayed signs of premature aging and had reduced lifespans, suggesting that increased fitness at an early age came at the cost of disadvantageous effects later in life [291]. In contrast, analyses of naturally occurring polymorphisms in populations of several animal species and humans do not support antagonistic pleiotropy, for no negative correlation between longevity and fertility has yet been observed [175]. Some authors further associate the above mentioned cellular senescence with antagonistic pleiotropy. A limited proliferative capacity of somatic cells protects the juvenile organism from developing cancer. At the same time, it inherently limits its tissue renewal capacity and accelerates aging [35].

1.1.2 Invertebrate Model Systems

The age of genomics has revolutionized aging research. Novel methods in biochemistry and genetics enabled the discovery of specific genes associated with longevity. This led to the understanding that senescence is a process whose rate is regulated by specific molecular signaling pathways. The vast majority of aging paradigms have initially been established in non-vertebrate model organisms. Their advantages lie in short lifespans and amenability to genetic manipulations.

Saccharomyces cerevisiae

Probably the first laboratory model organism to be used in aging research is the budding yeast *Saccharomyces cerevisiae*, dating back to the year 1959 when it was first reported that single cells can only undergo a limited number of cell divisions [214]. Besides this so-called *replicative lifespan*, a more recent concept, termed *chronological aging* has been developed. Chronological lifespan is defined as the time that cells can survive in a non-dividing state [78]. Most prominently, the conserved protein deacetylase silent information regulator 2 (*SIR2*) was initially identified in yeast to promote replicative lifespan [144, 149]. Although there is a consensus that sirtuins, the family of *SIR2* homologues, have a function as metabolic regulators [191], many details regarding their biological role remain unresolved. For example, *SIR2* deletion yeast strains have unaltered chronological lifespans and even live longer under nutrient deprivation [77]. The role of sirtuins in regulating longevity in higher organisms remains controversial and *SIRT1*, the closest homologue of yeast *SIR2* in mammals, does not appear to influence lifespan. Nonetheless, recent work in mouse models has demonstrated that *SIRT1* protects against diseases associated with a chronic high fat diet (reviewed in [125]) and is therefore seen as a promising target for pharmacological intervention.

The amenability of *S. cerevisiae* to genetic manipulations opened up the opportunity to conduct screens with isogenic single gene deletion libraries [306] to study their influence on aging. This led to the discovery of the target of rapamycin (TOR) signaling pathway as a negative regulator of lifespan and thus established a link between nutrient availability and longevity [145, 246]. Of note, interference with TOR signaling has since been shown to extend lifespan in a variety of organisms including nematodes, flies and mice [120, 139, 147]. Moreover, a reduction in nutrients extended both replicative and chronological lifespan and thus recapitulates the established concept of dietary restriction in yeast [141, 246, 254]. Collectively, these data demonstrate that even unicellular organisms such as *S. cerevisiae* can provide valuable insights into conserved biochemical and signaling pathways involved in lifespan regulation.

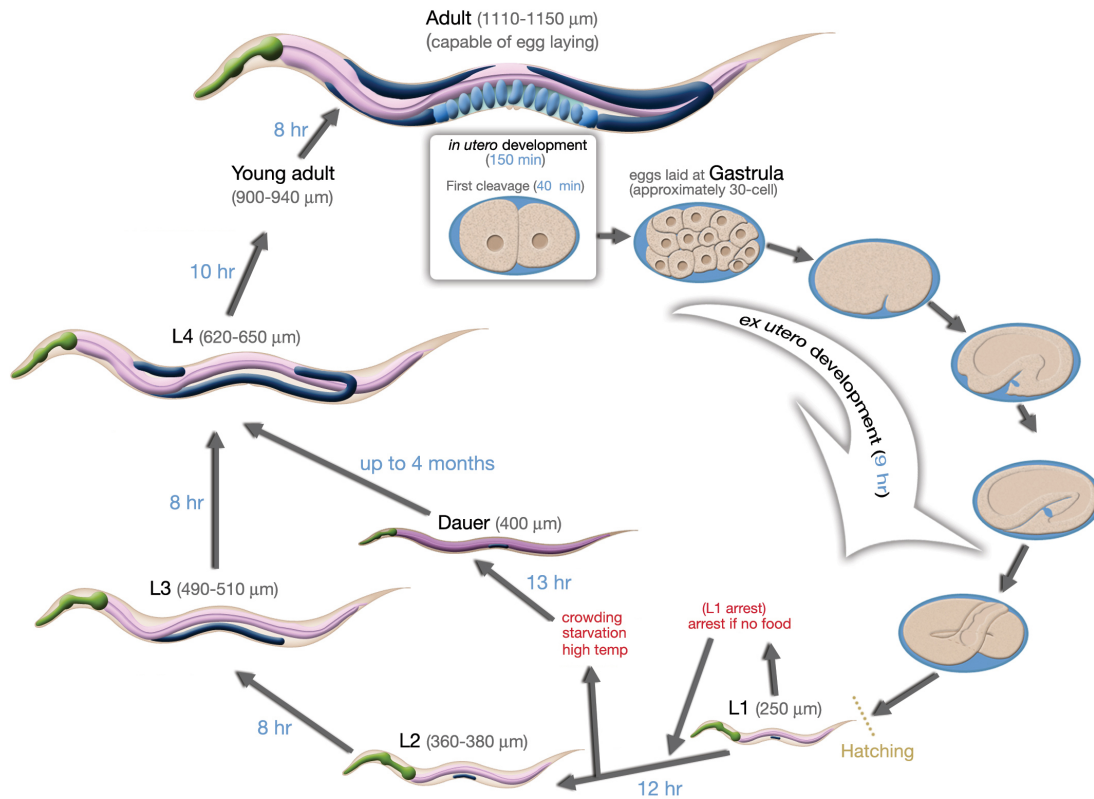


Figure 1.1.1: Developmental cycle of the *C. elegans* hermaphrodite. The nematode progresses through four consecutive larval stages (L1 to L4) before maturing into the reproductive adult after approximately 55 hours. In absence of nutrients, the development can be arrested either at the L1 larval stage, or the organism progresses into the highly long lived and stress resistant, albeit non-reproductive, dauer form. (Modified from <http://www.wormatlas.org/>.)

Caenorhabditis elegans

Having widely been studied by geneticists and developmental biologists since the 1970s, the small nematode *Caenorhabditis elegans* has matured into an indispensable tool in aging research since in the past two decades. In 1998 *C. elegans* became the first multicellular organism whose genome was published [31], and 20,513 protein coding genes are currently predicted (Wormbase release WS231). Advantages of employing *C. elegans* as a model system lie in its small adult body size of only approximately 1 mm, its fast life cycle of only 3 days under optimal growth conditions and its ability to survive cryogenic storage [25]. The self-fertilizing mode of reproduction of hermaphrodites further allows for maintenance of large populations without inbreeding depression

[142]. On the other hand, the high reproduction rate requires the induction of sterility by means of chemicals or temperature sensitive mutations to obtain age-synchronized populations. Some methods by which progeny is suppressed influence the organism's physiology and thereby lead to artifacts in lifespan experiments [5].

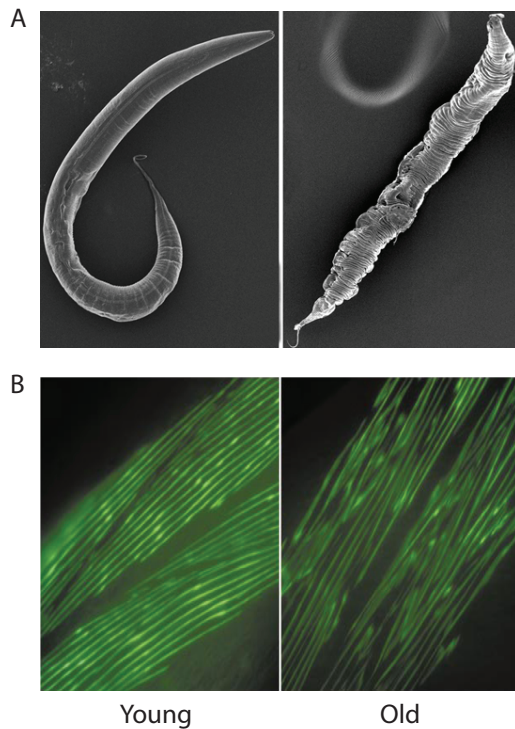


Figure 1.1.2: *C. elegans* as a model for aging. (A) Morphological differences between a young adult and an aged worm visualized by scanning electron microscopy. (B) Sarcopenia-like phenotype in the body wall muscle. Fluorescence microscopy images from worms expressing green fluorescent protein in muscle cells are displayed. (Adapted from <http://www.chp.edu/CHP/ghazilab> and [124].)

animals successively start to display signs of senescence, such as reduced motility or paralysis [158]. This is accompanied by morphological signs of deterioration in several, albeit not all, tissues. While neurons are relatively well preserved during aging, muscle fibers are more strongly affected and gradually display phenotypes resembling

After the embryonic stage, the animal's development comprises four successive larval stages before maturing into the reproductive adult worm. Under nutrient deprivation, heat stress or other environmental stimuli, *C. elegans* can form so-called *dauer* larvae, which are extremely long lived and stress resistant (1.1.1). In comparison to higher organisms, the anatomy of *C. elegans* is simple: Adult animals maintain a constant cell number, 959 or 1031 somatic cells in hermaphrodites or males, respectively, whose fate is predetermined during development [6]. Since cell division no longer takes place in adult worms, *C. elegans* is applied to study mechanisms of aging in post-mitotic tissues. Expectedly, telomere length, though strain dependent, is neither correlated with the animal's age nor its longevity [250].

Of particular interest for the use of *C. elegans* as a model organism in aging research is its short lifespan. When maintained at 20°C, wt hermaphrodites live for approximately two weeks. After a relatively short period of reproductive activity, typically lasting only 3 - 4 days, animals

human sarcopenia (Figure 1.1.2) [124].

A technological milestone towards identifying genetic determinants of longevity in metazoans was the development of a method which allowed determining the lifespan of worms in a high throughput format. To that end, a temperature sterile strain was subjected to chemical mutagenesis and several long-lived mutants were isolated. Phenotypes of these included constitutive dauer larvae formers as well as animals deficient in motility, chemotaxis or pharyngeal function. Thus, lifespan extension was mostly attributed to altered feeding behavior [159]. However, subsequent genetic mapping analysis revealed that several mutations had occurred in the *age-1* gene which is part of the insulin/insulin-like growth factor I (IIS) signaling pathway [90] and is described in more detail in a later section. Since then, the modulation of additional signaling pathways, for example target of rapamycin (TOR), Jun kinase and mitochondrial signaling, or biochemical pathways like protein translation, have been shown to extend lifespan in *C. elegans* [23, 166, 307]. The discovery of longevity genes has been greatly facilitated by the introduction of robust and convenient tools for reverse genetics experiments. Libraries of bacteria expressing RNAi constructs now allow for functional screens at a genome wide scale [146].

To gain insight into the causes of senescence on the molecular level, several studies profiled transcriptional changes during aging by microarray experiments. In an early report, age-synchronized populations of sterile mutant strains were analyzed at different time points during adult lifespan. Among the age-regulated genes was a large number of molecular chaperones, most of which peaked in transcript abundance in mid-life followed by a rapid decline in the later stages of life. The overall proportion of the genome with a significant change at the transcript level, however, was estimated to be less than 1% [188]. In contrast, more recent datasets, using amplified cDNA from several individual wt animals or RNA extractions from populations of temperature sensitive mutant suggested more extensional transcriptional remodulation [30, 102].

Drosophila melanogaster

The fruit fly *Drosophila melanogaster* with its lifespan of approximately eight weeks in a laboratory environment is another commonly used invertebrate model for the discovery of aging regulating genes. In contrast to nematodes, the fly anatomy and its diversity of tissues is much more complex. Several longevity genes were identified using forward or reverse genetic screens, or naturally occurring lifespan variability and mapping the corresponding chromosomal loci via quantitative trait locus analysis [236]. An even more extensive repertoire of genetics and genomics methods as compared to

C. elegans has been developed for *Drosophila*. These include the Gal4/UAS system [24] which allows for tissue specific overexpression of transgenes or transcript depletion via genome-wide RNAi libraries [64]. However, a major limitation of *Drosophila* in aging research is the inherently high mutation rate of the organism, making it challenging to generate transgenic lines with isogenic backgrounds [287].

The *Drosophila* model has served both to dissect previously identified pathways as well as to identify new longevity genes. For example, components of IIS, JNK and TOR signaling, which are known to regulate aging in worms, have also been shown to extend lifespan in *Drosophila* (reviewed in [236]). Novel longevity candidates include genes encoding for the G-protein coupled receptor *methuselah* (*mtl*) and its peptide ligands, *stunted* (*sun*) [55, 180].

1.1.3 Insulin/Insulin-like Growth Factor 1 Signaling

Components and Signaling Cascade of the IIS Pathway in *C. elegans*

One of the most extensively studied signaling pathways regulating longevity in *C. elegans* is the insulin/insulin-like growth factor 1 signaling (IIS) pathway. The first gene encoding one of its components was identified in 1988. In total, three mutations mapping to the same gene, termed *age-1*, yielded animals with an extended lifespan [89, 90]. More thorough morphological analysis revealed that age-related deterioration in multiple, although not all, tissues was delayed in these animals [124]. In 1993, a report showed that a point mutation in the *daf-2* gene, resulting in a single amino acid exchange from proline to serine, is sufficient to more than double the adult lifespan of hermaphrodite worms (Figure 1.1.3). This lifespan extension further required *daf-16*, a gene encoding a transcription factor [150]. Before the discovery of their role in adult lifespan determination, both *daf-2* and *daf-16* had already been identified as regulators of dauer larvae formation (*daf*), a highly stress resistant but non-reproductive form of nematodes [104, 256, 300]. Although mutations in both *age-1* and *daf-2* promote longevity, the phenotype of the latter mutant is more pronounced [168].

Further dissection of the pathway and the interplay of its component has led to the current model as depicted in Figure 1.1.4. A yet unidentified ligand binds to the tyrosin receptor kinase DAF-2, a homolog of the mammalian insulin receptor family. It has been suggested that activation occurs via autophosphorylation of tyrosine residues at the C-terminus of the protein analogous to the human insulin receptor [152]. Subsequently, DAF-2 recruits IST-1, an insulin receptor substrate orthologue, and the above mentioned phosphatidylinositol 3-kinase AGE-1/DAF-23 [213]. 3-phosphoinositide-dependent

kinase 1 (PKD-1) is activated by elevated phosphatidylinositol(3,4,5)triphosphate levels and phosphorylates three protein kinases: B/Akt homologs AKT-1 and AKT-2 [240]

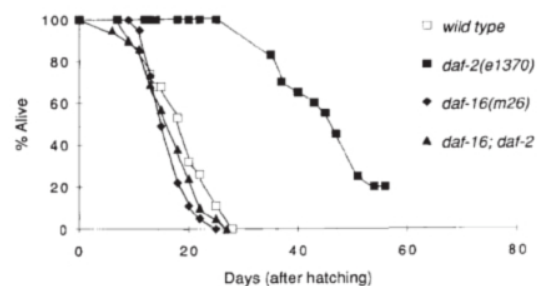


Figure 1.1.3: IIS-mediated lifespan extension in *C. elegans*. A point mutation in the *daf-2* gene, encoding a homolog of the mammalian insulin receptor, results in a strong lifespan extension. This phenotype further requires the *daf-16* gene encoding the transcription factor DAF-16, indicating that it acts downstream in the signaling cascade. (Adapted from [150].)

as well as the serum- and glucocorticoid-inducible kinase homolog SGK-1 [126]. This activation is counteracted by the phosphatase DAF-18, an orthologue of mammalian PTEN [225]. In parallel, AKT-1, AKT-2 and SGK-1 negatively regulate the activity of the transcription factor DAF-16 by phosphorylation of multiple serine and threonine residues. While AKT-1 and AKT-2 were reported to function predominantly in diapause regulation, the SGK-1 stimulus was most relevant for the regulation of lifespan and stress resistance [126]. As long as the IIS pathway is activated, DAF-16 remains phosphorylated and is retained in the cytosol, probably by sequestration via 14-3-3 protein binding as reported for mammalian cells [28]. Reduced IIS allows DAF-16 to enter the nucleus and activate transcription of its target genes [123]. Conflicting data exist in the literature as to the mechanism by which DAF-16 is inactivated. While Lee *et al.* reported that mutation of AKT phosphorylated residues resulted in dauer arrest induced by constitutive DAF-16 activation [172], Lin and colleagues observed that similarly mutated DAF-16 translocated into the nucleus but neither induced dauer formation nor extended lifespan. The authors of the latter study suggested that additional cues may be required for DAF-16 activation than the nuclear translocation alone [178].

The Transcriptional Response of DAF-16

DAF-16 belongs to the evolutionarily conserved forkhead box O (FOXO) group of transcription factors which are a subset of the HNF-3/forkhead structural family. In vertebrates, the FOXO group comprises up to five paralogs which have been implicated in a wide range of biological processes ranging from apoptosis, cell cycle arrest and DNA repair to oxidative stress resistance and metabolism [1, 13, 56, 106]. The most closely related members to DAF-16 in humans are the FOXO1/FKHR, FOXO3/FKHRL1 and FOXO4/AFX proteins with up to 67% sequence identity in their forkhead domains [177]. The observation that expression of human FKHRL1 can partially rescue the *daf-16* mutant phenotype in *C. elegans* further demonstrates the functional conservation of FOXO transcription factors [172]. Although *daf-16* is the only FOXO gene in *C. elegans*, three alternative splice isoforms with different amino termini termed a1/a2, b and d/f have been identified, the latter having the strongest effect on longevity [165, 177, 224]. By oligonucleotide selection, the conserved 8 bp DNA consensus sequence 5'-TTGTTTAC-3' was identified to which DAF-16 and its human orthologues AFX, FKHR and FKHRL1 bind. This sequence was hence termed *daf-16* family member binding element (DBE) [91].

Despite the fact that the FOXO transcription factor DAF-16 is recognized as the key

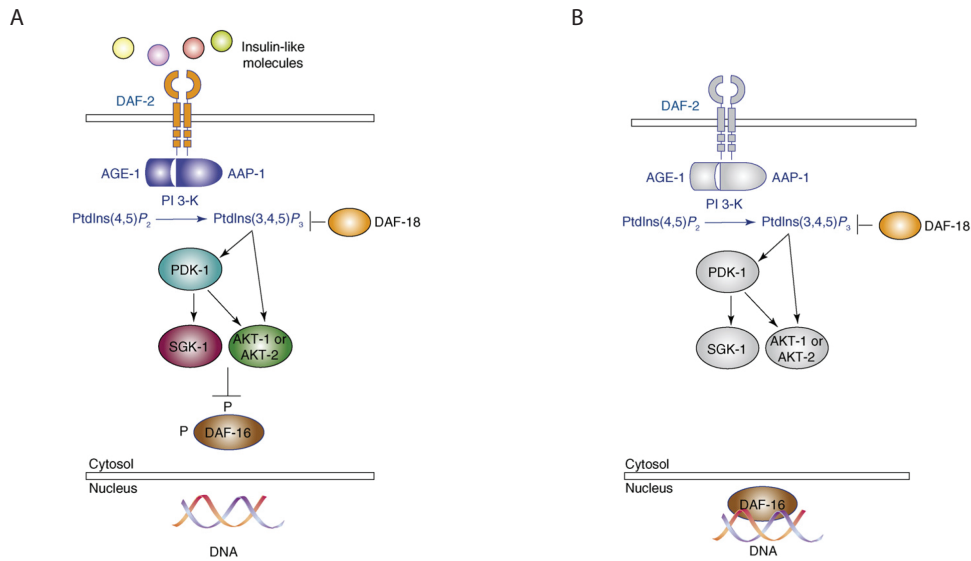


Figure 1.1.4: Model of the IIS signaling in *C. elegans*. (A) As long as the signaling pathway is activated by binding of ligands to the DAF-2 receptor, the PI3 kinase AGE-1 is activated. Via a downstream signaling cascade, the transcription factor DAF-16 is phosphorylated and retained in the nucleus. (B) If the function of DAF-2 or AGE-1 are reduced or the phosphatase DAF-18 is activated, DAF-6 translocates into the nucleus where it functions as a transcription factor. The transcriptional response of DAF-16 results in stress resistance and lifespan extension. (Adapted from [216].)

mediator of the IIS pathway, the molecular mechanism by which its activity extends lifespan remains elusive. Several microarray-based studies have tried to identify DAF-16 target genes. McElwee and colleagues used *daf-2* genetic mutants with *daf-2;daf-16* double mutants as controls and exclusively analyzed young adult worms. Their dataset showed that genes involved in stress resistance and detoxification, such as the mitochondrially located superoxide dismutase 3 (*sod-3*) and cytochrome P450 containing enzymes as well as molecular chaperones, including *hsp16*, *hsp-70* and *hsp-90* proteins, were expressed at higher levels in the *daf-2* mutant. The authors further suggested that the transcriptional profile was similar to that of dauer larvae [202]. The study by Murphy and coworkers used both genetic mutants as well as RNAi against *daf-2* and *daf-16* genes in sterile animals aged up to eight days across multiple time points. Similarly, multiple chaperones as well as genes with a role in oxidative stress defense, including catalases *ctl-1* and *ctl-2* and metallothionein *mtl-1*, were identified as targets of DAF-16. Additionally, antimicrobial proteins were reported to be upregulated in the long-lived *daf-2* mutants [218].

In a more recent report, serial analysis of gene expression (SAGE) was employed to address differential gene expression between *daf-2* genetic mutants and wt [113]. The experimental setup was more similar to that used by Murphy and co-workers, making use of temperature sensitive sterile strains and analyzing both young and old animals. However, the overlap of differentially expressed genes between the two studies was low. In contrast, the dataset provided by McElwee and colleagues was in much better agreement with the SAGE data. Apart from several heat shock proteins, genes encoding ribosomal and transthyretin-like proteins were overrepresented in *daf-2* mutants whereas other chaperones, metabolic enzymes, fat storage proteins and members of the protein turnover machinery were found downregulated. The authors suggested that the most relevant feature of *daf-2* mutants is a reduced metabolic rate.

To directly determine DAF-16 targets by identifying bound DNA sequences, another report applied chromatin immunoprecipitation (ChIP) using a polyclonal antibody raised against the protein [226]. The study used mixed developmental stages of wt, *daf-2* or *daf-16*; *daf-16* double mutants and extracted 103 genes from the identified sequences, that also contained the putative DAF-16 binding motif. These genes were involved in a variety of biological processes including metabolism, development, apoptosis, transcription and translation, signaling and stress response.

Finally, mass spectrometry-based quantitative proteomics has been applied in order to identify DAF-16 targets based on protein rather than transcript abundance [67]. To that end, nematodes were subjected to stable isotope labeling with ^{15}N and served as an internal standard to compare the proteomes of *daf-16*, *daf-2* and wt young adult populations. Only 86 of the identified proteins differed in abundance between the *daf-2* mutant strain and wt, of which only 35 had been identified as a DAF-16 target in any of the four above mentioned studies [173, 202, 218, 226]. The novel candidates were predominantly enzymes involved in carbohydrate metabolism, amino acid biosynthesis and ROS defense.

Evolutionary Conservation of IIS-mediated Longevity Regulation

Although IIS-related regulation of longevity is best established in nematodes, a growing body of evidence suggests that both the components and the basic molecular mechanisms of lifespan regulation are conserved in evolution from nematodes to humans (Figure 1.1.5). Just like *C. elegans*, the genome of the fruit fly *Drosophila melanogaster* contains a single gene, *InR*, which encodes for an insulin receptor homolog. While homozygous *InR* mutations are lethal [38, 81], heteroallelic combinations resulted in dwarf phenotypes with up to 85% maximum lifespan extension [279]. Similarly, mu-

tants for *chico*, the fly insulin receptor substrate/IST-1 homolog, displayed a longevity phenotype with 48 or 36% lifespan extension for homozygous or heterozygous animals, respectively [41]. Of note, the effect on lifespan was in both cases lower in males as compared to females [41, 279].

In contrast to nematodes and insects, the mammalian IIS receptor gene has diverged into three paralogs which together form the insulin receptor family: the insulin receptor (IR) [294], the insulin-like growth factor receptor (IGF-1R) [295] and the insulin receptor-related receptor (IRR) [269]. IRR is expressed primarily in kidney, stomach and pancreas [128, 197] and probably has a specialized function in sensing alkaline pH [63]. Both IR and IGF-1R are more widely expressed. While the role of IR and the downstream signaling is primarily in metabolic regulation, IGF-1R promotes cell growth, proliferation and survival. The role of IIS in mammalian aging remains controversial, primarily because insulin resistance and low insulin signaling are associated with diabetes and poor health in humans while ablation of the homologous pathway causes longevity

in lower organisms. Thus, this contradiction is sometimes referred to as *the insulin paradox* [44]. However, several reports support the notion that both reduced insulin and IGF-1 signaling can in some cases extend lifespan in mice and humans. For example, fat specific insulin receptor knockout mice are long lived by 18% while being protected against obesity, although maintaining normal food uptake [19]. A similar lifespan extension was achieved by systemic or brain-specific insulin receptor substrate 2 knockouts, despite the fact that these animals were hyperglycemic and overweight as compared to wt [277].

In contrast to insulin signaling, the role of IGF-1 signaling in aging is more firmly estab-

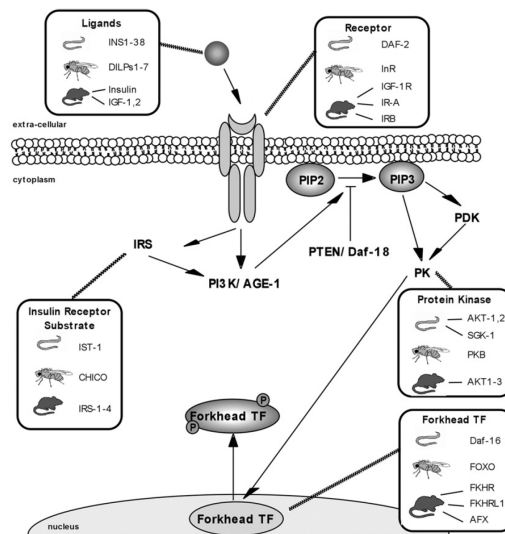


Figure 1.1.5: IIS signaling is conserved in evolution. Most component of the IIS signaling cascade have clear homologs in worm, fly and mouse, including the receptor and the downstream Forkhead transcription factor. However, single genes in *C. elegans* have often evolved into several paralogs in mammals, often with pronounced tissue specificity and specialized functions. (Adapted from [26].)

lished. Homozygous gene knockouts of the IGF-1R gene in mice (*Igf1r*) are lethal. Heterozygous animals, however, displayed a longevity phenotype and were more resistant to oxidative stress. Just like in flies, lifespan extension was only significant in females but not in males [129]. Interestingly, a study among a cohort of female Ashkenazi Jewish centenarians showed an over-representation of a heterozygous IGF-1R mutation [274]. Low levels of IGF-1 are further thought to contribute to the strongly delayed aging of Ames dwarf *Prop1^{df/df}* and Snell dwarf *Pit1^{dw/dw}* mice, which live more than 50% longer than wt [27, 82]. However, data as to whether FOXO transcription factors are required for increased longevity are still lacking.

Crosstalk between IIS and Other Signaling Pathways

Biochemical and genetics approaches revealed that IIS interacts with other cellular signaling pathways. These are either essential to allow DAF-16 action or adjust DAF-16 transcriptional response by activation or inactivation of coregulators. In *C. elegans* for example, the Dictyostelium suppressor of MEK null orthologue, *smk-1*, is required for longevity, oxidative and UV radiation stress resistance phenotypes. In contrast, SMK-1 depletion did not affect *daf-16*-dependent thermotolerance [307]. Similarly, host cell factor 1 homolog *hcf-1* and IIS synergistically regulate lifespan through DAF-16 action [138]. Both SMK-1 and HCF-1 colocalize with DAF-16 in the nucleus upon activation [138, 307].

Intriguingly, heat shock factor 1 (*hsf-1*) was identified as an additional gene essential for lifespan extension upon IIS inactivation [130, 212]. HSF-1 is a member of a conserved leucine-zipper containing family of transcription factors. While invertebrates, such as worm and fly, only possess a single member, up to four isoforms of heat shock factors have been reported in vertebrates [42, 92, 244]. In a state of folding homeostasis, some HSFs are thought to be sequestered by Hsp90 proteins from which they are released under heat stress. Under these conditions, HSFs homotrimerize, accumulate in the nucleus and strongly induce transcription of genes carrying heat shock response elements (HSEs), among which are multiple molecular chaperones [7, 39, 80, 154, 241, 260, 308, 309]. Very recently, the molecular mechanism linking HSF-1 and IIS signaling in *C. elegans* has been elucidated in more detail. As shown by yeast two hybrid and immunoaffinity experiments, a pool of HSF-1 is part of a heterooligomeric complex with *daf-16*-dependent longevity (DDL) proteins 1 and 2, as well as heat shock factor binding protein 1 (HSB-1) [39, 176, 261]. This complex, termed DDL-1 containing HSF-1 inhibitory complex (DHIC), has been suggested to dissociate and release HSF-1 under conditions of reduced IIS. This heat shock independent HSF-1

activation is thought to be achieved by DDL-1 phosphorylation via an as yet unidentified kinase [39]. These data hence provide a link between the regulation of lifespan and members of the proteostasis network (Figure 1.1.6).

Initially it was believed that that metazoan sirtuins, homologs of the yeast *Sir2* gene, act via the IIS pathway, suggesting that lifespan extension through dietary restriction is also facilitated by IIS. Several studies support this hypothesis, however, they are controversial. While an earlier report claimed that overexpression of *sir-2.1*, the most homologous *sir-2* gene in *C. elegans*, extended lifespan by up to 50% [283], it later became apparent that the observed phenotype was due to an unlinked mutation rather than *sir-2.1* dosage [299]. Thus, evidence that sirtuins affect lifespan in worms is lacking. Moreover, it has been proposed that sirtuins regulate FOXO transcription factors in mammalian cells, but it is not clear whether this regulation is positive or negative. SIRT1, the mammalian *Sir2*

ortholog was reported to repress Foxo3a and other mammalian forkhead transcription factors by deacetylation [29, 215] while the same protein appeared to activate Foxo1, the mouse homolog of FKHR via the same enzymatic activity [310].

Finally, DAF-16/FOXO can be activated or inactivated independently of the DAF-2 receptor. For example, the *daf-7*/TGF-beta signaling pathway also negatively regulates nuclear localization of DAF-16 in worms, although without affecting lifespan but rather dauer arrest regulation [172]. Conversely, Jun N-terminal (JNK) and Ste20-like kinase (MST1) pathways can activate FOXO transcription factors directly and thereby override the inhibitory IIS stimulus during cellular stress [296]. In mammalian cells, FOXO4 and FOXO3 were demonstrated to be activated via JNK or MST1, respectively [76, 174]. Moreover, overexpression of *cst-1*, the *C. elegans* homolog of MST1, extended lifespan in a *daf-16*-dependent manner while reduced expression shortened lifespan [174].

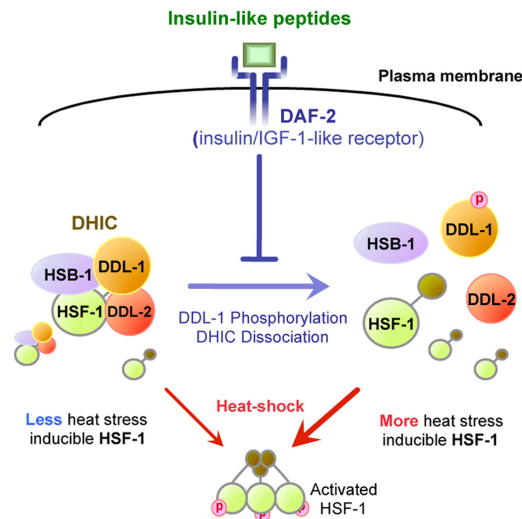


Figure 1.1.6: Proposed model for the interaction between IIS signaling and HSF-1. A pool of HSF-1 is sequestered by the DHIC complex. Interference with IIS results in HSF-1 release. (Adapted from [39].)

1.1.4 Proteostasis and Protein Aggregation during Aging

Modules of the Proteostasis Network

The term protein homeostasis, or *proteostasis*, is defined as “the cellular process that governs the life of proteins” [210]. The components involved in this process are referred to as the proteostasis system or network and are made up of a large number of proteins belonging to multiple biochemical pathways. These include RNA synthesis, degradation and processing, protein biosynthesis, protein folding and quality control, protein translocation, assembly and disassembly as well as degradation [11]. Individual pathways are often referred to as *hubs* within the proteostasis network (Figure 1.1.7). During proteostasis imbalance, caused by insults such as heat stress or the presence of aggregation prone proteins, each of these hubs should possess sufficient capacity to cope with the presence of denatured proteins and a reduced activity of other proteostasis components [210]. Under these conditions, the compromised function of any of the above mentioned hubs may result in proteostasis decline. This notion is supported by a genome-wide RNAi screen in *C. elegans* in which genes required for preventing protein aggregation were identified. Depletion of several individual proteins belonging to the proteostasis network resulted in premature polyQ aggregation [220].

Moreover, the occurrence of proteotoxic agents can weaken the proteostasis system. Artificial β -sheet forming peptides were shown to sequester a broad range of proteins in a human cancer cell line [232]. These proteins were mostly large in size, often contained unstructured regions and were involved in a broad range of cellular pathways, including protein folding and degradation. Furthermore, this sequestration displayed a preference for newly synthesized proteins. The authors therefore concluded that protein aggregation gradually compromises the biogenesis of proteins with high chaperone-mediated folding requirements and ultimately lead to a collapse of essential cellular functions.

If a chronic imbalance cannot be overcome by adjusting the capacities of the cellular proteostasis machinery it is likely that the system gradually deteriorates in a vicious cycle [210].

Proteostasis Decline during Aging

An increasing body of evidence suggests that the efficiency of many components of the proteostasis network becomes compromised during aging [69, 210]. In *C. elegans* for example, the response to heat and unfolded protein stress has been shown to be

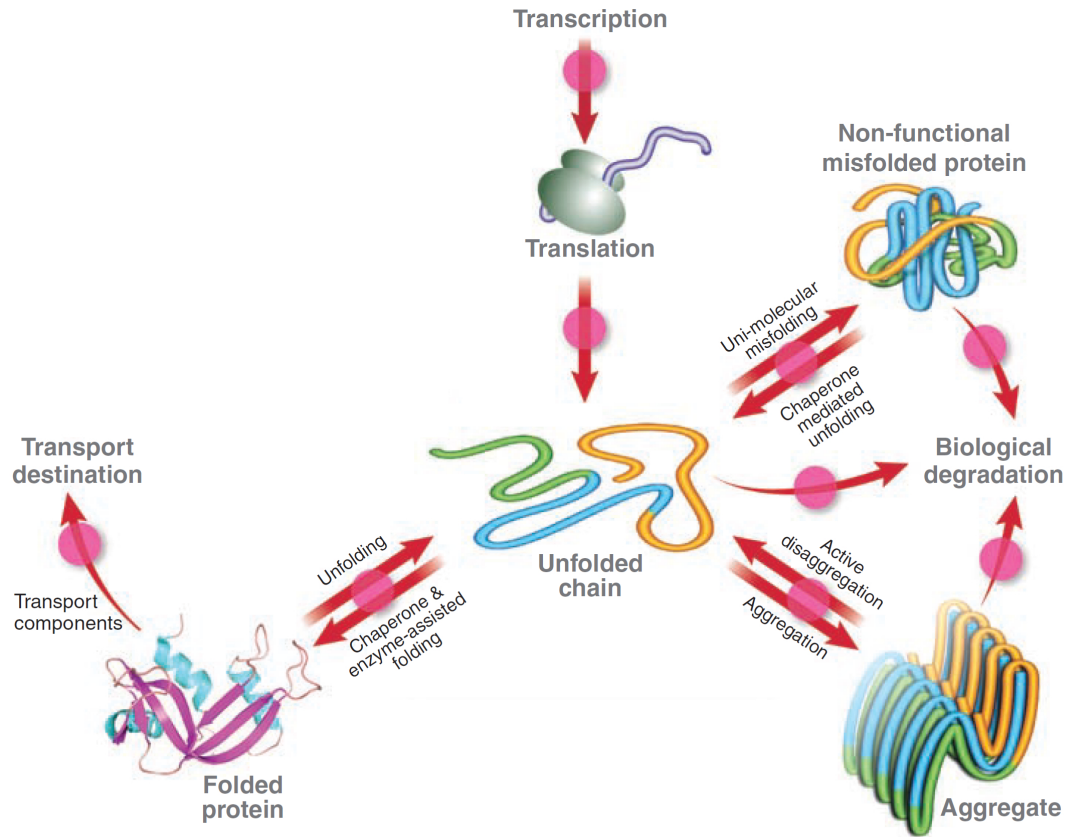


Figure 1.1.7: Proteostasis network hubs. Newly synthesized proteins are usually folded with the help of molecular chaperones to fulfill their function in the cell. Misfolded proteins in contrast are either renatured, degraded or form protein aggregates. Imbalance in the proteostasis system, for example during aging, can result in increased aggregate formation and ultimately cell death. (Modified from [11].)

dampened in aged compared to young animals [16]. Moreover, a decline in basal expression levels of small heat shock proteins was observed in microarray studies [188]. Interestingly, brain and muscle tissue of calorically restricted, and thereby long-lived, mice displayed elevated levels of Hsps over animals fed *ad libitum* [170, 171] while the extent of Hsp70 induction upon heat stress was reduced [127]. Similarly, caloric restriction rendered rats more thermotolerant and the extent of cellular damage induced by heat stress was reduced [114].

Besides protein folding, impaired function of chaperone-assisted autophagy [53] or the 26S proteasome pathway [285] in rat liver or flies, respectively, suggests a reduced clearance of misfolded protein aggregates with age. Of note, the proteasomal activ-

ity in rat liver was found to be unaltered throughout lifespan [268]. To directly assess the proteostasis capacity in worms, transgenic animals have been generated in which aggregation-prone proteins such as destabilized forms of myosin or paramyosin [16] or mutant forms of firefly luciferase fused to GFP [108] were expressed, and the formation of protein aggregates was assessed by microscopy. In all cases, the recombinant proteins were soluble at a young age and gradually formed aggregates later in life.

In line with the observed proteostasis decline in model organisms, age is the strongest risk determinant for the onset of a number of human neurodegenerative disorders caused by the accumulation of amyloid protein aggregates, including Alzheimer's, Huntington's and Parkinson's disease [44, 69, 151]. These amyloid folding diseases have been recapitulated in model organisms. For example, transgenic flies or worms expressing polyglutamines [58, 211] or A β peptides [43] as well as mouse models for Huntington's disease [304] consistently show an age related onset of aggregated formation and toxicity. Recent studies have shown that the occurrence of protein aggregates further weakens the proteostasis capacity [210]. In *C. elegans*, the expression of recombinant polyQ proteins increased the aggregation propensity of temperature sensitive cellular proteins, and vice versa [99].

The formation of insoluble protein deposits during aging has been observed in several organisms even in the absence of proteotoxic amyloid precursors. For example, in a proteomic study in *C. elegans* a strong increase in more than 700 SDS-insoluble proteins was detected in old as compared to young animals. These proteins were involved in diverse biological processes, including development, translation, protein folding and metabolic pathways [57]. An independent report also found age-related protein insolubility and further demonstrated that the depletion of highly aggregation-prone proteins by RNAi extended lifespan [253]. Protein aggregates in aging tissues were further reported in *Drosophila* [61].

Given that (a) the integrity of the proteostasis network becomes compromised with age and (b) its decline is enhanced by the presence of misfolded proteins, the occurrence of an eventual proteostasis collapse may set a limit to the lifespan of multicellular organisms [280].

Interaction between IIS and Proteostasis

Although the molecular mechanism by which reduced IIS extends lifespan remains ill defined, numerous reports indicate that a prolonged maintenance of the proteostasis network may at least be partially responsible for its longevity phenotype. As mentioned above, the transcription factor HSF-1, which facilitates the expression of multi-

ple molecular chaperones, is activated by IIS in the long lived *C. elegans daf-2* mutant [39]. In line with this observation, transcript levels of several chaperones were found to be elevated in a *daf-2* mutant background [113, 202, 218]. Experiments using aggregation prone proteins as folding sensors have substantiated the link between IIS and proteostasis more firmly. When a fusion protein consisting of 82 glutamine residues and YFP (Q82-YFP) was expressed in an *age-1* mutant background, both the onset of aggregation and signs of toxicity were reduced when compared to wt animals of the same age [211]. Conversely, depletion of DAF-16 or HSF-1 by RNAi accelerated the formation of Q40-YFP aggregates at an earlier time point in life [16]. Similarly, a variety of misfolding-related phenotypes in animals expressing destabilized forms of paramyosin or myosin heavy chain were increased upon RNAi against *hsf-1* or *daf-16* but decreased when the same genes were overexpressed or *age-1* was depleted [16]. Moreover, overexpression of *daf-16* homolog FOXO or the negative regulator of IIS, Pten, suppressed the formation of aggregates in fly muscle. Intriguingly, FOXO activation in muscle also provided a systemic protection against aggregate accumulation in other tissues [61]. Collectively, these results indicate that low levels of IIS and thereby increased transcriptional responses of DAF-16 and HSF-1 delay proteostasis decline during aging.

As some data suggest, DAF-16 and HSF-1 not only influence protein folding but also regulate clearance of misfolded protein aggregates. A study employing both an *in vivo* *C. elegans* Alzheimer's model as well as *in vitro* disaggregation assays concluded that HSF-1 promoted the disaggregation of toxic small molecular weight oligomers of A β peptides and thus made them accessible to proteasomal degradation [43]. DAF-16 in contrast did not decrease aggregation but lead to the formation of higher molecular weight assemblies with lower toxicity. The authors speculated that the clearance of these latter aggregates occurred either by secretion or a chaperone-dependent pathway at a slower rate. The notion that DAF-16/FOXO-dependent clearance of misfolded proteins occurs by other means than refolding is supported by a more recent report. FOXO activity was required for the clearance of insoluble deposits of polyubiquitinated proteins from fly muscle which occurred at least partially via the macroautophagy/lysosome pathway [61].

1.2 Mass Spectrometry-based Quantitative Proteomics

Mass spectrometry (MS)-based proteomics is a fast evolving field. Through constant improvements in instrumentation, quantification strategies and algorithms for data analysis it has in recent years emerged as an indispensable tool in biomedical research. The applications of MS-based proteomics now range from mere studies of protein expression levels to the analysis of posttranslational protein modifications and protein interactions.

1.2.1 Mass Analyzers for MS-Based Proteomics

A broad range of instrument types have been applied to proteomics since gentle ionization techniques, most importantly electrospray ionization (ESI) [79] and matrix-assisted laser desorption/ionization (MALDI) [148], have made peptides and proteins amenable to MS analysis. Besides linear ion trap and Orbitrap analyzers, which are discussed in more detail below, other commonly used instrument designs include time of flight (TOF) and triple quadrupole mass spectrometers [3, 115]. A milestone for high confidence peptide identification was the introduction of hybrid instruments between linear ion traps and Fourier transform ion cyclotron resonance (FTICR) analyzers with high resolving power and mass accuracy [276]. This instrument type, however, has lately been displaced by Orbitraps due to lower operating costs and successive performance improvements [265, 267].

Linear Ion Traps

Ion traps are devices capable of storing and isolating ions, and can additionally serve as mass analyzers. In the late 1980s, the first three-dimensional (3D) traps, also named Paul traps after their inventor, became commercially available [143]. These devices were applied in proteomics workflows by coupling them to liquid chromatography systems with online electrospray ionization [94]. A considerable increase in performance was achieved with the introduction of linear, or two-dimensional, ion traps. The linear trap designs outperformed commonly used 3D traps in many aspects, including injection efficiencies, ion storage capacities, dynamic range and sequencing speed [68, 198].

Linear traps consist of four parallel hyperbolic rods with a space in their center, to which oscillating electric fields are applied at radio frequency (RF). These so-called quadrupole fields are used to trap ions in radial trajectories. The ion motions are described by the Mathieu Equations.

$$q = \frac{4zeV}{m(x^2 + y^2)\Omega^2}$$

$$a = \frac{8zeU}{m(x^2 + y^2)\Omega^2}$$

q, a , trapping parameters

m , ion mass

e , ion charges

z , number of ion charge

V , amplitude of AC oscillation

U , DC offset

Ω , AC frequency

x, y , distances from the center of the trap to the X or Y rods, respectively

Using these equations, specific regions of a and q combinations can be calculated under which ions are stable in both x and y direction and thus remain trapped. Given that most variables, including the quadrupole dimensions and the applied radio frequency, are kept constant in a given instrument and that no DC offset is applied, the equations can be simplified to:

$$q = \frac{kV}{m/z}$$

$$a = 0$$

k , instrument constant

Stable ion trajectories can be expected for q values between 0 and 0.908. However, the upper q -limit for stable trajectories is reduced to 0.88 in the the ion trap designs used here when employed as a mass analyzer. This is due to the resonance ejection voltage, a supplemental AC voltage applied to the X-rods of the quadrupole [281].

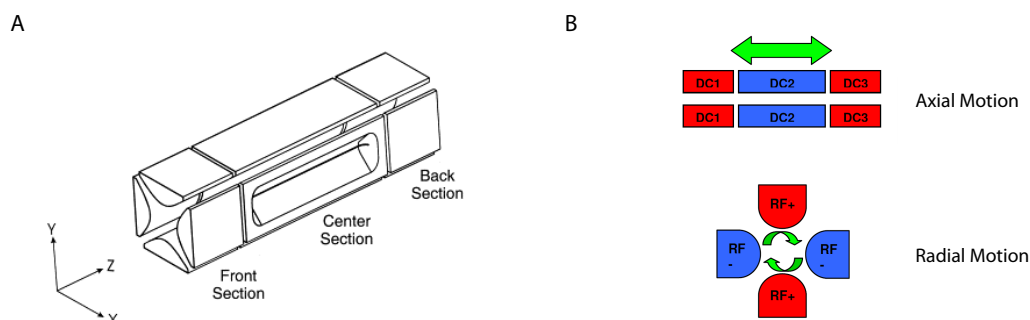


Figure 1.2.1: Linear Ion Trap. (A) Schematic drawing of the linear ion trap rod design. (B) Axial and longitudinal motions of ions in a linear trap are determined by DC trapping potentials of the front and back sections as well as an oscillating radio frequency AC potential applied to the opposing rods of the quadrupole. (Adapted with modifications from [264] and [281]).

While the quadrupole fields described above allow the trapping of ions in the the x-y plane, additional DC potentials restrict their movement along the z-axis (Figure 1.2.1). These stopping potentials can be provided by aperture plates located at the ends of the quadrupole rods [111]. More commonly, the quadrupole rods are split into three electrically isolated sections, and the stopping potential is applied to the outer sections of the ion trap. The combination of these two principles of radial and axial trapping confines ions with specific characteristics in a potential well.

When equipped with detectors, usually conversion dynodes coupled to photomultiplier tubes, linear ion traps can be used as mass analyzers. To that end, a population of ions is first confined and gradually "scanned out" of the trap by ramping the amplitude of the AC voltage V . By this means, ions assume q -values outside the stable range in the order of ascending m/z values, leave the trap and hit the detector. The linear ion trap is broadly used in MS-based proteomics because of its high sensitivity and sequencing speed. Moreover, gas phase reactions such as collision-induced dissociation (CID) can be performed in the same device. However, the applicability in proteomics is limited by its low mass accuracy and low resolving power. Therefore, ion traps are often combined with high resolution analyzers in hybrid instruments.

Orbitrap Mass Analyzer

The Orbitrap mass analyzer was introduced by Alexander Makarov in 2000 [192] and is reminiscent of an ion trap developed by Kingdon in the 1920s [153]. Both designs make

use of electrostatic fields to confine ions, rather than magnetic or oscillating electric fields as used in quadrupole or ICR analyzers, respectively. The Orbitrap cell consists of a central spindle surrounded by an outer electrode which is split into two isolated halves (Figure 1.2.2). Ions are injected tangentially into the cell and forced onto trajectories around the spindle by electric attraction which is counterbalanced by centrifugal forces. Trapping potentials are applied to the outer electrode to restrict the ions' axial movement and result in oscillations along the z -axis. The frequency ω of these oscillations is related to the mass/charge ratio (m/z) and can be described as

$$\omega = \sqrt{K \frac{z}{m}}$$

with K being an instrument constant [132]. By recording image current transients of the potential changes between both halves of the outer electrode, mass spectra can be deduced after Fourier transform analysis.

A major technical challenge during the development of Orbitrap instruments was the tangential transfer of ions into the cell. To this end, ions are first accumulated in a curved quadrupole ion trap, termed C-trap, and injected as a focused package by the application of a DC voltage [281]. The resolving power of the first generation of commercially available Orbitrap instruments was comparable to 7T FT-ICR instruments only in the high m/z range but was lower below 800 Th [266]. The application of a higher field strength [194] and a reduction in size [205] have further improved the performance of the Orbitrap cell which now outperforms most FT-ICR analyzers. The mass accuracy of Orbitrap instruments is typically within 3 ppm [193] but can be improved to values in the sub-ppm range by using ambient air ions for real time recalibration [229] or software-based recalibration [51].

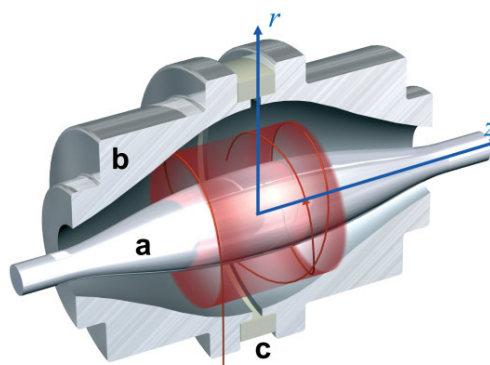


Figure 1.2.2: Orbitrap analyzer. The cell consists of a central electrode (a), also referred to as 'spindle', which is surrounded by two halves of the outer electrode (b) which are electrically isolated from each other by a ceramic ring (c). Ions move in stable trajectories around the spindle by electric attraction while simultaneously oscillating in the z -axis. (Adapted from [266].)

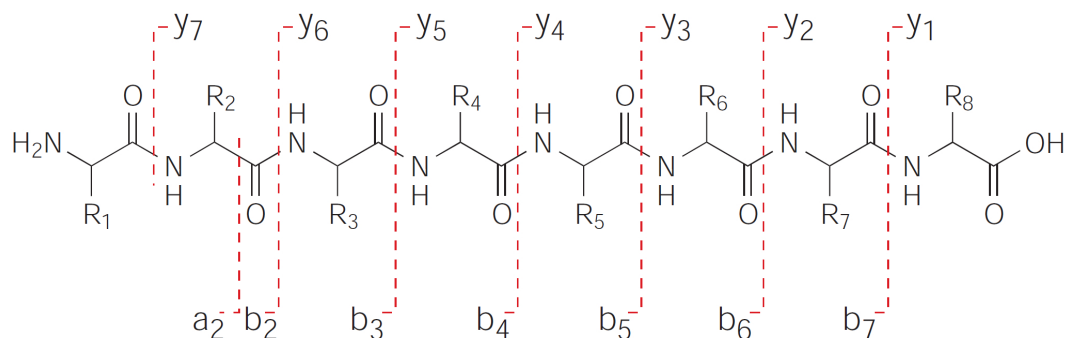


Figure 1.2.3: Roepstorff–Fohlmann–Biemann nomenclature. Fragment ion series obtained in fragmentation experiments are named with Latin letters according to the bonds in the peptide backbone at which the dissociation takes place. Additionally, fragments are numbered according to the distance from N- or C-terminus. (Adapted from [273].)

1.2.2 Fragmentation Methods in Tandem Mass Spectrometry

Peptide analysis by mass spectrometry in shotgun proteomics typically involves tandem MS (MS/MS or MS²) experiments. After ionization and isolation, the backbone of selected peptide ions is dissociated and, ideally, a ladder of fragment ions differing in mass by single amino acids is generated. By manual or computational analysis of the detected fragments, the amino acid sequence of the precursor can in principle be inferred. Depending on the cleaved chemical bond, peptide fragment ions are classified according to Roepstorff-Fohlmann-Biemann nomenclature as depicted in Figure 1.2.3 [273]. Fragmentation of peptides is usually achieved by collision with inert gas atoms, like in collision induced dissociation (CID) or higher energy collisional dissociation (HCD), or chemical reactions with radicals in the gas phase as in electron transfer dissociation (ETD).

In the hybrid mass spectrometers described in the following section, CID experiments are performed entirely in the linear ion trap section. In the first step, a precursor peptide ion selected for fragmentation is isolated. To this end, the precursor is brought to a high but stable q -value by increasing the quadrupole AC amplitude of the trap. In the next step, all undesired ions are ejected from the ion trap by applying a multi-frequency waveform which covers the resonator frequencies of ions with m/z values outside the isolation window. Before excitation, the q -value of the isolated ion population is reduced by altering the RF AC voltage of the ion trap to avoid the loss of small product ions. The selection of this so-called activation q is essential for the quality of the obtained fragmentation spectra. While low activation q values prevent sufficient

energy absorption and inefficient fragmentation, higher settings result in the loss of small fragment ions [54]. As a compromise, a typical activation q of 0.25 is chosen for the instrument types described in the following section. In this case, the lowest observable mass is one third of the fragmented precursor [219].

In the actual activation step, the isolated precursor ions are accelerated in the trap by applying a low amplitude AC waveform at its resonator frequency. Through collisions with surrounding inert gas atoms, often helium, the molecules accumulate vibrational energy until the peptide backbone dissociates. All steps of the CID experiment - precursor isolation, fragmentation and analysis of fragment ions - are typically performed in the same device, the linear ion trap.

HCD is an alternative fragmentation method for Orbitrap hybrid instruments [230]. After isolation in the linear ion trap, precursor ions are accelerated towards a special collision octopole or, in earlier setups, into the C-trap, where activation is achieved by collision with inert gas atoms at a relatively high pressure. Through the C-trap, product ions are then injected into the Orbitrap cell for analysis. Initially, the cycle time in HCD mode was considerably slower than to CID, but a comparable sequencing speed is achieved the more recently released generation of instruments [205]. Although much higher amounts of ions are required to perform HCD experiments, this method offers a number of advantages over CID fragmentation. First of all, fragmentation spectra are acquired at high resolution, and by that means identification scores are markedly improved. Secondly, all fragments are detectable and no low mass cutoff applies. This property for example helps in the identification of phosphotyrosine-containing peptides in which diagnostic reporter ions in the low region of the mass range are observed [9, 272]. Last, HCD reduces neutral losses during the fragmentation of phosphorylated peptides and thereby does not require additional activation steps [219].

Both CID and HCD fragmentation methods typically generate y- and b-type fragment ions, although the y-ion series is more dominant in HCD [230].

1.2.3 Instruments for High Resolution MS-Based Shotgun Proteomics

In bottom up shotgun proteomics experiments, protein mixtures are digested into peptides by proteolytic cleavage and analyzed by tandem mass spectrometry. The automated interpretation of mass spectra derived from these highly complex samples is challenging since the immense space of possible peptide assignments can yield false identifications. Instruments with high mass resolution and accuracy greatly improve the peptide identification confidence because the acquired spectra provide additional information on charge state and composition of precursor and/or fragment ions.

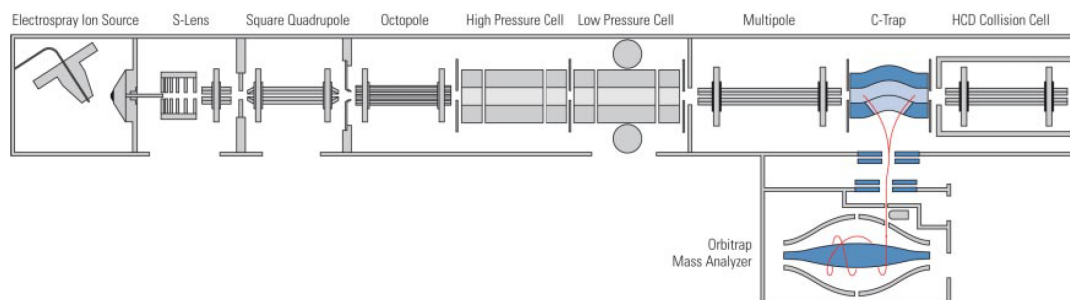


Figure 1.2.4: Schematic drawing of the Orbitrap-Velos hybrid mass spectrometer. (Modified from [231].)

For proteomics applications, high resolution mass analyzers are often combined with low resolution linear traps in hybrid instruments. For tandem MS experiments, the high resolution analyzer is typically used to acquire survey scans across a broad mass range. In parallel, selected peptide precursor ions can be sequentially isolated and subjected to CID fragmentation in the ion trap. These low resolution MS/MS scans are performed at higher speed, allowing several fragmentation events while the high resolution survey scan is acquired. Based on the resolution of survey and fragmentation scans, this mode of operation is referred to as *high-low* strategy [205]. Early hybrid instruments in which this strategy was pursued consisted of a linear ion trap coupled to an FT-ICR analyzer (FT-Ultra) [276] and, after the introduction of the Orbitrap cell, the LTQ-Orbitrap [193]. The time frame for a cycle consisting of a high resolution full scan and ten data dependent MS/MS events during analysis of complex mixture in these instruments was in the range of three seconds. A new ion trap design combined with increased ion transmission doubled the sequencing speed in the next generation of Orbitrap hybrid instruments (LTQ Orbitrap Velos, Figure 1.2.4) [231].

The mode of operation in which not only survey scans but also MS/MS scans are performed at high resolution is referred to as *high-high* strategy, to discriminate it from the previously described *high-low* strategy. Since the introduction of the LTQ Orbitrap Velos instrument, the *high-high* analysis of complex peptide mixtures using HCD fragmentation has become feasible. Higher ion currents into the instrument and improved transmission of fragment ions from the collision cell into the C-trap increased performance and speed. Cycles consisting of one survey and ten HCD fragmentation scans can be completed within a time frame of 2.6 s, although all spectra are acquired in the Orbitrap cell. [231]. Higher resolution Orbitrap analyzers have further increased scan speeds by allowing mass spectra to be acquired with shorter image current transients

at the same resolution [205]. Of note, a recently introduced instrument type, termed Q Exactive, uses an Orbitrap cell as its sole mass analyzer and is not designed as a hybrid mass spectrometer. Instead of a linear ion trap, a transmission quadrupole is used for isolation, resulting in lower fill times for MS/MS scans and faster cycle times in HCD mode [204].

1.2.4 Quantification Strategies

A major challenge in MS-based proteomics is the fact that peptides concentrations cannot be inferred directly from the signal intensities detected by a mass spectrometer. To circumvent this limitation, several strategies have been developed to allow either comparison of protein abundance between samples (relative quantification) or determination of protein copy numbers (absolute quantification) (Figure 1.2.6) .

Label-based Quantification

Label-based quantification makes use of the presence of two or more differentially modified versions of peptides from different samples in the same MS experiment. Abundance differences for each individual peptide can thereby be inferred by comparing intensity differences side by side in the same scan. Quantification labels can be introduced metabolically *in vivo* or chemically *in vitro*.

In metabolic labeling strategies, non-radioactive isotopes are incorporated into the proteome of an organism *in vivo*, causing a defined mass shift. The technically easiest way to achieve this is through supplying nutrients in which all atoms of a single element, often nitrogen, is replaced by a heavy isotope. For example, ^{15}N labeling has been used to compare proteomes of a wide range of organisms, including yeast [222] and cultured human cells [47, 134] as well as whole model organisms like *C. elegans*, *Drosophila* [160] and rats [200]. This technique, however, is limited to the comparison of two biological samples and incorporation rates are often suboptimal. Furthermore, the number of incorporated heavy atoms varies between proteolytic peptides. As a result, the mass shift between the signals obtained from a labeled peptide and its unmodified counterpart varies, causing difficulties in data analysis [105]. This challenge has been side stepped by introducing mass labels via heavy isotope-containing derivatives of essential amino acids, a method termed *stable isotope labeling by amino acids in cell culture* (SILAC) [233]. Typically, derivatives of lysine or both lysine and arginine are incorporated, followed by digestion with endopeptidase LysC or trypsin, respectively. By this means, a defined mass shift between labeled and unlabeled peptides is achieved (Figure 1.2.5). Commonly, up to three biological samples,

unlabeled and two different SILAC states, are measured simultaneously a single MS experiment. Although SILAC-based multiplexing with a higher number of different labels has been reported, the accuracy of quantifications in such experiments remains controversial because the isotope patterns of individual SILAC states are not clearly separated. Since the introduction of SILAC into culture, the concept has been extended to *in vivo* labeling of a wide range of model organisms, including bacteria [75, 107], yeast [60], nematodes [88, 167], fly [275] and mouse [163]. Notably, the SILAC based comparison of haploid and diploid yeast is the first published example of a quantitative, comprehensive proteomics dataset obtained in a eukaryotic organism [59].

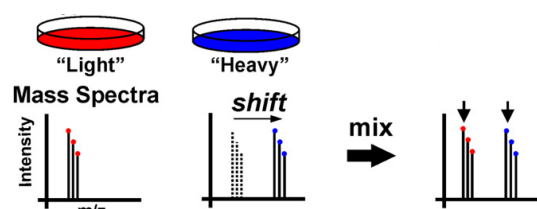


Figure 1.2.5: SILAC Quantification. Cells are grown in media containing heavy isotope derivatives of essential amino acids such as lysine and arginine. After proteolytic digestion, a defined mass shift can be observed in the acquired mass spectra. Mixing samples from unlabeled "light" and labeled "heavy" cells allows a direct comparison of peptide abundance in the same MS experiment. (Modified from [257]).

Peptide and protein quantification by metabolic labeling, in particular SILAC, is considered to be most accurate because biological samples can already be pooled on the protein level [12]. A limitation of this quantification strategy is the fact that not all biological samples can be subjected to metabolic labeling, e.g. human tissues and specific cell lines. However, a method termed *super-SILAC*, in which several cell lines are pooled to serve as an internal spike-in standard, makes the SILAC strategy more broadly amenable [95].

Chemical labels are introduced either before or after proteolytic digestion. An early example of the former approach is the isotope-coded affinity tag (ICAT) which covalently modifies cysteine residues and further contains a biotin group allowing for affinity enrichment [109]. Quantification, however, is limited to cysteine-containing peptides. Other isotope-coded peptide labels are introduced after digestion at the peptide level. These include the dimethyl strategy in which N-terminal α amino groups and ϵ amino groups of lysine residues are derivatized with light or isotope labeled formaldehyde in a Schiff-base reaction [21, 131]. Similar to SILAC, peptides from up to three protein samples can discriminated by their mass shift in survey scans. Isobaric tags such as the isobaric tag for relative and absolute quantification (iTRAQ) [243, 258] and the tandem mass tag (TMT) [282] in contrast achieve quantification by a different principle. These compounds, which are introduced via an amine specific reactive group, possess an identical total mass but yield

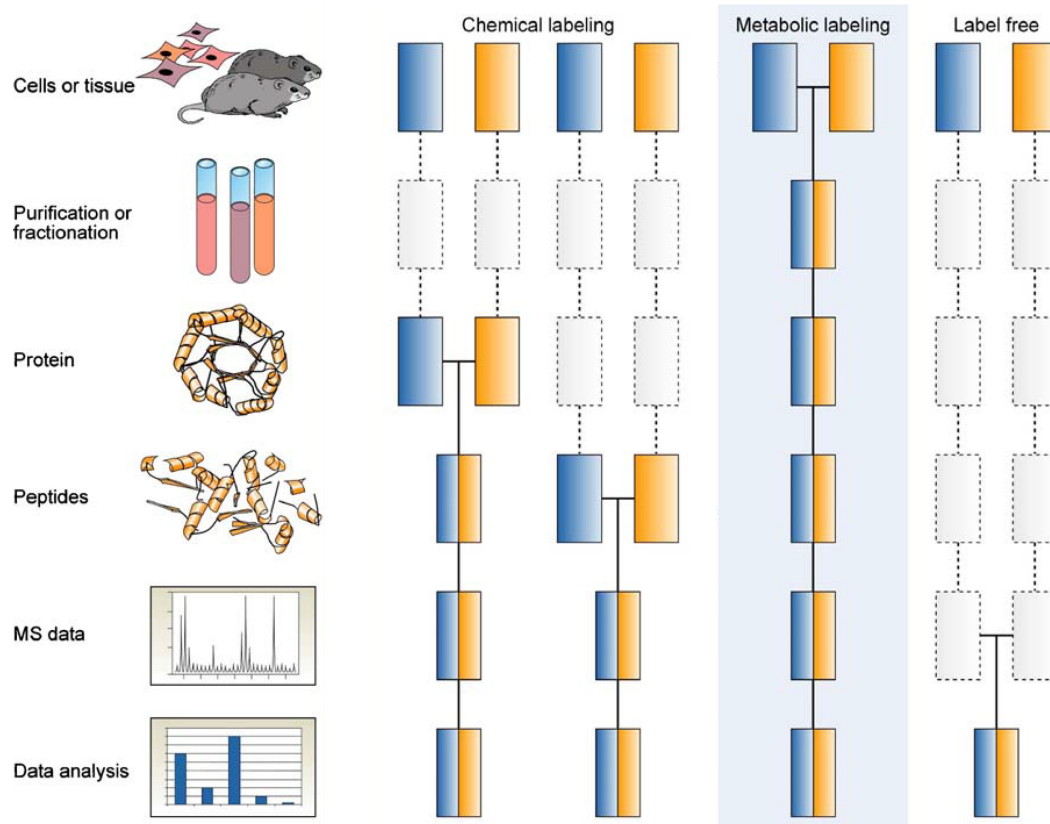


Figure 1.2.6: Strategies in Quantitative Proteomics. Quantification can either be achieved computationally between different experiments, so-called label free strategies, or by coding the peptides derived from different biological samples with heavy isotopes. Samples with metabolically introduced labels can already be pooled at a very early stage during sample preparation. Chemical labeling, in contrast, is performed later in the process, most commonly after proteolytic digestion. (Adapted from [12].)

different reporter ion masses upon fragmentation. These reporter ions can be observed in the low mass region of MS/MS spectra and the intensity ratios derived from the different states are subsequently used for peptide quantification. Although isobaric tagging has very high multiplexing capability and allows the simultaneous analysis of up to eight samples, the contamination of isolated precursor ions with co-eluting peptides may result in inaccurate quantification. An additional issue is the occurrence of undesired side reactions, posing difficulties in data analysis [12].

Label-free Quantification

Label-free quantification is a collective term for methods which allow absolute or relative protein quantification without introducing stable isotopes into peptides. It is considered the least accurate of all strategies but makes samples amenable to quantitative MS-based proteomics that cannot be subjected to labeling [12]. Label-free quantification is achieved by either comparing intensities or the numbers of identified MS/MS spectra or peptides. Virtually all label-free quantification strategies are based on one or a combination of these two principles.

The basis of the spectral counting approach is the observation that the number of spectra identifying a particular protein correlates well with the relative abundance of proteins in MS-based proteomics experiments [169, 181]. However, the accuracy of this method is controversial. When so-called *dynamic exclusion* is employed to avoid re-sequencing of peptides, spectral counting underestimates the concentration of highly abundant proteins. More importantly, a relatively high number of identified MS/MS spectra is required to detect small differences in protein abundance [228]. Peptide counting is a similar concept, however, the number of identified peptides rather than that of identified spectra is used as a proxy for abundance [12, 18, 100]. The peptide counting method was subsequently modified to account for differences between proteins to yield observable peptides. For example, the Protein Abundance Index (PAI) employs *in silico* digestion of proteins to determine how many tryptic peptides are expected to fall into the observable mass range of the employed mass spectrometer and corrects the number of identified peptides accordingly [251]. A further refinement, termed Exponentially Modified PAI (emPAI), makes use of the linear relationship between number of observed peptides and the logarithm of protein concentration for fitting [133]. Last, the Absolute Protein Expression Profiling (APEX) method is a machine learning-based method that corrects for probabilities to observe peptides from proteins. It has been reported to estimate absolute protein abundance in *E. coli* and yeast at an accuracy within one order of magnitude [186].

Intensity-based quantification methods are commonly used for relative quantification between different LC/MS experiments. Basic strategies such as the extracted ion current (XIC) compare integrated intensities over the elution windows of peptides across a set of samples [22]. Lately, an improved label-free quantification algorithm has been implemented into the MaxQuant software environment. Especially in highly complex samples, the quantification accuracy was improved via time-dependent retention time alignments. Ratios between normalized peak intensities are subsequently calculated for peptides shared between individual LC/MS experiments [187].

Finally, Intensity-based Absolute Quantification (iBAQ) represents a hybrid approach between peptide counting and intensity based quantification. Summed peak intensities of all identified peptides of a given protein are corrected for the number of observable peptides similar to the PAI method. After calibration with a defined protein standard, iBAQ yielded more accurate copy number estimates than merely spectral counting or intensity-based methods [263].

1.2.5 Computational Proteomics and Bioinformatics

The mass spectra acquired in high-resolution MS-based shotgun proteomics studies can often add up to data volumes in the range of hundreds of gigabytes. This requires efficient algorithms for the different steps of data processing, including feature extraction, peptide identification and quantification, protein assembly as well as downstream bioinformatic data analysis to interpret the results from a biological perspective.

Virtually all bottom-up proteomics experiments make use of protein sequence information which is either known or predicted from DNA sequencing data of the organism analyzed. *In silico* generated peptide lists are compared with the observed peptide ion masses in MS and MS/MS spectra in order to assign sequence identifications. Different approaches have been used to achieve this goal but usually integrate both data on peptide precursor masses and the fragmentation patterns observed in the corresponding MS/MS scans. The SEQUEST algorithm uses a list of the most intense m/z values of a given MS/MS spectrum. This peak list is correlated with theoretical fragmentation spectra of peptides whose masses lie within a certain threshold around that of the fragmented precursor ion [45, 311]. Mascot, another commonly used commercial software, reports probability-based identification scores, but no details on the equations by which they are calculated have been published to date [242]. The Andromeda search engine, which is integrated into the MaxQuant software environment, also uses probability-based matching. Briefly, the most intense ion peaks are extracted within windows of 100 Th, matched with expected y- and b-type ion series and the chances of random matches are calculated by means of a binomial distribution function [52].

A great advantage of an MS setup with high resolution and high mass accuracy over one with low resolution is that precursor peptide ions can be determined at very high accuracy. Several algorithms of the MaxQuant software use this information to improve protein and peptide identification as well as quantification. For example, the mass accuracy can further be refined by downstream computational processing steps such as averaging the measured mass over a number of survey scans and correcting for drifts in the Orbitrap analyzer in a time dependent manner [50, 51]. As accurate

precursor mass determination improves identification confidence with increasing peptide sequence length, MS/MS scores reported by the search engine can subsequently be adjusted accordingly and yield the final posterior error probability [50].

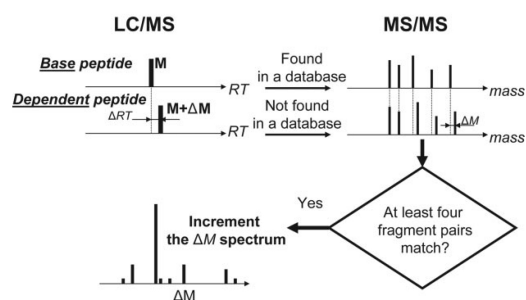


Figure 1.2.7: The ModifiComb algorithm. Successfully identified *base peptides* are used to identify *dependent peptides* in which part of the observed MS/MS signals display a defined mass shift. This approach allows to identify both established and novel posttranslational protein modification in an unbiased fashion. (Adapted from [262].)

After data processing and MS/MS database searches, a probability score is obtained for each fragmentation scan which serves as a measure how well the observed data fit that of an expected peptide from the database. A score cutoff is subsequently applied to guarantee that the assignment of peptide sequences to MS signals is backed by evidence of sufficient quality. A common method to set this threshold is the target decoy strategy. Fragmentation spectra searches are performed with a database containing both the regular and the reversed protein sequences of the organism analyzed. Peptide identifications are accepted up to a score threshold at which a particular proportion, often 1%, of the reversed sequences are re-

tained in the results list. Given that a specific proportion of false positive reverse sequences has been accepted, the same false discovery rate can be expected among the identified peptides [73]. The same basic principle can be applied during the reassembly step from identified peptide sequences back to proteins.

A growing field in MS-based proteomics is the identification and quantification of posttranslational protein modifications. To identify such modifications, different strategies can be employed. Typically, a particular type modification, such as phosphorylation or acetylation, is assumed a priori, for example because it has been specifically enriched for by biochemical procedure. During MS/MS database searches, specific mass shifts are subsequently considered for residues, on which the modification of interest may be localized [52, 242]. This biased approach, however, has the caveat that search engines may interpret fragmentation spectra incorrectly. For example, acetylation of the ϵ -amino group of lysine residues is a commonly occurring posttranslational modification *in vivo*, but can also be introduced at the termini of peptides during sample preparation *in vitro* [40]. A search engine with biased residue specificity would therefore

assign such *in vitro* modifications to proximal lysine residues and thereby yield false identifications. A completely different strategy to identify modified peptides is realized in the ModifiComb algorithm (Figure 1.2.7) [262]. Unidentified MS/MS spectra are searched for fragment patterns which closely resemble those of already identified spectra, but in which a series of peaks display a specific mass shift. For these so-called *dependent peptides* both the mass of the modification and the residue on which it is located are determined. A great strength of the ModifiComb approach is the fact that unknown or unexpected modifications can be identified. However, it is limited with respect to sensitivity because usually no specific biochemical enrichment strategy is performed during sample preparation. Moreover, the presence of an unmodified version of each modified peptide is required for its detection.

Once identification and quantification of peptides and proteins has been carried out, the resulting dataset is subjected to bioinformatic analysis. Specialized software environments, e. g. the Perseus framework [49] or the Bioconductor repository for the statistical programming language R [97], offer a range of statistical tools and algorithms to perform this task. Depending on the design of the performed experiment and the quantification method employed, downstream data analysis may differ substantially. Examples are the search for differentially regulated biological pathways between biological states in expression proteomics datasets or the search for novel protein complex members in protein-protein interaction studies.

1.2.6 Mitochondrial Organellar Proteomics

Mitochondria are essential eukaryotic organelles, harboring enzymes for oxidative respiration and many other biochemical pathways. Human diseases associated with mitochondrial dysfunction include disorders of oxidative ATP production, which can result in skeletal and heart muscle myopathy, organ failure or neurodegenerative diseases [33, 155].

Being enclosed by two membranes, mitochondria are divided into several subcompartments; the mitochondrial outer membrane (MOM), the mitochondrial inner membrane (MIM), the intermembrane space (IMS) and the matrix. The two mitochondrial membranes differ substantially in protein and lipid content and are further not homogeneous in nature but are structured into domains with distinct functions. Originating from bacterial endosymbionts, the organelle possesses its own genome. However, the human mitochondrial DNA (mtDNA) encodes for only thirteen proteins, which are transcribed and translated inside the organelle. All of the remaining mitochondrial proteins are encoded in the nucleus and are imported after translation in the cytosol

[303]. Their abundance range spans six orders of magnitude [157], and it is further estimated that approximately 15% of all mitochondrial proteins possess a dual cellular localization [87, 164]. Therefore, establishing an inventory of all mitochondrial proteins, the mitochondrial organellar proteome, poses a great challenge.

Currently, it is estimated that mammalian mitochondria harbor approximately 1500 proteins, corresponding to 7% of the open reading frames (ORFs) encoded in the genome [33]. Mitochondrial protein databases such as MitoP2 [74], MitoCarta [238] and MitoMiner [271] result from the integration of different data sources. First of all, *in silico* prediction algorithms are employed to identify mitochondrial localization signals. However, algorithms like TargetP, pTARGET, MitoPred or PSORT often have high false positive rates (reviewed in [93]). Moreover, not all mitochondrial proteins are recognized via canonical cleavable presequences but either contain internal sequences or are subject to special modes of insertion, most prominently proteins residing in the MOM. Secondly, protein localization data have been inferred from high throughput microscopy studies with tagged yeast ORF libraries or native antibodies [164, 292, 293]. Thirdly, and most importantly, organellar proteomics has facilitated the discovery of numerous novel mitochondrial proteins and helped validating *in silico* predictions.

Early proteomics studies were mainly non-quantitative and applied low-resolution MS to identify proteins in biochemically purified organelles. 2D gels of mammalian mitochondria suggested the presence of approximately 1200 protein spots, but only a small proportion of these was identified [185, 248]. A later, purely MS-based report with a quadrupole TOF instrument identified 399 proteins in mouse mitochondria of which 163 were not previously annotated to reside in the organelle [209].

With the increasing sensitivity of MS-based proteomics, it soon became apparent that qualitative approaches alone were insufficient to establish subcellular proteomes with high confidence. This is because biochemically isolated organelles are inherently contaminated with substantial amounts of proteins from other cellular compartments. Mitochondrial preparations from mouse heart were estimated to contain up to 14% impurities with respect to the total protein mass, even after extensive purification via density gradient centrifugation [84]. To address this problem, different strategies have been developed. For example, when subjected to a mild protease treatment, a significant proportion of contaminants from the cytosol or endoplasmic reticulum was removed. A disadvantage of this method is that several signal and tail-anchored proteins of the MOM with cytosolic domains were degraded and thus were not identified [83].

The application of quantitative strategies strongly helps to exclude contaminants from organellar proteome datasets. An example with a rather simple experimental design is the study by Kislinger and colleagues, in which lysates of multiple mouse organs were

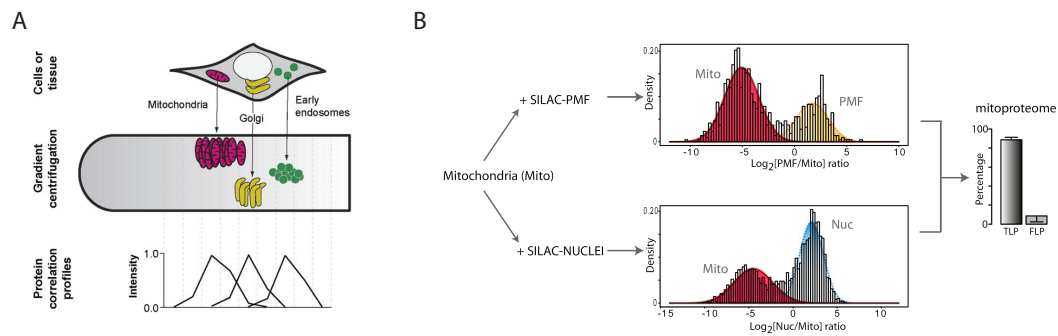


Figure 1.2.8: Different strategies to discriminate between genuine mitochondrial proteins and contaminants from other organelles. (A) Protein correlation profiling (PCP). Whole cell lysates or purified organelles are separated by density gradient centrifugation and fractions are analyzed by quantitative proteomics. Proteins residing in a particular organelle possess distinct abundance profiles. (B) Identification of mitochondrial proteins by Bayesian inference. Mitochondrial preparations are mixed with postmitochondrial (PMF) or nuclear (Nuc) fractions from SILAC labeled cells. The resulting abundance ratios represent an overlay of two distributions, based on which true (TLP) and false localization probabilities (FLP) can be determined for each protein. (Modified from [87] and [85], respectively.)

subjected to fractionated centrifugation to obtain four subcellular fractions: cytosol, microsomes, mitochondria and nuclei. The analysis yielded a dataset comprising of 4768 proteins which were subsequently assigned to one of eight compartments by machine learning algorithms [157]. However, the use of low resolution MS and spectral counting-based label-free quantification limit the quality of the presented data.

A more sophisticated method, termed protein correlation profiling (PCP), is based on cellular fractionation by density gradient centrifugation and was first employed to identify novel centrosomal proteins [8]. Foster and co-workers used this method, combined with high-resolution MS, to establish an organellar map of mouse liver cells. By matching abundance profiles across the density gradient with known organellar markers, a total of 1404 proteins were assigned to 10 subcellular compartments (Figure 1.2.8B) [86]. PCP has since been applied to determine contaminations in isolated mitochondrial fractions [84]. While these earlier studies used label free quantification, further improvements were obtained by implementing SILAC [62].

Conceptually related to PCP is Localization of Organelle Proteins by Isotope Tagging (LOPIT), in which cells are also separated by density gradient centrifugation, but quantification is achieved by chemical labeling. This method was first applied to *Arabidopsis* cells using self-generating iodixanol gradients and pairwise quantitative comparison between fractions via ICAT labeling [71]. Later, the protocol was improved by intro-

ducing fourplex iTRAQ labeling [259] and has since been extended to other species including *Drosophila* [278].

A different strategy to determine the mitochondrial proteome makes use of the distribution of proteins between different fractions of the biochemical fractionation procedure. Forner *et al.* achieved this by mixing mitochondrial preparations with either post-mitochondrial or nuclear fractions and determining the abundance ratios of individual proteins via SILAC quantitation. A probabilistic Bayesian model was subsequently applied to discriminate between contaminants and genuine mitochondrial proteins, and a false discovery estimate was calculated based on GO-annotation. The analysis yielded a mouse tissue mitochondrial proteome containing 689 high confidence entries [85] (Figure 1.2.8B). An independently presented report pursued a similar approach. Enrichment levels between crude and purified mitochondria were determined by label free quantification and subsequently used to identify contaminants [238].

While the above mentioned studies have expanded our knowledge of mitochondrial protein composition, few proteomics studies as yet have investigated suborganellar protein localization. For example, Zahedi and colleagues attempted to establish the mitochondrial sub-proteome of the MOM. To that end, they isolated "highly purified MOM vesicles" and performed analyses by 2D-gel electrophoresis and LC-MS. In total, 112 proteins were identified, among them a significant proportion of established MIM markers, which were interpreted as "pre-proteins" targeted towards their cellular destination [312]. Given that the study was non-quantitative and did not include controls, it is likely that a large part of the dataset represents contaminants. A crude subfractionation protocol of mitochondria for MS analysis was further presented in which intermembrane space, matrix and membrane associated proteins were separated by hyperosmotic swelling [84].

2 Results

2.1 Accurate Quantification of More Than 4000 Mouse Tissue Proteins Reveals Minimal Proteome Changes during Aging.

2.1.1 Aim and Summary

Age is the most important risk factor for numerous human diseases, most prominently neurodegenerative and metabolic disorders. Senescence leads to functional decline and morphological changes in mammalian tissues. However, the mechanism underlying the aging process at the molecular level is poorly understood. Several studies have addressed changes in mRNA or protein levels by microarrays [140, 171, 183, 221] or 2D gel electrophoresis [196], respectively, during aging in mice. The overlap between individual studies, however, was generally low and did not point at a specific mechanism. High resolution MS-based proteomics workflows using SILAC quantification have been employed in cell culture for many years. In contrast, quantification in lysates of mammalian tissue samples could until recently only be achieved by less accurate methods, for example by label-free or chemical labeling strategies, or by metabolic ^{15}N labeling with severe shortcomings in analysis depth. The development of the SILAC mouse [163] for the first time allowed highly accurate SILAC quantification in tissue samples of this important mammalian model organism. We employed this technology to compare the proteomes of five months old young adult animals with those of 26 months old animals, an age at which less than half of the original population remains alive. A focus of the study was on post-mitotic tissues, namely brain and heart muscle, in which the impact of senescence was expected to be strongest due to very low rates of cell replacement.

To our surprise, the observed proteome differences in tissues of young and aged animals were very low. Furthermore, the biological variability within age groups often surpassed the extent of changes inflicted by aging. In summary, the proteome in aging mice is efficiently maintained, at least for the more abundant half of the expressed cellular proteins.

2.1.2 Contribution

This project was designed conjointly between my supervisor, Matthias Mann, and myself. Under his mentoring, I obtained the biological samples, optimized sample preparation techniques and MS analysis methods. Furthermore, I performed both data acquisition and analysis. Together, we wrote the manuscript which led to the publication presented below.

2.1.3 Publication

This work has been published in the journal *Molecular and Cellular Proteomics*.

Mol Cell Proteomics. 2011 Feb;10(2)

“Accurate Quantification of More Than 4000 Mouse Tissue Proteins Reveals Minimal Proteome Changes during Aging.”

Dirk M. Walther and Matthias Mann

Accurate Quantification of More Than 4000 Mouse Tissue Proteins Reveals Minimal Proteome Changes During Aging*[§]

Dirk M. Walther[‡] and Matthias Mann^{‡§}

The biological process of aging is believed to be the result of an accumulation of cellular damage to biomolecules. Although there are numerous studies addressing mutation frequencies, morphological or transcriptional changes in aging mammalian tissues, few have measured global changes at the protein level. Here, we present an in depth proteomic analysis of three brain regions as well as heart and kidney in mice aged 5 or 26 months, using stable isotope labeling of whole animals (SILAC mouse) and high resolution mass spectrometry. In the frontal cortex and hippocampal regions of the brain, more than 4200 proteins were quantitatively compared between age groups. Proteome differences between individual mice were observable within and between age groups. However, mean protein abundance changes of more than twofold between young and old mice were detected in less than 1% of all proteins and very few of these were statistically significant. Similar outcomes were obtained when comparing cerebellum, heart, and kidney between age groups. Thus, unexpectedly, our results indicate that aging-related effects on the tissue proteome composition at the bulk level are only minor and that protein homeostasis remains functional up to a relatively high age. *Molecular & Cellular Proteomics* 10: 10.1074/mcp.M110.004523, 1–7, 2011.

Aging in higher organisms is a multifactorial process. It is commonly believed that lifespan is restricted because of the accumulation of cellular damage, ultimately interfering with crucial biological functions. In mammals, hallmarks of aging tissues include declining rates of self renewal capability and accumulating damages to DNA, proteins, and lipids (1, 2). Senescence in mice has been associated with transcriptional deregulation and an increased mutational burden. Interestingly, different tissues are not affected to the same extent - for example, mutation rates appear to be lower in brain (3–5). Aging-related changes in gene expression in the mouse brain have already been investigated by microarrays (6–9),

however, it is important to study the impact of senescence directly at the protein level to include the effects of post-transcriptional events such as translational regulation or altered protein degradation.

In recent years, great progress has been made in the field of high resolution mass spectrometry (MS)-based proteomics, now allowing for accurate identification of thousands of proteins (10–13). Since MS is not inherently quantitative, the majority of quantification methods rely on the simultaneous comparison of signal intensities between two or more samples during a single analysis following stable isotope coded labeling of peptides (14–16). For proteomic analysis of tissue samples, chemical labeling strategies such as the isotope-coded affinity tag (ICAT) (17) and the isobaric tag for relative and absolute quantification (iTRAQ) (18) have been widely applied. As an alternative, metabolic protein labeling approaches of mammalian model organisms *in vivo* have been described (19, 20). For example, full incorporation of ¹⁵N into the proteome of rats has been achieved by an isotope-pure diet (21). Arguably the most accurate method of protein quantitation by MS is stable isotope labeling with amino acids in cell culture (SILAC)¹ in which only heavy isotope containing derivatives of specific amino acids are used (22). This concept has recently been extended to mice to allow for quantitative comparison of tissue samples from *in vivo* experiments (23).

To date, few proteomics studies have investigated aging in mammalian tissues. Effects of senescence on the left rat heart ventricle was addressed using two-dimensional gel electrophoresis or iTRAQ labeling and matrix-assisted laser desorption/ionization (MALDI)-based quantitative mass spectrometry in which differential expression of metabolic enzymes, structural and antioxidant proteins were reported (24–26). Very recently, Mao *et al.* published a two-dimensional gel-based time course analysis of aging mouse brain. The authors suggest that aging is associated with a reduction in abundance of proteasomal subunits and an accumulation of non-functional proteins (27). In general, the depth and reliability of quantification of the above proteome studies was low because of technical limitations of the methods used.

[‡]From the Department of Proteomics and Signal Transduction, Max-Planck Institute of Biochemistry, D-82152 Martinsried, Germany
Received August 25, 2010, and in revised form, October 29, 2010
[§] Author's Choice—Final version full access.

Published, MCP Papers in Press, November 11, 2010, DOI 10.1074/mcp.M110.004523

¹ The abbreviations used are: SILAC, stable isotope labeling by amino acids in cell culture; LTQ, linear trap quadrupole; MS/MS, tandem mass spectrometry.

2 Results

Minimal Proteome Changes in Aging Mice

Here, we took advantage of the SILAC mouse technology and high resolution MS to study global effects of aging in mammalian tissues at the protein level. Using this technology, we compared the proteomes of each of four female C57BL/6JN mice aged 5 or 26 months and obtained highly accurate quantification over a broad range of tissues.

EXPERIMENTAL PROCEDURES

Mouse Tissues—Female C57BL/6JN mice aged 5 or 26 months, fed *ad libitum*, were obtained from the Aged Rodent Colonies (National Institute of Aging, Bethesda, MD). Animals were starved overnight and sacrificed by cervical dislocation. Brains were immediately removed and placed in ice cold PBS. The frontal cortex region was isolated by removal of olfactory tracts and cutting 1 mm posterior to the bregma. Subsequently, hippocampus and cerebellum were collected. Remaining corpses were perfused by injection of PBS into the heart before removal of kidneys and heart. All tissues and organs were washed in cold PBS and shock frozen in liquid nitrogen. For SILAC labeled standards, animals were fed for four generations with a diet containing exclusively $^{13}\text{C}_6$ lysine as previously described (23). Corresponding tissues were obtained from two 12-month-old females with 97.9% incorporation rate of heavy lysine. SILAC tissues were pooled from both animals before processing. All tissue samples were stored at -80°C until use.

Lysate Preparation and Protein Digestion—Tissues were blended with an Ultra-Turrax disperser (IKA, Staufen, Germany) in 150 mM Tris/HCl pH 8, 4 mM EDTA, 1 mM phenylmethylsulfonyl fluoride at 4°C . Hearts were ground in the frozen state in a mortar before homogenization. Immediately following homogenization, SDS was added to a final concentration of 4% (w/w) and samples were incubated at 95°C for 3 min. For shearing of DNA, samples were subjected to treatment with a Bioruptor ultra sonication bath (Diagenode, Liège, Belgium) at high energy setting for 10 min. Samples were heated again for 3 min at 95°C and clarified by centrifugation for 10 min at $20,000 \times g$. Protein content was determined using the BCA Protein Assay Kit (Thermo, Rockford, IL) according to the manufacturer's instructions. For frontal cortex and hippocampus, 100 μg protein from each animal were mixed with an identical amount of the corresponding SILAC labeled standard. For cerebellum and kidney, lysates were pooled within the young or old animal groups before mixing with SILAC standard. Reduction of disulfide bridges was achieved by addition of dithiothreitol to a final concentration of 0.1 M followed by incubation at 75°C for 5 min. Further processing for in-solution digestion was performed using the previously described filter-aided sample preparation method (28) with Microcon YM-30 devices (Millipore, Billerica, MA), but with the following minor modifications: Alkylation was carried out with 2-chloroacetamide instead of 2-iodoacetamide and proteins were digested exclusively with endoproteinase LysC (Wako Bioproducts, Richmond, VA) in 2 M urea, 25 mM Tris/HCl, pH 8 overnight at room temperature. Obtained peptides were acidified with trifluoroacetic acid and desalted via C_{18} solid phase extraction cartridges (3M, St. Paul, MN). Peptide mixtures were measured both directly and following fractionation into six fractions via strong anion exchange chromatography according to published procedures (29).

Mass Spectrometry—Liquid chromatography (LC)-MS experiments were essentially performed as described previously (30, 31). Briefly, reversed phase separation of peptides was performed using an Easy nLC nanoflow HPLC system (Proxeon Biosystems, Odense, Denmark now Thermo Fisher Scientific). Peptide mixtures were loaded onto a column with 15 cm length and 75 μm inner diameter, packed in-house with RepoSil-Pur C_{18} -AQ 3 μm resin (Dr. Maisch, Ammerbuch-Entringen, Germany) at 0.7 $\mu\text{m}/\text{min}$. Peptides were then eluted in fraction-

optimized nonlinear gradient from 3% to 60% acetonitrile in 0.5% acetic acid over a duration of 200 min. Eluting peptides were electrosprayed online via a nanospray ion source (Proxeon Biosystems) at a voltage of 2.2 kV into an LTQ Orbitrap XL mass spectrometer (Thermo Fisher Scientific, Bremen, Germany), except for unfractionated frontal cortex samples, which were acquired using an LTQ-FT mass spectrometer (Thermo Fisher Scientific). Survey scans were performed in the Orbitrap analyzer at a resolution of 60,000 at target values of 1,000,000 ions and maximum allowed fill times of 1 s over a mass range between m/z 350–1750. The 10 most intense peaks were subjected to fragmentation via collision induced dissociation in the LTQ. For each scan, 5000 ions were accumulated over a maximum allowed fill time of 250 ms and fragmented by wideband activation. Exclusion of precursor ion masses over a time window of 150 s was used to suppress repeated fragmentation of peaks. In all MS experiments except for the measurements of the hippocampus proteomes, internal lock mass recalibration was disabled and an Active Background Ion Repression Device (ABIRD, ESI Source Solutions, Woburn, MA) was used to increase the signal to noise ratio.

Data Analysis—Raw data consisting of 154 liquid chromatography-coupled tandem mass spectrometry (LC-MS/MS) files are deposited at Tranche and are freely available upon publication. Hash keys are provided in the [Supplemental Materials](#) section. Raw data was analyzed using the MaxQuant software environment, version 1.1.0.25. Retention time dependent mass recalibration was applied and peak lists were searched against a database containing all 56,729 entries from the International Protein Index mouse protein database version 3.68 and 255 frequently observed contaminants as well as reversed sequences of all entries. Searches were performed with the following settings: Precursor and fragment ion peaks were searched with an initial mass tolerance of 7 ppm and 0.5 Th, respectively. Enzyme specificity was set to LysC, additionally allowing cleavage between lysine and proline. Up to two missed cleavages were allowed and only peptides with at least six amino acids in length were considered. Carbamidomethylcysteine was set as a fixed modification whereas oxidation on methionine was set as a variable modification. Up to two missed cleavages were allowed. Precursor masses of already identified peptides were further searched within a 3 min time window in chromatograms derived from corresponding and adjacent peptide fractions ("match between runs" option in MaxQuant). For reliability estimation of peptide identifications, the posterior error probability for each top scoring hit was calculated. This metric is based on the tandem MS (MS/MS) score but additionally takes into account peptide length dependent histograms of forward and reverse hits to assess the probability of a false identification using the Bayes theorem (described in detail in (32)). Using a decoy database strategy (33), peptide identifications were accepted based on their posterior error probability until less than 1% reverse hits were retained in the list. Accepted peptide sequences were subsequently assembled into proteins in ascending order of their posterior error probability up to false discovery rate of 1% at the protein level. For successful protein identifications, at least two peptides and one peptide with a unique peptide sequence were required. If no unique peptide sequence to a single database entry was identified, the resulting protein identification was reported as an indistinguishable "protein group." Protein quantifications were based on the median SILAC ratios of at least two peptides (two valid "ratio counts") in each biological sample. Quantification of SILAC pairs was performed by MaxQuant with standard settings (32). Briefly, centroids of isotope clusters in the intensity- m/z plain were detected over multiple full scans and the median intensity ratios were used for the calculation of SILAC ratios.

For histogram representations, only proteins with at least one quantification per age group were considered. Mean normalized protein ratios between sample and SILAC standard were then calculated

within age groups and histograms were plotted using the R statistical programming language (34). For calculation of correlation coefficients and principal component analyses, datasets were filtered for entries with valid quantifications in all experiments (see above). Principal component analyses were performed using the Gene Expression Similarity Investigation Suite (Genesis) (35) following mean centering of expression data. Two-sided t-tests were carried out after filtering for proteins with at least three out of four quantifications under the assumption of unequal variance between age groups. Significance thresholds were then calculated via a permutation-based false discovery rate estimation of 1% (36). For comparison of microarray and proteome studies, median intensities for probes corresponding to Uniprot annotations of identified protein groups were calculated before statistical analyses analogous to the proteome data.

RESULTS

A Proteomic Screen to Detect Proteomic Changes With Aging in Mice—To quantify age-related proteome changes in mouse tissue, we used the SILAC technology *in vivo* and coupled it to high-resolution LC-MS/MS (Fig. 1). We labeled mice with a diet containing exclusively $^{13}\text{C}_6$ lysine over several generations and obtained virtually complete incorporation. To exclude potential effects because of the SILAC diet, we performed all experiments in a “spike-in” format, using the tissue from the SILAC mice as a common internal standard for all experiments. This design also allows comparison between multiple animals within and between each age group. For each experiment, equal amounts of protein sample from biological replicates and the corresponding SILAC standard were mixed, digested in solution with endoproteinase LysC using the filter-aided sample preparation method and peptides were fractionated via strong anion exchange chromatography (28, 29). These peptide fractions as well as unfractionated peptide preparations from each experiment were then analyzed by LC-MS/MS on a hybrid high resolution linear ion trap Orbitrap instrument (Fig. 1). Hippocampal and frontal cortex regions from the brains of four young and four old animals were processed individually, resulting in eight individual quantitative proteomes. We extended the study to cerebellum, kidney, and heart muscle but in contrast to the previous experiments, lysates within age groups were pooled for each of these three tissues.

The combined dataset over all five tissues comprises 154 LC-MS/MS experiments with 4 h gradients, during which more than 4.5 million MS/MS scans were acquired. The observed average absolute mass deviation for the corresponding precursor ions was 450 ppb. Following analysis with the MaxQuant software environment (32), more than 60% of the MS/MS scans were unambiguously identified. This led to 44,737 identified nonredundant peptide sequences and 5619 proteins (or protein groups) at a protein false discovery rate of less than 1%.

The Aging Tissue Proteomes of Frontal Cortex and Hippocampus—In frontal cortex and hippocampus, expression data for more than 4200 proteins of each four young and old mice were acquired individually. Of this subset of proteins, approximately two thirds were expressed and detected in at

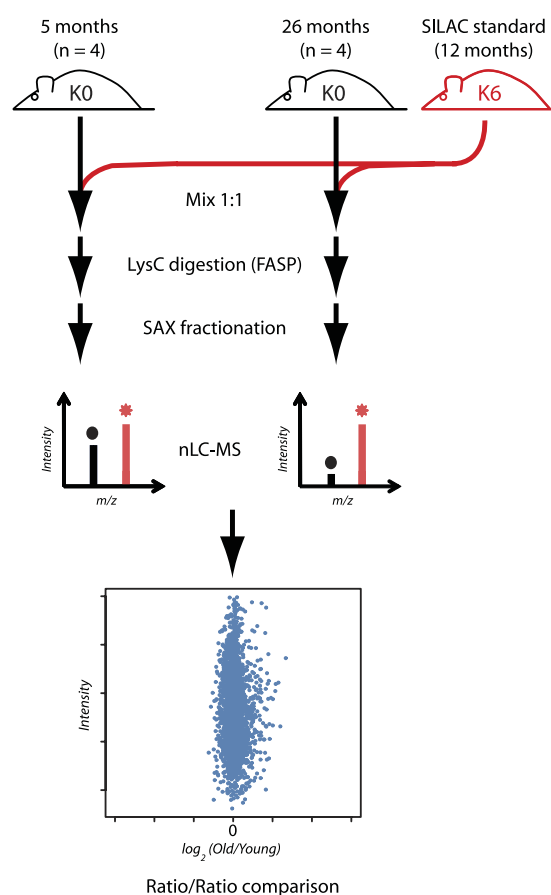


FIG. 1. Schematic of the workflow. Tissue lysates from each of four mice aged 5 or 26 months were analyzed in separate experiments and mixed each time with an identical standard derived from SILAC mice aged 12 months. Proteins were digested using the filter-aided sample preparation method (FASP) and fractionated before analysis by high resolution mass spectrometry. Proteins were quantified by dividing the individual SILAC peptide ratios of the proteomes to be compared (“ratio of ratios”).

least three out of four biological replicate experiments per age group (77 or 61% in frontal cortex or hippocampus, respectively, [Supplemental Tables 1 and 2](#)).

For protein quantification, our study employed an internal standard, which was added to all biological samples of a given tissue, to serve as a fixed reference point for all observed peptide ratios. To determine the quantitative reliability of this data set in more detail, we first extracted the typical number of quantification events per protein. In the above data set of a young animal it turned out to be 18 events on average (median of 8). This is because of the high redundancy of peptide based quantifications and compares favorably to two-dimensional gel experiments in which typically only one quantification event per protein is obtained in each individual sample. As a consequence, when comparing proteomes of

2 Results

Minimal Proteome Changes in Aging Mice

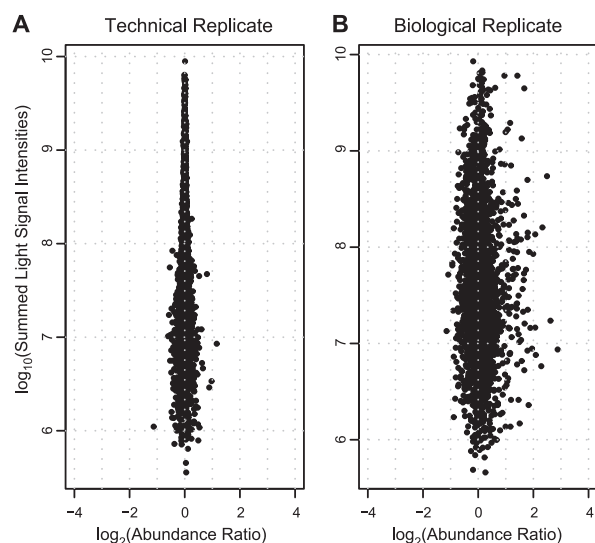


FIG. 2. Intensity-ratio distribution of protein abundances in hippocampus using an internal SILAC standard for quantitation between samples. *A*, Comparison between two technical replicates of a lysate derived from the same animal. *B*, Comparison between an old and a young animal.

two technical replicate experiments virtually all proteins were detected in equal quantities, demonstrating the usefulness of the method. This “ratio-of-ratios” distribution was narrow, with more than 99% of the proteins showing an apparent fold change of less than a factor of two (Fig. 2A). In contrast, a much broader abundance ratio distribution was observed when comparing two different biological samples (Fig. 2B). The figure also shows that the few outlier proteins, on the most part, have a higher abundance in the aged animals. However, most these changes are not statistically significant (see below). Next, we investigated the mean protein expression changes between the two age groups. Unexpectedly, the vast majority of proteins were found in equal quantities in old and young animals (Fig. 3A). An average expression change of more than twofold was detected in less than 1% of all quantified proteins and less than 3% changed by more than one third in both brain tissues (Supplemental Table 3). These data indicate that age-related changes on the protein level in mice are very minor in the two analyzed brain regions.

Statistical Analysis of Senescence-Related Proteome Changes in Frontal Cortex and Hippocampus—We asked whether aging causes specific changes in tissue proteomes. For this purpose we calculated the Pearson correlation coefficients between all pairs of biological samples using the abundance ratios of all quantified proteins. Specific age related proteome changes should be reflected by higher Pearson correlation coefficients between the animals of one age group as compared with the coefficients when comparing old and young animals. However, the correlation between pro-

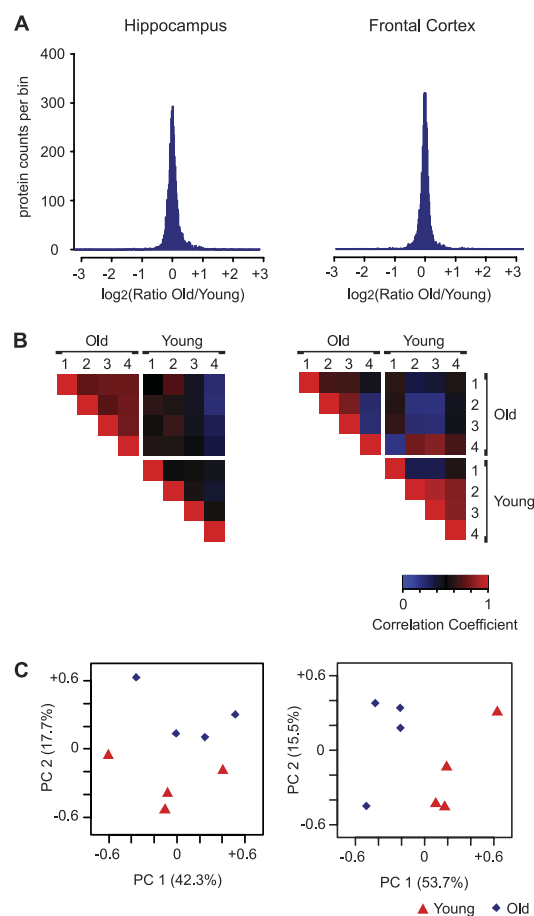


FIG. 3. A, Abundance of the vast majority of proteins is unchanged during aging in mice as indicated by a histogram representation of protein abundance ratios between old and young animals in hippocampus or frontal cortex. **B**, Pearson correlation between the proteomes of mice within the young or old age groups is not generally higher than between old and young individuals. Correlation coefficients in the matrix are color coded as shown. **C**, Principal component analysis of the individual proteomes.

teomes within young or aged animals was not generally higher than that between old and young mice (Fig. 3B). The differences between individual proteomes can be attributed to biological variability between the mice rather than to differences in sample preparation. This was apparent from the high degree of reproducibility obtained when analyzing each of three technical replicates of two selected hippocampal tissue lysates that were prepared and analyzed using the same protocol (Supplemental Fig. 1). To investigate the potential proteome differences between young and old mice by a different method we performed principal component analysis. The distances between the samples of the same age group was not generally smaller than the distances to samples from the other age group, confirming the findings ob-

tained by correlation analysis (Fig. 3C). Finally, statistical analysis of hippocampus and frontal cortex datasets via a two-sided *t* test at a permutation-based false discovery rate of 1% yielded only five significantly regulated proteins each (Supplemental Tables 1 and 2). Collectively, these results indicate that on the protein level of the two tissues, biological variability between individuals is more pronounced than changes induced by the process of aging, even in inbred mice with a matching genetic background.

The Aging Tissue Proteomes of Cerebellum, Heart, and Kidney—To investigate whether the absence of major changes in protein abundance is restricted to specific regions of the mouse brain, we additionally measured the proteomes of cerebellum, heart and kidney. In contrast to the previously described experiments, protein lysates within age groups of young or old animals were pooled, resulting in only two individual proteomes for each tissue. Similar to the situation in hippocampus and frontal cortex, the abundance of the vast majority of proteins was unaffected (Fig. 4, Supplemental Tables 3 and 4), therefore generalizing our findings to additional tissues.

Comparison with Other Large-Scale Studies—Age-related changes in transcript abundance in mammalian tissues have previously been investigated by microarrays. Although earlier investigations only reported a very small number of genes whose transcription changed during aging (6, 7), more recent publications did find a larger number of significantly regulated genes in mouse cortex (8, 9). However, in these latter studies, as in the proteome studies, the vast majority of transcripts did not change significantly. Furthermore, the transcripts that did appear to change during aging (8) generally did not exhibit corresponding changes in our quantitative proteomics dataset of frontal cortex (Supplemental Fig. 2). During the preparation of this manuscript a report appeared that addressed proteomic changes in the aging mouse brain by two-dimensional gel electrophoresis (27). The authors suggested significant changes in the abundance of several proteins such as proteasomal subunits, chaperones and mitochondrial proteins. Almost all these proteins were quantified in our data set in both the frontal cortex and the hippocampal datasets (111 out of 114 unique SwissProt identifiers). However, we did not detect any significant age-related changes of any of these proteins and their mean ratio changes were less than 5% (Supplemental Table 5).

As an orthogonal method, we substantiated the SILAC quantifications of selected candidate proteins by performing Western blots (Supplemental Fig. 3). We chose candidate proteins that appeared to change in aging mice in the above study (27), such as the mitochondrial protein VDAC1, the proteasomal subunit Psma5 and chaperones (calreticulin and Hsc71). As expected, the results verify our SILAC based finding that levels of these proteins remain virtually unchanged. We also obtained evidence that the few proteins that we did find to change are actually differentially expressed during aging.

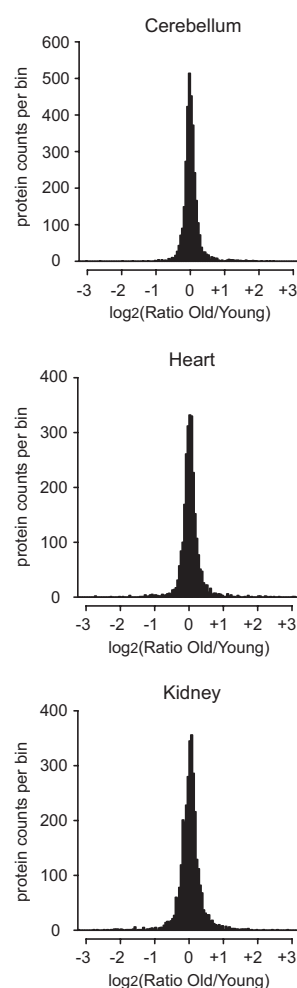


FIG. 4. Histograms of the protein abundance ratios between old and young animals in cerebellum, heart and kidney (representation analogous to Fig. 2A).

Specifically, the Western blot against complement C1q sub-component subunit B shows an about twofold accumulation with age in hippocampus, as expected from the SILAC ratio of 2.25.

DISCUSSION

Using high resolution mass spectrometry combined with the SILAC mouse technology, we performed the most comprehensive study of mammalian tissue aging at the proteome level to date. Reaching a depth of more than 4000 quantified proteins, our study covers the vast majority of tissue protein mass. Strikingly, our results indicate that abundance changes are low at least up to 26 months, an age at which less than half of the initial population survives (37). It should be noted that many low abundant proteins are not covered by our dataset. Nevertheless, if regulatory pathways in control of synthesis or

2 Results

Minimal Proteome Changes in Aging Mice

degradation of specific proteins subsets were affected in aging tissues, global changes at a larger scale would have been observed. Technological limitations are not likely to be the reason for not detecting profound proteome changes. Previous studies from our and other laboratories have demonstrated that SILAC-based quantitative proteomics is a sensitive method to measure effects on protein expression in knockout mice (23) or in the study of global differences in protein abundance between primary cells and cell lines from mice (12, 13, 38). Likewise, knockdowns of single genes can result in easily detectable abundance changes of hundreds of proteins (39). Finally, the recently described super-SILAC strategy, which also uses a complex SILAC-labeled proteome as an internal standard for tissue proteome quantification, readily detected the expected differences between tumor types (40). These studies clearly demonstrate that our experimental approach was well suited for the discovery of global proteomic changes in mice with aging.

We specifically focused on two brain regions, frontal cortex and hippocampus, for which acquisition of the proteomes of individual animals allowed us to perform statistical analysis of protein abundance between age groups. Multiple studies have addressed the effects of aging on the transcriptional level in mouse brain by microarrays (6–9). The overlap of significantly regulated candidate genes between individual studies was often low and the vast majority of mRNAs clearly did not change in abundance with age. Therefore, our observation of the absence of large scale gene expression changes at the proteome level generally reflects previous results at the level of the transcriptome.

In conclusion, this study demonstrates that expression levels of the vast majority of proteins remain virtually unchanged during aging in multiple mouse tissues. This suggests that the proteome is efficiently maintained to a relatively high age. As our data are averages obtained from a large number of cells, they do not exclude strong age-related variability between individual (5) or specific sub-populations of cells, such as tissue stem cells. As proteomic technology advances, it would be interesting to directly investigate these potential cell specific effects of aging.

Acknowledgments—We thank Juli Schlichtiger for help with the dissection of mouse brains, Sara Zanivan for maintenance of the SILAC mice, Juergen Cox, Michael L. Nielsen and Thanapit Viturawong for helpful discussions, Franz-Ulrich Hartl for kindly providing some of the antibodies and Boumediene Soufi for critically reading this manuscript.

* This work was supported by the European Union 7th Framework Program (HEALTH-F4-2008-201648/PROSPECTS) and NIH grant DK60837 (Diabetes Genome Anatomy Project).

☐ This article contains [supplemental Figs 1–3 and Tables 1–5](#).

§ To whom correspondence may be addressed: Department of Proteomics and Signal Transduction, Max-Planck Institute of Biochemistry, D-82152 Martinsried, Germany, Tel.: 49-89-8578-2557; Fax: 49-89-8578-2219; Email: mmann@biochem.mpg.de.

REFERENCES

1. Finkel, T., and Holbrook, N. J. (2000) Oxidants, oxidative stress and the biology of ageing. *Nature* **408**, 239–247
2. Sahin, E., and Depinho, R. A. (2010) Linking functional decline of telomeres, mitochondria and stem cells during ageing. *Nature* **464**, 520–528
3. Dollé, M. E., Giese, H., Hopkins, C. L., Martus, H. J., Hausdorff, J. M., and Vijg, J. (1997) Rapid accumulation of genome rearrangements in liver but not in brain of old mice. *Nat. Genet.* **17**, 431–434
4. Dollé, M. E., Snyder, W. K., Gossen, J. A., Lohman, P. H., and Vijg, J. (2000) Distinct spectra of somatic mutations accumulated with age in mouse heart and small intestine. *Proc. Natl. Acad. Sci. U.S.A.* **97**, 8403–8408
5. Bahar, R., Hartmann, C. H., Rodriguez, K. A., Denny, A. D., Busuttill, R. A., Dollé, M. E., Calder, R. B., Chisholm, G. B., Pollock, B. H., Klein, C. A., and Vijg, J. (2006) Increased cell-to-cell variation in gene expression in ageing mouse heart. *Nature* **441**, 1011–1014
6. Jiang, C. H., Tsien, J. Z., Schultz, P. G., and Hu, Y. (2001) The effects of aging on gene expression in the hypothalamus and cortex of mice. *Proc. Natl. Acad. Sci. U.S.A.* **98**, 1930–1934
7. Lee, C. K., Weindrich, R., and Prolla, T. A. (2000) Gene-expression profile of the ageing brain in mice. *Nat. Genet.* **25**, 294–297
8. Oberdoerffer, P., Michan, S., McVay, M., Mostoslavsky, R., Vann, J., Park, S. K., Hartlerode, A., Stegmüller, J., Hafner, A., Loerch, P., Wright, S. M., Mills, K. D., Bonni, A., Yankner, B. A., Scully, R., Prolla, T. A., Alt, F. W., and Sinclair, D. A. (2008) SIRT1 redistribution on chromatin promotes genomic stability but alters gene expression during aging. *Cell* **135**, 907–918
9. Loerch, P. M., Lu, T., Dakin, K. A., Vann, J. M., Isaacs, A., Geula, C., Wang, J., Pan, Y., Gabuzda, D. H., Li, C., Prolla, T. A., and Yankner, B. A. (2008) Evolution of the aging brain transcriptome and synaptic regulation. *PLoS One* **3**, e3329
10. Aebersold, R., and Mann, M. (2003) Mass spectrometry-based proteomics. *Nature* **422**, 198–207
11. de Godoy, L. M., Olsen, J. V., Cox, J., Nielsen, M. L., Hubner, N. C., Fröhlich, F., Walther, T. C., and Mann, M. (2008) Comprehensive mass-spectrometry-based proteome quantification of haploid versus diploid yeast. *Nature* **455**, 1251–1254
12. Selbach, M., Schwanhäusser, B., Thierfelder, N., Fang, Z., Khanin, R., and Rajewsky, N. (2008) Widespread changes in protein synthesis induced by microRNAs. *Nature* **455**, 58–63
13. Baek, D., Villén, J., Shin, C., Camargo, F. D., Gygi, S. P., and Bartel, D. P. (2008) The impact of microRNAs on protein output. *Nature* **455**, 64–71
14. Bantscheff, M., Schirle, M., Sweetman, G., Rick, J., and Kuster, B. (2007) Quantitative mass spectrometry in proteomics: a critical review. *Anal. Bioanal. Chem.* **389**, 1017–1031
15. Choudhary, C., and Mann, M. (2010) Decoding signalling networks by mass spectrometry-based proteomics. *Nat. Rev. Mol. Cell Biol.* **11**, 427–439
16. Wilm, M. (2009) Quantitative proteomics in biological research. *Proteomics* **9**, 4590–4605
17. Gygi, S. P., Rist, B., Gerber, S. A., Turecek, F., Gelb, M. H., and Aebersold, R. (1999) Quantitative analysis of complex protein mixtures using isotope-coded affinity tags. *Nat. Biotechnol.* **17**, 994–999
18. Ross, P. L., Huang, Y. N., Marchese, J. N., Williamson, B., Parker, K., Hattian, S., Khainovski, N., Pillai, S., Dey, S., Daniels, S., Purkayastha, S., Juhasz, P., Martin, S., Bartlett-Jones, M., He, F., Jacobson, A., and Pappin, D. J. (2004) Multiplexed protein quantitation in *Saccharomyces cerevisiae* using amine-reactive isobaric tagging reagents. *Mol. Cell Proteomics* **3**, 1154–1169
19. Gouw, J. W., Krijgsveld, J., and Heck, A. J. (2010) Quantitative proteomics by metabolic labeling of model organisms. *Mol. Cell Proteomics* **9**, 11–24
20. Bachi, A., and Bonaldi, T. (2008) Quantitative proteomics as a new piece of the systems biology puzzle. *J. Proteomics* **71**, 357–367
21. Wu, C. C., MacCoss, M. J., Howell, K. E., Matthews, D. E., and Yates, J. R., 3rd (2004) Metabolic labeling of mammalian organisms with stable isotopes for quantitative proteomic analysis. *Anal. Chem.* **76**, 4951–4959
22. Ong, S. E., Blagoev, B., Kratchmarova, I., Kristensen, D. B., Steen, H., Pandey, A., and Mann, M. (2002) Stable isotope labeling by amino acids in cell culture, SILAC, as a simple and accurate approach to expression proteomics. *Mol. Cell Proteomics* **1**, 376–386
23. Krüger, M., Moser, M., Ussar, S., Thievensen, I., Luber, C. A., Forner, F., Schmidt, S., Zanivan, S., Fässler, R., and Mann, M. (2008) SILAC mouse for quantitative proteomics uncovers kindlin-3 as an essential factor for

- red blood cell function. *Cell* **134**, 353–364
24. Dai, Q., Escobar, G. P., Hakala, K. W., Lambert, J. M., Weintraub, S. T., and Lindsey, M. L. (2008) The left ventricle proteome differentiates middle-aged and old left ventricles in mice. *J. Proteome Res.* **7**, 756–765
 25. Richardson, M. R., Lai, X., Mason, S. B., Miller, S. J., and Witzmann, F. A. (2008) Differential protein expression during aging in ventricular myocardium of Fischer 344 x Brown Norway hybrid rats. *Exp. Gerontol.* **43**, 909–918
 26. Grant, J. E., Bradshaw, A. D., Schwacke, J. H., Baicu, C. F., Zile, M. R., and Schey, K. L. (2009) Quantification of Protein Expression Changes in the Aging Left Ventricle of *Rattus norvegicus*. *J. Proteome Res.* **8**, 4252–4263
 27. Mao, L., Romer, I., Nebrich, G., Klein, O., Koppelstatter, A., Hin, S. C., Hartl, D., and Zabel, C. (2010) Aging in Mouse Brain Is a Cell/Tissue-Level Phenomenon Exacerbated by Proteasome Loss. *J. Proteome Res.* **9**, 3551–3560
 28. Wiśniewski, J. R., Zougman, A., Nagaraj, N., and Mann, M. (2009) Universal sample preparation method for proteome analysis. *Nat. Methods* **6**, 359–362
 29. Wiśniewski, J. R., Zougman, A., and Mann, M. (2009) Combination of FASP and StageTip-based fractionation allows in-depth analysis of the hippocampal membrane proteome. *J. Proteome Res.* **8**, 5674–5678
 30. Olsen, J. V., Ong, S. E., and Mann, M. (2004) Trypsin cleaves exclusively C-terminal to arginine and lysine residues. *Mol. Cellular Proteomics* **3**, 608–614
 31. Forner, F., Foster, L. J., Campanaro, S., Valle, G., and Mann, M. (2006) Quantitative proteomic comparison of rat mitochondria from muscle, heart, and liver. *Mol. Cell Proteomics* **5**, 608–619
 32. Cox, J., and Mann, M. (2008) MaxQuant enables high peptide identification rates, individualized p.p.b.-range mass accuracies and proteome-wide protein quantification. *Nat. Biotechnol.* **26**, 1367–1372
 33. Elias, J. E., and Gygi, S. P. (2007) Target-decoy search strategy for increased confidence in large-scale protein identifications by mass spectrometry. *Nat. Methods* **4**, 207–214
 34. R Foundation for Statistical Computing (2009) R: A language and environment for statistical computing
 35. Sturn, A., Quackenbush, J., and Trajanoski, Z. (2002) Genesis: cluster analysis of microarray data. *Bioinformatics* **18**, 207–208
 36. Tibshirani, R. (2006) A simple method for assessing sample sizes in microarray experiments. *Bmc Bioinformatics* **7**:106
 37. Turturro, A., Witt, W. W., Lewis, S., Hass, B. S., Lipman, R. D., and Hart, R. W. (1999) Growth curves and survival characteristics of the animals used in the Biomarkers of Aging Program. *J. Gerontol. A Biol. Sci. Med. Sci.* **54**, B492–501
 38. Pan, C., Kumar, C., Bohl, S., Klingmueller, U., and Mann, M. (2009) Comparative proteomic phenotyping of cell lines and primary cells to assess preservation of cell type-specific functions. *Mol. Cell Proteomics* **8**, 443–450
 39. Bonaldi, T., Straub, T., Cox, J., Kumar, C., Becker, P. B., and Mann, M. (2008) Combined use of RNAi and quantitative proteomics to study gene function in *Drosophila*. *Mol. Cell* **31**, 762–772
 40. Geiger, T., Cox, J., Ostasiewicz, P., Wiśniewski, J. R., and Mann, M. (2010) Super-SILAC mix for quantitative proteomics of human tumor tissue. *Nat. Methods* **7**, 383–385

2.2 Extensive Proteome Remodeling during Aging in *C. elegans* Revealed by Quantitative Proteomics

2.2.1 Aim and Summary

The nematode *Caenorhabditis elegans* is a commonly used model organism in aging research. Several molecular signaling pathways have been shown to regulate the rate of aging, most prominently the conserved insulin/insulin-like growth factor 1 (IIS) pathway. Interference with the function of the insulin receptor homologue DAF-2 or the effector kinase AGE-1 result in a strongly increased lifespan and stress resistance. The longevity phenotype further requires two transcription factors, DAF-16/FOXO and HSF-1. The molecular mechanism by which their transcriptional response increases longevity, however, remains ill defined. Some studies suggest that IIS plays an important role in the maintenance of protein homeostasis [280].

We therefore investigated the effects of aging in *C. elegans* by high-resolution mass spectrometry-based proteomics. To achieve accurate quantification, we performed *in vivo* SILAC labeling of worm by feeding them with a diet containing exclusively $^{13}\text{C}_6$ - $^{15}\text{N}_2$ -lysine. Lysates from these animals were spiked into biological samples as an internal standard. By this means, proteomes of synchronized worm populations of wt as well as *daf-2*, *daf-16* and *hsf-1* mutants at multiple time points throughout lifespan were obtained. In parallel, insoluble protein aggregates were biochemically isolated and analyzed.

Similar biochemical processes were affected by aging in the above mentioned strains. However, expression differences of specific subsets of proteins can be observed. In contrast to mouse, the proteome of *C. elegans* is extensively remodeled during aging. Approximately one third of the quantified proteins are subject to more than twofold abundance change between young adult and aged hermaphrodites. Moreover, the observed abundance changes were positively correlated with the rate at which the same proteins accumulate in aggregates. Depletion of highly aggregation prone proteins in return extended lifespan. In the long-lived *daf-2* mutant, both proteome remodeling and protein insolubility were delayed during senescence.

In conclusion, aging induces extensive proteome remodeling in *C. elegans* which results in a gradual upregulation of harmful aggregation-prone proteins and increased protein aggregation. It is conceivable that this deregulation eventually results in a collapse of the proteostasis network and thus limits the organism's lifespan.

2.2.2 Contribution

This project was initiated by the department of Franz-Ulrich Hartl. Together with Min Zheng, who performed the cultivation of synchronized worm populations, I established a protocol for SILAC labeling of *C. elegans*. I further developed SILAC-based pulse labeling and aggregate isolation procedures for which I also obtained the biological sample material. Moreover, I prepared all samples for MS analysis and carried out the data acquisition. Data analysis was performed in collaboration with Stefan Pinkert. During the biological and biochemical follow-up, I contributed some data, although the majority of these experiments were done by Prasad Kasturi. Ulrich Hartl and I wrote most sections of the manuscript.

2.2.3 Manuscript

The manuscript attached is currently in preparation.

Extensive Proteome Remodeling and Aggregation during Aging in *C. elegans* Revealed by Quantitative Proteomics

Dirk M. Walther^{1*}, Prasad Kasturi^{2*}, Stefan Pinkert², Prajwal Ciryam^{3,4}, Min Zheng², Michele Vendruscolo³, Richard I. Morimoto⁴, Christopher M. Dobson³, Matthias Mann¹,
and F.-Ulrich Hartl²

¹ Department of Proteomics and Signal Transduction, and

² Department of Cellular Biochemistry,

Max Planck Institute of Biochemistry, Am Klopferspitz 18, 82152 Martinsried, Germany

³ Department of Chemistry, University of Cambridge, Cambridge CB2 1EW, United Kingdom

⁴ Department of Molecular Biosciences, Northwestern University, Evanston, IL, 60208

*Equal contribution

Summary

A gradual loss of protein homeostasis (proteostasis) is thought to contribute to the process of aging. However, how these effects are reflected at the level of the proteome is poorly understood. Here, we employed SILAC labeling and quantitative proteomics to profile more than 6,000 proteins during the lifespan of *C. elegans*. Furthermore, we biochemically isolated aggregated protein species and analyzed the corresponding sub-proteomes. Among the proteins responsible for proteostasis maintenance, most prominently a decrease in the abundance of ribosomal and an increase in proteasomal subunits were observed and went alongside with changes in activity of protein synthesis and degradation, respectively. We found that the proteome underwent extensive remodeling during aging. Increasing protein abundance was positively correlated with the rate at which the same proteins accumulated in aggregates. Moreover, proteome remodeling was delayed in the long-lived *daf-2* mutant and proteins with a strong tendency to aggregate in wild type aggregated at slower rates in *daf-2*. Conversely, depletion of highly aggregation-prone proteins extended lifespan in wild type animals. We propose that age-dependent deterioration of proteome balance, driving aggregation, eventually causes proteostasis collapse, and thereby limits the lifespan of *C. elegans*.

Introduction

Protein homeostasis (or proteostasis), the state at which the proteome is in functional balance, must be tightly controlled in all cells (Balch et al, 2008). More than 10,000 different proteins are typically expressed simultaneously in the cells of higher eukaryotes (Nagaraj et al., 2011). Maintaining proper proteome balance requires a complex network of factors, including the machinery of protein biogenesis, molecular chaperones and proteolytic systems, for the regulation of the synthesis and folding of proteins, and the clearance of misfolded polypeptides (Balch et al., 2008; Hartl et al., 2011; Taylor and Dillin, 2011). An important role of this proteostasis network is the prevention of potentially toxic protein aggregation, particularly under conditions of cellular stress. However, as organisms age, the function of several components of protein quality control may become compromised (Douglas and Dillin, 2010), resulting in impaired responses to unfolded protein stress (Ben-Zvi et al., 2009; Morimoto, 2008), as well as in reduced tolerance of reactive oxygen species (Finkel and Holbrook, 2000). For example, a reduction in the expression of small heat shock proteins (HSPs), which are critical in aggregation prevention, has been observed in aging nematodes (Lund et al., 2002), and an age-dependent decline in protein degradation capacity was reported in rat liver and flies (Cuervo and Dice, 2000; Tonoki et al., 2009). Indeed, aging is considered the principal risk factor for the onset of a number of neurodegenerative disorders associated with aggregate deposition, such as Alzheimer's, Huntington's or Parkinson's disease (Cohen and Dillin, 2008; Douglas and Dillin, 2010; Kikis et al., 2010). The occurrence of protein aggregation may further impair proteostasis and thus accelerate the aging process by interfering with protein folding and clearance (Gidalevitz et al., 2006; Bence et al., 2001), and with numerous other processes,

resulting in cellular dysfunction and ultimately cell death (Balch et al., 2008; Gidalevitz et al., 2006; Olzscha et al., 2011; Vendruscolo, 2012). Understanding these relationships requires systematic analyses of the changes that occur in proteome composition and balance during aging.

The nematode *C. elegans* is one of the most extensively studied model organisms in aging research, owing to its relatively short lifespan and the availability of genetic tools to identify pathways that regulate longevity. A particularly well studied example is the insulin/insulin-like growth factor 1 signaling (IIS) pathway in which binding of ligands to the DAF-2 receptor activates a signaling cascade that down-regulates the activity of the transcription factor DAF-16/FOXO (Lin et al., 1997; Ogg et al., 1997). Inhibition of the IIS pathway, for example in strains carrying mutations in the genes encoding DAF-2 or the downstream PI(3) kinase AGE-1, activate DAF-16/FOXO and lead to dramatic lifespan extension along with increased stress resistance (Kenyon et al., 1993; Larsen et al., 1995; Lithgow et al., 1995). Several lines of evidence suggest that the lifespan-prolonging effect of IIS reduction involves an improvement of cellular proteostasis capacity through up-regulation of the machineries of protein folding and aggregation prevention. Importantly, in addition to DAF-16 activation, the longevity phenotype in *daf-2* mutants requires the function of HSF-1 (Hsu et al., 2003; Morley and Morimoto, 2004), the highly conserved transcription factor responsible for the expression of multiple heat-shock proteins and chaperones (Chiang et al., 2012; Halaschek-Wiener, 2005; McElwee et al., 2003; Murphy et al., 2003). Mutants for *daf-2* or *age-1* display a delayed onset of aggregate formation when expressing amyloid-forming peptides, such as polyglutamine proteins or the Alzheimer's β -(A β) peptide (Cohen et al., 2006; Cohen et al.,

2010; Morley et al., 2002). Similarly, overexpression of DAF-16 or HSF-1 rescued the phenotypes caused by a variety of temperature sensitive mutant proteins (Ben-Zvi et al., 2009) and maintained the solubility of several endogenous aggregation-prone proteins in aging *daf-2* mutant worms (David et al., 2010). Intriguingly, these pathways of proteostasis maintenance appear to be conserved in evolution. For example, A β peptides exhibited lower toxicity in mouse brain when IGF-1 signaling was impaired (Cohen et al., 2009).

Aging and the effect of the IIS pathway have been studied extensively in *C. elegans* by transcriptome analysis (Budovskaya et al., 2008; Golden et al., 2008; Golden and Melov, 2004; Lund et al., 2002). However, changes in transcript levels alone provide only limited information on effects at the proteome level, including protein aggregation, posttranslational modifications and turnover, in particular under conditions affecting the integrity of the proteostasis network. In recent years, significant progress has been made in the field of mass spectrometry-based proteomics, now allowing for the identification and quantitation of thousands of proteins in complex mixtures (Cox and Mann, 2011). Arguably, the most accurate quantification strategy is the use of stable isotope labeling with amino acids in cell culture (SILAC) (Ong et al., 2002), an approach that has been extended to multicellular model organisms such as mouse (Kruger et al., 2008), fly (Sury et al., 2010) and worm (Fredens et al., 2011; Larance et al., 2011).

Here, we used SILAC labeling and quantitative proteomics to profile the abundance levels of more than 6,000 proteins at various time points throughout the lifespan of *C. elegans*. We extended our study to short-lived and long-lived strains carrying mutations related to the IIS pathway and also quantified age-related protein aggregation. Our data show that during aging, the proteome of the animal undergoes extensive remodeling, reaching a state of proteome

imbalance that affects key components of the proteostasis network and drives protein aggregation. These changes are accelerated in short-lived mutant worms and are delayed in long-lived animals. Interestingly, a loss in X-chromosomal dosage compensation contributes to proteome imbalance in short-lived animals.

Results

Extensive Proteome Remodeling during Aging

To study proteomic changes in aging nematodes in depth and with high accuracy, we established a quantitative proteomics approach based on stable isotope labeling with amino acid derivatives (SILAC) (Ong et al., 2002). Near complete incorporation of heavy lysine into the proteome was achieved by feeding worms suspensions of metabolically labeled *E. coli* cells. We used a pool of lysates prepared from labeled animals of different ages as an internal standard for quantifying protein expression by mass spectrometry (MS) (Figure 1A). Synchronized populations of wild-type (WT) animals were collected in five to six day intervals, lysed and mixed with this standard before digestion, fractionation by isoelectric focusing and MS analysis. Replicate analysis across three time points indicated a high degree of reproducibility between individual experiments (Figure S1A). We analyzed the proteomes of adult worms in intervals from one day up to 22 days of age, when less than 30% of the animals remain alive. In total, close to 6,000 different proteins were identified and quantified at a false discovery rate of less than 1%.

We found that the proteome of *C. elegans* undergoes extensive remodeling during aging. One third (33%) of the quantified proteins increased or decreased in abundance at least

two-fold, with the most pronounced changes exceeding 200-fold (Figure 1B). To estimate the extent of proteome remodeling in terms of molar ratios, we employed label free absolute quantification, a measure which is linearly related to absolute abundance (Schwanhaussner et al., 2011). Those proteins increasing at least two-fold in abundance during lifespan contributed to almost half of total protein mass in highly aged animals (Figure S1B).

The majority of the observed changes in protein abundance were already notable between day 1 and day 6 but typically progressed throughout lifespan (Figure S1C). The proteins which were increased more than 2-fold in abundance in old worms (22 days) relative to young animals (day 1) showed a significant overrepresentation of signal peptides as predicted by the SignalP3 algorithm, indicating that a large proportion (493 out of 760; Benjamini-Hochberg false discovery rate 5.6×10^{-37}) of these proteins are targeted to the secretory pathway. This notion was confirmed by gene ontology (GO) term analysis which revealed a 4.8-fold enrichment of proteins localized in the extracellular matrix (Supplementary Table S1). Furthermore, all six of the egg storage proteins, known as vitellogenins, were among the predicted secreted proteins which accumulated strongly during aging, although egg formation does not continue after day 6. Other functional categories of up-regulated proteins included a variety of proteins involved in DNA replication and repair processes, such as DNA replication initiation and gap filling during excision repair (Figure 1D). These findings are surprising in light of the fact that all somatic cells of *C. elegans* enter the postmitotic phase after development is complete (Tissenbaum and Guarente, 2002) and that the activity of nucleotide excision repair has been reported to decrease in aged animals (Meyer et al., 2007). Among the proteins whose abundance declined markedly during aging were several factors involved in ribosome biogenesis and proteins

residing in the nucleolus (Figure 1C). Among this group of proteins with decreasing abundance was also a modest but significant overrepresentation of proteins with at least one predicted transmembrane segment (Krogh et al., 2001) (Benjamini-Hochberg FDR of 0.0014).

We next investigated whether proteins residing in specific subcellular compartments were particularly prone to age-related changes. Most compartments underwent abundance changes to a similar extent during aging (Figure 1E). Among the organelles most affected by a decrease in protein abundance were the mitochondria. Notably, the affected proteins included the constituents of the respiratory chain complex I, which decreased gradually in abundance by ~50% throughout lifespan (Figure S1D). A decline in complex I function has been associated with increased production of ROS and oxidative stress (Hirst, 2013). In contrast, subunits of complexes IV and V were expressed at more stable levels (data not shown). A marked abundance increase was more frequently observed for proteins predicted to reside in the extracellular space. Apart from the above mentioned vitellogenins, a large number of transthyretin-like as well as numerous uncharacterized proteins were noted to increase in abundance.

To discover distinct patterns of change in protein abundance, we employed the fuzzy c-means method (Kumar and Futschik, 2007) to group proteins into distinct clusters. Based on predicted expression scores (Chikina et al., 2009), we identified tissues that were specifically enriched in these protein clusters (Figures 1F and S1E). Proteins predicted to be predominantly expressed in the germline typically showed a strong increase within the first six days of adulthood while largely retaining constant levels later in life (cluster 1). This observation is consistent with the cessation of the reproductive phase after day 6. In contrast, proteins

enriched in neuronal cells frequently showed a continuous increase in abundance after day 6 (cluster 2). On the other hand, proteins predominantly expressed in muscle were subject to an either continuous abundance decline during lifespan (cluster 3) or a more pronounced reduction between day 1 and day 6 (cluster 4). A similar behavior was observed for proteins enriched in intestine and hypodermis (cluster 3).

Age-related Changes in Proteostasis Network Components

The proteostasis network in *C. elegans* as defined here comprises close to 700 components. 254 of these were quantified in our analysis, including 85 proteins required for transcription and translation, 108 molecular chaperones and chaperone regulators, 42 proteins required for the defense against oxidative stress, as well as 99 components involved in protein degradation by the ubiquitin proteasome system (UPS) and the autophagy/lysosomal pathways (Figure 2A, Table S2). Generally, most ribosomal proteins decreased in abundance during aging, while a large proportion of the UPS components tended to increase in abundance (Table S3). Such general trends were not observed for the PN constituents responsible for protein folding and the defense against oxidative stress. This is exemplified by the class of small heat shock proteins, a group of chaperones with a critical role in aggregation prevention (Figure 2B). Three of these proteins, SIP-1, HSP-43 and HSP-16.48, increased strongly (~13-90-fold), whereas others increased either more moderately or remained largely unchanged during lifespan. Among the components mediating defense against oxidative stress, the glutathione peroxidase isoform GPX-5 showed a marked increase. The superoxide dismutase isoform 4 (SOD4)

increased markedly throughout the lifespan, whereas other SODs were affected to a much lesser extent.

Systematic changes were observed in the abundance of the protein synthesis and degradation machineries. The levels of cytosolic and mitochondrial ribosomal proteins generally decreased while the subunits of the 20S proteasome increased in abundance (Figure 2C and D, Figure S2A). A ~25% reduction in cytosolic ribosomal proteins occurred between day 1 and day 12 (p-value < 3.2 E-19, 70 proteins quantified) while a stable median level of ribosomal proteins was maintained thereafter (Figure 2C). However, in animals aged day 12 and older a pronounced imbalance in the stoichiometry among ribosomal proteins was observed. While in cytosolic ribosomes the abundance of several subunits decreased more than 60% below the median at later stages in life (Figure 2C), certain subunits of mitochondrial ribosomes increased in abundance relative to day 1 and day 6 animals by up to 8-fold (Figure S2A).

The general decrease and the imbalance in the abundance of ribosomal proteins likely reflect a decline in ribosomal function and assembly and a potentially serious loss in proteostasis control. Indeed, labeling experiments showed that the production of newly-synthesized proteins decreased strongly with age. Animals at 1, 4, 6 or 12 days of age were shifted from unlabeled ("light") to $^{13}\text{C}_6$ - $^{15}\text{N}_2$ -lysine ("heavy") labeled bacteria as a food source and the ratio between newly-synthesized and preexisting proteins was quantified after 24 hours (Figure 2E). In young animals (day 1), the amount of newly synthesized protein generally exceeded that of preexisting protein, reflecting active growth of the animals. In contrast, virtually no incorporation of heavy label was observed in moderately aged animals at day 12. To analyze protein synthesis later in lifespan more accurately, we shifted animals at the age of 5

days to heavy lysine and measured the accumulation of labeled protein throughout the remaining lifespan. Again, labeling efficiency declined sharply with age (Figure S2B). We note that this effect was not caused by reduced food uptake in aged worms as animals of a mutant strain deficient in pharyngeal pumping, *eat-2*, showed normal labeling compared to WT despite their strong defect in food uptake (Figure S2C).

The observed increase in abundance of proteasomal core subunits (~2-fold at day 22) was somewhat steeper between day 1 and day 6, followed by a milder continuous increase up to day 22 (Figure 2D). Unlike the effect on ribosomal proteins, there was no significant imbalance in the stoichiometry of proteasomal subunits, suggesting that their increase reflects an activation of proteasome function. This interpretation was confirmed by measuring proteasome activity in worm lysates. To this end, the chymotryptic activity of the proteasome under native-like conditions was analyzed via the cleavage rate of fluorogenic peptides, demonstrating an increase to a similar degree as the abundance change when comparing day 12 and day 1 animals (Figure 2F). Only negligible activities were observed in the presence of proteasomal inhibitors MG132 and lactacystin, demonstrating the specificity of the assay.

In summary, the levels and activities of two main branches of proteostasis control, protein synthesis and degradation, change in opposite directions during aging. While the decrease in ribosomal subunit proteins appears to be accompanied by a severe deregulation of ribosome assembly and thus is likely to contribute to aging, the increase in proteasome core subunits is more likely to reflect an attempt at mitigating the consequences of proteome imbalance. Other notable changes in the proteostasis system during lifespan include the

increase in abundance of several small Hsps and of components involved in the defense against oxidative stress.

Proteome Changes in Long-lived and Short-lived Mutant Animals

To better understand the relationship between the observed proteome changes during lifespan and the aging process, we next performed a proteomic analysis of long-lived *daf-2*, and short-lived *daf-16* and *hsf-1* mutants. The extent of proteome remodeling observed in WT animals among the proteins that increased in abundance was delayed in *daf-2* animals and accelerated in the short-lived *daf-16* and *hsf-1* strains (Figure 3A). To identify novel proteins that may contribute to IIS-mediated lifespan extension, we selected seven proteins whose expression levels were markedly lower in the long-lived *daf-2* mutant strain as compared to WT (Figure S3A). Most of these proteins are largely uncharacterized and have diverse predicted functions, including a putative metalloprotease, a peptide synthetase and two membrane transporters (Table S4). These candidates were tested for possible a lifespan extension when down-regulated in WT worms from L1 stage. When we depleted these proteins by RNA interference, we achieved a mild but robust lifespan extension, indicating a role in the regulation of longevity (Figure 3B, Table S5). This lifespan extension was not observed in a *daf-16* mutant background, suggesting that the down-regulated proteins act in the IIS pathway and their lifespan extension is dependent on *daf-16* (Figure S3B, Table S6).

The changes in components of the proteostasis network observed in long-lived and short-lived mutant strains occurred again predominantly in protein synthesis and degradation pathways, albeit at different rates as compared to WT animals (Figure 4). In the long-lived *daf-2*

mutant (Figure 4A), the up-regulation of proteasomal subunits occurred earlier and to a stronger degree than in WT animals (Figure 4B), while it occurred to a lesser degree in the short-lived *daf-16* and *hsf-1* strains (Figure 4C and D). The depletion of ribosomal proteins was delayed in *daf-2* (Figure 4A) but was more extensive in *daf-16* worms (Figure 4C). In contrast, down-regulation of ribosomal proteins was less pronounced in *hsf-1* animals (Figure 4D).

Interestingly, we observed marked differences in abundance levels between WT and *daf-2* mutant animals for PN components involved in the oxidative stress response. For example, catalases CTL-1, CTL-2 and CTL-3 as well as superoxide dismutases SOD-1, SOD-2 and SOD-3 were consistently up-regulated in *daf-2* worms compared to WT (Figure 4E and F, and data not shown).

Association of Hsf-1 and Daf-16 Deficiency with X-chromosomal Dosage

Compensation

Surprisingly, we found that in aged *hsf-1* and *daf-16* mutant animals the abundance of at least 430 quantified X-chromosomally encoded proteins was mildly but consistently increased over autosomally encoded proteins, reaching a mean increase by 16% in *daf-16* animals at day 17. To investigate the nature of this abundance difference further, we used a genome profiling algorithm, which was developed to detect chromosomal aberrations in cancer cell lines by testing for significantly elevated expression levels of proteins encoded on neighboring positions on each chromosome (Geiger et al., 2010) (Figure 5A). This method confirmed that X-chromosomally encoded proteins were systematically expressed at higher levels in aged *daf-16* and *hsf-1* animals from day 12 onward. It seemed plausible that this effect resulted from a

compromised X dosage compensation regulation. We therefore tested whether the observed phenotype could be reproduced in a strain containing a mutation in *dpy-28*, a gene encoding a component of the X-dosage compensation machinery (Meyer, 2005). Compared to *hsf-1* and *daf-16* mutants, the loss of DPY-28 function resulted in a more pronounced elevation of expression levels of X-chromosomally encoded proteins (Figure 5A). This phenotype could already be observed in day 1 animals, because X-chromosomal repression in *dpy-28* mutants is impaired independent of age (data not shown). Notably, loss of dosage compensation was not observed in a *dpy-5* mutant strain, carrying a mutation unrelated to dosage compensation but displaying a morphology phenotype (shorter and stouter) similar to that of *dpy-28* (Hartman and Ishii, 2007) (Figure 5A).

We hypothesized that even a moderate increase in protein expression might have a negative effect on overall proteostasis of aging cells if it affects a substantial proportion of the genome (Siegel and Amon, 2012). We therefore utilized a *C.elegans* polyglutamine (polyQ) protein aggregation model in which a Q40-YFP fusion protein is expressed in muscle cells (Morley et al., 2002). It has previously been demonstrated that a reduction in HSF-1 and DAF-16 levels results in an early onset of visible aggregation of the model protein (Hsu et al., 2003). To test whether deregulation of dosage compensation causes a similar phenotype, we expressed the same transgene in the dosage compensation deficient *dpy-28* mutant. In line with our hypothesis, the number of observable Q40-YFP inclusions increased markedly in *dpy-28* animals compared to WT already after 24 h or 48h post L1 stage (Figure 5B and C, and Figure S4 A, B and C), although Q40-YFP was expressed at equal levels (Figure S4D, E and F).

Collectively, these results indicate that proteome imbalance with mildly increased abundance of a substantial fraction of the proteome is sufficient to cause proteostasis stress as exemplified by accelerated aggregation of pathological proteins. Thus, premature proteome imbalance may contribute to the decreased lifespan of the short-lived *daf-16* mutant worms.

Quantification of Age-related Protein Aggregation

Declining proteostasis capacity is thought to facilitate the accumulation of proteins in insoluble aggregates. Recent studies reported the age-dependent formation of SDS-insoluble aggregates in *C. elegans* (David et al., 2010; Reis-Rodrigues et al., 2012). However, protein aggregates, including amyloid fibrils and insoluble proteins accumulating upon conformational stress, vary in biophysical properties and are typically not SDS-insoluble, raising the possibility that extraction protocols using SDS may underestimate the extent of aggregation. We therefore developed a procedure allowing the sensitive analysis and quantification of protein aggregates. For validation we used animals expressing FlucDM-GFP, a mutationally destabilized version of firefly luciferase which forms visible inclusions upon heat stress (Gupta et al., 2011). Young worms were subjected to heat shock for 90 min at 33°C, whole cell lysates were prepared and fractionated by centrifugation. The pellet fraction obtained was washed with mild detergents to obtain the insoluble protein fraction. While less than 5% of total FlucDM-GFP was insoluble in control animals, approximately 50% of the recombinant protein was recovered in the insoluble fraction after heat shock (Figure S5A). However, extraction with SDS containing buffer resulted in considerable loss of recovery of both total insoluble protein and insoluble FlucDM-GFP (Figure S5C). Isolation of aggregated proteins from aged animals yielded significantly more total protein as compared to young animals (Figure S5D). Importantly, using the less stringent

isolation procedure we observed that the proportion of FlucDM-GFP in the insoluble fraction increased not only upon heat shock (Figure S5B) but also increased more than 5-fold during aging (Figure S5E). Age-dependent aggregation was also detected for another model protein, Q35-YFP, consistent with previous observations (Morley et al., 2002) (Figure S5F and G).

We next measured aggregation at the proteome level in synchronized worm populations at different times during aging. A pool of total lysates from heavy lysine labeled worms of different strains and ages was used as an internal standard for quantitation (see Experimental Procedures). Insoluble proteins were separated by SDS-PAGE and subjected to in gel digestion prior to MS analysis. In total, we identified and quantified more than 3300 proteins. The vast majority (82%) of these proteins increased significantly in the insoluble fraction of WT worms at 12 days compared to young animals at day 1 (Figure 6A, Figure S6A). Aggregate formation occurred mainly between day 6 and day 12, i.e. after the hermaphrodite animals cease to lay eggs. The majority of these aggregation-prone proteins were not previously identified, presumably owing to the lower stringency of the isolation procedure (Figure S6B). The aggregated proteins showed a similar subcellular distribution as the proteins in total lysates (Figure S6C). Notably, the proteins which accumulated at the highest rate in WT animals were typically found in lower amounts in the insoluble fractions of long-lived *daf-2* animals (Figure 6B), indicating that lifespan extension correlates with a better ability of the animals to maintain proteostasis. In contrast, no such reduction in aggregation was observed for the short-lived *daf-16* and *hsf-1* mutants (Figure S6E and F).

Age-dependent Increase in Protein Abundance Correlates with Aggregation Propensity

To determine the propensity of proteins to form aggregates during aging, we performed aggregate isolations from aged WT animals at day 12 and measured the fraction of total protein in the aggregate. Comparable protein solubility values were obtained in three biological replicates (Pearson correlation coefficients >0.78). The measured aggregation propensities covered a range of more than two orders of magnitude, with a median value of 7.7% of individual proteins being insoluble (Figure S6I). Thus, while the total aggregate load increases dramatically during aging, for the majority of proteins depletion by aggregation would not result in a loss of function.

Previous studies have reported a negative correlation between aggregation propensities predicted computationally from protein sequence properties and protein abundance in *E. coli* or human tissues (de Groot and Ventura, 2010; Tartaglia et al., 2009; Tartaglia and Vendruscolo, 2009). For a small number of proteins, this trend has been confirmed by measuring aggregation properties of recombinant proteins *in vitro* (Baldwin et al., 2011; Tartaglia et al., 2007). Our SILAC-based proteomics dataset enabled us to experimentally validate this dependency at the proteome-wide scale. To this end, we grouped proteins into quantiles according to their aggregated proportion at day 12 and estimated the total abundance of each protein in the whole cell lysate using intensity-based label-free absolute quantification (LFAQ, Figure 6C) (Schwanhaussner et al., 2011). Indeed, the median abundance of the most aggregation-prone proteins (median aggregation 26% of total) was more than 10-fold lower than that of the most soluble proteins (median aggregation 2% of total), and this difference was highly significant (p-

value $<1.5 \times 10^{-11}$) (Figure 6D). For example, glycolytic enzymes or proteins residing in the mitochondrial matrix tend to be more soluble, correlating with their relatively high abundance.

Interestingly, despite the higher aggregation propensity of low-abundant proteins, we found that the best predictor of a protein contributing to the aggregate fraction was its absolute abundance in the total proteome. A Spearman's rank correlation of 0.76 was observed between the absolute abundance of specific proteins in the aggregated fraction and the abundance of the same proteins in the corresponding whole cell lysate (Figure 6E). This indicates that highly abundant proteins contribute greatly to the overall aggregate load in spite of their lower relative aggregation propensities. Moreover, when comparing abundance changes in the aggregated fraction between days 1 and 12 with the corresponding abundance changes in the total proteome, we also observed a positive correlation (Spearman's rank correlation coefficient 0.49, Figure 6F).

Given that the extent of aggregation varied over more than two orders of magnitude between individual proteins, we further investigated whether aggregation propensity correlated with the functional categories of proteins. GO analysis suggested that proteins involved in nucleic acid metabolism (specifically DNA-replication) tend to aggregate more strongly (Table S7). Interestingly, all identified members of the small HSP family of chaperones displayed a high degree of insolubility (Figure 6G). Notably, several of these chaperones increased in total abundance during aging (Figure 2C), presumably reflecting an attempt of the organism to reduce protein aggregation.

Aggregate formation is generally indicative of cellular stress and declining protein homeostasis. We therefore asked whether reducing the expression levels of highly aggregation-

prone proteins ameliorates organismal health and thereby extends lifespan. We selected four largely uncharacterized genes that were among the proteins which accumulated most strongly in the insoluble protein fractions during aging, and targeted them with RNA interference. The selected proteins were highly abundant but nevertheless showed aggregation propensities above median (Table S8). Remarkably, even though these aggregation-prone proteins individually contribute at most ~1% to total protein abundance, their removal was sufficient to cause a mild but significant lifespan extensions (Figure 6H, Table S9). These results suggest strongly that aggregation resulting from age-dependent proteome imbalance contributes to limiting lifespan in *C. elegans*.

Discussion

We have applied SILAC-based quantitative proteomics to map protein abundance changes during aging in the nematode *C. elegans*. One of the most important results of this study is the large extent of proteome remodeling occurring during aging. In WT animals, approximately one third of the quantified proteins are more than twofold up- or down-regulated during adult lifespan. This finding is in striking contrast to the situation in tissues of aged mice, where negligible proteomic changes were detected with a comparable experimental setup (Walther and Mann, 2011). Similarly, early microarray studies addressing aging in *C. elegans* suggested that only a small number of genes were significantly altered in transcription level (Lund et al., 2002). Although more recently published transcriptome datasets (Budovskaya et al., 2008; Golden and Melov, 2004) found more pronounced differences between young and old worms, the correlation with our SILAC-based protein quantification was relatively low (Figure S1F and

G). Much of the observed discrepancies between transcript and protein abundance may be attributed to posttranscriptional regulatory mechanisms. In mammalian cell lines typically more than one third of the protein abundance variation cannot be explained by transcript abundance alone (Schwanhausser et al., 2011; Vogel et al., 2010), but is ascribed to control of translation initiation and elongation efficiency, or protein stability (Vogel and Marcotte, 2012). Similar correlations were reported for *C. elegans* (Laurent et al., 2010). However, given the decline in proteostasis network function in aging nematodes (Cohen et al., 2006; Morley et al., 2002), a more pronounced discrepancy of our data from microarray studies can be expected due to altered protein synthesis and turnover rates.

We found that aging affected multiple nodes of the proteostasis system, most prominently protein biosynthesis and protein degradation. Firstly, an increase in abundance and activity of the proteasome was observed, which may be compensatory to counteract the rising burden of protein aggregation. Secondly, a gradual reduction in levels of ribosomal proteins occurred, and was associated with a marked decline in protein biosynthesis rates as demonstrated by SILAC and pulse labeling experiments. It is unclear whether these changes represent an adaptation to altered physiological requirements of the aged organism, or are at least in part causative of senescence. On the one hand, ribosomal decline went along with a down-regulation of the pathway required for their biogenesis, which may be an adaptation to a reduced requirement for protein synthesis once the developmental and reproductive phases are completed. On the other hand, aging was associated with an imbalance in the stoichiometry of the cytosolic and mitochondrial ribosomal proteins. This finding suggests impaired

transcriptional regulation or altered stability of specific ribosomal proteins and could be indicative of a deleterious effect.

Proteostasis decline with aging is evolutionarily conserved from nematodes to humans (Dillin and Cohen, 2011). In line with this notion, two recent publications reported the occurrence of SDS insoluble protein aggregates in old worms (David et al., 2010; Reis-Rodrigues et al., 2012). We employed a protocol with less stringent extraction for biochemical aggregate isolations, which probably accounts for the fact that the above mentioned studies have missed most of the aggregation-prone proteins identified here. We have previously demonstrated that proteins sequestered by amyloid type aggregate precursors in human cells have a preference for unstructured regions and have large molecular weights (Olzscha et al., 2011). In contrast, the more than 3,000 proteins of our *C. elegans* “aggregome” dataset, representing a significant proportion of the proteome, appeared to be largely devoid of common physico-chemical properties. This may point at a different mechanism underlying the aggregation process, which remains to be elucidated. Nonetheless, a negative correlation was found between absolute abundance and aggregation propensity, suggesting that proteins with high copy numbers are optimized in terms of folding requirements and solubility.

The integration of multiple experiments, addressing the total cellular proteome as well as its insoluble subset in WT and several longevity mutants, allowed us to detect dependencies between proteome remodeling and protein aggregation in aging worms. Proteome remodeling, or proteome imbalance, was accompanied by the increased expression of highly aggregation prone proteins. Moreover, the accumulation of these proteins in aggregates was attenuated in the long lived *daf-2* mutant. In *daf-16* animals, an overexpression of X-chromosomally encoded

proteins was observed, probably posing additional stress on the proteostasis network. Strikingly, the depletion even of individual proteins, that are highly aggregation-prone, resulted in a moderate but significant lifespan extension. This indicates that the observed protein aggregation indeed causes cytotoxicity.

Collectively, our data suggest that aging in *C. elegans* is associated with deleterious proteome imbalance, which drives protein aggregation. This may contribute to a successive proteostasis decline and thereby restrict the organism's lifespan.

Experimental Procedures

C. elegans Strains

C. elegans strains were maintained by standard methods (Brenner, 1974). The Bristol strain N2 was used as wild-type. The following mutants and transgenic strains were employed: CB1370 [*daf-2 (e1370)III*], TJ1052 [*age-1 (hx546)II*], CF1038 [*daf-16 (mu86)I*], PS3551 [*hsf-1 (sy441)I*], DA1113 [*eat-2 (ad1113)II*], CB428 [*dpy-21 (e428)V*], TY148 [*dpy-28 (y1)III*], AM140 [*rmls132 [P(*unc-54*) Q35::YFP]*], AM141 [*rmls133 [P(*unc-54*) Q40::YFP]*] and FUH135 [*marIs135 [P(*unc-54*) FLuc-DM::GFP]*].

E. coli Feeding Strains

Unless otherwise specified, *C. elegans* cultures were maintained with *E. coli* strain OP50 as a food source. For large scale SILAC labeling of worms the lysine auxotroph *E. coli* strain ET505 (CGSC#: 7088) was used. For pulse labeling experiments, a lysine auxotroph strain of OP50 was

generated by disrupting the *lysA* gene via the λ phage Red recombinase system as previously described (Datsenko and Wanner, 2000).

Growth Conditions

Worms were routinely maintained at 20°C on solid nematode growth medium (NGM). Cultures were synchronized by sodium hypochloride treatment followed by starvation-induced L1 arrest for 24 h. At L4 stage, larvae were transferred to media containing 10 μ M fluorodeoxyuridine to suppress progeny. For total proteome measurements, progeny was removed by repeated sedimentation. Dead worms were removed manually before harvesting. Bacterial cultures for SILAC labeling were grown in $^{13}\text{C}_6$ - $^{14}\text{N}_2$ -lysine (Cambridge Isotope Laboratories, Andover, MA) containing M63 minimal media, harvested by centrifugation and washed. Suspensions were spotted onto nitrogen-free agarose plates (Krijgsveld et al., 2003). The incorporation of heavy lysine into the proteome of *C. elegans* was more than 99% after four reproductive cycles.

Sample Preparation for Total Proteome Measurements

Worms were rinsed off plates and washed with M9 minimal salt solution to minimize bacterial contamination. Pellets were resuspended in lysis buffer (4% SDS, 0.1 M Tris/HCl pH 8.0, 1 mM EDTA), incubated at 95°C for 5 min and sonicated in a Bioruptor (Diagenode, Liège, Belgium) ultrasonication bath for 10 min at high energy setting. After heating for 3 minutes, lysates were clarified by centrifugation (20,000 rcf, 10 min) and protein content was quantified using the BCA assay kit (Pierce, Rockford, IL). In a typical experiment, 40 μ g of total protein lysate was mixed with an equal amount of a $^{13}\text{C}_6$ - $^{14}\text{N}_2$ -lysine labeled lysate pool with equal contributions of

WT animals aged 1, 6, 12 and 17 days. Proteins were reduced, alkylated and digested with endoproteinase LysC (Wako Bioproducts, Richmond, VA) using the filter aided sample preparation method (FASP) (Wisniewski et al., 2009). Obtained peptide mixtures were either analyzed without fractionation or desalted via C18 solid phase extraction (SPE) cartridges (3M, St. Paul, MN) and subjected to isoelectric focusing on an Offgel system (Agilent, Santa Clara, CA) using 13 cm linear immobilized pH gradient strips with a pH range from 3 to 10 according to published procedures (de Godoy et al., 2008; Hubner et al., 2008). Fractionated or unfractionated peptides were purified via StageTips (Rappsilber et al., 2007).

Biochemical Isolation of Protein Aggregates

Approximately 600 worms were resuspended in 550 μ l lysis buffer (50 mM Tris/HCl pH 8.0, 0.5 M NaCl, 4 mM EDTA, 1% (v/v) Igepal CA630, Complete proteinase inhibitor cocktail (Roche Diagnostics, Mannheim, Germany)) and sonicated for 8 min at 0°C in a Bioruptor sonication bath. Lysates were clarified (1,000 rcf, 1 min, 4°C) and protein content was adjusted to equal levels. For proteome measurements, a lysate pool of $^{13}\text{C}_6$ - $^{14}\text{N}_2$ -lysine labeled animals was mixed with each of the samples. Insoluble proteins were sedimented by ultracentrifugation (500,000 rcf, 4°C, 10 min) and subsequently washed twice with modified RIPA buffer (50 mM Tris/HCl pH 8.0, 0.15 M NaCl, 4 mM EDTA, 1% (v/v) Igepal CA630, 0.5% sodium deoxycholate, Complete proteinase inhibitor cocktail) before solubilization in 2% SDS containing sample buffer for 10 min at 95°C. Proteins were resolved on SDS-PAGE gels and either analyzed by Coomassie staining or Western blotting, or processed for MS analysis by in gel digestion and StageTip purification.

Mass Spectrometry and Data Analysis

Peptides were separated on C18 reversed phase nHPLC columns (Nagaraj et al., 2011; Walther and Mann, 2011) with gradient durations of 140 or 280 min for fractionated or unfractionated samples, respectively, and sprayed online into LTQ-Orbitrap Velos or Orbitrap Elite mass spectrometer (Thermo Fisher Scientific, Bremen, Germany)(Michalski et al., 2012; Olsen et al., 2009). In each scan cycle, fragmentation spectra of the 10 most intense peptide precursors in the survey scan were acquired in the higher-energy collisional dissociation (HCD) mode. Raw data were processed in the MaxQuant software environment (Cox and Mann, 2008) and peak lists were searched with Andromeda (Cox et al., 2011) against a database containing the translation of all predicted proteins listed in Uniprot (release January 15, 2012) as well as a list of contaminants including commonly observed human keratins as well as the NCBI protein database of *E. coli* strain K12 (release date January 25, 2010). The minimal required peptide length was set to seven amino acids and both protein and peptide identifications were accepted at a false discovery rate of 1%.

Bioinformatic Analysis

Prediction of subcellular localization, signal sequences and transmembrane segments were performed using WoLF PSORT (Horton et al., 2007), SignalP (Petersen et al., 2011) and TMHMM v. 2.0 (Krogh et al., 2001) algorithms, respectively. Further annotation included predicted tissue specificity of expression (Chikina et al., 2009), Pfam protein families (Finn et al., 2008) and gene ontology databases (Ashburner et al., 2000). One- and two-dimensional annotation enrichment analysis was performed in the Perseus data analysis suite (Cox and Mann, 2012). Fuzzy c-means

clustering of time course profiles was carried out using the Mfuzz package in the statistical programming language R (Kumar and Futschik, 2007).

Proteasomal Activity Assays

Worms were lysed by ultrasonication in the presence of 2mM ATP and proteasomal activity was performed as previously described using the fluorogenic substrate Z-Gly-Gly-Leu-AMC (Kisselev and Goldberg, 2005; Vilchez et al., 2012).

Lifespan Assays

RNAi by feeding was performed as described previously (Kamath et al., 2001) using RNAi bacteria from the Ahringer library (Kamath et al., 2003). All RNAi clones used in this study were verified by sequencing. RNAi bacterial cultures were grown in LB+ampicillin (50 µg/ml) for 8 h at 37°C and then seeded onto RNAi plates (NGM plates with 2mM IPTG and 25µg/ml carbenicillin). *E. coli* strain HT115 (DE3) carrying the L4440 plasmid (empty vector) was used as control. Lifespan assays were performed at 20°C. Synchronized L1 larvae were added to RNAi plates seeded with corresponding RNAi bacteria and grown on these plates until reaching the L4 stage. Approximately 100 L4 larvae were then transferred to fresh RNAi plates containing 10 µM 5-fluorodeoxyuracile (FUDR) to prevent growth of progeny and this day of the transfer was considered as day 0 in the adult lifespan assay. Worms were then moved to new plates every 5-7 days for the rest of the assay. Lifespan was assessed every other day and worms were scored as dead when they did not move or respond to gently prodding with a platinum wire. Worms that crawled onto the wall of the plates or died from vulval bursting were excluded.

Quantification of Q40 Aggregates and Microscopy

Worms expressing Q40-YFP were mounted on 2% agar pad on glass slides and immobilized in 1 mM levamisole. Aggregates were scored at 24 h and 48h post-L1 stage, using a Leica fluorescent stereomicroscope. A minimum of 20 worms were scored for each strain and time point analyzed. Worms expressing FlucDM-EGFP were fixed in ethanol and mounted on slides using Dako fluorescent mounting medium. Fluorescence imaging was performed on a Zeiss Axiovert fluorescence microscope.

Acknowledgements

We would like to thank the *Caenorhabditis* Genetics Center for providing most of the strains used in this study. Our work is supported by the European Union 7th Framework Program (HEALTH-F4-2008-201648/PROSPECTS)

References

- Ashburner, M., Ball, C.A., Blake, J.A., Botstein, D., Butler, H., Cherry, J.M., Davis, A.P., Dolinski, K., Dwight, S.S., Eppig, J.T., *et al.* (2000). Gene ontology: tool for the unification of biology. The Gene Ontology Consortium. *Nat Genet* 25, 25-29.
- Balch, W.E., Morimoto, R.I., Dillin, A., and Kelly, J.W. (2008). Adapting proteostasis for disease intervention. *Science* 319, 916-919.
- Baldwin, A.J., Knowles, T.P., Tartaglia, G.G., Fitzpatrick, A.W., Devlin, G.L., Shammass, S.L., Waudby, C.A., Mossuto, M.F., Meehan, S., Gras, S.L., *et al.* (2011). Metastability of native proteins and the phenomenon of amyloid formation. *J Am Chem Soc* 133, 14160-14163.
- Ben-Zvi, A., Miller, E.A., and Morimoto, R.I. (2009). Collapse of proteostasis represents an early molecular event in *Caenorhabditis elegans* aging. *Proc Natl Acad Sci U S A* 106, 14914-14919.
- Bence, N.F., Sampat, R.M., and Kopito, R.R. (2001). Impairment of the ubiquitin-proteasome system by protein aggregation. *Science* 292, 1552-1555.
- Brenner, S. (1974). The genetics of *Caenorhabditis elegans*. *Genetics* 77, 71-94.
- Budovskaya, Y.V., Wu, K., Southworth, L.K., Jiang, M., Tedesco, P., Johnson, T.E., and Kim, S.K. (2008). An elt-3/elt-5/elt-6 GATA transcription circuit guides aging in *C-elegans*. *Cell* 134, 291-303.
- Chiang, W.-C., Ching, T.-T., Lee, Hee C., Mousigian, C., and Hsu, A.-L. (2012). HSF-1 Regulators DDL-1/2 Link Insulin-like Signaling to Heat-Shock Responses and Modulation of Longevity. *Cell* 148, 322-334.

- Chikina, M.D., Huttenhower, C., Murphy, C.T., and Troyanskaya, O.G. (2009). Global prediction of tissue-specific gene expression and context-dependent gene networks in *Caenorhabditis elegans*. *PLoS Comput Biol* 5, e1000417.
- Cohen, E., Bieschke, J., Perciavalle, R.M., Kelly, J.W., and Dillin, A. (2006). Opposing activities protect against age-onset proteotoxicity. *Science* 313, 1604-1610.
- Cohen, E., and Dillin, A. (2008). The insulin paradox: aging, proteotoxicity and neurodegeneration. *Nat Rev Neurosci* 9, 759-767.
- Cohen, E., Du, D., Joyce, D., Kapernick, E.A., Volovik, Y., Kelly, J.W., and Dillin, A. (2010). Temporal requirements of insulin/IGF-1 signaling for proteotoxicity protection. *Aging Cell* 9, 126-134.
- Cohen, E., Paulsson, J.F., Blinder, P., Burstyn-Cohen, T., Du, D., Estepa, G., Adame, A., Pham, H.M., Holzenberger, M., Kelly, J.W., *et al.* (2009). Reduced IGF-1 Signaling Delays Age-Associated Proteotoxicity in Mice. *Cell* 139, 1157-1169.
- Cox, J., and Mann, M. (2008). MaxQuant enables high peptide identification rates, individualized p.p.b.-range mass accuracies and proteome-wide protein quantification. *Nat Biotechnol* 26, 1367-1372.
- Cox, J., and Mann, M. (2011). Quantitative, high-resolution proteomics for data-driven systems biology. *Annu Rev Biochem* 80, 273-299.
- Cox, J., and Mann, M. (2012). 1D and 2D annotation enrichment: a statistical method integrating quantitative proteomics with complementary high-throughput data. *BMC Bioinformatics* 13 Suppl 16, S12.
- Cox, J., Neuhauser, N., Michalski, A., Scheltema, R.A., Olsen, J.V., and Mann, M. (2011). Andromeda: A Peptide Search Engine Integrated into the MaxQuant Environment. *Journal of Proteome Research* 10, 1794-1805.
- Cuervo, A.M., and Dice, J.F. (2000). Age-related decline in chaperone-mediated autophagy. *Journal of Biological Chemistry* 275, 31505-31513.
- Datsenko, K.A., and Wanner, B.L. (2000). One-step inactivation of chromosomal genes in *Escherichia coli* K-12 using PCR products. *Proceedings of the National Academy of Sciences of the United States of America* 97, 6640-6645.
- David, D.C., Ollikainen, N., Trinidad, J.C., Cary, M.P., Burlingame, A.L., and Kenyon, C. (2010). Widespread Protein Aggregation as an Inherent Part of Aging in *C. elegans*. *Plos Biology* 8.
- de Godoy, L.M.F., Olsen, J.V., Cox, J., Nielsen, M.L., Hubner, N.C., Frohlich, F., Walther, T.C., and Mann, M. (2008). Comprehensive mass-spectrometry-based proteome quantification of haploid versus diploid yeast. *Nature* 455, 1251-U1260.
- de Groot, N.S., and Ventura, S. (2010). Protein Aggregation Profile of the Bacterial Cytosol. *PLoS One* 5, e9383.
- Dillin, A., and Cohen, E. (2011). Ageing and protein aggregation-mediated disorders: from invertebrates to mammals. *Philos Trans R Soc Lond B Biol Sci* 366, 94-98.
- Douglas, P.M., and Dillin, A. (2010). Protein homeostasis and aging in neurodegeneration. *J Cell Biol* 190, 719-729.
- Finkel, T., and Holbrook, N.J. (2000). Oxidants, oxidative stress and the biology of ageing. *Nature* 408, 239-247.
- Finn, R.D., Tate, J., Mistry, J., Coghill, P.C., Sammut, S.J., Hotz, H.R., Ceric, G., Forslund, K., Eddy, S.R., Sonnhammer, E.L., *et al.* (2008). The Pfam protein families database. *Nucleic Acids Res* 36, D281-288.
- Fredens, J., Engholm-Keller, K., Giessing, A., Pultz, D., Larsen, M.R., Hojrup, P., Moller-Jensen, J., and Faergeman, N.J. (2011). Quantitative proteomics by amino acid labeling in *C. elegans*. *Nature Methods* 8, 845-U109.
- Geiger, T., Cox, J., and Mann, M. (2010). Proteomic Changes Resulting from Gene Copy Number Variations in Cancer Cells. *Plos Genetics* 6.

- Gidalevitz, T., Ben-Zvi, A., Ho, K.H., Brignull, H.R., and Morimoto, R.I. (2006). Progressive disruption of cellular protein folding in models of polyglutamine diseases. *Science* 311, 1471-1474.
- Golden, T.R., Hubbard, A., Dando, C., Herren, M.A., and Melov, S. (2008). Age-related behaviors have distinct transcriptional profiles in *Caenorhabditis elegans*. *Aging Cell* 7, 850-865.
- Golden, T.R., and Melov, S. (2004). Microarray analysis of gene expression with age in individual nematodes. *Aging Cell* 3, 111-124.
- Gupta, R., Kasturi, P., Bracher, A., Loew, C., Zheng, M., Villella, A., Garza, D., Hartl, F.U., and Raychaudhuri, S. (2011). Firefly luciferase mutants as sensors of proteome stress. *Nature Methods* 8, 879-U155.
- Halaschek-Wiener, J. (2005). Analysis of long-lived *C. elegans* daf-2 mutants using serial analysis of gene expression. *Genome Res* 15, 603-615.
- Hartl, F.U., Bracher, A., and Hayer-Hartl, M. (2011). Molecular chaperones in protein folding and proteostasis. *Nature* 475, 324-332.
- Hartman, P.S., and Ishii, N. (2007). Chromosome dosage as a life span determinant in *Caenorhabditis elegans*. *Mech Ageing Dev* 128, 437-443.
- Hirst, J. (2013). Mitochondrial complex I. *Annu Rev Biochem* 82, 551-575.
- Horton, P., Park, K.J., Obayashi, T., Fujita, N., Harada, H., Adams-Collier, C.J., and Nakai, K. (2007). WoLF PSORT: protein localization predictor. *Nucleic Acids Res* 35, W585-587.
- Hsu, A.-L., Murphy, C.T., and Kenyon, C. (2003). Regulation of Aging and Age-Related Disease by DAF-16 and Heat-Shock Factor. *Science* 300, 1142-1145.
- Hubner, N.C., Ren, S., and Mann, M. (2008). Peptide separation with immobilized pI strips is an attractive alternative to in-gel protein digestion for proteome analysis. *Proteomics* 8, 4862-4872.
- Kamath, R.S., Fraser, A.G., Dong, Y., Poulin, G., Durbin, R., Gotta, M., Kanapin, A., Le Bot, N., Moreno, S., Sohrmann, M., *et al.* (2003). Systematic functional analysis of the *Caenorhabditis elegans* genome using RNAi. *Nature* 421, 231-237.
- Kamath, R.S., Martinez-Campos, M., Zipperlen, P., Fraser, A.G., and Ahringer, J. (2001). Effectiveness of specific RNA-mediated interference through ingested double-stranded RNA in *Caenorhabditis elegans*. *Genome Biol* 2, RESEARCH0002.
- Kenyon, C., Chang, J., Gensch, E., Rudner, A., and Tabtiang, R. (1993). A *C. elegans* mutant that lives twice as long as wild type. *Nature* 366, 461-464.
- Kikis, E.A., Gidalevitz, T., and Morimoto, R.I. (2010). Protein homeostasis in models of aging and age-related conformational disease. *Adv Exp Med Biol* 694, 138-159.
- Kisselev, A.F., and Goldberg, A.L. (2005). Monitoring activity and inhibition of 26S proteasomes with fluorogenic peptide substrates. *Methods Enzymol* 398, 364-378.
- Krijgsveld, J., Ketting, R.F., Mahmoudi, T., Johansen, J., Artal-Sanz, M., Verrijzer, C.P., Plasterk, R.H.A., and Heck, A.J.R. (2003). Metabolic labeling of *C-elegans* and *D-melanogaster* for quantitative proteomics. *Nature Biotechnology* 21, 927-931.
- Krogh, A., Larsson, B., von Heijne, G., and Sonnhammer, E.L. (2001). Predicting transmembrane protein topology with a hidden Markov model: application to complete genomes. *J Mol Biol* 305, 567-580.
- Kruger, M., Moser, M., Ussar, S., Thievensen, I., Luber, C.A., Forner, F., Schmidt, S., Zanivan, S., Fassler, R., and Mann, M. (2008). SILAC mouse for quantitative proteomics uncovers kindlin-3 as an essential factor for red blood cell function. *Cell* 134, 353-364.
- Kumar, L., and Futschik, M.E. (2007). Mfuzz: a software package for soft clustering of microarray data. *Bioinformatics* 2, 5-7.
- Larance, M., Bailly, A.P., Pourkarimi, E., Hay, R.T., Buchanan, G., Coulthurst, S., Xirodimas, D.P., Gartner, A., and Lamond, A.I. (2011). Stable-isotope labeling with amino acids in nematodes. *Nature Methods* 8, 849-U114.

- Larsen, P.L., Albert, P.S., and Riddle, D.L. (1995). Genes that regulate both development and longevity in *Caenorhabditis elegans*. *Genetics* 139, 1567-1583.
- Laurent, J.M., Vogel, C., Kwon, T., Craig, S.A., Boutz, D.R., Huse, H.K., Nozue, K., Walia, H., Whiteley, M., Ronald, P.C., *et al.* (2010). Protein abundances are more conserved than mRNA abundances across diverse taxa. *Proteomics* 10, 4209-4212.
- Lin, K., Dorman, J.B., Rodan, A., and Kenyon, C. (1997). *daf-16*: An HNF-3/forkhead family member that can function to double the life-span of *Caenorhabditis elegans*. *Science* 278, 1319-1322.
- Lithgow, G.J., White, T.M., Melov, S., and Johnson, T.E. (1995). Thermotolerance and extended life-span conferred by single-gene mutations and induced by thermal stress. *Proceedings of the National Academy of Sciences* 92, 7540-7544.
- Lund, J., Tedesco, P., Duke, K., Wang, J., Kim, S.K., and Johnson, T.E. (2002). Transcriptional profile of aging in *C.-elegans*. *Current Biology* 12, 1566-1573.
- McElwee, J., Bubbs, K., and Thomas, J.H. (2003). Transcriptional outputs of the *Caenorhabditis elegans* forkhead protein DAF-16. *Aging Cell* 2, 111-121.
- Meyer, B.J. (2005). X-Chromosome dosage compensation. *WormBook*, 1-14.
- Meyer, J.N., Boyd, W.A., Azzam, G.A., Haugen, A.C., Freedman, J.H., and Van Houten, B. (2007). Decline of nucleotide excision repair capacity in aging *Caenorhabditis elegans*. *Genome Biol* 8, R70.
- Michalski, A., Damoc, E., Lange, O., Denisov, E., Nolting, D., Muller, M., Viner, R., Schwartz, J., Remes, P., Belford, M., *et al.* (2012). Ultra high resolution linear ion trap Orbitrap mass spectrometer (Orbitrap Elite) facilitates top down LC MS/MS and versatile peptide fragmentation modes. *Mol Cell Proteomics* 11, O111 013698.
- Morimoto, R.I. (2008). Proteotoxic stress and inducible chaperone networks in neurodegenerative disease and aging. *Genes Dev* 22, 1427-1438.
- Morley, J.F., Brignull, H.R., Weyers, J.J., and Morimoto, R.I. (2002). The threshold for polyglutamine-expansion protein aggregation and cellular toxicity is dynamic and influenced by aging in *Caenorhabditis elegans*. *Proceedings of the National Academy of Sciences of the United States of America* 99, 10417-10422.
- Morley, J.F., and Morimoto, R.I. (2004). Regulation of longevity in *Caenorhabditis elegans* by heat shock factor and molecular chaperones. *Mol Biol Cell* 15, 657-664.
- Murphy, C.T., McCarroll, S.A., Bargmann, C.I., Fraser, A., Kamath, R.S., Ahringer, J., Li, H., and Kenyon, C. (2003). Genes that act downstream of DAF-16 to influence the lifespan of *Caenorhabditis elegans*. *Nature* 424, 277-284.
- Nagaraj, N., Wisniewski, J.R., Geiger, T., Cox, J., Kircher, M., Kelso, J., Paabo, S., and Mann, M. (2011). Deep proteome and transcriptome mapping of a human cancer cell line. *Mol Syst Biol* 7.
- Ogg, S., Paradis, S., Gottlieb, S., Patterson, G.I., Lee, L., Tissenbaum, H.A., and Ruvkun, G. (1997). The Fork head transcription factor DAF-16 transduces insulin-like metabolic and longevity signals in *C.-elegans*. *Nature* 389, 994-999.
- Olsen, J.V., Nielsen, M.L., Damoc, N.E., Griep-Raming, J., Moehring, T., Makarov, A., Schwartz, J., Horning, S., and Mann, M. (2009). Characterization of the Velos, an Enhanced LTQ Orbitrap, for Proteomics. *Molecular & Cellular Proteomics*, S40-S40.
- Olzscha, H., Schermann, S.M., Woerner, A.C., Pinkert, S., Hecht, M.H., Tartaglia, G.G., Vendruscolo, M., Hayer-Hartl, M., Hartl, F.U., and Vabulas, R.M. (2011). Amyloid-like aggregates sequester numerous metastable proteins with essential cellular functions. *Cell* 144, 67-78.
- Ong, S.E., Blagoev, B., Kratchmarova, I., Kristensen, D.B., Steen, H., Pandey, A., and Mann, M. (2002). Stable isotope labeling by amino acids in cell culture, SILAC, as a simple and accurate approach to expression proteomics. *Mol Cell Proteomics* 1, 376-386.
- Petersen, T.N., Brunak, S., von Heijne, G., and Nielsen, H. (2011). SignalP 4.0: discriminating signal peptides from transmembrane regions. *Nat Methods* 8, 785-786.

- Rappsilber, J., Mann, M., and Ishihama, Y. (2007). Protocol for micro-purification, enrichment, pre-fractionation and storage of peptides for proteomics using StageTips. *Nature Protocols* 2, 1896-1906.
- Reis-Rodrigues, P., Czerwieniec, G., Peters, T.W., Evani, U.S., Alavez, S., Gaman, E.A., Vantipalli, M., Mooney, S.D., Gibson, B.W., Lithgow, G.J., *et al.* (2012). Proteomic analysis of age-dependent changes in protein solubility identifies genes that modulate lifespan. *Aging Cell* 11, 120-127.
- Schwanhauser, B., Busse, D., Li, N., Dittmar, G., Schuchhardt, J., Wolf, J., Chen, W., and Selbach, M. (2011). Global quantification of mammalian gene expression control. *Nature* 473, 337-342.
- Siegel, J.J., and Amon, A. (2012). New Insights into the Troubles of Aneuploidy. *Annu Rev Cell Dev Biol*.
- Sury, M.D., Chen, J.-X., and Selbach, M. (2010). The SILAC Fly Allows for Accurate Protein Quantification in Vivo. *Molecular & Cellular Proteomics* 9, 2173-2183.
- Tartaglia, G.G., Pechmann, S., Dobson, C.M., and Vendruscolo, M. (2007). Life on the edge: a link between gene expression levels and aggregation rates of human proteins. *Trends Biochem Sci* 32, 204-206.
- Tartaglia, G.G., Pechmann, S., Dobson, C.M., and Vendruscolo, M. (2009). A Relationship between mRNA Expression Levels and Protein Solubility in *E. coli*. *Journal of Molecular Biology* 388, 381-389.
- Tartaglia, G.G., and Vendruscolo, M. (2009). Correlation between mRNA expression levels and protein aggregation propensities in subcellular localisations. *Molecular BioSystems* 5, 1873-1876.
- Taylor, R.C., and Dillin, A. (2011). Aging as an event of proteostasis collapse. *Cold Spring Harb Perspect Biol* 3.
- Tissenbaum, H.A., and Guarente, L. (2002). Model organisms as a guide to mammalian aging. *Dev Cell* 2, 9-19.
- Tonoki, A., Kuranaga, E., Tomioka, T., Hamazaki, J., Murata, S., Tanaka, K., and Miura, M. (2009). Genetic Evidence Linking Age-Dependent Attenuation of the 26S Proteasome with the Aging Process. *Molecular and Cellular Biology* 29, 1095-1106.
- Vendruscolo, M. (2012). Proteome folding and aggregation. *Curr Opin Struct Biol*.
- Vilchez, D., Morantte, I., Liu, Z., Douglas, P.M., Merkwirth, C., Rodrigues, A.P., Manning, G., and Dillin, A. (2012). RPN-6 determines *C. elegans* longevity under proteotoxic stress conditions. *Nature*.
- Vogel, C., Abreu Rde, S., Ko, D., Le, S.Y., Shapiro, B.A., Burns, S.C., Sandhu, D., Boutz, D.R., Marcotte, E.M., and Penalva, L.O. (2010). Sequence signatures and mRNA concentration can explain two-thirds of protein abundance variation in a human cell line. *Mol Syst Biol* 6, 400.
- Vogel, C., and Marcotte, E.M. (2012). Insights into the regulation of protein abundance from proteomic and transcriptomic analyses. *Nat Rev Genet* 13, 227-232.
- Walther, D.M., and Mann, M. (2011). Accurate Quantification of More Than 4000 Mouse Tissue Proteins Reveals Minimal Proteome Changes During Aging. *Molecular & Cellular Proteomics* 10.
- Wisniewski, J.R., Zougman, A., Nagaraj, N., and Mann, M. (2009). Universal sample preparation method for proteome analysis. *Nat Methods* 6, 359-362.

Figure Legends

Figure 1: Proteomic analysis of aging in *C. elegans*. (A) Experimental design. Synchronized worm populations at different time points were lysed and mixed with a metabolically (SILAC) labeled internal protein standard. After digestion, peptides were either analyzed directly or after fractionation by isoelectric focusing by nLC coupled mass spectrometry. (B) Histogram representations of proteome changes in WT between young adults (day 1) and animals of the indicated ages. The proportion of proteins which were affected at least twofold in abundance during aging are marked in red. (C, D) Significantly affected functional categories within the two-fold up- or down-regulated proteins between young (day 1) and aged (day 22) nematodes via Gene Ontology (GO) term enrichment. The enrichment factor is plotted against the p-value derived from Fisher Exact test. Each term is represented by a circle, whose size encodes for the number of proteins affected. (E) Changes in subcellular compartments are divided into unchanged (grey) or 1.5-fold up- (gold) or down-regulated (blue) proteins between young (day 1) and aged (day 22) nematodes. The area of the circles reflects the number of proteins identified. (F) Clustering of time course expression patterns in WT animals using the fuzzy c-means algorithm. Specifically enriched major tissues are indicated for each cluster, which are based on predicted genome-wide expression scores.

Figure 2: Changes in specific subsets of the proteostasis network. (A) We classified the proteostasis network into the three basic categories governing synthesis, maintenance and degradation, which were further subdivided as indicated. (B) Examples of time course abundance profiles of proteins facilitating protein maintenance. Members of the small heat

shock protein family as well as proteins involved in oxidative stress response displayed. (C) Boxplot representation of abundance changes of ribosomal proteins during lifespan. (D) Boxplots of abundance changes of the fourteen 20S proteasomal core particle subunits during lifespan. (E) Decline of label incorporation rate during aging determined by pulsed SILAC. Animals aged 1, 4, 6 or 12 days were transferred to a heavy lysine-labeled food source for 24 h, lysed, digested and subsequently analyzed by mass spectrometry (F). Quantification of the chymotryptic proteolytic activity of the proteasome in lysates derived from old (day 12) and young (day 1) worms as measured by the cleavage rate of a fluorogenic synthetic peptide. Assays were performed either in the presence of the indicated specific proteasomal inhibitors or without inhibitors (Mock). Error bars represent standard deviations obtained from each six biological replicate experiments per time point.

Figure 3: Impact of IIS on the *C. elegans* proteome. (A) Proteome imbalance scoring late in life. Expression differences between animals at the indicated time points and animals at an intermediate age past the reproductive phase (day 6) were summed up individually for up- and down-regulated proteins for each strain and normalized to the number of quantified proteins. (B) Lifespan of WT animals upon depletion of proteins that were found to be underrepresented in the long-lived *daf-2* strain (Figure S3A). Animals were fed with bacteria expressing RNAi knockdown constructs against the indicated genes or subjected to mock treatment.

Figure 4: Remodeling of the proteostasis network during aging in WT worms (B) and longevity mutant strains *daf-2* (A), *daf-16* (C) and *hsf-1* (D). Each time point is represented by a concentric

circle. Expression changes within the indicated categories with respect to the abundance level at strain-specific day 1 are color coded as indicated. (E,F,G) Abundance profiles of selected proteostasis in the indicated strains during aging: catalases (E), superoxide dismutases (F) and small heat shock proteins (G).

Figure 5: X-chromosomal deregulation in the short-lived IIS mutants *daf-16* and *hsf-1*.

(A) Genome profiling of expression ratios between *daf-16* or *hsf-1* and WT. A sliding window approach is used to determine chromosomal regions with significant overrepresentation of the encoded proteins in the proteome. The same phenotype can be recapitulated when comparing the ratio between the dosage compensation-deficient mutant strain *dpy-28* and WT. However, this is not the case for *dpy-5*, a mutant strain with a similar morphology phenotype as *dpy-28*. (B, C) X-chromosomal deregulation results in premature aggregation of muscle-specific polyglutamines (Q40-YFP). (B) Representative fluorescence images of Q40-YFP-expressing animals 48h past L1 stage in WT or *dpy-28* mutant background. (C) Quantification of observed protein aggregates across populations of the same animals.

Figure 6: Proteomic analysis of protein aggregation during aging. (A) Boxplots of protein abundance in the insoluble fraction during the course of aging in WT using SILAC quantification. (B) The long lived *daf-2* mutant displays an attenuated accumulation of highly aggregation-prone proteins in the insoluble fraction. The accumulation of each protein in WT in the aggregated fraction between day 01 and day 12 is plotted against the abundance difference between *daf-2* and WT animals at day 12. (C) Histogram of aggregation propensities in WT

animals at day 12. Whole cell lysates and isolated insoluble proportions were quantified against the same SILAC standard and ratios between the two experiments were calculated for each protein. (D) Relationship between aggregation propensity and total protein abundance. Proteins were divided into five quantiles based on their measured insoluble proportion. Label-free absolute quantitation (LFAQ) in the corresponding whole cell lysate was used to estimate concentrations. (E) Absolute abundance of proteins in the aggregated fraction is positively correlated with absolute abundance in the total proteome. Data for aged WT animals at day 12 are displayed. The Spearman's rank correlation ρ is indicated. (F) A positive correlation exists between age related abundance changes in the aggregated fraction and abundance changes of the same proteins in the total proteome. Differences between old (day 12) and young (day 1) WT animals are plotted on both axes. (G) Aggregation propensities and age-dependent accumulation in aggregates between young (day 1) and aged (day 12) of small heat shock proteins with respect to the distribution of all identified proteins. (H) Depletion of highly aggregation-prone proteins extends lifespan. Experiments were performed as described in the legend to Figure 4B.

Figure 7: Model for proteome maintenance during aging in *C.elegans*. In young adult worms, proteostasis is maintained. The load of misfolded proteins is reduced by the action of chaperones that prevent aggregation and/or by proteasome-mediated degradation. In aged animals, functional folding of newly synthesized proteome declines and the load of misfolded or aggregation-prone proteins increases. This results in an up-regulation of specific chaperones

and proteasomal subunits. Despite these cellular responses, the burden of protein aggregation cannot entirely be compensated and eventually results in proteostasis collapse.

Supplementary Materials Legends

Supplementary Figures

Figure S1: (A) Reproducibility of SILAC-based proteomic analyses. Each four biological replicates of WT animals at the indicated ages were collected and quantified against the same SILAC spike-in standard. Each one of the four replicates (open circles) was prepared on a different day than the remaining three (closed circles). Principal component analysis plots are displayed. (B) Absolute proportion in terms of molar concentrations the proteome subsets shown in Figure 1B that is affected by a more than twofold increase or decrease during aging between day 1 and day 22 in WT animals as estimated by label free absolute quantification. (C) Comparison of GO categories affected in the early (day 6 vs. day 1) and late stage in life (day 22 vs. day 6) of WT animals. All terms that were significantly affected in either of the two periods are displayed (Wilcoxon rank sum test at 5% FDR) and their relative changes were plotted against each other. The dashed grey line indicates the position of categories which are equally affected early and late in life. Selected outliers are indicated in the plot. (D) Abundance change of quantified subunits of the mitochondrial respiratory chain complex I. (E) Remaining clusters from time course expression patterns displayed in Figure 1E. Extent (F) and correlation (G) between the microarray study of Golden and Melov (Golden and Melov, 2004) and our proteomics dataset. The Pearson correlation R between both datasets is displayed.

Figure S2: (A) Protein abundance of subunits of the mitochondrial ribosome. (B) SILAC pulse labeling experiments. Worms were shifted to heavy media at day 5 (time point 0) and allowed to grow on the heavy food source for the indicated time. Boxplots of the H/L ratios at the

indicated time points are displayed. (C) Comparison of SILAC pulse labeling performed with WT and *eat-2* mutant worms, which are partially deficient in food uptake. Animals were shifted to a heavy food source at day 5 and harvested after six days of labeling.

Figure S3: Expression profiles of the candidates tested for lifespan extension due to decreased expression in the *daf-2* mutant as compared to WT. (B) Lifespan assays as shown in Figure 4B performed in *daf-16* mutant background.

Figure S4: Q40-YFP aggregation in dosage compensation deficient mutants. A muscle specific Q40-YFP transgene was introduced into the indicated genetic backgrounds and visible aggregates were quantified by fluorescence microscopy. (A) Representative microscopic images of animals 24h or 48h after L1 stage. (B, C) Quantification results 24h or 48h past L1 stage, respectively. Observations were grouped according to the numbers indicated in the figure legend. (D) Western blot showing the amount of Q40-YFP protein in wild-type and *dpy-28* mutant strains, using an antibody against GFP. Actin was used as loading control. (E and F) Q40-YFP transcript levels in wild-type and *dpy-28* mutant strains were detected by semi quantitative RT-PCR and quantified. Actin was used as loading control and values were normalized to actin level.

Figure S5: Validation of the biochemical aggregate isolation procedure using synthetic model proteins. Worms were lysed by ultrasonication and aggregates were isolated from clarified lysates by ultracentrifugation. Pellets were extracted twice with RIPA buffer, solubilized by

boiling in SDS and analyzed by SDS-PAGE and Western blotting. (A) Purification steps from animals expressing the aggregation-prone mutated firefly luciferase fused to GFP (FlucDM-GFP). The experiment was performed on worms grown at normal conditions or after a heat shock at 33°C for 90 min. (B) FlucDM-GFP recovery from animals before or after heat shock, or after 90 min recovery from heat shock. Western blot signals were quantified both in whole cell lysates and in insoluble fractions to determine the relative aggregation propensity of the model protein. Error bars represent standard deviations in three biological replicate experiments. (C) Influence of SDS on the recovery of aggregated FlucDM protein. A Coomassie stained gel and Western blot analysis after aggregate isolations from heat-shocked animals are displayed. (E) Aggregation propensity of FlucDM-GFP in young (day 1) and aged (day 19) worm populations (n=4). Western blot signals using an antibody against firefly luciferase of the same samples used in Figure S5D were quantified in total and aggregated fractions and relative insoluble proportions were calculated. (E, F) Insoluble and soluble proportions of the model protein Q35-YFP in young (day 1) and aged (day 7) worms (n=4) as determined by quantitative Western blotting using an antibody raised against GFP.

Figure S6: (A) T-test results of replicate analysis of aggregated fractions in young (day 1) and aged (day 12) animals. The proportions of proteins that were found to be significantly increased or decreased in aged worms at a 5% false discovery rate are shown. (B) Overlap between the significantly accumulated proteins found in the published datasets by Reis-Rodrigues *et al.*, David *et al.*, and this study. (C) Proportions of predicted subcellular localizations of all quantified proteins in aggregate fractions and the corresponding whole cell lysates of aged

WT animals (day 12). (D) Proportions of proteins that are predicted to contain at least one transmembrane segment. (E, F) Aggregate accumulation vs. abundance differences in the aggregated fractions of short lived strains *daf-16* and *hsf-1* as described in the legend to Figure 6B. (G) Experimental design of the SILAC-based quantitation of protein aggregation propensities. Total lysates of aged animals (day 12) were subjected to aggregate isolation. Whole cell lysates as well as insoluble and soluble fractions were quantified against an identical SILAC standard to determine the aggregated and soluble proportions of each protein. (H) Histograms of SILAC ratios measured in total lysate, insoluble and soluble fractions using the experimental setup depicted in Figure S6G. (I) Histogram of measured aggregation propensities in WT animals at day 12. (J, K, L) Properties of aggregation-prone proteins tested for lifespan extension with respect to the entire proteome. Candidates were selected for high rates of accumulation in the aggregated fractions between day 1 and day 12 (J). Additionally, aggregation propensities at day 12 (K) and absolute abundance as determined by label-free absolute quantification (L) are displayed.

Supplementary Tables

Table S1: GO term analysis of proteins with at least two-fold expression changes during aging in WT animals. Statistical data from Fisher Exact tests are provided. Only terms with an enrichment factor of greater than two are displayed. Benj. Hoch. FDR, Benjamini-Hochberg false discovery rate.

Table S2: Constituents of the proteostasis system and log2 fold-changes between young (day 1) and highly aged animals (day 22) in the total proteome.

Table S3: Categories of the proteostasis network affected during aging in WT.

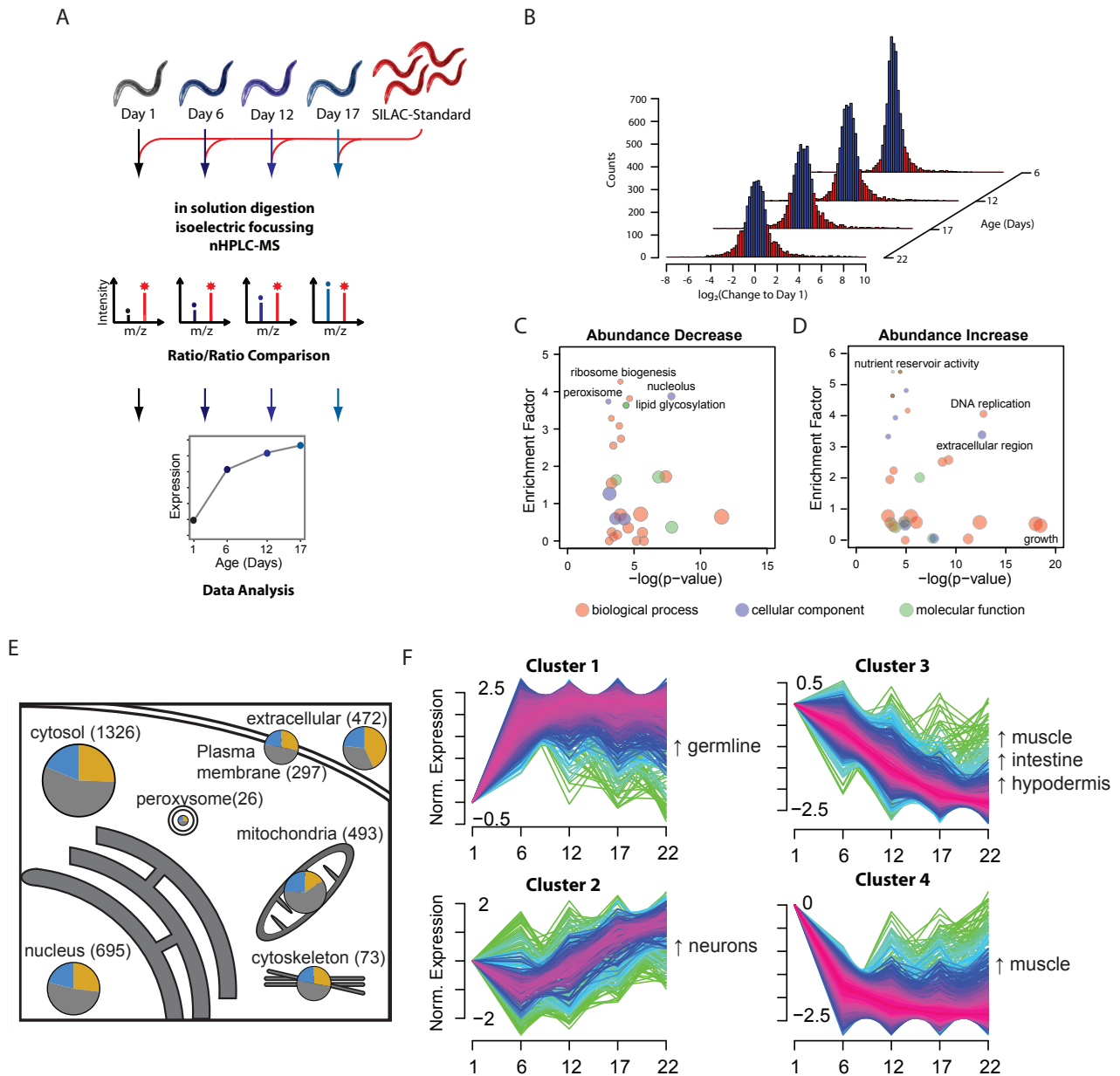
Table S4: Gene names and descriptions of candidates selected due to expression differences between *daf-2* and WT for lifespan assays as well as RNAi constructs used.

Table S5: Results and statistics of three individual lifespan experiments with WT animals maintained on bacteria expressing RNAi constructs against the indicated genes.

Table S6: The same experiments as described in the legend to Table S5 performed in *daf-16* mutant animals.

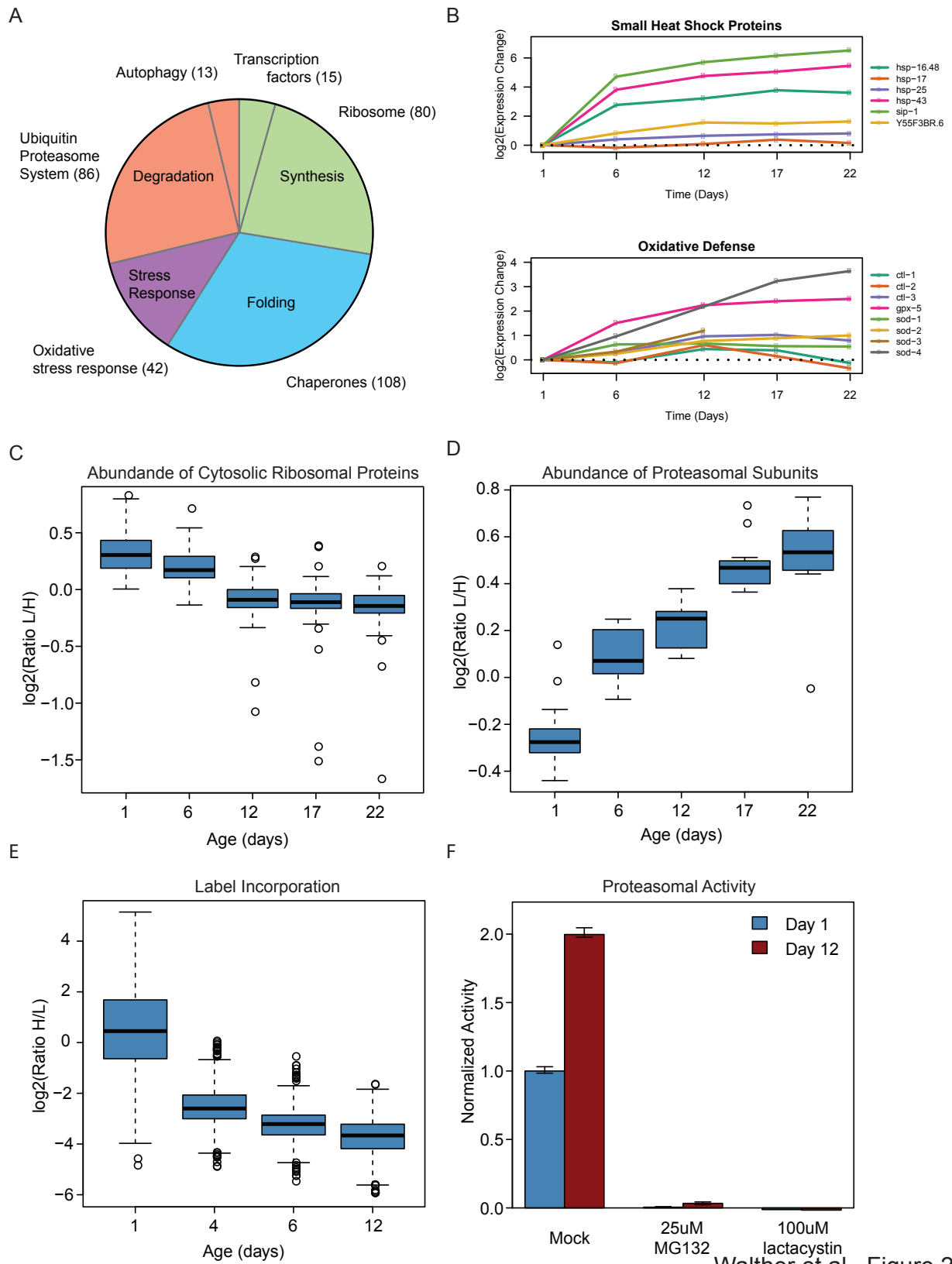
Table S7: 1D annotation distribution analysis of GO terms based on protein aggregation propensities in WT animals aged 12 days. Higher difference values indicate that the indicated terms are predominantly associated with highly aggregation-prone proteins.

Table S8 – S10: Lifespan assay data for candidates selected because of their aggregation properties as provided in tables S4 to S6.



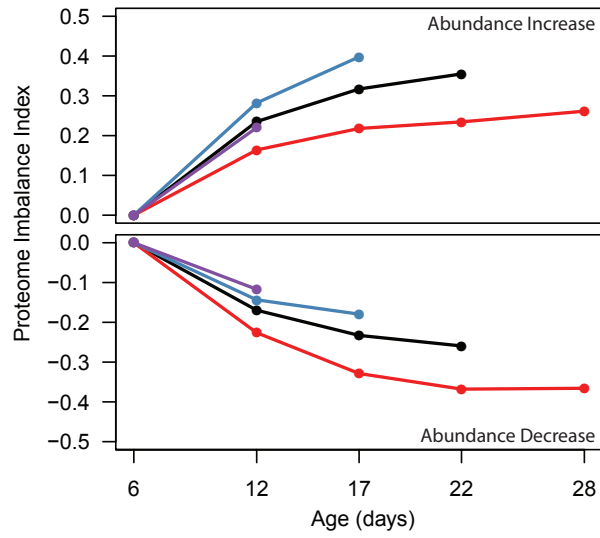
Walther et al., Figure 1

2 Results

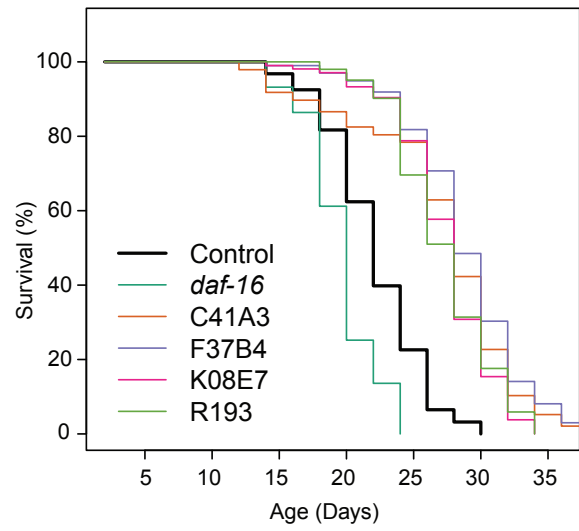


Walther et al., Figure 2

A

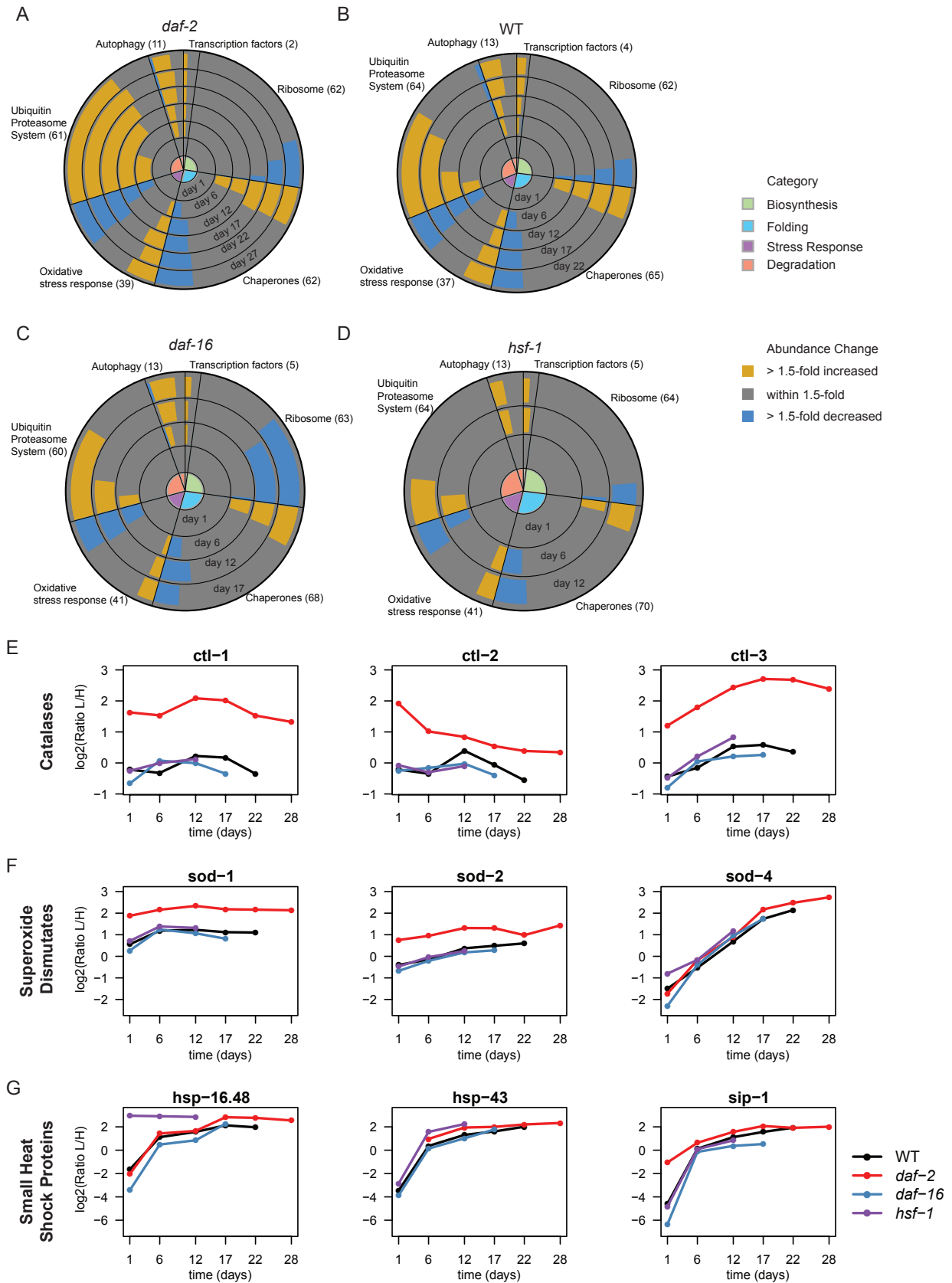


B



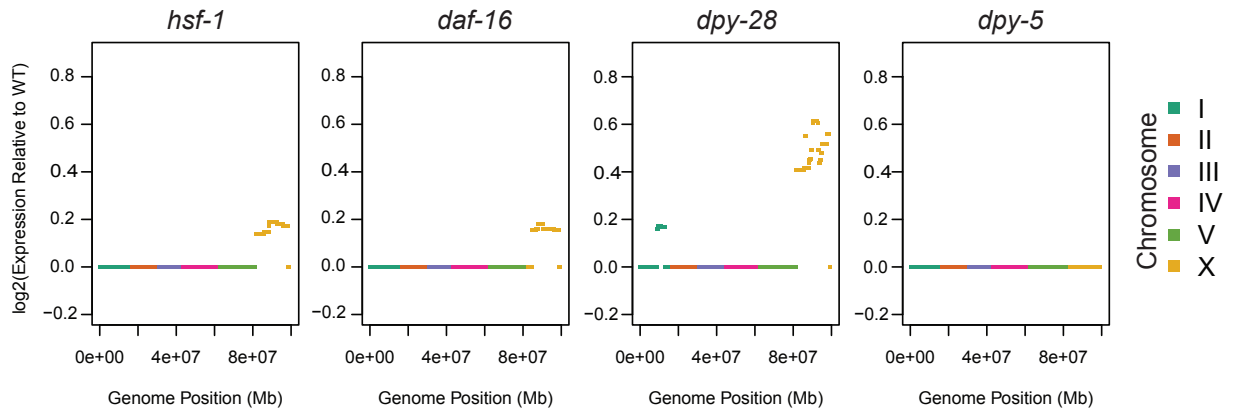
Walther et al., Figure 3

2 Results

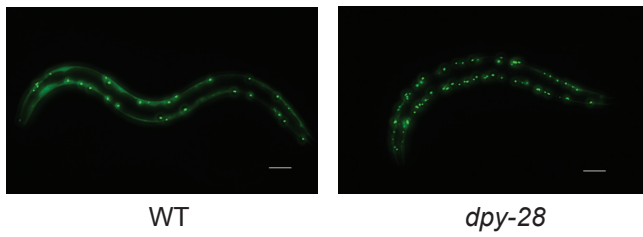


Walther et al., Figure 4

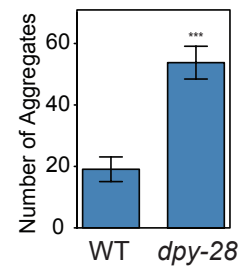
A



B

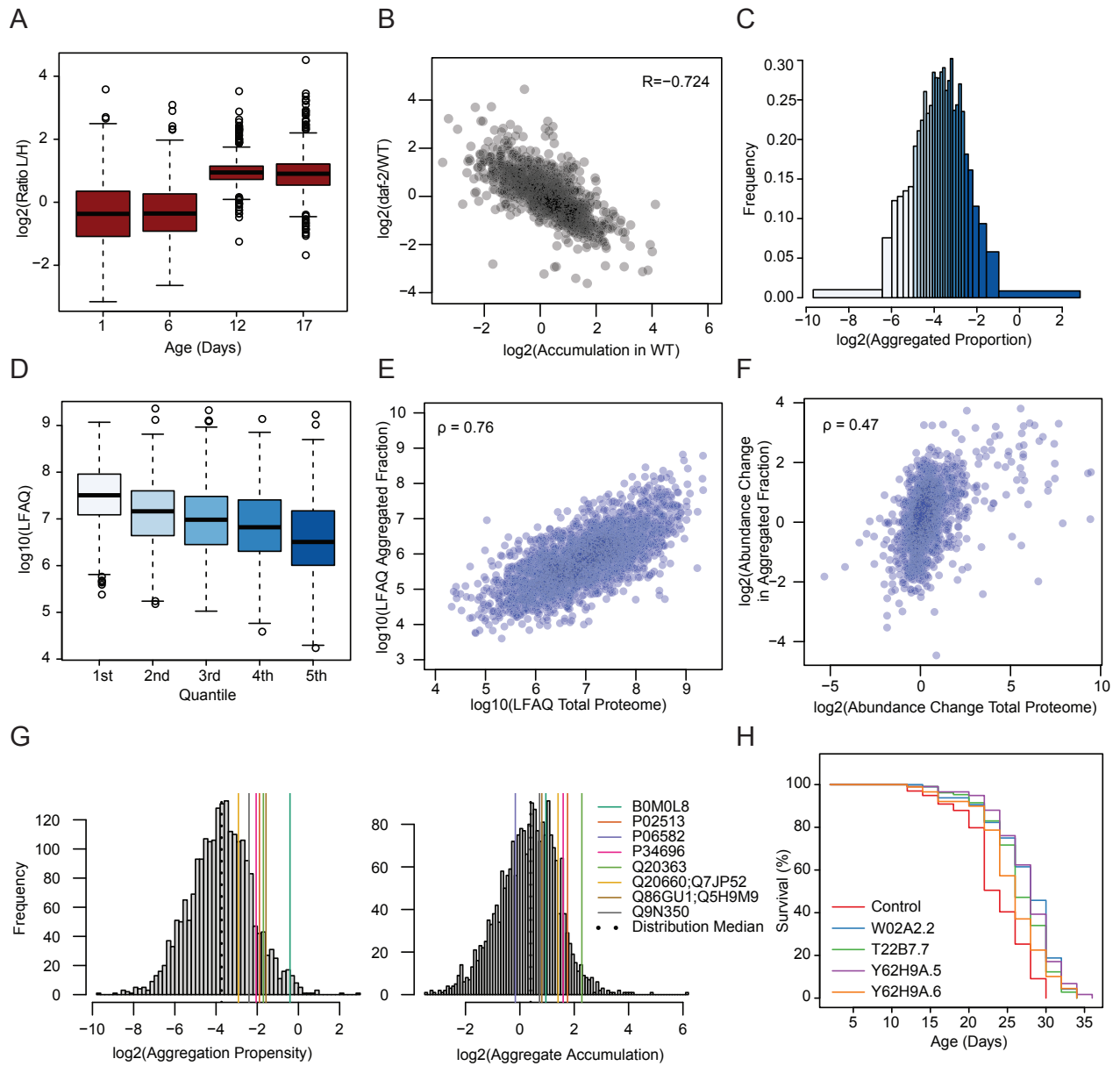


C

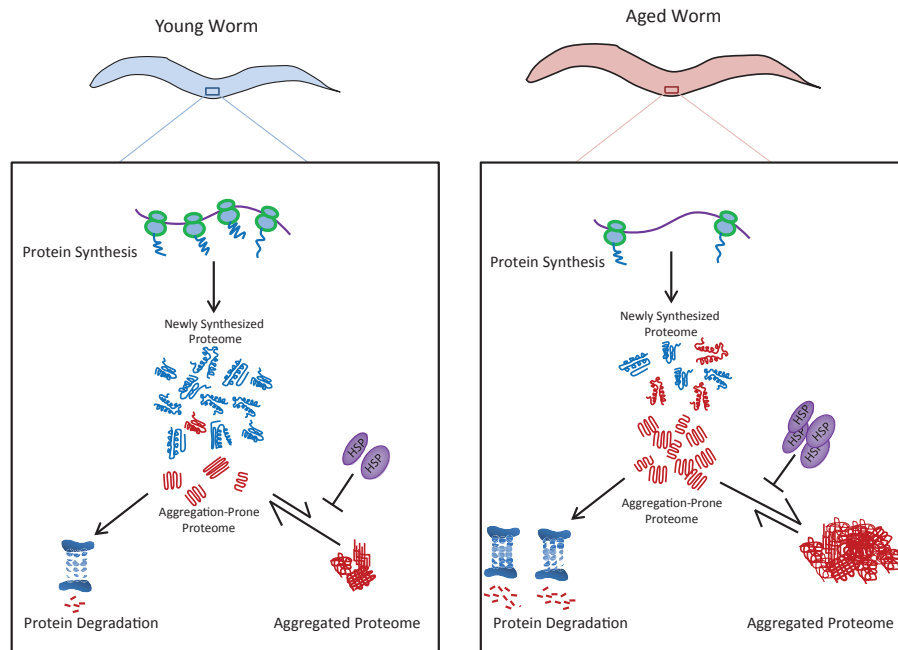


Walther et al., Figure 5

2 Results

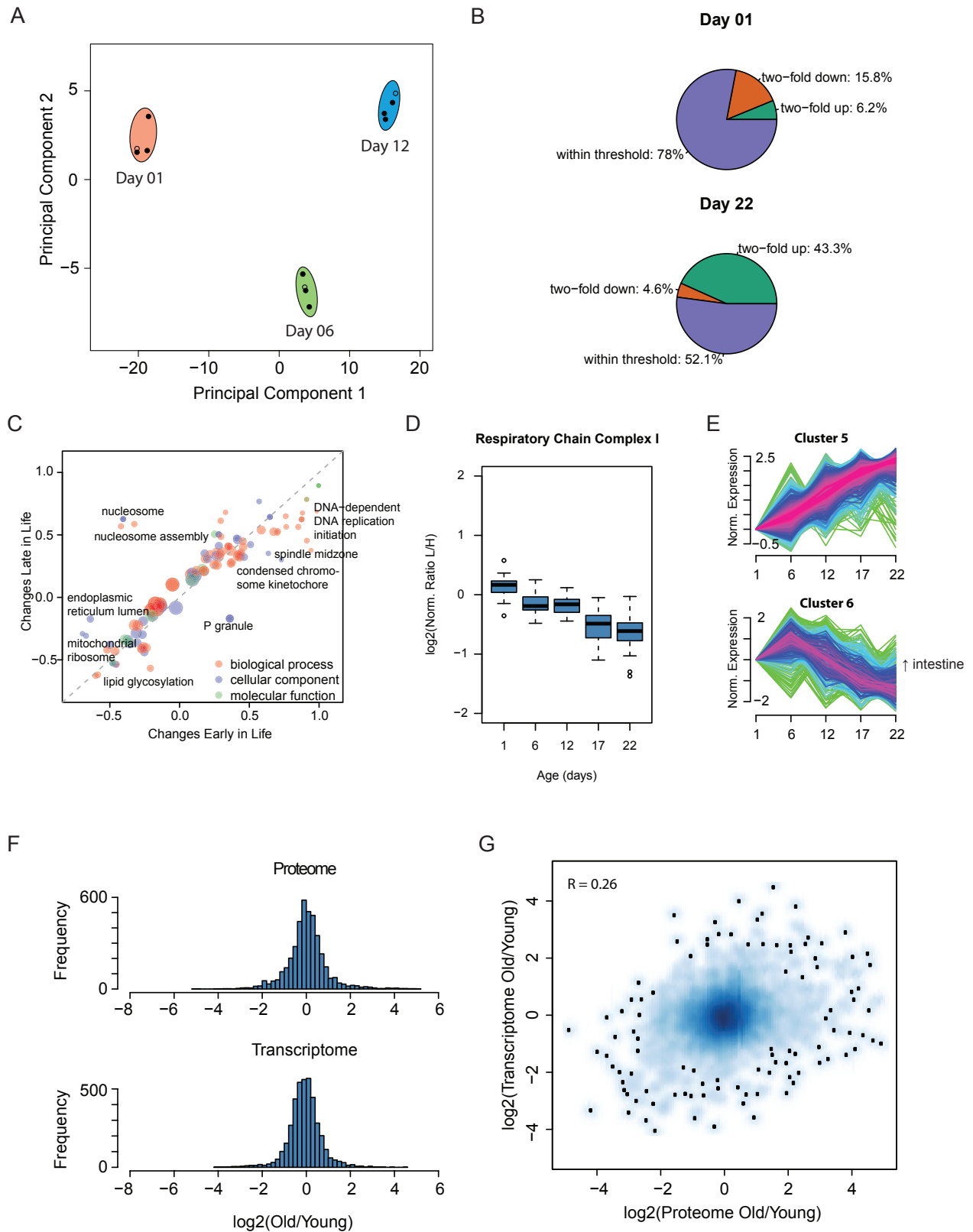


Walther et al., Figure 6

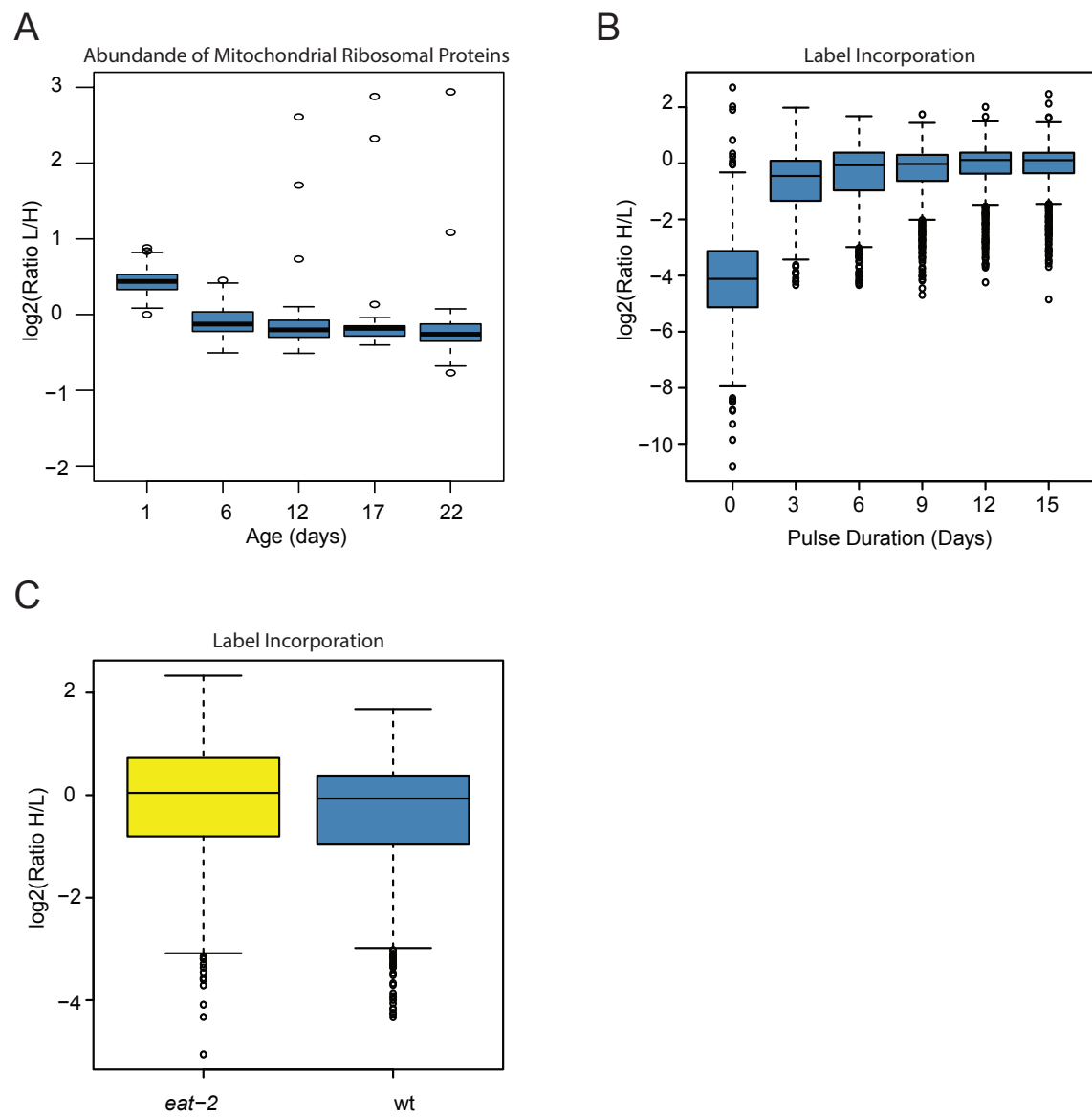


Walther et al., Figure 7

2 Results



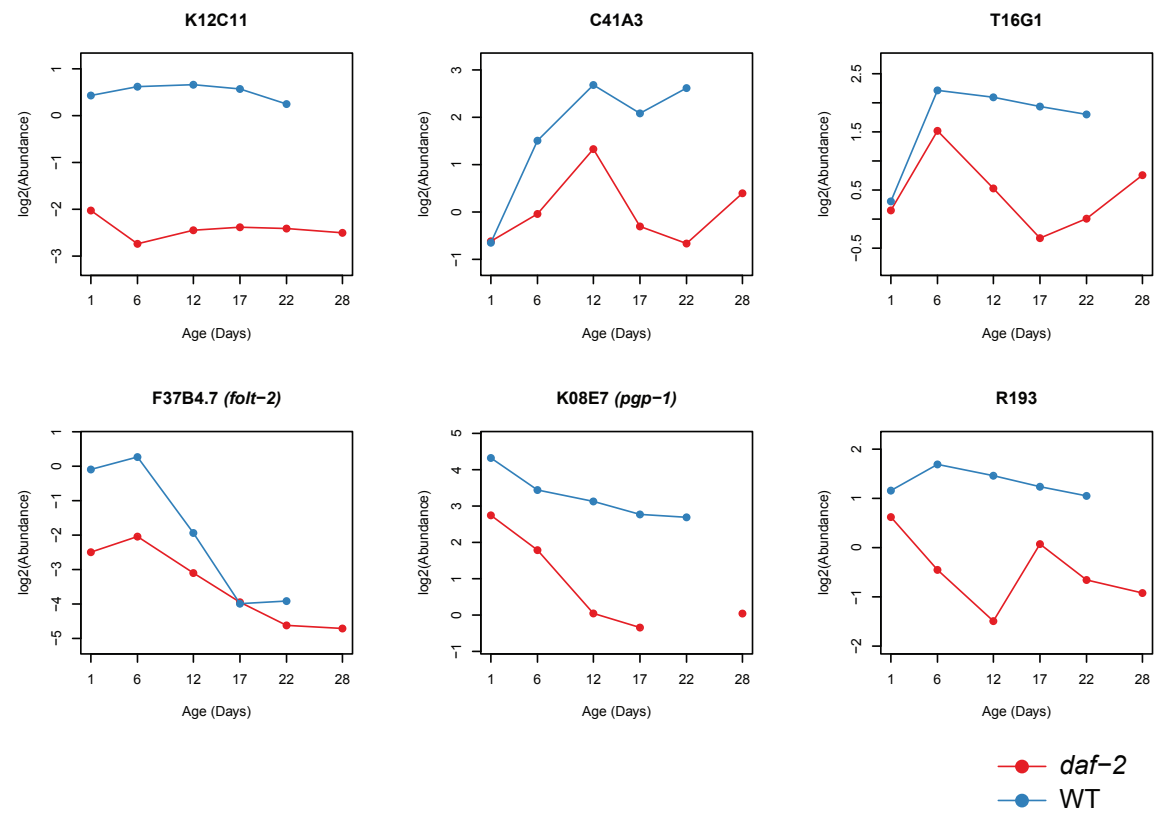
Walther et al., Suppl. Figure 1



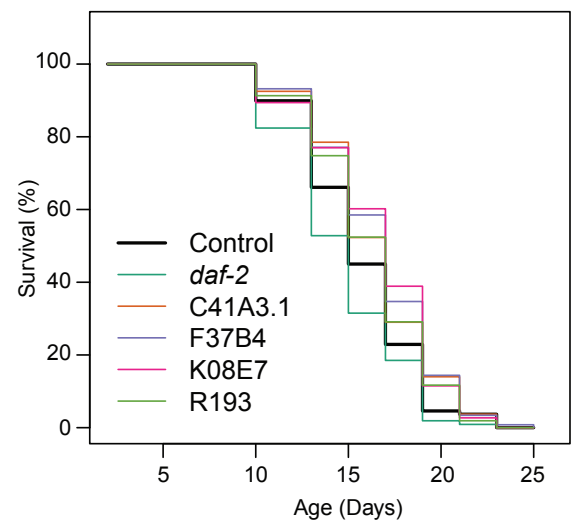
Walther et al., Suppl. Figure 2

2 Results

A

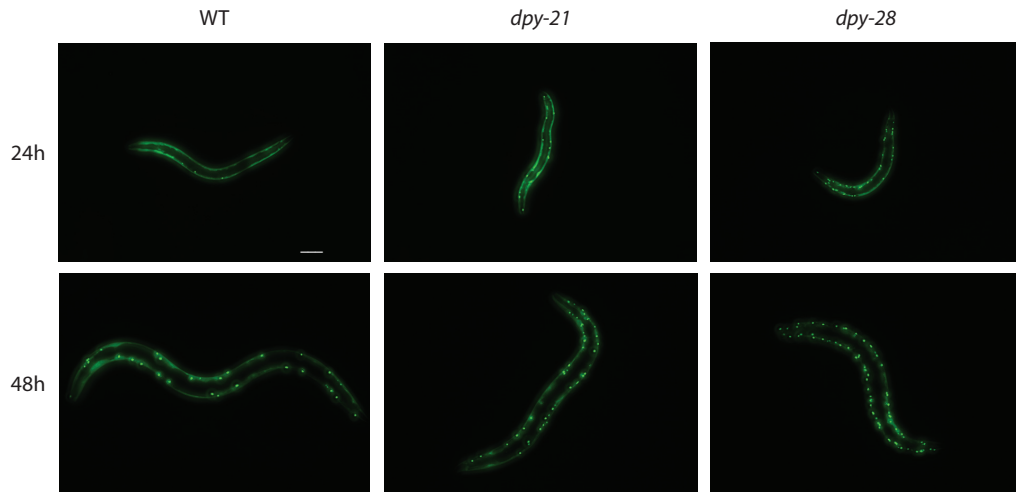


B

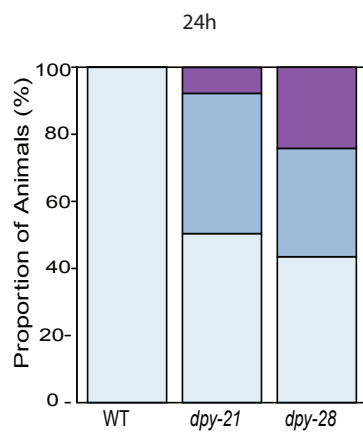


Walther et al., Suppl. Figure 3

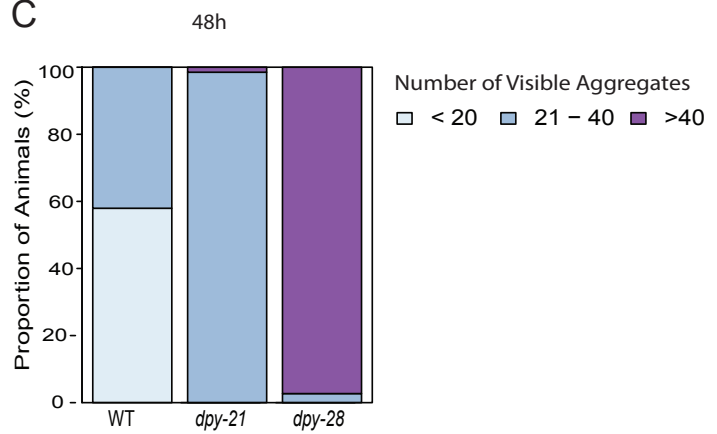
A



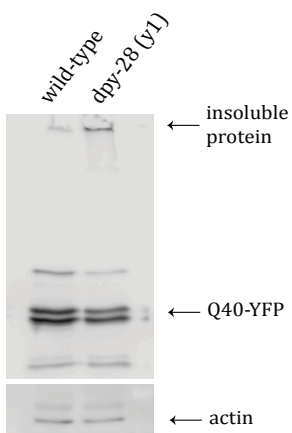
B



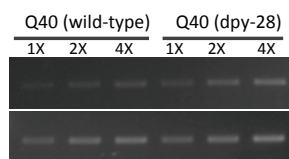
C



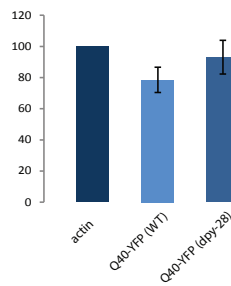
D

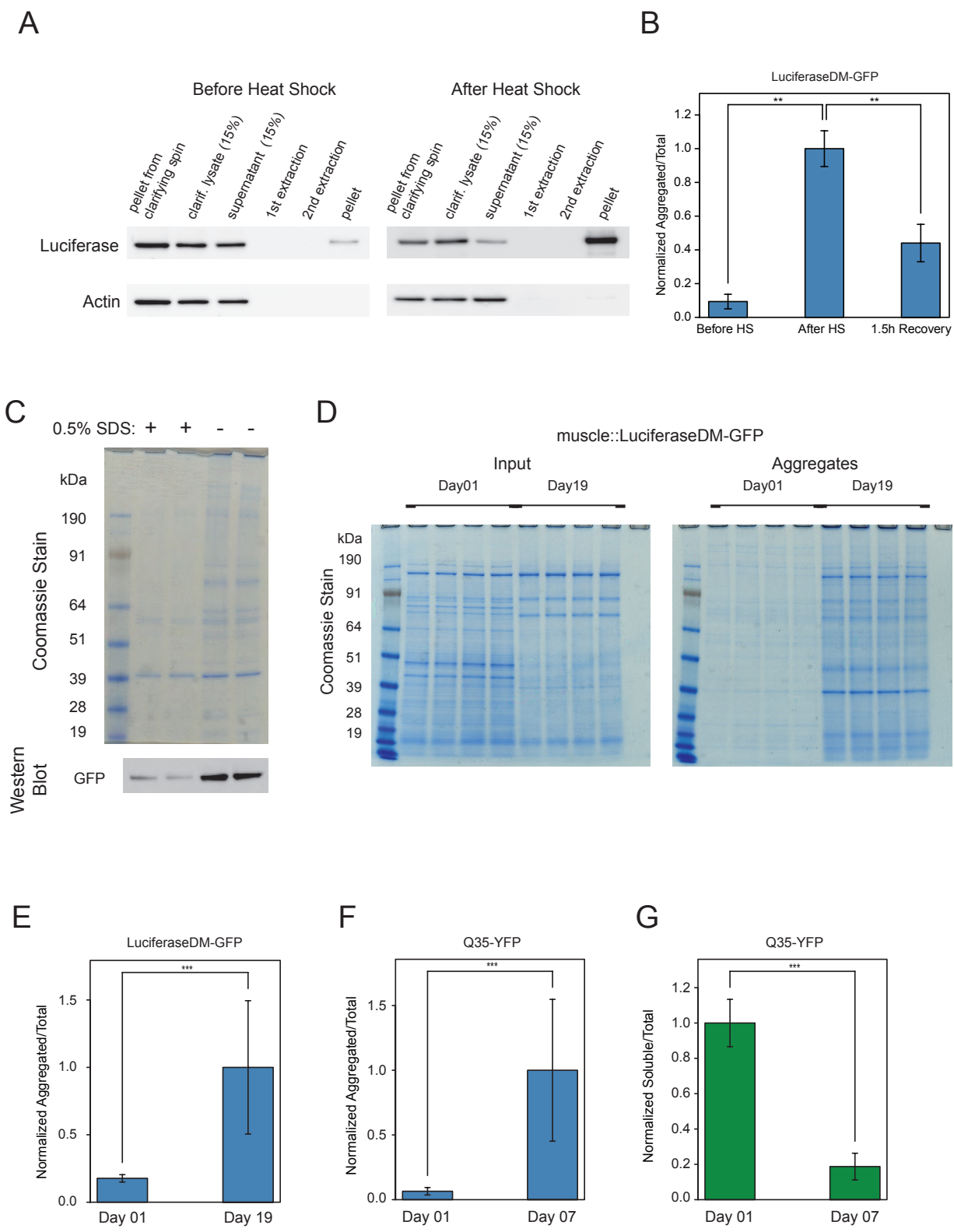


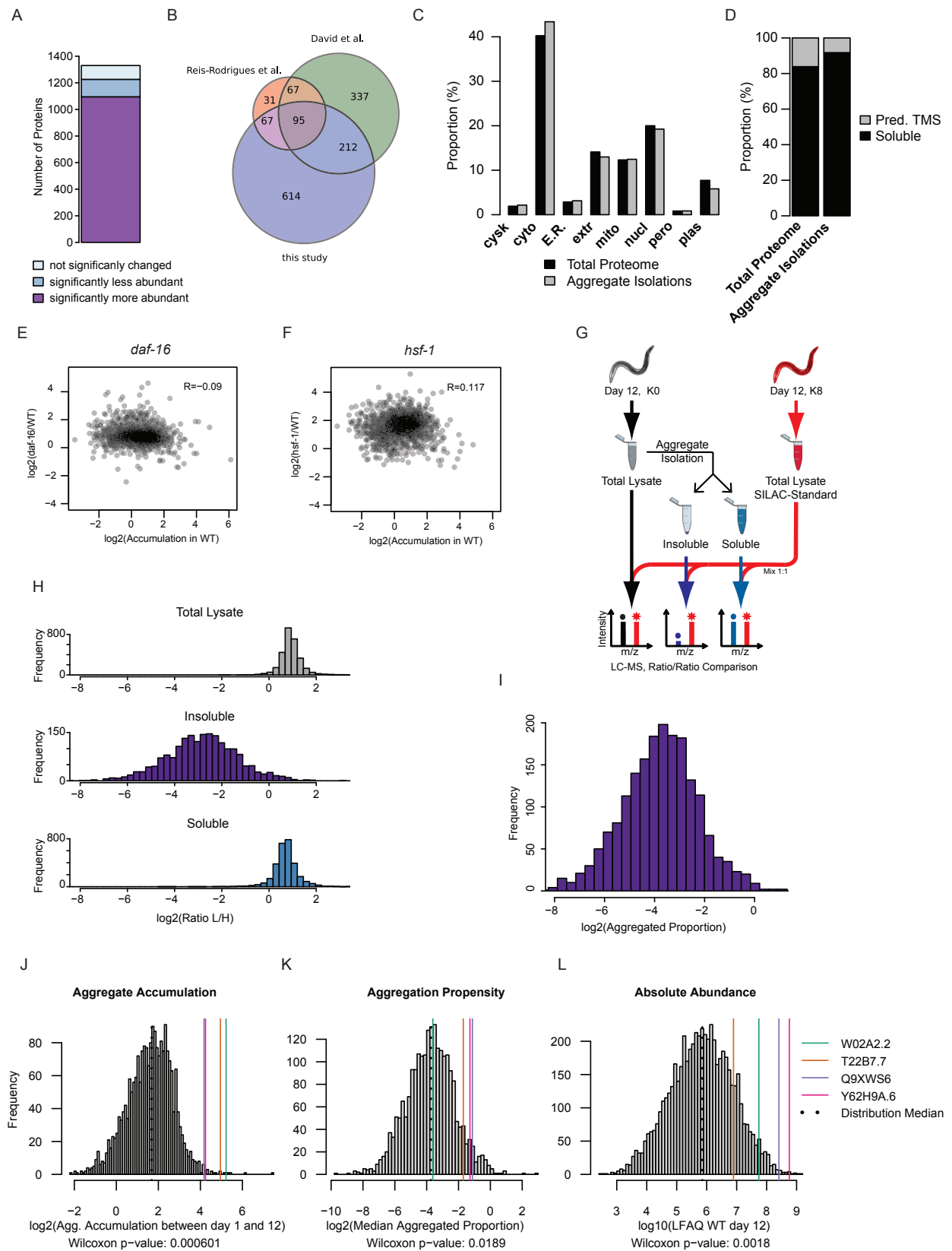
E



F







2 Results

Table S1: GO Term Enrichment of Proteins with >Two-fold Expression Change During Aging
>Two-fold Up-regulated

GO Category	GO Term	Enrichment factor	P value	Benj. Hoch. FDR
molecular_function	nutrient reservoir activity	5.41	3.92E-05	1.37E-02
molecular_function	magnesium chelatase activity	5.41	2.13E-04	4.25E-02
molecular_function	lipid transporter activity	5.41	3.92E-05	1.56E-02
biological_process	DNA-dependent DNA replication initiation	5.41	3.92E-05	4.28E-03
cellular_component	extracellular space	4.81	9.69E-06	1.47E-03
cellular_component	spindle midzone	4.64	2.24E-04	1.69E-02
molecular_function	DNA-directed DNA polymerase activity	4.64	2.24E-04	4.16E-02
biological_process	lipid transport	4.64	2.24E-04	1.63E-02
biological_process	mitotic sister chromatid segregation	4.16	6.90E-06	8.94E-04
biological_process	DNA replication	4.06	1.71E-13	1.50E-10
cellular_component	condensed chromosome	3.94	1.19E-04	1.05E-02
cellular_component	extracellular region	3.38	2.45E-13	2.60E-10
cellular_component	lysosome	3.33	6.17E-04	3.84E-02
biological_process	cell division	2.58	5.50E-10	1.60E-07
biological_process	cytokinesis	2.51	2.24E-09	6.04E-07
biological_process	mitosis	2.24	1.80E-04	1.40E-02
molecular_function	DNA binding	2.01	4.33E-07	2.42E-04

>Two-fold Down-regulated

Category column	Category value	Enrichment factor	P value	Benj. Hoch. FDR
biological_process	ribosome biogenesis	4.27	1.07E-04	9.59E-03
cellular_component	nucleolus	3.88	1.56E-08	4.13E-06
biological_process	lipid glycosylation	3.81	2.19E-05	2.55E-03
cellular_component	peroxisome	3.73	8.55E-04	4.77E-02
molecular_function	transferase activity, transferring hexosyl groups	3.63	3.94E-05	1.10E-02
molecular_function	carbohydrate binding	3.63	3.94E-05	1.22E-02
biological_process	cellular metabolic process	3.29	5.08E-04	3.17E-02
biological_process	rRNA processing	3.08	1.28E-04	1.07E-02
biological_process	lipid metabolic process	2.74	9.63E-05	8.86E-03
biological_process	biosynthetic process	2.56	3.63E-04	2.54E-02

table S2

Table S2: Components of the protestasis network				
Majority protein IDs	Protein ID	PN Category	Gene Name	log2(Abundance Change) Day 22 vs. Day 01
Q9BL02	Q9BL02	TFs	ceh-44	-0.819572
O44499	O44499	TFs	R02D3.3	0.393971
Q18034	Q18034	TFs	tag-182	0.73797
Q22703	Q22703	TFs	dpl-1	0.981504
Q95PZ4	Q95PZ4	TFs	Y66D12A.15	1.322669
Q8MYM8	Q8MYM8	TFs	Y39B6A.36	2.407454
P48162	P48162	Ribosome	rpl-25.1	-2.270054
Q21930	Q21930	Ribosome	rpl-28	-1.040522
P49181	P49181	Ribosome	rpl-36	-1.025348
O01868	O01868	Ribosome	rpl-24.1	-0.885498
P91128	P91128	Ribosome	rpl-13	-0.810403
Q09533	Q09533	Ribosome	rpl-10	-0.786909
O45946	O45946	Ribosome	rpl-18	-0.671873
P91913	P91913	Ribosome	rla-1	-0.629733
O45226	O45226	Ribosome	rpl-29	-0.598498
P49041	P49041	Ribosome	rps-5	-0.591549
O01802	O01802	Ribosome	rpl-7	-0.580656
Q9XVE9	Q9XVE9	Ribosome	rpl-14	-0.576073
Q19877	Q19877	Ribosome	rps-23	-0.570765
P48166	P48166	Ribosome	rpl-41	-0.542129
O18650	O18650	Ribosome	rps-19	-0.532733
Q9XVF7	Q9XVF7	Ribosome	rpl-8	-0.486366
O01504	O01504	Ribosome	rpa-2	-0.475205
Q95Y90	Q95Y90	Ribosome	rpl-9	-0.464085
O17570	O17570	Ribosome	rpl-38	-0.456047
O02056	O02056	Ribosome	rpl-4	-0.43422
Q94300	Q94300	Ribosome	rpl-11.1	-0.426663
P34334	P34334	Ribosome	rpl-21	-0.425077
P34662	P34662	Ribosome	rpl-35	-0.388672
Q20206	Q20206	Ribosome	rps-11	-0.383896
A3QMC5	A3QMC5	Ribosome	rpl-34	-0.381042
O01692	O01692	Ribosome	rps-17	-0.365086
Q1XFY9	Q1XFY9	Ribosome	rps-24	-0.358892
Q9XVP0	Q9XVP0	Ribosome	rps-15	-0.354444
P48156	P48156	Ribosome	rps-8	-0.350309
Q9U1X9	Q9U1X9	Ribosome	rla-2	-0.348633
P91914	P91914	Ribosome	rpl-27	-0.344512

table S2

O45499	O45499	Ribosome	rps-26	-0.344217
P49197	P49197	Ribosome	rps-21	-0.324447
P49405	P49405	Ribosome	rpl-5	-0.311332
P49180	P49180	Ribosome	rpl-33	-0.309192
O02639	O02639	Ribosome	rpl-19	-0.301762
Q9U2A8	Q9U2A8	Ribosome	rpl-43	-0.296358
P52821	P52821	Ribosome	rps-25	-0.29269
P48152	P48152	Ribosome	rps-3	-0.278364
Q27389	Q27389	Ribosome	rpl-16	-0.259682
P47991	P47991	Ribosome	rpl-6	-0.258502
P48158	P48158	Ribosome	rpl-23	-0.257623
P52819	P52819	Ribosome	rpl-22	-0.255299
Q20228	Q20228	Ribosome	rps-9	-0.254919
O18240	O18240	Ribosome	rps-18	-0.234986
Q93572	Q93572	Ribosome	rpa-0	-0.23301
P49196	P49196	Ribosome	rps-12	-0.223988
P91374	P91374	Ribosome	rpl-15	-0.208308
P51403	P51403	Ribosome	rps-2	-0.207857
Q8WQA8	Q8WQA8	Ribosome	rps-20	-0.204029
Q9TXP0	Q9TXP0	Ribosome	rps-27	-0.199306
O01869	O01869	Ribosome	rps-10	-0.195596
Q22054	Q22054	Ribosome	rps-16	-0.186814
Q23312	Q23312	Ribosome	rps-7	-0.183804
P51404	P51404	Ribosome	rps-13	-0.177431
P46769	P46769	Ribosome	rps-0	-0.173889
O44480	O44480	Ribosome	rpl-20	-0.168853
Q9NEN6	Q9NEN6	Ribosome	rps-6	-0.156726
P48154	P48154	Ribosome	rps-1	-0.144399
Q9XWS4	Q9XWS4	Ribosome	rpl-30	-0.113173
P48150	P48150	Ribosome	rps-14	-0.11106
Q9N3X2	Q9N3X2	Ribosome	rps-4	0.035463
Q20647	Q20647	Ribosome	rpl-25.2	0.085422
P49632	P49632	Ribosome	ubq-2	0.213662
Q23338	Q23338	Chaperones	fkf-4	-3.300837
Q17770	Q17770	Chaperones	pdi-2	-1.870924
P34329	P34329	Chaperones	C14B9.2	-1.590235
P27798	P27798	Chaperones	crt-1	-1.181437
P91189	P91189	Chaperones	dnj-7	-1.030239
Q18421	Q18421	Chaperones	C34C12.8	-1.02002
Q17438	Q17438	Chaperones	dnj-1	-1.019141
P52014	P52014	Chaperones	cyn-6	-0.998941

table S2

Q8MPX3	Q8MPX3	Chaperones	dnj-20	-0.845115
Q20752	Q20752	Chaperones	stc-1	-0.82132
Q9XWE1	Q9XWE1	Chaperones	dnj-27	-0.808008
P27420	P27420	Chaperones	hsp-3	-0.797316
Q11067	Q11067	Chaperones	tag-320	-0.681787
Q965Q1	Q965Q1	Chaperones	Y22D7AL.10	-0.469788
G5EDB6	G5EDB6	Chaperones	ppgn-1	-0.411907
Q94216	Q94216	Chaperones	dnj-11	-0.400285
Q2L6Y6	Q2L6Y6	Chaperones	R151.7	-0.393951
P52013	P52013	Chaperones	cyn-5	-0.353362
Q9N4L6	Q9N4L6	Chaperones	ZK973.11	-0.303759
P50140	P50140	Chaperones	hsp-60	-0.280751
Q21993	Q21993	Chaperones	pfd-5	-0.230403
P52554	P52554	Chaperones	pfd-6	-0.227796
Q8TA83	Q8TA83	Chaperones	dnj-10	-0.214883
O16303	O16303	Chaperones	dnj-19	-0.178579
Q9N5M2	Q9N5M2	Chaperones	pdf-2	-0.1676
Q9N3T5	Q9N3T5	Chaperones	spg-7	-0.128894
O45502	O45502	Chaperones	dnj-12	-0.119789
P54812	P54812	Chaperones	cdc-48.2	-0.093031
P11141	P11141	Chaperones	hsp-6	-0.05989
Q22758	Q22758	Chaperones	T24H7.2	-0.052601
Q9N456	Q9N456	Chaperones	glrx-10	-0.02015
Q17967	Q17967	Chaperones	pdi-1	-0.01018
P47208	P47208	Chaperones	cct-4	-0.00122
G5ED07	G5ED07	Chaperones	pdi-3	0.036827
P52009	P52009	Chaperones	cyn-1	0.052393
Q9N4J8	Q9N4J8	Chaperones	cct-3	0.058982
P41988	P41988	Chaperones	cct-1	0.075503
Q9U2S6	Q9U2S6	Chaperones	cyn-13	0.082081
P47207	P47207	Chaperones	cct-2	0.10071
P91243	P91243	Chaperones	dnj-9	0.109249
Q9N358	Q9N358	Chaperones	cct-8	0.10928
Q9XTU9	Q9XTU9	Chaperones	glrx-5	0.115571
Q9NAF9	Q9NAF9	Chaperones	pinn-4	0.222311
Q9XXI7	Q9XXI7	Chaperones	cyn-16	0.233219
P46550	P46550	Chaperones	cct-6	0.235433
P09446	P09446	Chaperones	hsp-1	0.253885
P52018	P52018	Chaperones	cyn-11	0.329666
Q05036	Q05036	Chaperones	C30C11.4	0.330965
Q18688	Q18688	Chaperones	daf-21	0.353901

table S2

P20163	P20163	Chaperones	hsp-4	0.414079
Q95Y44	Q95Y44	Chaperones	dnj-30	0.425666
Q20774	Q20774	Chaperones	dnj-13	0.43117
P52012	P52012	Chaperones	cyn-4	0.441249
O16259	O16259	Chaperones	sti-1	0.463122
O44739	O44739	Chaperones	bag-1	0.466069
O17002	O17002	Chaperones	dnj-22	0.480879
Q18445	Q18445	Chaperones	cyn-12	0.482127
P34652	P34652	Chaperones	cnx-1	0.488331
Q9U2Q8	Q9U2Q8	Chaperones	fkf-2	0.526578
Q9U1Q3	Q9U1Q3	Chaperones	cyn-15	0.635047
P54811	P54811	Chaperones	cdc-48.1	0.730264
Q9N492	Q9N492	Chaperones	pinn-1	0.745625
O45418	O45418	Chaperones	fkf-6	0.791455
G5EE04	G5EE04	Chaperones	hip-1	0.893728
G5ECY6	G5ECY6	Chaperones	chn-1	0.918543
Q22751	Q22751	Chaperones	dnj-23	1.557921
Q9N350	Q9N350	Chaperones	Y55F3BR.6	1.623039
P02513	P02513	Chaperones	hsp-16.48	3.854937
B0M0L8	B0M0L8	Chaperones	hsp-43	5.500406
Q20363	Q20363	Chaperones	sip-1	6.517886
O02089	O02089	oxSR	msra-1	-3.592271
A8WFK6	A8WFK6	oxSR	gpx-7	-2.114834
O17397	O17397	oxSR	F52H2.6	-1.8946
Q21032	Q21032	oxSR	idh-1	-1.875446
Q17770	Q17770	oxSR	pdi-2	-1.870924
G5EE41	G5EE41	oxSR	cuc-1	-1.750963
Q21219	Q21219	oxSR	pept-1	-1.742017
P34329	P34329	oxSR	C14B9.2	-1.590235
G5EC91	G5EC91	oxSR	dpy-11	-1.377119
O02621	O02621	oxSR	F26E4.12	-1.191312
Q9N2W7	Q9N2W7	oxSR	Y94H6A.8	-0.809261
Q9XWE1	Q9XWE1	oxSR	dnj-27	-0.808008
Q9N357	Q9N357	oxSR	Y55F3AR.2	-0.803335
Q11067	Q11067	oxSR	tag-320	-0.681787
P90925	P90925	oxSR	pah-1	-0.643779
O18236	O18236	oxSR	nuo-3	-0.613147
Q17688	Q17688	oxSR	C06A6.5	-0.547203
Q27487	Q27487	oxSR	ctl-2	-0.393489
Q9N4L6	Q9N4L6	oxSR	ZK973.11	-0.303759
Q9BKU4	Q9BKU4	oxSR	phb-1	-0.194577

table S2

Q9TW67	Q9TW67	oxSR	png-1	-0.175902
P91442	P91442	oxSR	T10H10.2	-0.025716
Q17967	Q17967	oxSR	pdi-1	-0.01018
G5ED07	G5ED07	oxSR	pdi-3	0.036827
O62327	O62327	oxSR	R05H10.5	0.144879
P50093	P50093	oxSR	phb-2	0.157412
Q3Y409	Q3Y409	oxSR	F52E1.13	0.381529
Q6EZG4	Q6EZG4	oxSR	glrx-3	0.414082
G5EFF8	G5EFF8	oxSR	C30H7.2	0.421277
Q20117	Q20117	oxSR	gcs-1	0.495269
Q10664	Q10664	oxSR	mek-2	0.627131
Q9TXY8	Q9TXY8	oxSR	trx-4	0.689014
Q19683	Q19683	oxSR	F21D5.5	0.790692
G5EES9	G5EES9	oxSR	txl	0.872802
P31161	P31161	oxSR	sod-2	0.982488
O61213	O61213	oxSR	bli-3	1.526075
Q93204	Q93204	oxSR	gpx-5	2.677219
Q03598	Q03598	UPS	C40H1.6	-0.772614
Q21106	Q21106	UPS	dcaf-1	-0.756369
Q9U1Y9	Q9U1Y9	UPS	skr-4	-0.435981
Q18447	Q18447	UPS	hecd-1	-0.391766
G5EDD8	G5EDD8	UPS	skr-2	-0.323651
P52478	P52478	UPS	ubc-1	-0.290564
G5EDT9	G5EDT9	UPS	F36A2.13	-0.130791
P91430	P91430	UPS	T03F1.1	-0.013457
Q10051	Q10051	UPS	T10F2.4	0.005989
Q9XVK5	Q9XVK5	UPS	ubc-12	0.017965
G5ECU1	G5ECU1	UPS	skr-1	0.065153
Q9XTT9	Q9XTT9	UPS	rpt-6	0.271356
O76371	O76371	UPS	rpt-5	0.357458
P91477	P91477	UPS	pbs-4	0.419447
P52012	P52012	UPS	cyn-4	0.441249
Q17820	Q17820	UPS	aos-1	0.444061
Q9GUP2	Q9GUP2	UPS	eel-1	0.447582
O01524	O01524	UPS	F19F10.9	0.46922
Q9GZH5	Q9GZH5	UPS	rpn-1	0.47625
P35129	P35129	UPS	let-70	0.489518
P91133	P91133	UPS	ubr-1	0.503064
Q20585	Q20585	UPS	rpn-7	0.514255
Q18217	Q18217	UPS	ula-1	0.52189
Q95XX0	Q95XX0	UPS	ubc-13	0.525489

table S2

Q23449	Q23449	UPS	rpn-12	0.525525
Q9BKS1	Q9BKS1	UPS	elc-1	0.538547
G5ECR7	G5ECR7	UPS	elb-1	0.555126
Q04908	Q04908	UPS	rpn-3	0.569564
O61742	O61742	UPS	rpn-10	0.585565
O61792	O61792	UPS	rpn-8	0.589338
Q09583	Q09583	UPS	pas-7	0.60294
P46502	P46502	UPS	rpt-3	0.61424
Q96618	Q96618	UPS	pbs-1	0.62596
Q21554	Q21554	UPS	ddb-1	0.655003
Q27481	Q27481	UPS	uba-1	0.656036
O62102	O62102	UPS	pbs-2	0.679783
Q18787	Q18787	UPS	rpt-1	0.684665
O17736	O17736	UPS	D2085.4	0.686212
Q22253	Q22253	UPS	rpn-9	0.686457
Q95017	Q95017	UPS	ubc-9	0.689047
Q95005	Q95005	UPS	pas-4	0.693026
G5EBK4	G5EBK4	UPS	atg-7	0.711062
P34477	P34477	UPS	ubc-7	0.723635
O16368	O16368	UPS	rpt-2	0.744974
Q9N599	Q9N599	UPS	pas-3	0.764344
Q27488	Q27488	UPS	pas-2	0.812707
Q23237	Q23237	UPS	pbs-3	0.813749
O76577	O76577	UPS	rpn-11	0.81496
Q19324	Q19324	UPS	rpn-5	0.839889
Q23457	Q23457	UPS	rbx-1	0.839969
Q95008	Q95008	UPS	pas-5	0.862351
P90868	P90868	UPS	pbs-7	0.872052
O44156	O44156	UPS	pas-6	0.877004
Q9TZ69	Q9TZ69	UPS	ubc-20	0.88807
G5ECY6	G5ECY6	UPS	chn-1	0.918543
Q9XUV0	Q9XUV0	UPS	pbs-5	0.925739
Q19360	Q19360	UPS	uba-3	0.93582
O17586	O17586	UPS	pas-1	0.973252
Q17392	Q17392	UPS	cul-4	1.063987
P34286	P34286	UPS	pbs-6	1.133585
Q9N369	Q9N369	UPS	atg-3	1.14194
Q17389	Q17389	UPS	cul-1	1.177409
Q9NAN1	Q9NAN1	UPS	uba-2	1.342353
Q21633	Q21633	UPS	ubc-18	1.43499
Q95QN6	Q95QN6	UPS	EEED8.16	1.436282

table S2

Q17391	Q17391	UPS	cul-3	1.47004
G5EG38	G5EG38	UPS	emb-27	1.607611
Q22342	Q22342	Autophagy	atg-11	-0.086027
Q23669	Q23669	Autophagy	ZK930.1	0.146815
O16466	O16466	Autophagy	atg-18	0.214917
Q17796	Q17796	Autophagy	hgrs-1	0.348715
Q9NA30	Q9NA30	Autophagy	atg-4.1	0.409934
Q9XWU8	Q9XWU8	Autophagy	epg-3	0.50184
Q22799	Q22799	Autophagy	dlc-1	0.6007
G5EBK4	G5EBK4	Autophagy	atg-7	0.711062
Q9N369	Q9N369	Autophagy	atg-3	1.14194
Q09490	Q09490	Autophagy	lgg-1	1.239914

2 Results

Table S3: Components of the proteostasis network affected by aging.

	all	TFs	Ribosome	Chaperone	oxSR	UPS	Autophagy
>1.5-fold up	65	4	0	11	7	39	4
>1.5-fold down	42	1	10	13	16	2	0
changed	107	5	10	24	23	41	4
sum	254	6	64	70	37	67	10

Table S4: Lifespan candidates selected from total proteome

Gene	Description	RNAi Clone	Expression cluster (wormbase)
K12C11.1	Putative metallopeptidase (498 aa)	I-1O11	
C41A3.1	Non-ribosomal peptide synthetase/polyketide synthase (7829 aa)	X-3E19	differentially_expressed_with_age_medoid_6
T16G1.4	Predicted small molecule kinase (436 aa)	V-8J17	
K08D8.6	Uncharacterized (CUB-like domain) (491 aa)	IV-6H18	
F37B4.7 (folt-2)	putative folate transporter (424 aa)	V-2J03	age_regulated_genes
K08E7.9 (pgp-1)	pgp-1 encodes a transmembrane protein that is a member of the P-glycoprotein subclass of the ATP-binding cassette (ABC) transporter superfamily (1321 aa)	IV-6P19	
R193.2	Uncharacterized (SEA domain) (1899 aa)	X-1E16	age_regulated_genes

2 Results

Table S5: Lifespan Assays, candidates selected from total proteomes (wild-type worms)

RNAi	Mean Lifespan	% change	Log Rank p-value	Total animals died/Total
eV	22.11 +/- 0.37			93/120
eV	21.95 +/- 0.67			81/100
eV	22.55 +/- 0.73			76/100
daf-2	36.88	66.8%		103/120
daf-16	19.59 +/- 0.26	-11.4%	6.10E-09	80/120
daf-16	17.71 +/- 0.39	-19.3%	0.00E+00	89/100
daf-16	19.29 +/- 0.39	-14.5%	0.00E+00	85/100
K12C11.1	24.48 +/- 0.45	10.5%	2.00E-06	96/120
K12C11.1	23.42 +/- 0.68	6.7%	0.053	90/100
K12C11.1	23.91 +/- 0.56	6.0%	0.6022	85/100
C41A3.1	27.05 +/- 0.61	22.1%	0.00E+00	97/120
C41A3.1	24.82 +/- 0.74	11.5%	0.0001	100/115
C41A3.1	25.75 +/- 0.74	14.2%	0.0013	63/75
T16G1.4	23.78 +/- 0.41	7.5%	8.00E-04	101/120
T16G1.4	26.56 +/- 0.63	21.0%	4.50E-07	79/100
T16G1.4	NA	NA		NA
K08D8.6	26.12 +/- 0.38	18.1%	0.00E+00	103/120
K08D8.6	26.67 +/- 0.74	21.5%	1.70E-08	90/100
K08D8.6	28.83 +/- 0.64	27.8%	0.00E+00	84/100
F37B4.7	28.77 +/- 0.45	30.0%	0.00E+00	99/120
F37B4.7	24.3 +/- 0.59	10.7%	0.0136	92/100
F37B4.7	25.18 +/- 0.49	11.6%	5.29E-02	93/100
K08E7.9	27.29 +/- 0.36	23.4%	0.00E+00	104/120
K08E7.9	22.23 +/- 0.57	1.3%	0.4457	77/100
K08E7.9	24.72 +/- 0.52	9.6%	0.0675	104/120
R193.2	27.18 +/- 0.36	22.9%	0.00E+00	102/120
R193.2	24.29 +/- 0.63	10.6%	0.0042	98/110
R193.2	26.54 +/- 0.52	17.7%	0.0001	83/100

Table S6: Lifespan Assays (*daf-16* mutant background), candidates selected from total proteomes

RNAi	Mean Lifespan	% change	Log Rank value	p- Total animals died/Total
eV	15.54 +/- 0.3			109/120
eV	17.45 +/- 0.35			91/120
daf-2	14.58 +/- 0.3	-6.2%	0.0451	108/120
daf-2	16.89 +/- 0.35	-3.2%	0.3522	99/120
K12C11.1	15.28 +/- 0.31	-1.7%	0.5183	103/120
K12C11.1	16.93 +/- 0.27	-2.9%	0.1358	110/120
C41A3.1	16.33 +/- 0.31	5.1%	0.0909	107/120
C41A3.1	17.91 +/- 0.32	2.6%	0.3574	109/120
T16G1.4	16.23 +/- 0.32	4.4%	0.1158	103/120
T16G1.4	17.12 +/- 0.3	-1.9%	3.77E-01	107/120
K08D8.6	16.6 +/- 0.31	6.8%	0.0142	107/120
K08D8.6	17.1 +/- 0.3	-2.0%	3.56E-01	102/120
F37B4.7	16.58 +/- 0.3	6.7%	0.016	118/120
F37B4.7	17.74 +/- 0.32	1.6%	0.6789	99/120
K08E7.9	16.49 +/- 0.31	6.1%	0.018	113/120
K08E7.9	18.15 +/- 0.41	4.0%	0.073	95/120
R193.2	16.14 +/- 0.31	3.9%	0.1975	103/120
R193.2	17.16 +/- 0.3	-1.6%	0.3782	98/120

2 Results

Table S7: 1D Annotation Distribution of Aggregation Propensities in wt Animals at Day 12

GO Category	GO Term	Difference	P value	Benj. Hoch. FDR
cellular_component	M band	0.62	3.74E-04	1.49E-02
cellular_component	intermediate filament	0.58	5.45E-04	1.58E-02
cellular_component	striated muscle dense body	0.53	4.36E-04	1.39E-02
cellular_component	P granule	0.52	1.15E-05	1.22E-03
molecular_function	helicase activity	0.51	1.34E-07	2.13E-05
molecular_function	ATP-dependent helicase activity	0.47	6.57E-06	7.48E-04
biological_process	DNA replication	0.44	7.56E-05	8.80E-03
molecular_function	DNA binding	0.43	7.57E-10	6.03E-07
molecular_function	nucleic acid binding	0.32	2.89E-08	7.67E-06
molecular_function	RNA binding	0.29	3.86E-06	5.12E-04
biological_process	morphogenesis of an epithelium	0.27	1.07E-05	1.60E-03
molecular_function	structural constituent of ribosome	0.24	2.44E-04	1.95E-02
cellular_component	nucleus	0.23	5.48E-08	1.74E-05
cellular_component	ribosome	0.23	2.92E-04	1.33E-02
biological_process	translation	0.22	1.19E-04	1.14E-02
cellular_component	intracellular	0.21	1.36E-05	1.08E-03
biological_process	hermaphrodite genitalia development	0.17	7.53E-06	1.32E-03
molecular_function	ATP binding	0.16	3.63E-05	3.61E-03
biological_process	embryo development	0.16	9.14E-11	4.79E-08
biological_process	reproduction	0.13	4.80E-07	1.26E-04
biological_process	nematode larval development	0.10	1.89E-04	1.65E-02

Table S8: Lifespan candidates selected from aggregated subproteome

Gene	Description	RNAi Clone	Expression cluster (wormbase)
W02A2.2 (far-6)	Fatty Acid/Retinol binding protein (184 aa)	IV-7G05	age_regulated_genes
T22B7.7	Acyl-CoA thioesterase (393 aa)	X-3K09	age_regulated_genes
Y62H9A.5	Novel Protein (165 aa)	X-5N13	
Y62H9A.6	Novel Protein (181 aa)	X-5N15	age_regulated_genes

2 Results

Table S9: Lifespan Assays, candidates selected from aggregated subproteome (wild-type worms)

RNAi	Mean Lifespan	% change	Log Rank value	p- Total animals died/Total
eV	20.99 +/- 0.3			119/140
eV	23.52 +/- 0.44			99/120
eV	22.55 +/- 0.73			76/100
W02A2.2	24.48 +/- 0.37	16.6%	0.00E+00	116/140
W02A2.2	27.29 +/- 0.46	16.0%	0.00E+00	96/120
W02A2.2	25.61 +/- 0.65	13.5%	0.0016	79/100
T22B7.7	22.99 +/- 0.36	9.5%	9.30E-06	111/140
T22B7.7	26.64 +/- 0.44	13.2%	6.00E-08	106/120
T22B7.7	24.6 +/- 0.73	9.1%	0.1193	58/75
Y62H9A.5	22.74 +/- 0.31	8.3%	0.0001	127/140
Y62H9A.5	27.56 +/- 0.38	17.1%	0.00E+00	117/120
Y62H9A.5	25.32 +/- 0.55	12.2%	0.0197	91/100
Y62H9A.6	22.6 +/- 0.3	7.7%	0.0007	126/140
Y62H9A.6	25.6 +/- 0.48	8.8%	0.0004	89/100
Y62H9A.6	26.2 +/- 0.54	16.1%	0.0005	91/100

Table S10: Lifespan Assays (daf-16 mutant background), candidates selected from aggregated subproteome

RNAi	Mean Lifespan	% change	Log Rank value	p- Total animals died/Total
eV	20 +/- 0.31			113/140
eV	17.32 +/- 0.29			112/120
W02A2.2	20.62 +/- 0.32	3.10%	5.34E-02	119/140
W02A2.2	17.61 +/- 0.33	1.67%	3.10E-01	112/120
T22B7.7	20.11 +/- 0.36	0.45%	0.4173	108/130
T22B7.7	17.48 +/- 0.3	0.92%	0.8583	97/120
Y62H9A.5	20.71 +/- 0.36	3.55%	0.027	99/120
Y62H9A.5	17.89 +/- 0.35	3.29%	0.0861	108/120
Y62H9A.6	19.95 +/- 0.32	-0.25%	9.89E-01	119/140
Y62H9A.6	17.29 +/- 0.32	-0.18%	7.84E-01	84/120

2.3 The Mitochondrial Contact Site Complex, a Determinant of Mitochondrial Architecture.

2.3.1 Aim and Summary

Mitochondria are enclosed by two membranes with distinct functions and substantial differences in lipid and protein content. Mitochondrial contact sites (CS) - interactions between these two membranes - have been observed in electron micrographs of mitochondria [110]. However, the proteins facilitating their formation are largely unknown. To identify proteins involved in CS formation, membrane vesicles of yeast mitochondria were generated by mild sonication and separated via sucrose gradient centrifugation. SILAC-based protein correlation profiling was subsequently employed to compare abundance distributions of individual proteins across the gradient. By this means, five largely uncharacterized proteins were identified whose profiles matched that of Fcj1, which had previously been shown to be enriched in the protrusions of the inner membrane towards CS, termed cristae junctions (CJ) [249]. Biochemical assays and electron microscopy confirmed that these proteins form a complex required for CS formation which we named MICOS. Deletion of MICOS subunits resulted in partial or complete loss of CJ and an impaired growth on carbon sources requiring respiration.

2.3.2 Contribution

This project was designed and initiated by the group of Walter Neupert at the Adolf-Butenandt Institute for Physiological Chemistry, Ludwig-Maximilians University in Munich, Germany. Max Harner optimized the gradient centrifugation procedure and, together with Christian Körner, performed the majority of the follow up work. My contribution was to establish the experimental strategy that allowed us to identify proteins involved in CS formation. I further optimized the sample preparation conditions, performed the measurements and contributed to the data analysis.

2.3.3 Publication

This work has been published in *The EMBO Journal*.

EMBO J. 2011 Oct 18;30(21):4356-70.

“The Mitochondrial Contact Site Complex, a Determinant of Mitochondrial Architecture.”

Max Harner*, Christian Körner*, **Dirk M. Walther**, Dejana Mokranjac, Johannes Kaesmacher, Ulrich Welsch, Janice Griffith, Matthias Mann, Fulvio Reggiori, and Walter Neupert

*equal contribution

The mitochondrial contact site complex, a determinant of mitochondrial architecture

Max Harner^{1,2,6}, Christian Körner^{1,2,6},
Dirk Walther³, Dejana Mokranjac²,
Johannes Kaesmacher^{1,2}, Ulrich Welsch⁴,
Janice Griffith⁵, Matthias Mann³,
Fulvio Reggiori⁵ and Walter Neupert^{1,2,*}

¹Department of Cellular Biochemistry, Max Planck Institute of Biochemistry (MPIB), Martinsried, Germany, ²Adolf Butenandt Institute, Ludwig-Maximilians-Universität München, Munich, Germany, ³Department of Proteomics and Signal Transduction, Max Planck Institute of Biochemistry (MPIB), Martinsried, Germany, ⁴Anatomical Institute, Ludwig-Maximilians-Universität München, Munich, Germany and ⁵Department of Cell Biology and Institute of Biomembranes, University Medical Centre Utrecht, Utrecht, The Netherlands

Mitochondria are organelles with a complex architecture. They are bounded by an envelope consisting of the outer membrane and the inner boundary membrane (IBM). Narrow crista junctions (CJs) link the IBM to the cristae. OMs and IBMs are firmly connected by contact sites (CS). The molecular nature of the CS remained unknown. Using quantitative high-resolution mass spectrometry we identified a novel complex, the mitochondrial contact site (MICOS) complex, formed by a set of mitochondrial membrane proteins that is essential for the formation of CS. MICOS is preferentially located at the CJs. Upon loss of one of the MICOS subunits, CJs disappear completely or are impaired, showing that CJs require the presence of CS to form a superstructure that links the IBM to the cristae. Loss of MICOS subunits results in loss of respiratory competence and altered inheritance of mitochondrial DNA.

The EMBO Journal (2011) 30, 4356–4370. doi:10.1038/emboj.2011.379; Published online 18 October 2011

Subject Categories: membranes & transport; cell & tissue architecture; cellular metabolism

Keywords: contact site proteins; crista junction; MICOS; mitochondrial membrane proteome; molecular architecture of mitochondria

Introduction

The ability to determine the relationship between the molecular architecture of proteins and the functions of proteins has been key to progress in cell biology to a large extent. The relationship between the molecular architecture of cell organelles, the next higher level of cellular organization, and their function is much less understood. Organelles are composed of membranes and it is much more difficult to link the

structure of membrane proteins and of lipids to a specific architecture. This is particularly challenging in the case of mitochondria because these organelles have a unique and quite complex membrane system, which is the basis for their numerous intricate functions (Scheffler, 2011). Mitochondria catalyse a plethora of metabolic reactions, in particular transducing energy by oxidative phosphorylation. Mitochondria replicate and inherit the mitochondrial genome and synthesize proteins and lipids. They are involved in apoptosis, cellular ageing and in a large number of diseases (Pellegrini and Scorrano, 2007; Wallace and Fan, 2009; Larsson, 2010). Mitochondria are dynamic organelles that have the ability to continuously divide and fuse (Gripapic *et al.*, 2004; Okamoto and Shaw, 2005; Hoppins and Nunnari, 2009). They move in the cell by association with the cytoskeleton (Boldogh and Pon, 2006; Chan *et al.*, 2006; Westermann, 2010). They import proteins from the cytosol and lipids from the endoplasmic reticulum (ER).

The most prominent architectural elements of the mitochondria are their membranes (Frey and Mannella, 2000; Reichert and Neupert, 2002; Perkins *et al.*, 2004; Mannella, 2006, 2008). Mitochondria are bounded by an envelope, which is comprised of the outer membrane (OM) and inner boundary membrane (IBM), two membranes of completely different composition and properties. The cristae protrude from the IBM into the inner space of the mitochondria, the matrix. The cristae and the IBM together make up the inner membrane (IM). The structure of the cristae, their arrangement in the matrix, their number and surface area are highly diverse in different types of cells, tissues and organisms (Fawcett, 1981). The connections between IBM and the cristae are the crista junctions (CJ). These are small, usually very short tubule or slot-like structures. The space between the OM and the IBM, the intermembrane space (IMS), is rather narrow in comparison to the space between cristae sheets, also called intracrista space. Furthermore, there are sites of firm interaction between OM and IBM that become apparent when isolated mitochondria are in a low-energy state or exposed to hypertonic medium. Under these conditions, the matrix condenses and the IBM retracts from the OM (Hackenbrock, 1968). These connections have been termed mitochondrial contact sites (CS), yet their molecular nature has remained elusive.

It has been discussed that these various membranes are shaped essentially by the lipid components (Renken *et al.*, 2002). However, mutations have been described in which the overall shape of mitochondria as observed by light microscopy is altered (Shaw and Nunnari, 2002; Okamoto and Shaw, 2005). More recently, and important in the present context, mutations affecting mitochondrial ultrastructure as revealed by electron microscopy (EM) were reported (Dimmer *et al.*, 2002; Meeusen *et al.*, 2006; Tamai *et al.*, 2008; Rabl *et al.*, 2009). In most cases, the phenotype observed was loss of mitochondrial DNA and of respiratory competence. Thus, it seems reasonable to assume that there

*Corresponding author. Max Planck Institute of Biochemistry, Am Klopferspitz 18, Martinsried D-82152, Germany. Tel.: +49 89 8578 3078; Fax: +49 89 2180 77095; E-mail: Neupert@biochem.mpg.de
⁶These authors contributed equally to this work

Received: 5 July 2011; accepted: 29 September 2011; published online: 18 October 2011

are groups of proteins that determine the various structural elements of mitochondria.

Here, we report on a search for proteins that determine CS by which the IBM and OM are attached to each other. We reasoned that it should be possible to isolate a fraction of the mitochondrial membranes that contains CS. To identify CS, we generated a novel marker by expressing in yeast cells a fusion protein that permanently spans both outer and IBM. We subfractionated mitochondria, separated vesicles and analysed the fractions by protein correlation profiling, a mass spectrometry-based organellar proteomics technique (Andersen *et al*, 2003; Foster *et al*, 2006; Dengjel *et al*, 2010). In this approach, we used an SILAC standard (Ong *et al*, 2002) to identify proteins with the same distribution as the marker. Resulting protein candidates were characterized in terms of their submitochondrial location, topology, importance for cell growth and mitochondrial respiratory competence. Six proteins were found that form a mitochondrial contact site (MICOS) complex. They are associated with the IM and interact with the OM by binding to the TOB/SAM complex and the Ugo1 protein. The MICOS complex is critically involved in the formation of CJs and cristae, as well as in several important functions of the mitochondria. We conclude that the MICOS complex represents the long searched molecular scaffold of mitochondrial contact sites.

Results

Identification of protein candidates of mitochondrial contact sites

Examination of mitochondria by EM in their cellular environment yields images in which the OM and IBM are closely apposed to each other ('orthodox state'). CS cannot be distinguished under these conditions. When mitochondria are isolated and subjected to hyperosmotic treatment, the IBM retracts, the matrix shrinks and the mitochondria assume a 'condensed state' (Hackenbrock, 1968). The IBM remains in close contact with the OM, however, only at few sites (Figure 1A, upper left panel). The gaps at these sites are filled with stain, indicating the presence of proteins (Figure 1A, upper right panel). Importantly, we observed that these contacts in most cases are present right next to where cristae merge with the IBM, at the CS. This is illustrated in a drawing in which an orthodox mitochondrion is reconstructed from a condensed mitochondrion (Figure 1A, middle panels). Taken together, these observations led us to hypothesize that CS forming proteins are present in these areas.

On the basis of this reasoning, we devised an approach in which the proteins that are forming the CS could be identified. We designed a marker protein for these sites. Previous attempts to identify components of CS led to successful subfractionation of mitochondria but the absence of a marker prevented the identification of mitochondrial contact site (Mcs) proteins (Werner and Neupert, 1972; Pon *et al*, 1989). As a prerequisite, the marker must be permanently spanning OM and IBM. The design of this protein was based on our work on the structure and topology of yeast Tim23, an essential component of the protein conducting TIM23 translocase (Donzeau *et al*, 2000). We generated a fusion protein of GFP with Tim23, which locks Tim23 in the desired position, with the GFP domain being present on the mitochondrial surface (Harner *et al*, 2011). GFP-Tim23 expressed in cells

lacking wild-type Tim23 has the intriguing property of complementing the function of the TIM23 translocase (Vogel *et al*, 2006). Figure 1A (middle panel) depicts the distribution of proteins of OM and IM, as well as of Tim23 in wild-type cells (left side, green squares) and of GFP-Tim23 in cells expressing this marker (right side, green dumbbells). The predicted different behaviour of these two proteins upon condensation of mitochondria will result in accumulation of GFP-Tim23 in CS, but not of Tim23. Therefore, vesicle fractions containing CS (Figure 1A, lower panels) will contain GFP-Tim23 as marker protein for the Mcs proteins.

Subfractionation of mitochondria and analysis of protein components by immunoblotting. To verify this concept, we subjected mitochondria to mild sonication and separation of fragments by density gradient flotation centrifugation. In a first set of experiments, we analysed the gradient fractions with antibodies against the designed marker and a number of OM and IM proteins. We compared mitochondria from wild-type cells and from cells expressing GFP-Tim23 instead of Tim23 (Figure 1B, left versus right panel). IM proteins were recovered at the bottom of the gradient and to a lower degree in the middle of the gradient of both wild-type and GFP-Tim23 expressing cells. Wild-type Tim23 was distributed in a similar manner as other IM proteins. In contrast, in mitochondria containing GFP-Tim23, this fusion protein was present exclusively in the middle of the gradient, being virtually absent in the bottom fractions. The submitochondrial location of intermediates of precursor proteins stalled upon import into isolated mitochondria was analysed previously by fractionation of the mitochondria and sucrose gradient centrifugation. The majority of the intermediates were recovered in fractions of intermediate density, in agreement with the localization of the TIM23 import machinery in these fractions shown here (Pon *et al*, 1989). OM proteins such as VDAC/porin and subunits of the TOM complex were present in the top fractions of the gradient and to a low degree in the fractions containing the GFP-Tim23 marker in both types of cells. Interestingly, Fc11, a protein with an essential role in the formation of CJ (Rabl *et al*, 2009) showed a very similar distribution as GFP-Tim23. We concluded that we were able to resolve the CS containing vesicles and have identified a first component of this fraction.

Proteome of the CS fraction by quantitative mass spectrometry. In a further experiment, we used quantitative mass spectrometry (SILAC) to identify proteins specifically enriched in the CS fraction using protein correlation profiling via an internal SILAC standard. Cells were grown in media containing ^{12}C and ^{14}N ('light') or ^{13}C and ^{15}N ('heavy') lysine. Mitochondria were isolated, fragmented and subjected to gradient centrifugation as in Figure 1B. Gradient fractions 10–15 from the 'heavy' gradient were pooled and served as a metabolically labelled internal standard for SILAC-based protein quantitation. Individual fractions (the odd numbered ones of a total of 21) of the 'light' gradient were mixed with aliquots of this internal standard, digested with endoproteinase LysC to peptides and analysed by high-resolution mass spectrometry. Proteins were identified and quantified in each of the fractions based on their isotope ratios using the MaxQuant framework (Cox and Mann, 2008). Proteins of the various mitochondrial subcompartments showed

2 Results

Molecular architecture of mitochondria
M Harner *et al*

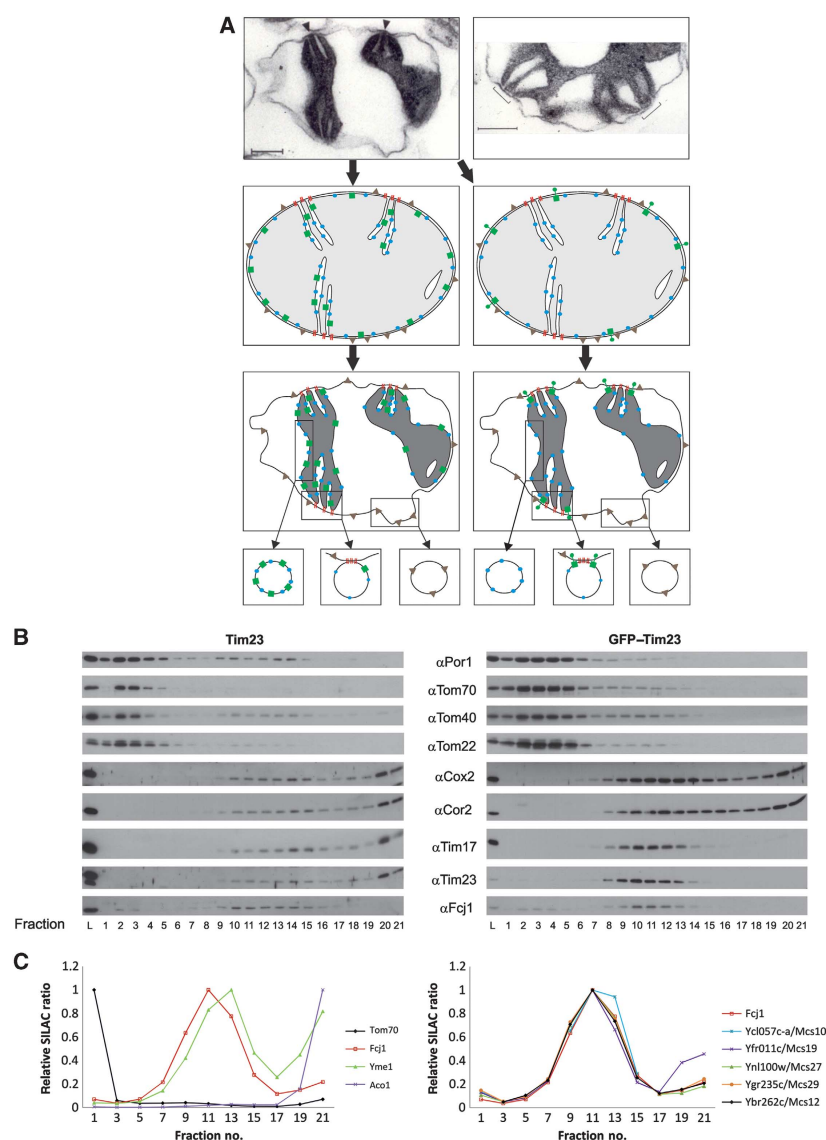


Figure 1 Identification of Mcs proteins. (A) Rationale for the analysis of distribution of membrane proteins in mitochondria. (Upper panels) Electron micrographs of sections of mitochondria from *Neurospora crassa* subjected to osmotic shrinking ('condensed configuration'). Size bars, 200 nm. Arrowheads show regions of attachment between IM and OM (contact sites, CS); brackets indicate CS at higher magnification where two cristae invaginate in close neighbourhood. (Middle panels) 'Orthodox configuration' was reconstructed from the electron micrograph in the upper panel (see arrows). Left, mitochondria from wild type, expressing untagged Tim23; right, mitochondria from cells expressing GFP-Tim23. (Lower panels) Distribution of proteins indicated above after shrinking of mitochondria and theoretically generated vesicles. Symbols: red lines, putative proteins of CS; blue balls, IM proteins; green squares, Tim23; green dumbbells, GFP-Tim23; grey triangles, OM proteins. (B) Separation of vesicles of mitochondria from Tim23 and GFP-Tim23 expressing cells (left and right panels, respectively) by flotation equilibrium gradient centrifugation. Fractions were analysed by SDS-PAGE and immunodecorated with the indicated antibodies. L, load fraction. Odd numbered fractions of the gradients were analysed. (C) Analysis of mitochondrial fractions prepared as in (B) by quantitative mass spectrometry (SILAC). Distribution of marker proteins and of proteins qualifying as components of CS. (Left panel) Profiles of examples of OM proteins, IM proteins, matrix proteins and Fcj1. (Right panel) Profiles of six proteins that qualify as Mcs proteins. See also Supplementary Figure S1 for further controls.

characteristic profiles (Figure 1C; see also Supplementary Figure S1 and Supplementary Dataset File F1). IM proteins peaked in fraction 13 with a high isotope ratio in the bottom fraction. OM proteins, including subunits of the

TOM complex, were prominent in the top fraction, and present to a minor extent in the middle of the gradient. Soluble matrix proteins were only present in the bottom fractions. Apparently, soluble proteins remained in IM

vesicles or were released from the vesicles when experiencing the high osmotic pressure of the bottom fractions of the gradient. The procedure was highly reproducible and precise. The profiles of the same protein in two different mass spectrometry experiments were virtually identical. The same was true when comparing two different subunits of one complex (Supplementary Figure S1). The mitochondrial preparation in these experiments was intentionally not optimized for purity in order not to damage the architecture of mitochondria during isolation. Proteins of the ER originating either from contamination or from association of ER with the mitochondria showed a well-defined profile that can be easily discriminated from the profiles of mitochondrial proteins (Supplementary Figure S1).

Importantly, in contrast to the profile of IM proteins, Fcj1 showed a peak of isotope ratio in fraction 11 and a rather low ratio in the bottom fractions. We examined the ~350 mitochondrial membrane proteins, which were detected in the SILAC analysis for having a profile like Fcj1 and thereby GFP-Tim23. This screen yielded a list of five proteins whose gradient profiles are shown in Figure 1C, right panel. These proteins are present in the *Saccharomyces cerevisiae* genome database (<http://www.yeastgenome.org>), where they are listed as mitochondrial proteins of unknown function. Three of them are present in a collection of proteins, resulting from a screen for altered inheritance of mitochondrial DNA (AIM) (Hess *et al*, 2009), which comprises a total of 46 entries.

We conclude that we have identified a set of six proteins, which, according to their co-fractionation with the marker protein, qualify as components of the IBM/CS. From now on, we address these proteins as Mcs proteins and by their calculated molecular mass in kDa. These proteins are Mcs29 (Ygr235c), Mcs27 (Ynl100w, AIM37), Mcs19 (Yfr011c, AIM13), Mcs12 (Ybr262c, AIM5), Mcs10 (Ycl057c-a) and Fcj1 (Ykr016w, AIM28).

The MICOS complex

Co-isolation of Mcs proteins. To investigate whether the proteins identified interact with each other, we performed both co-isolation and molecular sizing experiments. A summary of the interactions observed upon co-isolation is presented in Figure 2A. All six proteins showed interactions between each other but not with any of the other mitochondrial proteins tested. Interestingly, Fcj1 could be co-isolated together with all five C-terminally His-tagged Mcs proteins. However, pull down of C-terminally tagged Fcj1 led to co-isolation of only trace amounts of Mcs proteins (Figure 2A, left panel). This was surprising, in particular since C-terminally tagged Fcj1 was able to rescue the deletion of Fcj1. Therefore, we suspected that the presence of the tag leads to a weakened interaction of Fcj1 with other Mcs proteins. We then expressed N- or C-terminally tagged Fcj1 versions from a plasmid in an Fcj1 deletion strain. Indeed, all the Mcs proteins were co-isolated only when the tag was present at the N-terminus (Figure 2A, right panel). This observation indicates the importance of the conserved C-terminal domain of Fcj1 for interaction with the other complex components. Altogether, these results demonstrate the existence of a complex network of physical interactions between the various Mcs proteins. Whether the intensities observed in

this assay are a reflection of the strength of binding or are influenced by the experimental conditions is not clear.

Relative abundance of Mcs proteins in mitochondria. We checked the relative abundance of the Mcs proteins by tagging them with a C-terminal HA-tag and expressing them under their endogenous promoters from the chromosome. Isolated mitochondria were analysed by SDS-PAGE (polyacrylamide gel electrophoresis) and immunoblotting with an antibody against the HA-tag. The experimental approach used obviously provides only a rough estimate of the abundance due to the limitations of the method. Yet, it appears that Fcj1, Mcs12, Mcs19 and Mcs29 are of roughly equal abundance, whereas Mcs27 and, in particular, Mcs10 are present at higher levels (Figure 2B).

Complexes formed by the Mcs proteins. In order to analyse complexes formed by the Mcs proteins, we subjected mitochondria to lysis with digitonin followed by gel filtration (Figure 2C). All of the Mcs proteins were present in two large complexes of ~1.5 and 0.7 MDa apparent molecular mass, which we termed MICOS I and MICOS II, respectively. Some of the Mcs proteins, however, were not completely or only partly recovered in MICOS I and II. In particular, very little of Mcs10 was found with the large complexes, but rather in fractions of about 200 kDa. These species probably contain oligomers of Mcs10 since untagged Mcs10 could be co-isolated with tagged Mcs10 when expressed together (not shown). Mcs29 was recovered only to a lower extent in MICOS I and II; however, more was present in the low molecular mass range. Finally, Mcs12 was present to a higher extent in MICOS II than in MICOS I. The TOM complex that served as a control eluted with an apparent mass of 400–500 kDa as to be expected (Kunkele *et al*, 1998). To test whether the absence of the majority of Mcs10 from the large complexes was due to a minor contribution to MICOS I and II or whether Mcs10 easily dissociates from the other Mcs proteins upon solubilization of mitochondria, we performed Blue native (BN)-PAGE. Immunoblotting with antibodies against Fcj1, Mcs27 or Mcs29 revealed two high molecular mass complexes of roughly 1.5 and 0.7 MDa. The sizes of these two complexes matched very well with those obtained upon gel filtration. The antibody against Mcs10 did not recognize its antigen upon BN-PAGE; therefore, we analysed mitochondria harbouring his-tagged Mcs10. Immunoblotting using antibody against the His-tag (penta-His; Qiagen) revealed again two high molecular complexes with similar sizes as observed upon immunodecoration with the other Mcs proteins (Supplementary Figure S2A). This indicates that Mcs10 has the tendency to dissociate from the complex after detergent solubilization of mitochondria and gel filtration.

Steady-state levels of Mcs proteins in deletion strains. We further asked as to whether deletion of one of the Mcs proteins would affect the steady-state levels of the other Mcs proteins (Figure 2D). Indeed, severe reduction of the levels of proteins of the MICOS complex occurred (with the exception of deletion of Mcs12), but not of other proteins of the different mitochondrial subcompartments. Deletion of Fcj1, in particular, resulted in a strong reduction of the levels of all other subunits of the MICOS complex. Interestingly, not only downregulation was observed; deletion of Mcs29 caused upregulation of Mcs27. These results

Molecular architecture of mitochondria

The MICOS complex fell apart when one of the Mcs proteins was missing as observed by filtration analysis

A

Western blot analysis showing the levels of αFcj1, αMcs10, αMcs19, αMcs27, αMcs29, αMcs12, αAco1, and αTom40 in WT, Mcs19-6xHis, Mcs27-6xHis, Fcj1-6xHis, Mcs29-6xHis, Mcs10-6xHis, and Mcs12-6xHis strains. The blots are organized by strain and probed with different antibodies.

B

Western blot analysis showing the levels of αHA and αTom40 in strains expressing Fcj1-3xHA, Mcs10-3xHA, Mcs19-3xHA, Mcs27-3xHA, and Mcs29-3xHA. The blots show the localization of these proteins relative to Tom40.

C

Fractionation of Msc proteins by size exclusion chromatography. Fractions I and II are indicated. Molecular weight markers (669, 440, 158, 48, 25 kDa) are shown. Blots for αFcj1, αMcs10, αMcs19, αMcs27, αMcs29, αHA (Mcs12), and αTom40 are shown across fractions L and Fractions 1–22.

D

Western blot analysis showing the levels of αFcj1, αMcs10, αMcs19, αMcs27, αMcs29, αMcs12, αAco1, αTim23, αTim50, αTom40, and αTob55 in WT, Δfcj1, Δmcs10, Δmcs19, Δmcs27, Δmcs29, and Δmcs12 strains. The blots show the effect of deleting these genes on other Msc proteins.

E

PK treatment and alkaline extraction of Msc proteins. PK treatment (+/-) and TX (-) are indicated. Alkaline extraction (extr.) is also indicated. Blots for αFcj1, αMcs10, αMcs19, αMcs27-N, αMcs27-C, αMcs29-N, αMcs29-C, αMcs12-C, αTom70, αTim50, and αHep1 are shown. Schematic diagrams illustrate the topology of these proteins in the membrane.

from MICOS I to MICOS II was observed. We conclude that the six different Mcs proteins cooperate in an intricate manner to generate the MICOS complex.

Topology of Mcs proteins. In order to determine the topology of the Mcs proteins, we performed protease accessibility and alkaline extraction assays followed by immunoblotting (Figure 2E). This list includes the previously established topology of Fc11 (Rabl *et al*, 2009). Mcs10 is integrated into the IM with a predicted transmembrane segment located about 50 residues from the N-terminus. A topology in which the N-terminal part is located in the matrix and the C-terminal part in the IMS is supported by the loss of C-terminal His or HA tags upon protease treatment of mitochondria (not shown). However, in view of the absence of a classical targeting signal other topologies cannot be excluded. Mcs19 is present in the IMS; it is apparently not an integral membrane protein, as it could be extracted from membranes at alkaline pH, a notion supported by the absence of a predicted membrane anchor. Since it is not lost during hypo-osmotic swelling, most of Mcs19 is likely bound to the IM. The relatively high isotope ratio at the top of the gradient (see Figure 1C) raises the possibility that part of the protein is associated with the OM. On the other hand, the comparatively high ratio at the bottom of the gradient may suggest that part of it is present in cristae membranes. Mcs27 and Mcs29 are also integral proteins of the IM. They have two predicted transmembrane spanning helices; the hydrophilic parts are present in the IMS. Mcs12 is anchored to the IM with its N-terminus exposing a hydrophilic domain of about 70 residues into the IMS. In summary, the six proteins found to participate in CS formation are inserted into or associated with the IM.

Submitochondrial location of the Mcs proteins

To determine the location of the various Mcs proteins at the submitochondrial level, immunolabelling with gold particles of cryosections was performed. It should be noted that with this procedure, gold particles can be present at a distance of up to 20 nm from the epitopes. Cells expressing the HA-tagged Mcs proteins were grown on lactate or glycerol (Figure 3A; see also Supplementary Figure S3A). Fc11 was predominantly found at the mitochondrial envelope, very often in close proximity to CJ, in agreement with our previous work. Most intriguingly, the Mcs10 protein had a very similar distribution. It was also associated with the mitochondrial

envelope and in most cases present at CJ. The observed immune reactions are specific as background labelling in wild-type cells was negligible (not shown). To analyse the distribution of Mcs10 in more detail, cells were also grown on glycerol where fewer cristae are present. Under these conditions, a close association of Mcs10 with CJ was conspicuous (Figure 3B). A third protein with a similar distribution is Mcs19, which, however, was also found at cristae. The latter location appears to be consistent with its higher levels in gradient fractions that correspond to crista membranes (cf Figure 1C, right panel, and see below Figure 4A). Mcs27, Mcs29 and Mcs12 also showed a preferential location at the envelope with very few gold particles found in the interior of mitochondria. Notably, the immunoreactivity of the cryosections was in agreement with the estimated levels of the Mcs proteins (Figure 2B).

The distribution of a number of other mitochondrial proteins was studied for comparison (Figure 3C). Isocitrate dehydrogenase (Idh1), an abundant matrix protein was distributed all over the internal space of the mitochondria. VDAC/porin (Por1) was only found on or close to the OM. Likewise, Tob38/Sam35 and Mas37/Tob37/Sam37, components of the TOB complex, were present at the OM. Tim50 and Tim16, components of the TIM23 protein import machinery, in contrast, were found at the envelope membranes and to a lower degree in the interior of the mitochondria, in agreement with a previous study (Vogel *et al*, 2006) (see also Supplementary Figure S3B). Quantitative analysis of the immunolabelling of the Mcs proteins showed that some 35–45% of the gold particles were present at CJ; in contrast, only 5–8% of those marking control proteins were found at CJ (Figure 3D; Supplementary Table SI). Since CJs are small structures, they are not always visible in case of grazing sections; therefore, the number of Mcs proteins at CJs may be underestimated. On the other hand, a fraction of Mcs proteins may also be present outside CJ.

In summary, immuno-EM revealed that the MICOS complex is indeed located predominantly or entirely at the mitochondrial envelope strongly supporting the results of analysis of mitochondrial subfractions. Most interestingly, the MICOS complex is predominantly located at CJs.

Interaction of Mcs proteins with OM proteins

In a search for components of the mitochondrial OM that might be interaction partners of the Mcs proteins, we checked the gradient fractions of Figure 1 for OM proteins that overlap

Figure 2 The MICOS complex. (A) Co-isolation of Mcs proteins. His-tagged versions of the Mcs proteins were expressed under control of their own promoters (left panel) or from the pYX242 plasmid (right panel) in the respective deletion strain. Mitochondria were isolated, solubilized with digitonin and incubated with Ni-NTA beads. Total (T, 5% of total), supernatant (S, 5% of total) and bound material (B, 100%) were analysed by SDS-PAGE and immunodecoration with the indicated antibodies. Mitochondria from wild-type cells served as control. (B) Relative abundance of Mcs proteins. HA-tagged versions of the Mcs proteins were expressed under their own promoters. Equal amounts of mitochondria were analysed by SDS-PAGE and immunoblotting with antibodies against the HA-tag (α HA) and against Tom40 (α Tom40), the loading control. (C) Molecular sizing of Mcs proteins from wild-type mitochondria. Mitochondria were lysed with digitonin and lysates subjected to gel filtration on a Superose 6 column. The fractions were analysed by SDS-PAGE and immunoblotting using the indicated antibodies; in case of Msc12, a strain was used which expressed HA-tagged Msc12 and immunoblotting was with α HA antibody. Msc10 blots were exposed for two different time periods. The TOM complex (Tom40) was decorated as a control. I and II, MICOS complex I and II. Positions of marker proteins for calibration are indicated with arrows. L, load (10% of material applied to column). See also Supplementary Figure S2A. (D) Steady-state levels of Mcs proteins in cells in which one of the MCS genes was deleted. Mitochondria were analysed by SDS-PAGE and immunoblotting. See also Supplementary Figure S2B. (E) Membrane integration and orientation of Mcs proteins. (Left) Mitochondria from wild-type cells were left untreated or treated with proteinase K (PK) either directly, after subjecting them to osmotic swelling (SW) or after lysis with Triton X-100 (TX); bars indicate the apparent molecular masses of the full-length proteins. (Right) Mitochondria were exposed to alkaline extraction at pH 12. Soluble (S) and membrane integrated (P, pellet) material were separated by centrifugation. Aliquots were subjected to SDS-PAGE and immunodecoration with antibodies against the indicated proteins. Arrowhead, unspecific cross-reaction.

2 Results

Molecular architecture of mitochondria M Harner *et al*

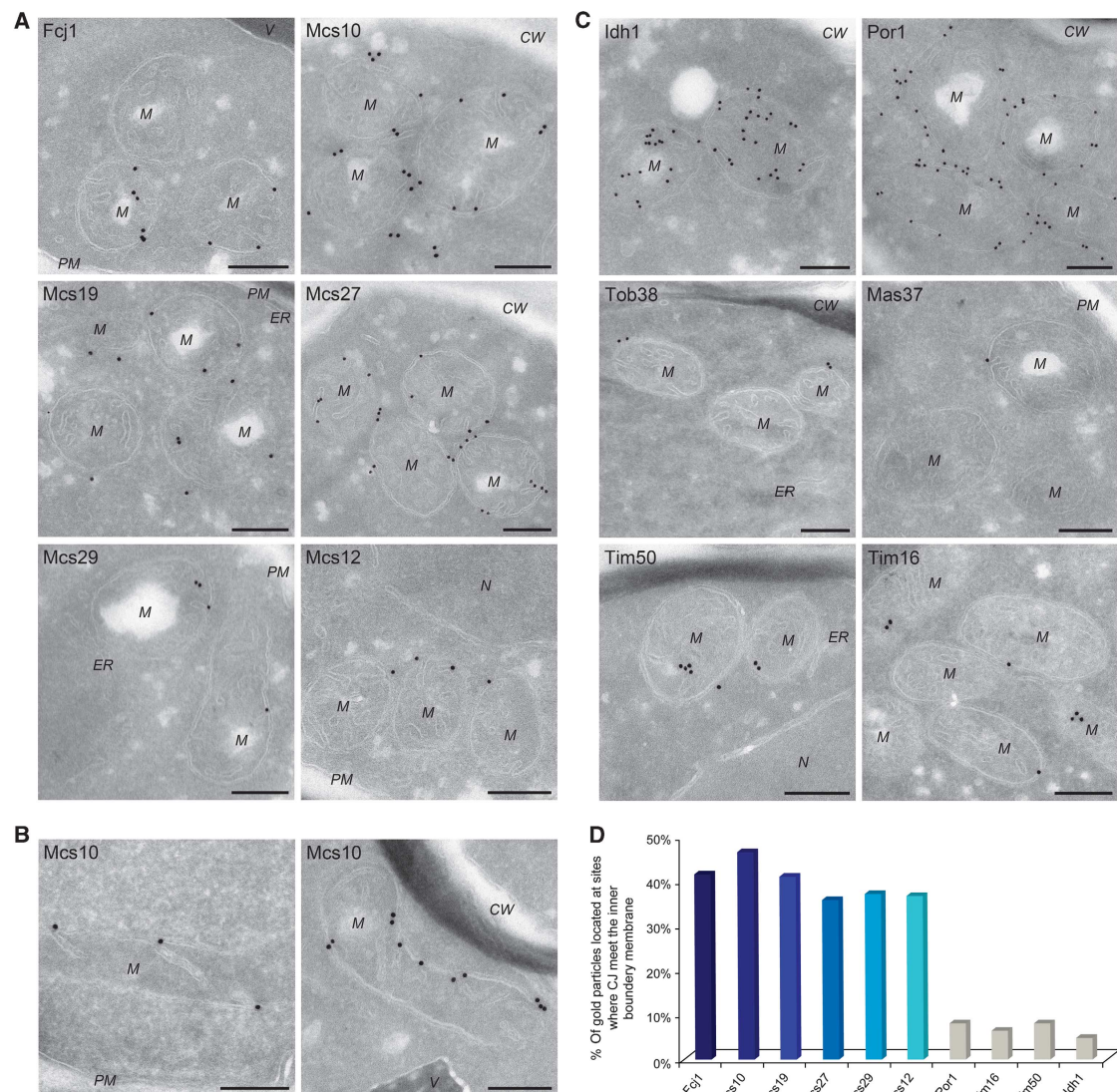


Figure 3 Localization of Mcs proteins by immuno-EM. Cells expressing C-terminally HA-tagged versions of Mcs proteins, were processed for immuno-EM, cryosections were labelled with anti-HA antibodies and protein A bound gold particles, with the exception of Por1, for which specific antibodies were used. **(A)** Distribution of Mcs proteins in cells grown on lactate. **(B)** Mcs10 localization in cells grown on glycerol. **(C)** Distribution of proteins of various mitochondrial subcompartments in cells grown on lactate. Matrix (Idh1); OM, (Por1, Tob38 and Mas37/Tob37); inner boundary and crista membrane (Tim50 and Tim16). CW, cell wall; M, mitochondrion; N, nucleus; PM, plasma membrane; V, vacuole. Size bars, 200 nm. Additional examples in Supplementary Figure S3. **(D)** Quantitative analysis of the distribution of Mcs and control proteins at sites where the CJ meet the IBM. For each labelling, the percentage of gold particles present at the CJ was determined.

with the characteristic profile of Mcs proteins. Subunits of the TOM complex and OM45 were present in the middle of the gradient to a very low degree. They probably represent the pieces of OM that adhere to the IBM in the CS fractions. There were conspicuous exceptions. The levels of components of the TOB/SAM complex that mediates the insertion of β -barrel proteins into the mitochondrial OM (Kozjak *et al*, 2003; Paschen *et al*, 2003) were significantly higher in the fractions containing the Mcs proteins as seen both with immunoblotting and mass spectrometry (Figure 4A

and B). A more detailed evaluation was performed by subtracting the profile of proteins such as the TOM complex subunit Tom40. Thereby, a clear coincidence of the profiles of TOB/SAM components with that of the Mcs proteins was observed (Figure 4C). The precision of the SILAC measurements allows this operation; subtraction of two OM proteins from each other yielded a reproducible zero line (Figure 4D). We conclude that a fraction of the TOB/SAM complex and Mcs proteins belong to a common structure.

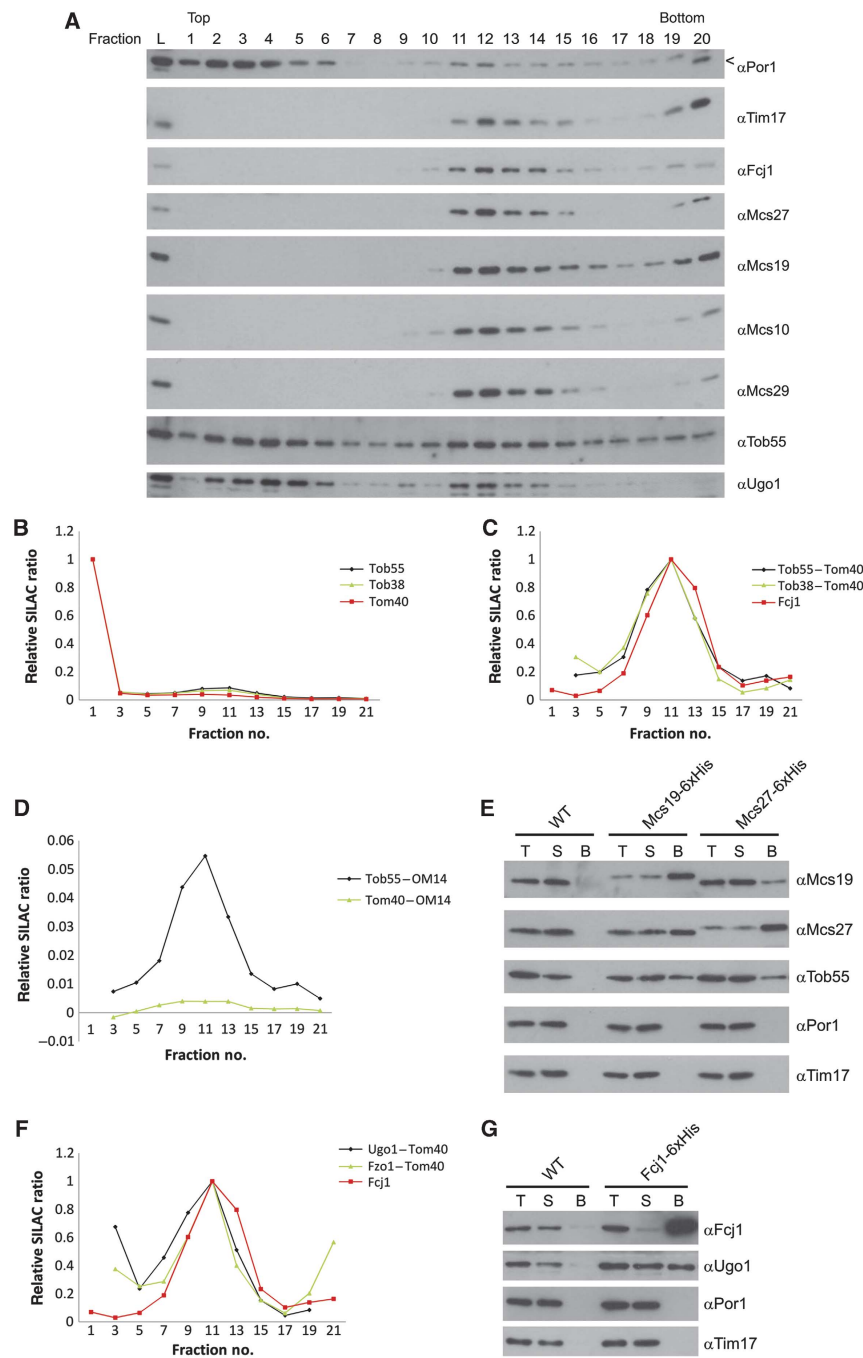


Figure 4 Interaction of Mcs proteins with components of the OM. (A) Wild-type mitochondria were fractionated and subjected to density flotation centrifugation as in Figure 1B. Fractions were subjected to SDS-PAGE and immunodecoration with antibodies against Por1, Tim17, Mcs proteins, Tob55 and Ugo1. (B) Analysis of the distribution on flotation gradients of Tob55 and Tob38 compared with Tom40 by mass spectrometry. (C) Differential profiles of Tob55 and Tob38 after subtraction of the profile of Tom40. (D) Subtraction of the profiles of two OM proteins, Tom40 and OM14, from each other. (E) Co-isolation of Tob55 with Mcs19 and Mcs27. For details see Figure 2A. (F) Density gradient profiles of Ugo1 and Fzo1 processed as in (C). (G) Co-isolation of Ugo1 with Fcj1. Analysis as in (E), with the exception that Triton X-100 was used for solubilization. Arrow head, unspecific cross reaction.

2 Results

Molecular architecture of mitochondria
M Harner *et al*

To analyse whether TOB/SAM components can be co-isolated with Mcs proteins, mitochondria were solubilized with the mild detergent digitonin and interaction with Mcs proteins was studied (Figure 4E). Indeed, Tob55 was observed to bind to both Mcs27 and Mcs19. In a separate study, the interaction of Tob55 with Fcj1 was analysed. Fcj1-His interacted with Tob55, however, in a rather inefficient way. A mutational study of Fcj1 revealed a role of the C-terminus of Fcj1 in the interaction with Tob55 (Körner, Reichert *et al*, unpublished data). No interaction was seen with components of the TOM complex and other OM proteins such as OM45 (not shown). We conclude that a fraction of the TOB/SAM complexes in the OM is present in CS and interacts with Mcs proteins that are associated with the IM.

Two further proteins of the OM were found that shared the gradient profile of the TOB/SAM proteins, Ugo1 and Fzo1 (Figure 4A and F). When the SILAC profiles of typical OM proteins such as Tom40 or OM45 were subtracted from the SILAC profiles of Ugo1 and Fzo1, a peak in the characteristic Mcs protein fraction 11 remained, indicating that a fraction of these latter proteins were present in CS. Interaction of Ugo1 with Fcj1 was observed by co-isolation (Figure 4G). The OM protein Ugo1 is required for mitochondrial fusion and is associated with the fusion protein Fzo1 (Sesaki and Jensen, 2001, 2004; Wong *et al*, 2003). Thus, a fraction of Ugo1 seems to play a role in tethering Fcj1 to the OM and thereby to localize Fzo1 to CS.

To corroborate these results, we analysed vesicles by sucrose gradient centrifugation that were generated from mitochondria of a $\Delta fcl1$ strain (Supplementary Figure S4A). Strikingly, Mcs proteins and Ugo1 showed a different distribution in these cells compared with wild type (Figure 4A). Mcs10 and Mcs29 were shifted from fractions of intermediate density to fractions of high density so that their profiles were very similar to that of Tim17, an IM protein. The subpopulation of Ugo1 that was present in vesicles of intermediate density from wild-type mitochondria was almost completely absent in the gradient fractions of vesicles of $\Delta fcl1$ mitochondria. These results confirm the role of Fcj1 in bringing together proteins of the IM with proteins of the OM, and also substantiate our concept of the enrichment of Mcs proteins in gradient fractions of intermediate density.

We also studied the ultrastructure of mitochondria in $\Delta ugo1$ cells (Supplementary Figure S4B). These cells did not grow on non-fermentable carbon source and therefore were grown on glucose and compared with wild-type and $\Delta mcs10$ cells grown on glucose. Their mitochondria were grossly altered. In particular, the number of CJs was extremely low; crista-like structures were almost completely absent. Apparently, Ugo1 has a role in the fusion of mitochondria, but is also critically involved in determining the architecture of mitochondria as shown here.

Functional characterization of Mcs proteins

Role of Mcs proteins for the architecture of mitochondria. Figure 5 shows representative EM micrographs of cells in which each of the MCS genes was deleted, together with a quantitative evaluation of morphological parameters (see also Supplementary Figure S5 and Supplementary Table SII). The deletion of Fcj1 led to virtually complete loss of CJ, to an increase of crista stacks and to an increased

number of crista rims/endings/apexes as previously reported (Rabl *et al*, 2009). Likewise, deletion of Mcs10 caused virtually complete loss of CJ, accumulation of crista stacks and an increase of crista rims. The deletion of Mcs19 led to a massive loss of CJ and cristae showed bizarre shapes with frequent kinks. Notable are the abundant branches of the cristae. In $\Delta mcs27$ mitochondria, CJ were reduced by about 60%, there were crista stacks but much fewer than in $\Delta fcl1$ mitochondria. Deletion of Mcs29 resulted in a slight reduction of the number of CJ. Yet in contrast to $\Delta fcl1$ mitochondria, stacks were sometimes observed to be connected to the IBM by CJ. Upon deletion of Mcs12, fewer CJ were seen than in wild type, but similar to Mcs27 some of the crista stacks were connected to the IBM.

In conclusion, these data show that the proteins found in the search for components of CS are characterized by a complete or partial deficiency in CJ and altered crista morphology, such as increased number of crista rims or crista branching.

Growth behaviour of cells. Each one of the strains depleted of the various Mcs proteins grew like wild type on rich glucose-containing (YPD) medium (Figure 6). On fermentable carbon sources, some of the deletion mutants showed severe ($\Delta fcl1$, $\Delta mcs10$) or mild ($\Delta mcs27$ and $\Delta mcs12$) growth defects, partly depending on growth temperature. Thus, deletion of the MCS genes leads to loss or reduction of the capacity of mitochondria for oxidative phosphorylation, demonstrating that the architecture of mitochondria is key to basic metabolic processes of the mitochondria.

Discussion

In this work, we describe a novel complex with an important role in determining the architecture and function of mitochondria (Figure 7). This large multisubunit complex, which we term MICOS complex, is anchored to the IBM and extends across the IMS to reach specific OM proteins, the TOB/SAM and the Ugo1–Fzo1 complexes. Interaction of the Ugo1–Fzo1 complex with the IM has been reported previously (Fritz *et al*, 2001); however, the interaction partner in the IM remained obscure so far. Why the TOB/SAM complex serves as an anchor for Mcs proteins is an intriguing question. Perhaps equivalent interactions were present in the gram-negative ancestors of the mitochondria, the elusive Bayer's junctions (Bayer, 1991), and maintained during evolution of mitochondria for similar or new purposes.

MICOS is preferentially located at sites where the cristae originate from the IBM. Two of the six Mcs proteins identified, Mcs10 and Fcj1, are essential for forming CJ, the others affect the presence of CJ to different degrees. Among these, Mcs19 is not only important for the presence of CJ, but also for the formation of intact cristae, as its depletion leads to appearance of branches in cristae. It remains to be determined whether Ugo1 and Fzo1 are present in the MICOS complex like the other Mcs proteins. Ugo1 was found also in association with Mgm1, a dynamin-like GTPase (Wong *et al*, 2003; Sesaki and Jensen, 2004). It is also possible that they form a separate complex with different composition and function.

Our findings shed new light on the architectural organization of mitochondria and at the same time raise a number of

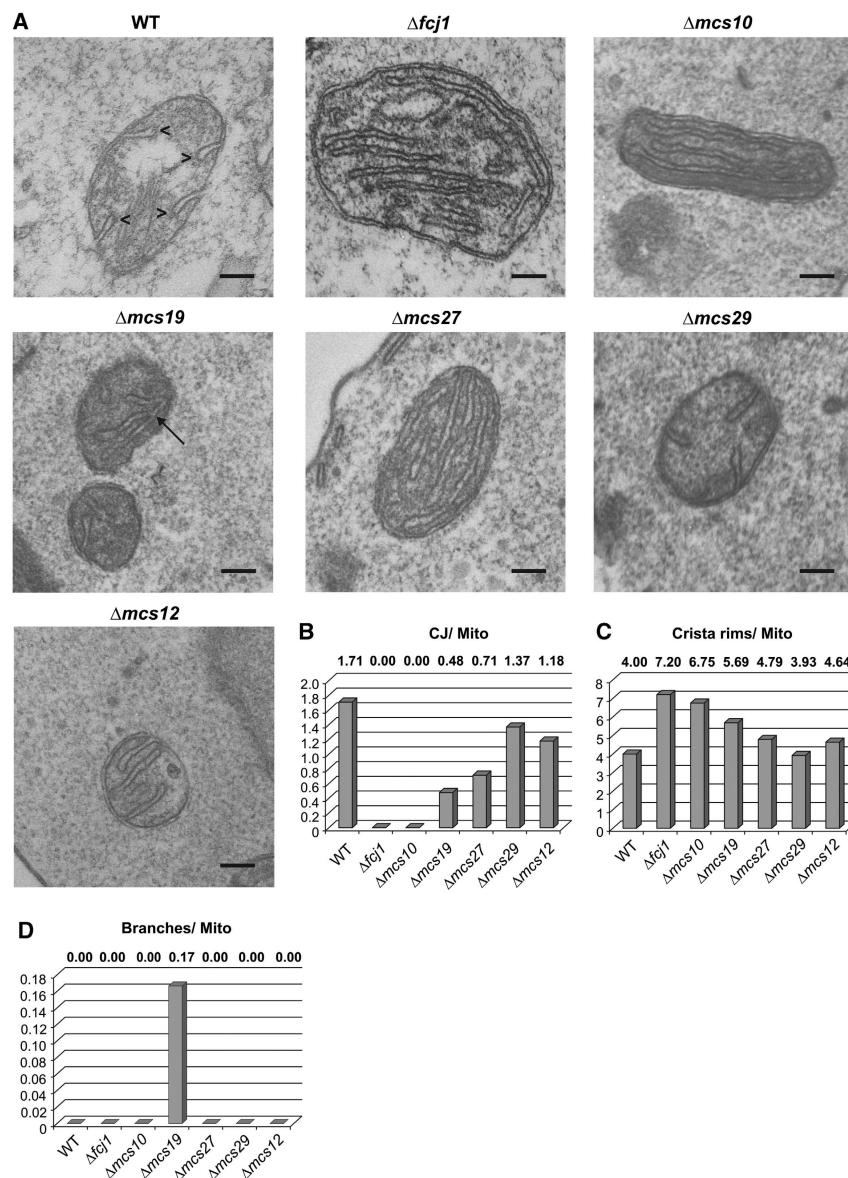


Figure 5 Morphological roles of Mcs proteins. (A) Electron micrographs of mitochondria of wild-type cells and of cells lacking the various Mcs proteins. Cells were fixed with glutaraldehyde and sections contrasted with OsO_4 . Size bar, 100 nm. (B–D) Quantitative evaluation of images. Average numbers of (B) CJs, (C) crista rims and (D) crista branches per mitochondrial profile. Additional examples and quantifications in Supplementary Figures S4B and S5 and Supplementary Table SII. Arrowheads, crista rims; arrow, crista branch.

intriguing questions. They strongly support our initial hypothesis on the existence of firm contacts between OM and IBM at sites where the CJs merge with the IBM. The MICOS complex appears to be important for mitochondrial architecture, dynamics and function in several respects. First, it is necessary for the formation of CJs. Second, it is critical for the capacity of mitochondria for oxidative phosphorylation and inheritance of mitochondrial DNA, as highlighted by the presence of four of the

MCS genes in the AIM collection (Hess *et al*, 2009). Third, changes in the buoyant density of membrane vesicles from mitochondria depleted of Fcj1 would suggest that the transfer of membrane lipids to and between mitochondrial membranes is dependent on the MICOS complex (unpublished results).

The definition of the CS as important specific architectural elements leads us to some speculations regarding so far unexplained processes in mitochondria. We speculate that

2 Results

Molecular architecture of mitochondria
M Harner *et al*

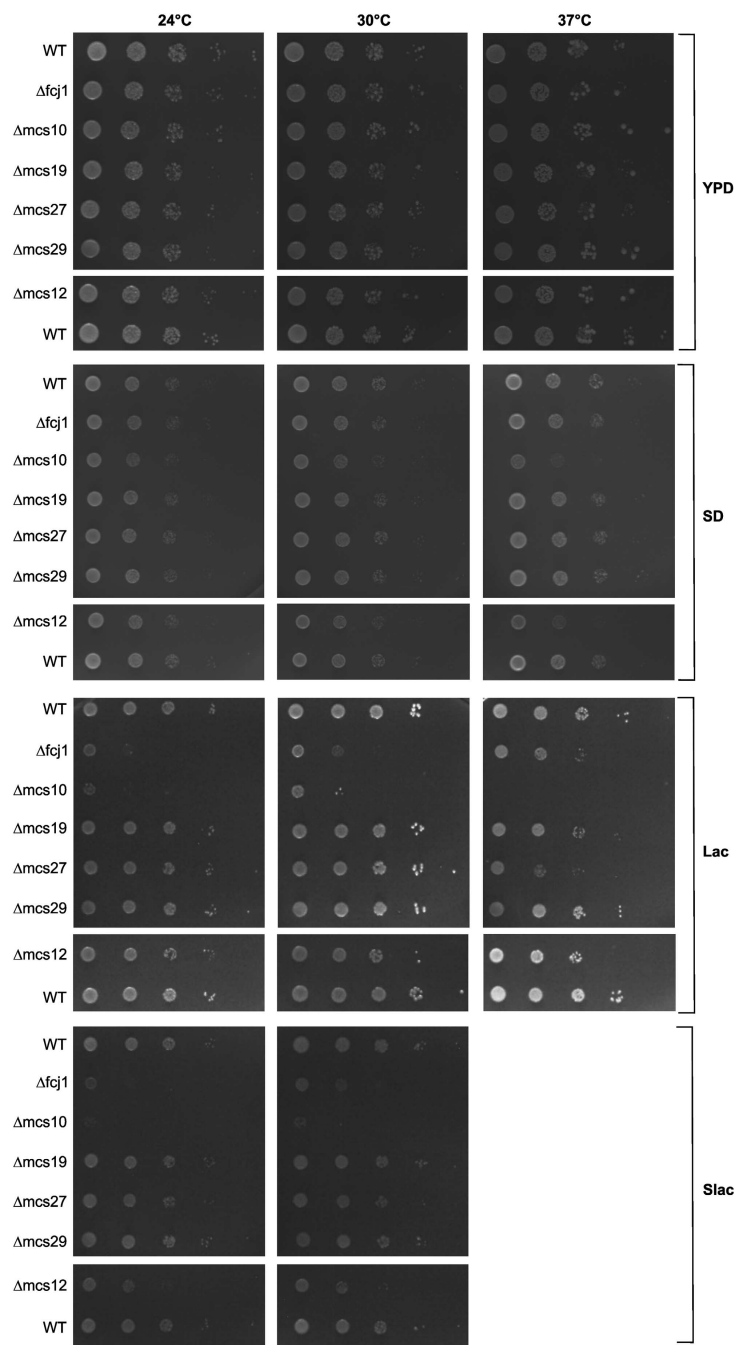


Figure 6 Growth characteristics of cells lacking Mcs proteins. Cells were spotted in 10-fold dilution steps on agar plates containing one of the following media: glucose and yeast extract (YPD); glucose-containing synthetic medium (SD); lactate-containing medium (Lac); lactate-containing synthetic medium (Slac). Plates were incubated at the indicated temperatures. None of the strains grew on Slac at 37°C.

the MICOS complex may control the lateral diffusion of newly imported IM proteins into the cristae after their insertion into the IBM. As a consequence, the MICOS complex may influence the composition and structure of both the IBM and the

crista membrane. Furthermore, by shaping cristae junctions, the MICOS complex might be involved in the release of components of the intracrista space, an important process in apoptosis in higher eukaryotes. Such a role of CS and

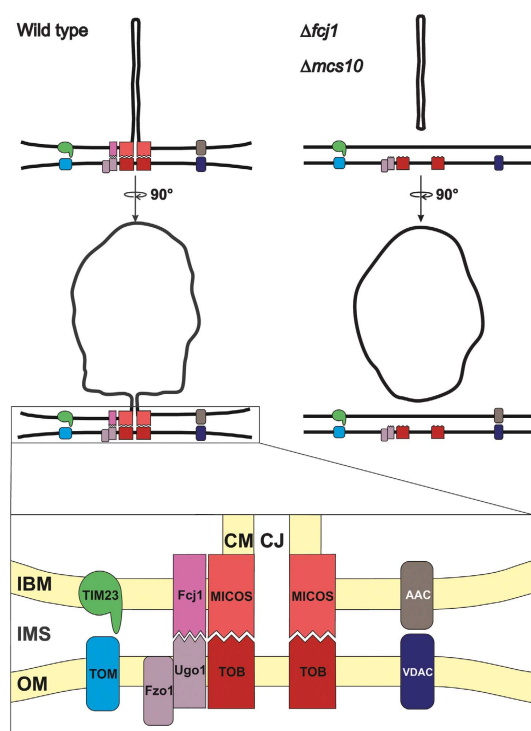


Figure 7 Working model of the role of the MICOS complex in mitochondrial architecture. (Upper panels) Mitochondrion of wild-type cells (left) and of cells lacking Fcj1 or Mcs10 (right) in two orientations. (Lower panel) Blow-up of CS with interaction of MICOS-TOM and of Fcj1-Ugo1-Fzo1. Dynamic interaction of TOM and TIM protein import complexes, and of AAC (ADP/ATP carrier) and VDAC/porin bridging the IMS, supported by CS. For further explanation and abbreviations see Discussion.

several others have been previously proposed (Frey and Mannella, 2000; Mannella, 2008).

Our results also bring up the exciting possibility that the connection of cristae with the IBM is not static but dynamic. It has been suggested that the width of CJ may limit the diffusion of proteins like cytochrome *c* from the intracrista space into the space between IMS (Scorrano *et al*, 2002). We speculate that CJ can undergo a time dependent opening and closing, governed by fusion and fission at the CS. The MICOS complex could be a scaffold for maintenance of defined sites of fusion and participate in controlling the equilibrium of fusion and fission. Such a dynamic structure of the mitochondria would have far reaching implications for the efficiency of oxidative phosphorylation. Cristae in a closed state would be able to maintain the proton gradient generated by the respiratory chain to a much higher extent than cristae, which are continuously open to the IMS and therefore to the cytosolic compartment. The question of whether the proton gradient usually measured in mitochondria is sufficient for optimal ATP production is an issue in mitochondrial bioenergetics. Several possible mechanisms have been proposed that might prevent proton equilibration with the bulk phase (Mulikidjanian *et al*, 2005; Strauss *et al*, 2008).

Protein translocases of OM and IBM, the TOM and TIM23 complexes, were shown to interact closely, yet transiently. The MICOS complex may not be essential for this process, but CS could increase the efficiency of matching TOM with the TIM and TOB complexes (Figure 7). Likewise, export of ATP from the mitochondria by a joint action of the ADP/ATP translocase, VDAC/porin and hexokinase (Brdiczka *et al*, 2006) may not need the presence of CS. On the other hand, the MICOS complex might increase the efficiency of their interactions by providing a scaffold for matching of the protein complexes residing in IBM and OM.

Is the complex which we describe here a common structure in all eukaryotes? Mcs10 is a highly conserved protein (Supplementary Figure S6A). Its sequence is remarkable in several aspects. It is a small protein with a single predicted transmembrane segment, containing a GX₃G motif, followed by a GXGXGXG motif in which the X residues are hydrophobic. The C-terminal motif is particularly interesting. Since Mcs10 apparently forms homo-oligomers both elements might be involved in the self-association. Fcj1 was found previously to have sequence similarity to mammalian mitofilin and homologues are present in metazoa. Downregulation of mitofilin led to mitochondria with altered cristae and absence of CJ. Mitofilin was therefore recognized as a protein controlling crista morphology (Odgren *et al*, 1996; John *et al*, 2005; Rabl *et al*, 2009). Mcs29 and Mcs27 proteins might be evolutionarily related (Supplementary Figure S6B). Both contain two predicted transmembrane segments at similar positions. However, we found no obvious homologues in higher eukaryotes. Mcs19 also does not show related sequences in higher organisms, even among fungi conservation is very limited. However, the very C-terminal part shows somewhat higher similarity. Interestingly, a CX₁₀C motif in the latter part is conserved among fungal species. It could possibly serve as a motif for the disulphide relay system for import into the IMS (Hell, 2008). Mcs12 also belongs to the group of Mcs proteins with low-sequence similarity even among fungi.

Interestingly, two recent reports describe proteins that appear to play a role in the ultrastructure of mitochondria of higher eukaryotes. ChChd3 in mammalian cells is located on the IM facing the IMS and is involved in maintaining cristae integrity and mitochondrial function (Darshi *et al*, 2011). None of the Mcs proteins can be recognized as a homologue; however, both Mcs19 and ChChd3 have a myristoylation motif and pairs of cysteine residues close to the C-terminus. A homologue of this protein in *Caenorhabditis elegans*, CHCH-3, was suggested to have a role as a chaperone. Furthermore, the protein MOMA-1 in *C. elegans* was proposed to display low-sequence similarity to Mcs27 and Mcs29 (Head *et al*, 2011). Although we could not detect significant sequence similarity (Supplementary Figure S6B), the overall structures of Mcs27, Mcs29 and MOMA-1 are similar. MOMA-1 was found mainly in the OM (Head *et al*, 2011), in contrast to Mcs27 and Mcs29, which are integrated into the IM of yeast mitochondria. It will be important to clarify as to whether the submitochondrial location of MOMA-1 is different from that of Mcs27 and Mcs29 or the sequence similarity is too low to predict homology.

Irrespective of possible homologies, there are similarities in the observed interactions, knockdown phenotypes and possible functions between ChChd3 and MOMA-1 and the

2 Results

Molecular architecture of mitochondria

M Harner *et al*

respective yeast proteins. The mammalian ChChd3 interacts with mitofilin and Sam50/Tob55; morphological aberrations such as clustering of mitochondria around the nucleus, fragmented and tubular cristae and reduced opening diameter of CJ were observed (Xie *et al*, 2007; Darshi *et al*, 2011). Mutations in MOMA-1 and in the mitofilin homologue in *C. elegans*, IMMT-1, led to altered crista morphology. Furthermore, the phenotypes of knockdown studies suggested an interaction of MOMA-1, the ChChd3 homologue, CHCH-3, and IMMT-1.

Thus, in view of these similarities, our discovery and biochemical and functional characterization of the MICOS complex are relevant not only for lower eukaryotes but apparently for the whole eukaryotic world. We believe that it opens the door for a profound and detailed analysis of the molecular basis of mitochondrial architecture, also in higher eukaryotic cells.

Materials and methods

Yeast strains and cell growth

For analysis of submitochondrial fractions, strains W303 {*leu2-3,112 trp1-1 can1-100 ura3-1 ade2-1 his3-11,15*} and W303 Δ *tim23* harbouring pRS315GFP-Tim23 under the endogenous Tim23 promoter were used (Vogel *et al*, 2006). For the SILAC analysis of submitochondrial fractions, YPH499 {*ura3-52, lys2-801^{amber}, ade2-101^{pcr}, trp1- Δ 63, his3- Δ 200, leu2- Δ 1*} was used because of its lysine auxotrophy. Chromosomal manipulations (knockouts, C-terminal 6 \times His- and 3 \times HA-tagging) were performed in the YPH499 background (Longtine *et al*, 1998; Knop *et al*, 1999). For the generation of deletion strains, the coding regions of *FCJ1*, *YCL057C-A/MCS10*, *YFR011C/MCS19*, *YNL100W/MCS27*, *YGR235C/MCS29* and *YBR262C/MCS12* were replaced by a *HIS3* cassette using the pFA6a-His3MX6 plasmid as the PCR template. The 6 \times His-tags were introduced using the pYM9 plasmid as the PCR template. The 3 \times HA-tags were introduced using the pYM2 vector as the PCR template. All strains expressing tagged versions were tested for growth and all were found to grow like wild type. Wild-type morphology of mitochondria in cells expressing the HA-fusion proteins was also confirmed by EM (see Figure 3). Strains were grown on 2% lactate medium (Lac) (containing 3 g yeast extract, 1 g NH₄Cl, 1 g KH₂PO₄, 0.5 g CaCl₂ \times 2H₂O, 0.5 g NaCl, 1 g MgSO₄ \times 7H₂O, and 3 mg FeCl₃ per litre) at 24°C for analysis of submitochondrial fractions (Sherman, 1991).

For growth analysis and mitochondrial preparations, strains were cultured as indicated at 24, 30 or 37°C in Lac medium, in YPD medium (1% yeast extract, 2% peptone, 2% glucose) (Sherman, 1991), or synthetic medium (1.7 g Yeast Nitrogen Base and 5 g (NH₄)₂SO₄ per l) containing either 2% lactate (SLac) or 2% glucose (SD) (see Supplementary data for details).

Subfractionation of mitochondria

Mitochondria were swollen for 30 min on ice. Sucrose concentration was adjusted to 0.5 M followed by incubation for 15 min at 0°C and mild sonication. After a clarifying spin (20 000 g, 20 min, 4°C), vesicles were concentrated by centrifugation (120 000 g, 100 min, 4°C). Vesicles were resuspended and separated by a centrifugation of a continuous flotation sucrose gradient (200 000 g, 24 h, 4°C). For detailed protocol see Supplementary data.

Mass spectrometry analysis of proteins from submitochondrial fractions

For sample preparation and mass spectrometry, equal volumes of sucrose gradient fractions were mixed with SILAC standards and supplemented with twice the volume of denaturation buffer (9 M urea, 3 M thiourea, 100 mM Tris/HCl pH 8, 1.5 mM DTT). After alkylation with 2-iodoacetamide, proteins were digested overnight with endoproteinase LysC (Wako Bioproducts, Richmond, VA, USA) and peptides were desalted and concentrated via C18 StageTips (Rappsilber *et al*, 2003). LC-MS experiments with an Easy nLC nanoflow HPLC system coupled to an LTQ Orbitrap XL mass spectrometer (Thermo Fisher Scientific) were performed essentially

as described previously (Olsen *et al*, 2004; Forner *et al*, 2006) with modifications. Columns of 40 cm length and an inner diameter of 75 μ m, packed with 1.8 μ m beads (Reprosil-AQ Pur, Dr Maisch, Entringen, Germany) (Thakur *et al*, 2011), were used and the gradient length was 5 h.

Raw data were analysed using the MaxQuant software environment (Cox and Mann, 2008). Peak lists were searched with Mascot (Perkins *et al*, 1999) against a database containing the translation of all 6809 gene models from the *Saccharomyces* Genome Database release from 12 December 2007 and 175 frequently observed contaminants as well as the reverse sequences of all entries. Both peptide and protein identification were accepted at a 1% false discovery rate, using a decoy database strategy. Protein quantification was exclusively based on peptides with unique sequences.

Electron microscopy

For standard EM, cells were fixed with glutaraldehyde, contrasted with osmium tetroxide, sectioned and subjected to EM (see Supplementary data for details).

For immuno-EM, cells were grown in lactate or glycerol medium to the exponential phase, chemically fixed, embedded in 12% gelatin and cryosectioned as described (Griffith *et al*, 2008). Sections were immunogold labelled using either anti-HA (a kind gift of Guojun Bu, Washington University) or anti-porin (Molecular Probes) antibodies and a protein A-gold 10 nm conjugate before being viewed in a JEOL 1010 electron microscope (JEOL, Tokyo, Japan). The quantitative evaluation of the gold-labelling experiments was performed as follows. A gold particle was assigned to the CJ if at a distance not >20 nm from this site. Likewise, and assigned to the mitochondrial envelope if at a distance not >20 nm from the OM/IM and not localizing to the CJ. The remaining particles present in the interior of the mitochondria were considered in the inner space, which comprises both the cristae and the matrix.

Miscellaneous

Proteolytic susceptibility assay. In all, 50 μ g mitochondria were incubated with either SM buffer (0.6 M sorbitol, 20 mM MOPS, pH 7.4), swelling buffer (20 mM MOPS, pH 7.4) or lysis buffer (1% (v/v) Triton X-100, 20 mM MOPS, pH 7.4) for 30 min on ice. Proteinase K (final concentration of 0.2 mg/ml) was added and the suspension was incubated at 4°C for 15 min. Proteinase K was inhibited by the addition of phenylmethanesulfonyl fluoride (PMSF) to a final concentration of 4 mM and incubation for 10 min on ice. Samples were centrifuged for 20 min (20 000 g, 4°C), resuspended in SM buffer, and precipitated by addition of trichloroacetic acid (TCA; final concentration of 14%). The precipitate was resuspended in Laemmli buffer, subjected to SDS-PAGE and analysed by immunoblotting.

Alkaline extraction. In all, 100 mg mitochondria were resuspended in 75 μ l 20 mM HEPES and 75 μ l 200 mM Na₂CO₃ were added. The suspension was mixed by vortexing for 15 s, incubated for 30 min on ice and centrifuged for 30 min (135 000 g, 4°C). The pellet was resuspended in Laemmli buffer. In all, 30% of the supernatant was TCA precipitated and resuspended in Laemmli buffer. Samples were subjected to SDS-PAGE and analysed by immunoblotting.

Co-isolation assays. For co-isolation of proteins with His-tagged Fcj1, Mcs10, Mcs19, Mcs27, Mcs29 or Mcs12, 1 mg mitochondria isolated from the respective strains were lysed with 1% (w/v) digitonin or 1% (v/v) Triton X-100 as indicated. After Ni-NTA affinity chromatography, fractions were analysed by SDS-PAGE followed by immunoblotting.

Size exclusion chromatography. Isolated mitochondria were incubated for solubilization in digitonin buffer (30 mM Hepes pH 7.4, 100 mM potassium acetate pH 7.4, 5 mM EDTA and 1 mM PMSF, 1% digitonin) at a protein/digitonin ratio of 1/1 for 30 min on ice. After centrifugation for 15 min at 60 000 g and 4°C, cleared lysates were subjected on Superose 6 size exclusion column (GE Healthcare; Elution buffer: 30 mM Hepes pH 7.4, 150 mM KAc pH 7.4, 5 mM EDTA, 1 mM PMSF, 0.1% digitonin). Fractions were analysed by SDS-PAGE and immunoblotting.

Blue native PAGE. Mitochondria (150 μ g protein) were incubated with 20 μ l solubilization buffer (50 mM NaCl, 50 mM imidazole,

2 mM 6-aminohexanoic acid, 1 mM EDTA, 1 mM PMSF, 3% digitonin, pH 7.0) for 15 min at 4°C followed by a clarifying spin for 20 min at 15 000 g and 4°C (Wittig *et al.*, 2006). The supernatant was mixed with 2 µl Native PAGE™ 5% G-250 Sample Additive (Invitrogen) and subjected to BN-PAGE (Native PAGE 3–12% Bis-Tris, Invitrogen). After blotting on PVDF membranes (Roth), immunodecoration using the indicated antibodies was performed.

Supplementary data

Supplementary data are available at *The EMBO Journal* Online (<http://www.embojournal.org>).

Acknowledgements

We thank Petra Heckmeyer, Sabine Tost, Christiane Kotthoff and Petra Robisch for excellent technical assistance. We are grateful

to Kai Hell and Martin Ott for helpful discussions, the late Professor Fritz Miller for the EM micrographs of *Neurospora* mitochondria and Regina Rabl for providing the construct with N-terminally his-tagged Fcjl. This work was supported by the Deutsche Forschungsgemeinschaft, SFB 594. FR is supported by the Netherlands Organization for Health Research and Development (ZonMW-VIDI-917.76.329) and by the Netherlands Organization for Scientific Research (Chemical Sciences, ECHO Grant-700.59.003).

Author contributions: MH, CK, DW, DM, JK and JG performed the experiments. UW, MM and FR supervised the study. WN was involved in conception of the project, supervision and writing of the manuscript.

Conflict of interest

The authors declare that they have no conflict of interest.

References

- Andersen JS, Wilkinson CJ, Mayor T, Mortensen P, Nigg EA, Mann M (2003) Proteomic characterization of the human centrosome by protein correlation profiling. *Nature* **426**: 570–574
- Bayer ME (1991) Zones of membrane adhesion in the cryofixed envelope of *Escherichia coli*. *J Struct Biol* **107**: 268–280
- Boldogh IR, Pon LA (2006) Interactions of mitochondria with the actin cytoskeleton. *Biochim Biophys Acta* **1763**: 450–462
- Brdiczka DG, Zorov DB, Sheu SS (2006) Mitochondrial contact sites: their role in energy metabolism and apoptosis. *Biochim Biophys Acta* **1762**: 148–163
- Chan D, Frank S, Rojo M (2006) Mitochondrial dynamics in cell life and death. *Cell Death Differ* **13**: 680–684
- Cox J, Mann M (2008) MaxQuant enables high peptide identification rates, individualized p.p.b.-range mass accuracies and proteome-wide protein quantification. *Nat Biotechnol* **26**: 1367–1372
- Darshi M, Mendiola VL, Mackey MR, Murphy AN, Koller A, Perkins GA, Ellisman MH, Taylor SS (2011) ChChd3, an inner mitochondrial membrane protein, is essential for maintaining crista integrity and mitochondrial function. *J Biol Chem* **286**: 2918–2932
- Dengjel J, Jakobsen L, Andersen JS (2010) Organelle proteomics by label-free and SILAC-based protein correlation profiling. *Methods Mol Biol* **658**: 255–265
- Dimmer KS, Fritz S, Fuchs F, Messerschmitt M, Weinbach N, Neupert W, Westermann B (2002) Genetic basis of mitochondrial function and morphology in *Saccharomyces cerevisiae*. *Mol Biol Cell* **13**: 847–853
- Donzeau M, Kaldi K, Adam A, Paschen S, Wanner G, Guiard B, Bauer MF, Neupert W, Brunner M (2000) Tim23 links the inner and outer mitochondrial membranes. *Cell* **101**: 401–412
- Fawcett DW (1981) *The Cell*. Philadelphia: W.B. Saunders
- Forner F, Foster LJ, Campanaro S, Valle G, Mann M (2006) Quantitative proteomic comparison of rat mitochondria from muscle, heart, and liver. *Mol Cell Proteomics* **5**: 608–619
- Foster LJ, de Hoog CL, Zhang Y, Xie X, Mootha VK, Mann M (2006) A mammalian organelle map by protein correlation profiling. *Cell* **125**: 187–199
- Frey TG, Mannella CA (2000) The internal structure of mitochondria. *Trends Biochem Sci* **25**: 319–324
- Fritz S, Rapaport D, Klanner E, Neupert W, Westermann B (2001) Connection of the mitochondrial outer and inner membranes by fzo1 is critical for organellar fusion. *J Cell Biol* **152**: 683–692
- Griffith J, Mari M, De Maziere A, Reggiori F (2008) A cryosectioning procedure for the ultrastructural analysis and the immunogold labelling of yeast *Saccharomyces cerevisiae*. *Traffic* **9**: 1060–1072
- Griparic L, Head BP, Van der Bliek AM (2004) Mitochondrial division and fusion. *Topics Curr Genet* **8**: 227–249
- Hackenbrock CR (1968) Chemical and physical fixation of isolated mitochondria in low-energy and high-energy states. *Proc Natl Acad Sci USA* **61**: 598–605
- Harner M, Neupert W, Deponte M (2011) Lateral release of proteins from the TOM complex into the outer membrane of mitochondria. *EMBO J* **30**: 3232–3241
- Head BP, Zulaika M, Ryazantsev S, van der Bliek AM (2011) A novel mitochondrial outer membrane protein, MOMA-1, that affects cristae morphology in *Caenorhabditis elegans*. *Mol Biol Cell* **22**: 831–841
- Hell K (2008) The Erv1-Mia40 disulfide relay system in the intermembrane space of mitochondria. *Biochim Biophys Acta* **1783**: 601–609
- Hess DC, Myers CL, Huttenhower C, Hibbs MA, Hayes AP, Paw J, Clore JJ, Mendoza RM, Luis BS, Nislow C, Giaever G, Costanzo M, Troyanskaya OG, Caudy AA (2009) Computationally driven, quantitative experiments discover genes required for mitochondrial biogenesis. *PLoS Genet* **5**: e1000407
- Hoppins S, Nunnari J (2009) The molecular mechanism of mitochondrial fusion. *Biochim Biophys Acta* **1793**: 20–26
- John GB, Shang Y, Li L, Renken C, Mannella CA, Selker JM, Rangell L, Bennett MJ, Zha J (2005) The mitochondrial inner membrane protein mitofilin controls cristae morphology. *Mol Biol Cell* **16**: 1543–1554
- Knop M, Siegers K, Pereira G, Zachariae W, Winsor B, Nasmyth K, Schiebel E (1999) Epitope tagging of yeast genes using a PCR-based strategy: more tags and improved practical routines. *Yeast* **15**: 963–972
- Kozjak V, Wiedemann N, Milenkovic D, Lohaus C, Meyer HE, Guiard B, Meisinger C, Pfanner N (2003) An essential role of Sam50 in the protein sorting and assembly machinery of the mitochondrial outer membrane. *J Biol Chem* **278**: 48520–48523
- Kunkele KP, Heins S, Dembowski M, Nargang FE, Benz R, Thieffry M, Walz J, Lill R, Nussberger S, Neupert W (1998) The preprotein translocation channel of the outer membrane of mitochondria. *Cell* **93**: 1009–1019
- Larsson NG (2010) Somatic mitochondrial DNA mutations in mammalian aging. *Annu Rev Biochem* **79**: 683–706
- Longtine MS, McKenzie III A, Demarini DJ, Shah NG, Wach A, Brachat A, Philippsen P, Pringle JR (1998) Additional modules for versatile and economical PCR-based gene deletion and modification in *Saccharomyces cerevisiae*. *Yeast* **14**: 953–961
- Mannella CA (2006) The relevance of mitochondrial membrane topology to mitochondrial function. *Biochim Biophys Acta* **1762**: 140–147
- Mannella CA (2008) Structural diversity of mitochondria: functional implications. *Ann NY Acad Sci* **1147**: 171–179
- Meeusen S, DeVay R, Block J, Cassidy-Stone A, Wayson S, McCaffery JM, Nunnari J (2006) Mitochondrial inner-membrane fusion and crista maintenance requires the dynamin-related GTPase Mgm1. *Cell* **127**: 383–395
- Mulkiyanian AY, Cherepanov DA, Heberle J, Junge W (2005) Proton transfer dynamics at membrane/water interface and mechanism of biological energy conversion. *Biochemistry (Mosc)* **70**: 251–256
- Odgren PR, Toukatly G, Bangs PL, Gilmore R, Fey EG (1996) Molecular characterization of mitofilin (HMP), a mitochondria-associated protein with predicted coiled coil and intermembrane space targeting domains. *J Cell Sci* **109**(Part 9): 2253–2264
- Okamoto K, Shaw JM (2005) Mitochondrial morphology and dynamics in yeast and multicellular eukaryotes. *Annu Rev Genet* **39**: 503–536

2 Results

Molecular architecture of mitochondria

M Harner *et al*

- Olsen JV, Ong SE, Mann M (2004) Trypsin cleaves exclusively C-terminal to arginine and lysine residues. *Mol Cell Proteomics* **3**: 608–614
- Ong SE, Blagoev B, Kratchmarova I, Kristensen DB, Steen H, Pandey A, Mann M (2002) Stable isotope labeling by amino acids in cell culture, SILAC, as a simple and accurate approach to expression proteomics. *Mol Cell Proteomics* **1**: 376–386
- Paschen SA, Waizenegger T, Stan T, Preuss M, Cyrklaff M, Hell K, Rapaport D, Neupert W (2003) Evolutionary conservation of biogenesis of beta-barrel membrane proteins. *Nature* **426**: 862–866
- Pellegrini L, Scorrano L (2007) A cut short to death: Parl and Opa1 in the regulation of mitochondrial morphology and apoptosis. *Cell Death Differ* **14**: 1275–1284
- Perkins DN, Pappin DJ, Creasy DM, Cottrell JS (1999) Probability-based protein identification by searching sequence databases using mass spectrometry data. *Electrophoresis* **20**: 3551–3567
- Perkins GA, Ellisman MH, Fox DA (2004) The structure-function correlates of mammalian rod and cone photoreceptor mitochondria: observations and unanswered questions. *Mitochondrion* **4**: 695–703
- Pon L, Moll T, Vestweber D, Marshallsay B, Schatz G (1989) Protein import into mitochondria: ATP-dependent protein translocation activity in a submitochondrial fraction enriched in membrane contact sites and specific proteins. *J Cell Biol* **109**: 2603–2616
- Rabl R, Soubannier V, Scholz R, Vogel F, Mendl N, Vasiljev-Neumeyer A, Korner C, Jagasia R, Keil T, Baumeister W, Cyrklaff M, Neupert W, Reichert AS (2009) Formation of cristae and crista junctions in mitochondria depends on antagonism between Fc1 and Su e/g. *J Cell Biol* **185**: 1047–1063
- Rappsilber J, Ishihama Y, Mann M (2003) Stop and go extraction tips for matrix-assisted laser desorption/ionization, nanoelectrospray, and LC/MS sample pretreatment in proteomics. *Anal Chem* **75**: 663–670
- Reichert AS, Neupert W (2002) Contact sites between the outer and inner membrane of mitochondria-role in protein transport. *Biochim Biophys Acta* **1592**: 41–49
- Renken C, Siragusa G, Perkins G, Washington L, Nulton J, Salamon P, Frey TG (2002) A thermodynamic model describing the nature of the crista junction: a structural motif in the mitochondrion. *J Struct Biol* **138**: 137–144
- Scheffler I (ed). (2011) *Mitochondria*, 2nd edn. New York: Wiley and Sons Ltd
- Scorrano L, Ashiya M, Buttle K, Weiler S, Oakes SA, Mannella CA, Korsmeyer SJ (2002) A distinct pathway remodels mitochondrial cristae and mobilizes cytochrome c during apoptosis. *Dev Cell* **2**: 55–67
- Sesaki H, Jensen RE (2001) UGO1 encodes an outer membrane protein required for mitochondrial fusion. *J Cell Biol* **152**: 1123–1134
- Sesaki H, Jensen RE (2004) Ugo1p links the Fzo1p and Mgm1p GTPases for mitochondrial fusion. *J Biol Chem* **279**: 28298–28303
- Shaw JM, Nunnari J (2002) Mitochondrial dynamics and division in budding yeast. *Trends Cell Biol* **12**: 178–184
- Sherman F (1991) Getting started with yeast. *Methods Enzymol* **194**: 3–21
- Strauss M, Hofhaus G, Schroder RR, Kuhlbrandt W (2008) Dimer ribbons of ATP synthase shape the inner mitochondrial membrane. *EMBO J* **27**: 1154–1160
- Tamai S, Iida H, Yokota S, Sayano T, Kiguchiya S, Ishihara N, Hayashi J, Mihara K, Oka T (2008) Characterization of the mitochondrial protein LETM1, which maintains the mitochondrial tubular shapes and interacts with the AAA-ATPase BCS1L. *J Cell Sci* **121**: 2588–2600
- Thakur SS, Geiger T, Chatterjee B, Bandilla P, Froehlich F, Cox J, Mann M (2011) Deep and highly sensitive proteome coverage by LC-MS/MS without pre-fractionation. *Mol Cell Proteomics* **10**: M110.003699
- Vogel F, Bornhøvd C, Neupert W, Reichert AS (2006) Dynamic subcompartmentalization of the mitochondrial inner membrane. *J Cell Biol* **175**: 237–247
- Wallace DC, Fan W (2009) The pathophysiology of mitochondrial disease as modeled in the mouse. *Genes Dev* **23**: 1714–1736
- Werner S, Neupert W (1972) Functional and biogenetical heterogeneity of the inner membrane of rat-liver mitochondria. *Eur J Biochem* **25**: 379–396
- Westermann B (2010) Mitochondrial fusion and fission in cell life and death. *Nat Rev Mol Cell Biol* **11**: 872–884
- Wittig I, Braun HP, Schagger H (2006) Blue native PAGE. *Nat Protoc* **1**: 418–428
- Wong ED, Wagner JA, Scott SV, Okreglak V, Holewinski TJ, Cassidy-Stone A, Nunnari J (2003) The intramitochondrial dynamin-related GTPase, Mgm1p, is a component of a protein complex that mediates mitochondrial fusion. *J Cell Biol* **160**: 303–311
- Xie J, Marusich MF, Souda P, Whitelegge J, Capaldi RA (2007) The mitochondrial inner membrane protein mitofilin exists as a complex with SAM50, metaxins 1 and 2, coiled-coil-helix coiled-coil-helix domain-containing protein 3 and 6 and DnaJC11. *FEBS Lett* **581**: 3545–3549

2.4 A Crucial Role of Mim2 in the Biogenesis of Mitochondrial Outer Membrane Proteins.

2.4.1 Aim and Summary

The mitochondrial outer membrane (MOM) contains proteins involved in numerous biological processes, such as mitochondrial protein import, cytoskeletal attachment and mtDNA inheritance. Integral MOM proteins are inserted with different topologies, ranging from single and multi alpha-transmembrane helices to beta-barrel structures. Since its identification as a factor involved in mitochondrial protein import [207], the essential protein Mim1 has been implicated in the insertion of single and multispan proteins as well as the translocase of the outer mitochondrial membrane (TOM) complex assembly. Mim1 is further known to be part of a higher molecular weight assembly [14, 135, 239, 245, 302].

To elucidate the function of this complex, we screened for novel interactors of Mim1. To this end, we generated GFP-tagged variants of Mim1, subjected mitochondria to mild detergent lysis and performed immunoprecipitation experiments. Interactors were identified by high resolution MS-based proteomics. SILAC quantification was used to discriminate between specific and unspecific binders.

We identified Mim2 as an interactor of Mim1 and both proteins form the MIM complex. Cells devoid of Mim2 were severely impaired in growth and showed defects in mitochondrial morphology and protein import.

2.4.2 Contribution

This project resulted from a collaboration between the department of Matthias Mann at the MPI of Biochemistry and the group of Doron Rapaport from the Interfaculty Institute of Biochemistry in Tübingen, Germany. To enable the identification of new Mim1 interactors, I developed an immunoprecipitation protocol suited for labile mitochondrial outer membrane protein complexes. I further optimized sample preparation workflows, as well as acquired and analyzed the data of the MS-based interaction screen. The generation of the tagged yeast strains as well as the follow up experiments were performed in Doron Rapaport's laboratory.

2.4.3 Publication

This work is currently in press at the *Journal of Cell Science*.

J Cell Sci. 2012 Mar 30. [Epub ahead of print]

“A Crucial Role of Mim2 in the Biogenesis of Mitochondrial Outer Membrane Proteins.”

Kai S. Dimmer, Drazen Papic, Benjamin Schumann, Desiree Sperl, Katrin Krumpe, **Dirk M. Walther**, and Doron Rapaport

A crucial role for Mim2 in the biogenesis of mitochondrial outer membrane proteins

Kai S. Dimmer¹, Dražen Papić¹, Benjamin Schumann^{1,*}, Desirée Sperl¹, Katrin Krumpe¹, Dirk M. Walther² and Doron Rapaport^{1,‡}

¹Interfaculty Institute of Biochemistry, University of Tübingen, 72076 Tübingen, Germany

²Max Planck Institute of Biochemistry, 82152 Martinsried, Germany

*Present address: Max Planck Institute for Colloids and Interfaces, 14476 Potsdam, and Free University Berlin, 14195 Berlin, Germany

‡Author for correspondence (doron.rapaport@uni-tuebingen.de)

Accepted 12 March 2012

Journal of Cell Science 125, 3464–3473

© 2012. Published by The Company of Biologists Ltd

doi: 10.1242/jcs.103804

Summary

Most of the mitochondrial outer membrane (MOM) proteins contain helical transmembrane domains. Some of the single-span proteins and all known multiple-span proteins are inserted into the membrane in a pathway that depends on the MOM protein Mitochondrial Import 1 (Mim1). So far it has been unknown whether additional proteins are required for this process. Here, we describe the identification and characterization of Mim2, a novel protein of the MOM that has a crucial role in the biogenesis of MOM helical proteins. Mim2 physically and genetically interacts with Mim1, and both proteins form the MIM complex. Cells lacking Mim2 exhibit a severely reduced growth rate and lower steady-state levels of helical MOM proteins. In addition, absence of Mim2 leads to compromised assembly of the translocase of the outer mitochondrial membrane (TOM complex), hampered mitochondrial protein import, and defects in mitochondrial morphology. In summary, the current study demonstrates that Mim2 is a novel central player in the biogenesis of MOM proteins.

Key words: Mim2, MIM complex, Mitochondria, Outer membrane, Protein import

Introduction

The mitochondrial outer membrane (MOM) harbors a diverse set of proteins with functions ranging from biosynthetic pathways, morphogenesis and inheritance of the organelle to protein import into mitochondria (Burri et al., 2006; Schmitt et al., 2006; Zahedi et al., 2006). As all MOM proteins are encoded in the nucleus and translated on ribosomes in the cytosol, they have to be targeted to the organelle and inserted into the membrane (Neupert and Herrmann, 2007; Chacinska et al., 2009; Endo and Yamano, 2009; Walther and Rapaport, 2009). Despite recent progress, the various insertion mechanisms by which MOM proteins are incorporated into the membrane are still poorly understood.

MOM proteins can be divided according to their topologies into different families (Dukanovic and Rapaport, 2011). The β -barrel proteins form one family and are unique to the outer membranes of chloroplasts, mitochondria and Gram-negative bacteria. Their mitochondrial import route via the dedicated complex for topogenesis of outer membrane β -barrel proteins (TOB), also known as sorting and assembly machinery (SAM) complex, is the best studied among the MOM proteins. Three additional protein families contain a single helical transmembrane domain (TMD). The so called tail-anchored (TA) and signal-anchored (SA) proteins bear this domain at their very C- or N-terminus, respectively (Wattenberg and Lithgow, 2001; Waizenegger et al., 2003; Ahting et al., 2005). An additional group is comprised of proteins that contain a central TMD, thus exposing domains to both the cytosol and the intermembrane space (IMS). Finally, a unique group is composed of MOM proteins that transverse the membrane via multiple helical TMDs.

The import pathways of helical MOM proteins are ill defined. Some evidence exists that tail- and signal-anchored proteins

insert into the MOM without participation of a dedicated insertion machinery (Setoguchi et al., 2006; Kemper et al., 2008; Meineke et al., 2008). Other reports suggest a partial overlap in insertion pathways of polytopic and TA proteins (Rojo et al., 2002; Otera et al., 2007).

Two recent reports shed new light on the insertion mechanism of multispan proteins. They demonstrate that the outer membrane protein Mitochondrial Import 1 (Mim1) plays a crucial role in the insertion of multispan MOM proteins (Becker et al., 2011; Papić et al., 2011). The results suggest that precursor proteins are first recognized by Tom70 and then handed over to a Mim1-containing complex. Mim1 was originally identified in a systematic screen as a mutant that accumulates mitochondrial precursor proteins. It is a small integral protein of the MOM with a molecular mass of roughly 13 kDa (Mnaimneh et al., 2004; Dimmer and Rapaport, 2010). Later studies reported that Mim1 is a component of a higher molecular weight complex and that the protein is necessary for biogenesis of Tom20 and Tom70 and therefore also for the assembly of the TOM complex (Ishikawa et al., 2004; Waizenegger et al., 2005; Becker et al., 2008; Hulett et al., 2008; Popov-Celeketić et al., 2008; Lueder and Lithgow, 2009; Becker et al., 2010; Thornton et al., 2010).

Whereas the involvement of Mim1 in the biogenesis of outer membrane (OM) helical proteins is well documented, it has been unclear so far whether additional proteins are required for this process. Furthermore, the actual composition of the Mim1-containing complex and its mode of function are still unknown. Here, we report on the identification and characterization of a novel outer membrane protein, Mim2 that is crucial for proper growth of yeast cells. Mim2 and Mim1 are components of the same functional

2 Results

complex that is playing a central role in the biogenesis of MOM proteins.

Results

Identification of Mim2

Mim1 was reported to be a subunit of a higher molecular weight complex of unknown composition. To search for additional components of the Mim1-containing complex, we performed immunoprecipitation in combination with stable isotope labeling with amino acids in cell culture (SILAC) (Ong et al., 2002). This method has been widely used to identify protein-protein interactions (Selbach and Mann, 2006; Hubner et al., 2010; Vermeulen et al., 2010; Walther and Mann, 2010). Mitochondria were isolated from a *mim1Δ* strain transformed with a vector encoding either Mim1 or GFP–Mim1, organelles were lysed with digitonin, and the lysate was incubated with beads specifically binding GFP. Bound material was digested with the protease LysC and resulting peptides were analyzed by high-resolution mass spectrometry followed by data processing with the MaxQuant software environment (Cox and Mann, 2008). Among the identified proteins particularly the putative open reading frame (ORF) *YLR099W-A* displayed an enrichment very similar to that of the bait protein Mim1 (supplementary material Fig. S1). Due to its identification as an interaction partner of Mim1, we named this ORF *MIM2*. According to the *Saccharomyces* Genome Database (SGD, www.yeastgenome.org), this small ORF is an essential gene and encodes a protein of 87 amino acids. Mim2 has no homologs in higher eukaryotes but is conserved in fungi like *Schizosaccharomyces pombe* and *Neurospora crassa* (Fig. 1A). Although several hydrophobic amino acids are clustered in the middle of the primary sequence (Fig. 1A), no transmembrane domain was predicted by commonly used programs.

Mim2 is an integral protein of the MOM

To investigate the subcellular localization of Mim2, yeast cells deleted for the chromosomal copy of *MIM2* were transformed with a vector encoding either native Mim2 or Mim2 with a C-terminal HA-tag. Both Mim2 and Mim2–HA expressed in this way were functional as they rescued the growth defect of *mim2Δ* cells (supplementary material Fig. S2 and text below). Subcellular fractionation demonstrated that Mim2–HA is present in the mitochondrial fraction (Fig. 1B). Next, we subjected mitochondria harboring Mim2–HA to an alkaline extraction treatment in which soluble and peripheral membrane proteins can be separated from integral membrane proteins by centrifugation. As shown in Fig. 1C, Mim2–HA, like the integral membrane protein Tom40, was enriched in the pellet fraction, suggesting that Mim2 is a mitochondrial membrane protein.

Since mitochondria have two distinct membranes, we wanted to investigate in which membrane Mim2 is located and study its membrane topology. Mitochondria containing Mim2–HA were either left intact or their OM was ruptured under hypo-osmolar conditions. Thereafter samples were treated with proteinase K (PK). In intact mitochondria, Mim2–HA is cleaved and a smaller fragment of about 11 kDa was detected (Fig. 1D, second lane). This fragment was not observed when the MOM was ruptured or when mitochondria were solubilized with detergent (Fig. 1D). The IMS localized protein Dld1 and the matrix protein Mge1 served to control the integrity of the outer and inner membranes,

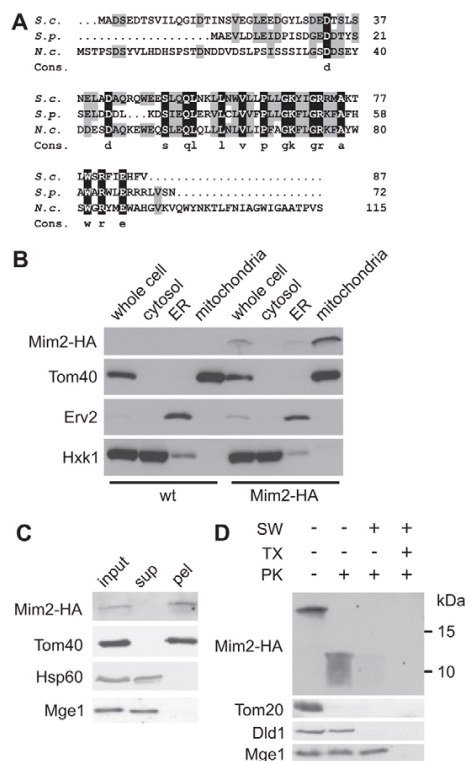


Fig. 1. Mim2 is an integral protein of the MOM with its C-terminus facing the intermembrane space. (A) Mim2 is conserved among fungi. Amino acid sequences of Mim2 from *Saccharomyces cerevisiae* (S.c.), *Schizosaccharomyces pombe* (S.p.) and *Neurospora crassa* (N.c.) are shown. Identical residues are depicted in white on black background, similar residues are highlighted in gray. (B) Mim2 is a mitochondrial protein. Whole-cell lysate (whole cell) and fractions corresponding to cytosol, light microsomal fraction (ER) and mitochondria of either wild-type cells or cells expressing Mim2–HA were analyzed by SDS-PAGE and immunodecoration with antibodies against the HA-tag, the mitochondrial protein Tom40, the ER protein Erv2 and a marker protein for the cytosol (hexokinase, Hxk1). (C) Mim2 is a membrane-embedded protein. Mitochondria isolated from cells expressing Mim2–HA were subjected to carbonate extraction. The supernatant (sup) and pellet (pel) fractions were analyzed by SDS-PAGE and immunodecoration with antibodies against the indicated proteins. Tom40, an integral OM protein; Hsp60 and Mge1, soluble matrix proteins. (D) The C-terminus of Mim2 is protected from protease digestion by the MOM. Mitochondria isolated from cells expressing Mim2–HA were treated with proteinase K (PK) under different conditions. Mitochondria were kept intact, the outer membrane was ruptured by hypo-osmolar swelling (SW) or mitochondria were lysed completely by the addition of the detergent Triton X-100 (TX). Samples were precipitated with trichloroacetic acid and analyzed by SDS-PAGE and immunodecoration with antibodies against the HA-tag, or the indicated mitochondrial proteins. Tom20, an OM protein exposed to the cytosol; Dld1, an IMS protein; Mge1, a matrix protein.

respectively. These results demonstrate that Mim2 is anchored in the MOM with its C-terminus facing the IMS.

An unusual feature of Mim2 is the distribution of charged amino acid residues along its sequence. Negatively charged residues cluster at the N-terminal region, whereas the C-terminal part is positively charged. While low concentrations of the

rather unspecific protease PK were sufficient to cleave Mim2–HA, treating intact mitochondria with high concentrations of trypsin, a protease cutting C-terminally to positively charged amino acids, did not result in a cleavage of Mim2–HA (supplementary material Fig. S3). These results further support

our proposal that the positively charged C-terminal region of Mim2 is protected by the MOM. Taken together our findings suggest that Mim2 is an integral membrane protein of the MOM with its N-terminus located in the cytosol and the C-terminus residing in the IMS.

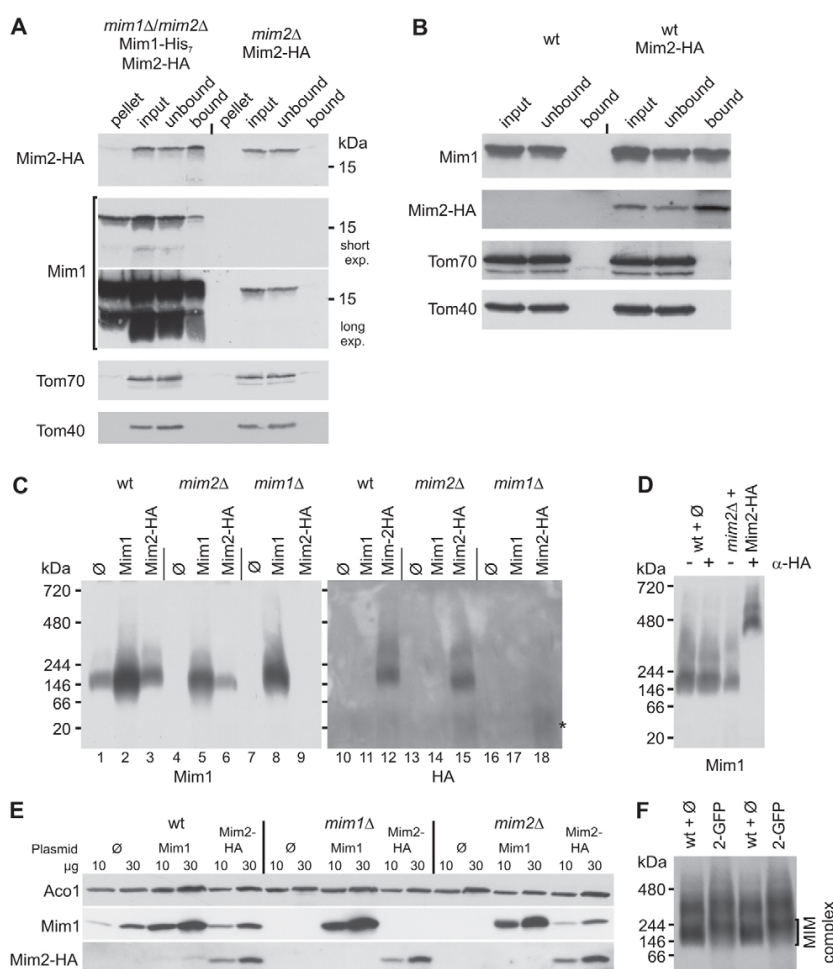


Fig. 2. Mim1 and Mim2 physically interact and are components of the same protein complex. (A) Mitochondria isolated from either the double-deletion strain *mim1Δ/mim2Δ* overexpressing Mim1–His₇ and Mim2–HA or a single deletion strain *mim2Δ* overexpressing Mim2–HA were employed. Organelles were lysed in digitonin-containing buffer and cleared supernatants were incubated with Ni–NTA beads. Non-solubilized matter (pellet), cleared supernatant (input, 20% of total), supernatant after binding to the beads (unbound, 20% of total) and material bound to the beads (bound, 100% of total) were analyzed by SDS-PAGE and immunodecoration with the indicated antibodies. (B) Mitochondria isolated from a strain overexpressing Mim2–HA (Mim2–HA) and the corresponding wild-type strain were lysed in digitonin-containing buffer. Cleared supernatants were incubated with ProteinG Sepharose beads preincubated with an antibody against the HA-tag. Supernatants before (input, 10% of total) and after (unbound, 10% of total) binding to the beads as well as bound material (bound, 100% of total) were analyzed by SDS-PAGE and immunodecoration with the indicated antibodies. (C) Mitochondria isolated from wild-type, *mim1Δ* or *mim2Δ* strains harboring an empty plasmid (Ø) or overexpressing either Mim1 or Mim2–HA were lysed in digitonin and analyzed by BN-PAGE. For analysis of Mim1 and Mim2–HA containing complexes, the membrane was immunodecorated with antibodies against Mim1 and the HA-tag, respectively. An unassembled species of Mim2–HA is indicated with an asterisk. (D) Mitochondria isolated from a wild-type or *mim2Δ* strains containing either empty plasmid (Ø) or overexpressing Mim2–HA were solubilized in digitonin, the lysate was cleared by centrifugation and then incubated with or without an antibody against the HA-tag (α-HA). Samples were analyzed by BN-PAGE and immunodecoration with an antibody against Mim1. (E) Two different amounts (10 µg and 30 µg) of the mitochondria described above in the legend to panel (C) were analyzed by SDS-PAGE and immunodecoration with the indicated antibodies. The matrix protein aconitase (Aco1) served as a control. (F) Mitochondria isolated from a wild-type strain containing empty plasmid (Ø) and a *mim2Δ* strain overexpressing GFP–Mim2 (2-GFP) were solubilized in digitonin, and samples were analyzed by BN-PAGE and immunodecoration with an antibody against Mim1. For easier observation of the small size difference, the same samples were loaded twice in alternating lanes. The MIM complex is indicated.

Mim1 and Mim2 physically interact and are components of the same complex

Although we identified Mim2 as a protein that associates with GFP-Mim1 we wanted to substantiate the interaction between the two proteins by additional pull-down experiments. Mitochondria were isolated from a *mim1Δ/mim2Δ* double-deletion strain overexpressing Mim1-His₇ (Popov-Celeketić et al., 2008) and Mim2-HA. A *mim2Δ* strain overexpressing Mim2-HA that contains non-tagged endogenous Mim1 served as a control (Fig. 2A). The isolated organelles were lysed and proteins were incubated with Ni-NTA beads to pull down Mim1-His₇. Subsequent SDS-PAGE and immunodecoration showed that Mim2-HA specifically bound to the affinity beads together with Mim1-His₇. No unspecific binding of Mim2-HA to the beads was observed with the control sample. Of note, the enrichment of Mim2-HA in the bound material was even higher than that of Mim1-His₇, suggesting a tight association of both proteins. A further potential explanation for this enrichment of Mim2 is that the binding of Mim2 to Mim1-His₇ causes a conformational change in the latter protein that in turn results in an increased accessibility of the His-tag for binding to the affinity beads.

To further verify this interaction, we performed the reciprocal co-immunoprecipitation experiment. Mitochondria isolated from a strain expressing Mim2-HA were solubilized with the mild detergent digitonin and then incubated with beads loaded with antibody specific for the HA-tag. A significant amount of the endogenous Mim1 was co-precipitated together with Mim2-HA (Fig. 2B). No unspecific binding of Mim1 to the beads was observed when the corresponding wild-type mitochondria were used as a control (Fig. 2B).

Mim1 was reported to be a component of a high molecular weight complex (Ishikawa et al., 2004; Waizenegger et al., 2005; Becker et al., 2008; Popov-Celeketić et al., 2008). Our results show that Mim1 and Mim2 tightly interact and indicate that Mim2 is a novel component of this Mim1-containing complex

that we refer to as the MIM complex. To confirm this hypothesis, mitochondria from *mim1Δ* or *mim2Δ* strains overexpressing either Mim1 or Mim2-HA were analyzed by blue native gel electrophoresis (BN-PAGE). Both Mim1 and Mim2-HA migrated as a complex of approximately 200 kDa (Fig. 2C, compare lanes 3 and 12 and supplementary material Fig. S4) confirming that the two proteins are indeed components of the same oligomeric structure. Expression of Mim2-HA in the strain lacking endogenous Mim2 only partially restored the levels of the MIM complex as assessed by BN-PAGE (Fig. 2C, compare lane 6 to lane 1) although the steady-state levels of Mim1 as monitored by SDS-PAGE were almost normal (Fig. 2E). These observations suggest that even though Mim2-HA complements the *mim2Δ* growth phenotype, the HA-tag might interfere with the optimal interaction of Mim2 with Mim1.

Next, we investigated the importance of Mim2 and Mim1 for the formation of the MIM complex. Of note, no Mim1-containing oligomeric species could be detected in the absence of Mim2 and the protein could not be detected in SDS-PAGE and immunodecoration (Fig. 2C, lane 4; 2E). Hence, Mim2 is a crucial player in the biogenesis of Mim1 and the MIM complex. The absence of Mim1 has different effects as it leads to a loss of a detectable Mim2-HA-containing complex but unassembled species of the protein is present (Fig. 2C, lane 18; supplementary material Fig. S5) and expression levels of the protein are unaffected (Fig. 2E).

To further substantiate the participation of both proteins in the same complex we used mitochondria isolated from wild-type and *mim2Δ* cells transformed with either Mim2-HA encoding vector or an empty plasmid as control. Next we lysed the organelles with detergent and performed an antibody-shift assay where antibodies against the HA-tag were added to the lysed organelles before their analysis by BN-PAGE. The antibodies caused a shift in the migration of the Mim1 signal (Fig. 2D), suggesting that both Mim1 and Mim2 are subunits of the same MIM complex.

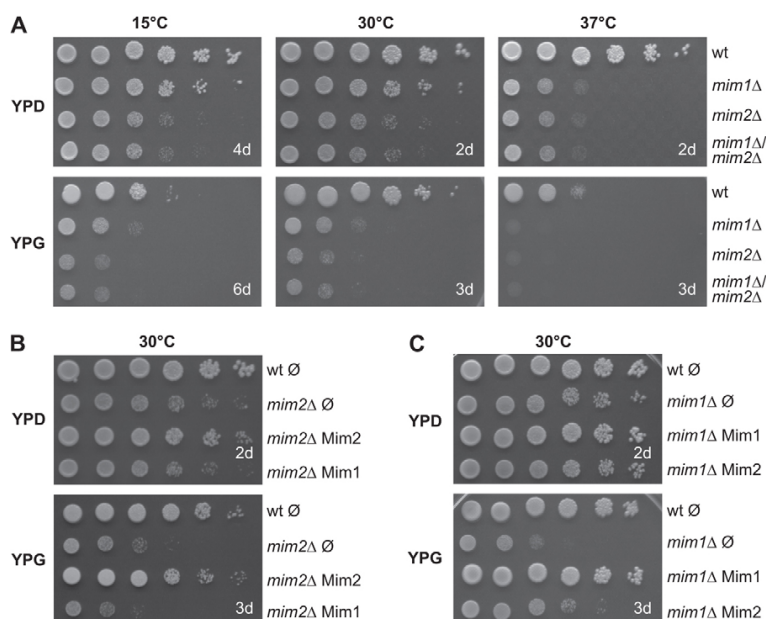


Fig. 3. Deletion of MIM2 results in severe growth phenotypes. (A) Cells that lack Mim1, Mim2 or both proteins show reduced growth at all conditions. The indicated strains were tested at three different temperatures by drop-dilution assay for growth on rich medium containing the fermentable carbon source glucose (YPD) or the non-fermentable carbon source glycerol (YPG). Pictures were taken after the indicated number of days. (B) Overexpression of Mim1 does not rescue the growth defect of a *mim2Δ* strain. Wild-type cells transformed with an empty plasmid and *mim2Δ* cells transformed with an empty plasmid, Mim2 encoding plasmid or Mim1 encoding plasmid were analyzed by drop-dilution assay on YPD or YPG medium. (C) Overexpression of plasmid-borne Mim2 partially rescues the growth defect of the *mim1Δ* strain. Wild-type cells transformed with an empty plasmid and *mim1Δ* cells transformed with an empty plasmid, Mim1 encoding plasmid, or Mim2 encoding plasmid were analyzed by drop-dilution assay on YPD or YPG medium.

Of note, overexpression of Mim1 in the absence of Mim2 resulted in a complex with apparent similar migration behavior to the native complex (Fig. 2C, compare lane 1 to 5). Hence, it seems that Mim2 is not absolutely required for the formation of Mim1-containing complex. This observation further suggests that the native MIM complex probably contains only one or two copies of Mim2. Therefore the absence of Mim2 causes only a minor difference of 10–20 kDa in the mass of the MIM complex and such a difference in turn is hard to resolve by BN-PAGE. In order to obtain further support for our assumption that the two proteins are components of the same native complex, we analyzed the MIM complex in organelles harbouring GFP-tagged Mim2. If Mim1 is a component in the same complex as Mim2, the additional mass of the GFP moiety should shift also the band of the Mim1-containing complex as analyzed by BN-PAGE. Indeed, clear slower migration behavior of the Mim1-complex was observed in the organelles harboring the GFP-tagged Mim2 (Fig. 2F). Taken together, our results suggest that Mim1 and Mim2 are components of the same protein complex.

Deletion of MIM2 causes severe growth phenotype

The ORF *YLR099W-A/MIM2* was reported in a systematic deletion attempt to be an essential gene (Kastenmayer et al., 2006). We wanted to confirm the reported lethality by deleting the complete ORF of *MIM2* in the diploid yeast strain W303a/ α and then performing tetrad analysis. After sporulation and tetrad dissection, haploid *mim2 Δ* strains were retrieved as confirmed by PCR (data not shown). In contrast to the reported lethality, this deletion strain was viable although it showed a severe growth reduction on fermentable and non-fermentable carbon sources at all tested temperatures (Fig. 3A). The growth behavior of the *mim2 Δ* strain is even worse than that of the strain lacking Mim1 and the double-deletion strain grows like the *mim2 Δ* strain (Fig. 3A). To exclude the possibility that the observed phenotypes were caused by unrelated changes, e.g. changes in the promoter region of the essential *ERG27* gene – which is in close proximity on the chromosome to the *MIM2* gene – we aimed to complement these phenotypes by plasmid-encoded Mim2. Overexpression of native or the C-terminally tagged version of Mim2 could rescue the growth phenotype of the deletion mutant confirming that the observed phenotypes are related to the absence of the Mim2 protein (supplementary material Fig. S2).

MIM2 and MIM1 genetically interact

Our results suggest that Mim1 and Mim2 physically interact and are components of the same protein complex. Hence we asked whether the two ORFs also genetically interact. We could not observe a synthetic growth phenotype by deletion of both genes (Fig. 3A). Of note, overexpression of Mim1 in yeast cells lacking Mim2 slightly hampered the growth of the *mim2 Δ* strain (Fig. 3B). Accordingly, the steady-state levels of the MIM substrate Ugo1 are somewhat reduced in these cells (supplementary material Fig. S6). On the other hand, overexpression of Mim2 in a *mim1 Δ* strain led to partial rescue of the growth phenotype (Fig. 3C). This partial rescue was observed in six independent transformants and was paralleled by elevated levels of Ugo1. Furthermore, the overexpression of Mim2–HA in the *mim1 Δ* strain caused higher levels of Tom40 and less unassembled Tom40 molecules as compared to *mim1 Δ*

cells (supplementary material Fig. S7). These results suggest that higher levels of Mim2 can reduce the dependency on Mim1 for some processes. Collectively, in addition to their physical association, *MIM1* and *MIM2* genetically interact.

Deletion of MIM2 leads to abnormal mitochondrial morphology

It was previously reported that downregulation of Mim1 leads to altered mitochondrial morphology (Altmann and Westermann, 2005; Dimmer and Rapaport, 2010). It is assumed that this phenotype results from the impaired assembly of the TOM complex and the subsequent insufficient import of morphology

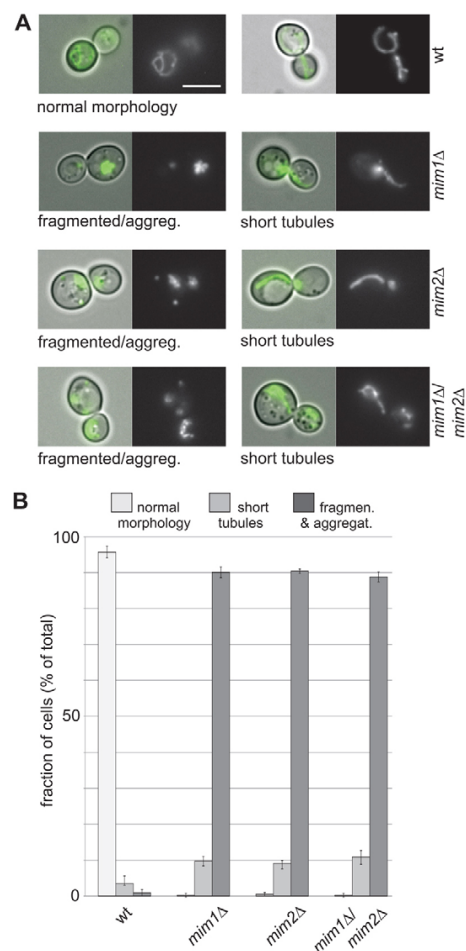


Fig. 4. Cells that lack Mim1, Mim2 or both proteins show altered mitochondrial morphology. (A) Cells of the indicated strains transformed with mitochondrially targeted GFP (pSu9-GFP) were analyzed by fluorescence microscopy. Examples of predominant phenotypes (fragmented/aggregated and short tubular) for each strain are shown (scale bar: 5 μ m). (B) Analyzed cells of the various strains were grouped into three different morphology phenotypes (normal, short tubules, and fragmented and aggregated). Statistical analysis of four different experiments, in which ≥ 100 cells per experiment were analyzed, was performed and the various occurrences of the phenotypes are presented.

relevant proteins. We verified this phenotype by deletion of *MIM1* in the wild-type background W303 (Fig. 4A). Typically for this deletion strain, mitochondria were fragmented and aggregated in approximately 90% of the cells (Fig. 4B). Very similar morphological phenotype was observed upon deletion of *MIM2* alone or in the *mim1Δ/mim2Δ* double-deletion strain (Fig. 4A,B). These results provide further evidence that Mim1 and Mim2 function in the same molecular pathway.

Loss of Mim2 leads to reduced biogenesis of mitochondrial proteins

To gain further insight into the function of Mim2, we analyzed the steady-state levels of proteins in mitochondria isolated from *mim2Δ* cells. Of note, Mim1 was hardly detectable in these organelles and a severe reduction was observed in the levels of the MOM proteins Tom20, Fzo1 and Ugo1 – known substrates of Mim1 (Fig. 2E; Fig. 5A, left panel) (Waizenegger et al., 2005; Becker et al., 2011; Papic et al., 2011). In contrast to Tom20, the levels of all other TOM components tested – Tom40, Tom22 and Tom70 – did not show a significant reduction in mitochondria lacking Mim2. Similarly, the steady-state levels of other mitochondrial proteins like the MOM β-barrel protein Por1, the tail-anchored protein Fis1, the inner membrane proteins Oxa1 and Dld1, as well as the matrix proteins Hsp60 and aconitase were unaltered in comparison to those in wild-type organelles (Fig. 5A, right panel).

We next compared the assembly status of the TOM complex in mitochondria isolated from strains lacking Mim2, Mim1 or both. The amount of assembled TOM complex as assessed by immunodecoration with antibodies against Tom40 and Tom22 was drastically reduced when *MIM1*, *MIM2* or both were deleted

(Fig. 5B). Concomitantly, an unassembled species of Tom40 was observed in the mutated cells. The observations regarding the reduced stability of the TOM complex in *mim1Δ* cells are in line with previous reports (Ishikawa et al., 2004; Waizenegger et al., 2005). The assembly of the TOB complex as monitored by BN-PAGE was unchanged in these deletion strains (Fig. 5B). Collectively, the absence of Mim2 resulted in reduced steady-state levels of Tom20 and multispan MOM proteins as well as reduced stability of the TOM complex.

Mitochondria lacking Mim2 show compromised import of multispan MOM proteins

Since the steady-state levels of certain mitochondrial proteins were reduced in mitochondria lacking Mim2, we investigated its role in mitochondrial protein import. To this end we first analyzed whole-cell extracts for accumulation of mitochondrial precursor proteins, a phenotype that was observed in cells lacking Mim1 (Ishikawa et al., 2004; Mnaimneh et al., 2004; Waizenegger et al., 2005). We observed a clear accumulation of unprocessed precursor form of the matrix protein Hep1 in extracts from cells lacking Mim1 or Mim2 or both proteins (Fig. 6A). This indicates a global import defect of mitochondria lacking Mim2.

Next we investigated the in vitro import for model substrates located in the different mitochondrial compartments. Isolated mitochondria were incubated with radioactive precursor proteins for different time points and import was assessed by SDS-PAGE and autoradiography. The import efficiencies for the matrix destined preprotein pSu9-DHFR, the inner membrane protein AAC, as well as the β-barrel precursor porin were reduced (Fig. 6B). Of note, the most pronounced reduction was in the case of the MOM multispan proteins Ugo1 and Fzo1 (Fig. 6B). In

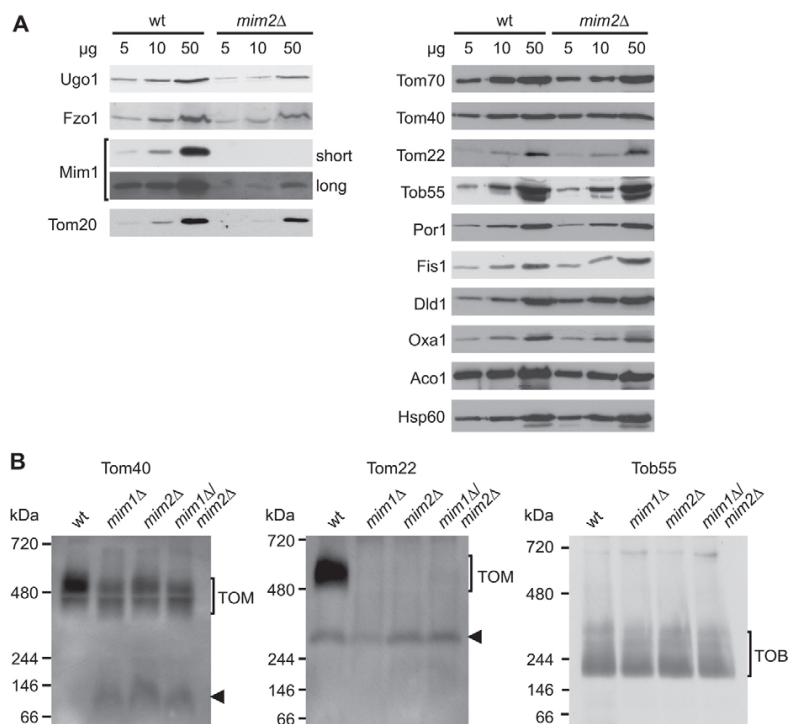
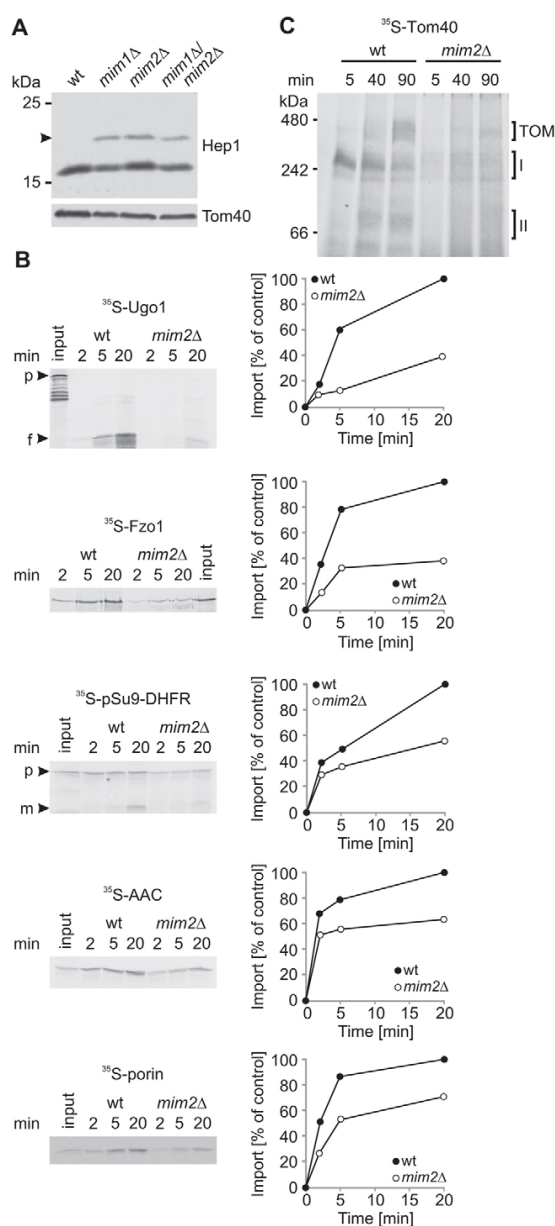


Fig. 5. Absence of Mim2 leads to reduced steady-state levels of helical MOM proteins and a compromised assembly of the TOM complex. (A) Various amounts of mitochondria (5, 10 and 50 μg) isolated from wild-type and *mim2Δ* cells were analyzed by SDS-PAGE and immunodecoration with the indicated antibodies. A representative experiment of three different independent repeats is presented. (B) Mitochondria of the indicated strains were first lysed in 1% digitonin (for TOM analysis) or in 0.5% Triton X-100 (for TOB analysis) and then subjected to BN-PAGE and immunoblotting with the indicated antibodies. Arrowheads indicate the Tom40-containing low molecular mass species and the Tom22 assembly intermediate. The assembled TOM and TOB complexes are indicated. A representative experiment of three different independent repeats is presented.

contrast, the import of the tail-anchored MOM protein Fis1, which is inserted independently of any known import factors (Kemper et al., 2008), was unaffected by the absence of Mim2 (data not shown). The global defect in mitochondrial import results most probably from a reduced number of functional TOM complexes. In accordance with the reduced steady-state levels of assembled TOM complex in mitochondria lacking Mim2 (Fig. 5B), the assembly of newly synthesized Tom40 molecules into the TOM complex is severely hampered in *mim2Δ* cells (Fig. 6C).



We aimed to analyze the direct import defects due to lower levels of Mim2 avoiding the global outcome resulting from compromised biogenesis of Tom components and hampered assembly of the TOM complex. To that end a yeast strain in which the expression of *MIM2-HA* was under the control of the *GAL1* promoter was constructed. In the presence of galactose the cells grew like wild-type cells whereas growth on glucose was strongly compromised. We first tested the levels of various mitochondrial proteins in total cell lysates from the *GAL1-MIM2-HA* cells grown at various time periods after the shift from galactose- to glucose-containing medium (data not shown). On the basis of this analysis we isolated mitochondria from cells grown for 15 h on glucose and analyzed their proteins by immunodecoration. Of note, Mim2 and its partner protein Mim1 were hardly detectable in these organelles whereas the Tom components were still in normal levels (supplementary material Fig. S8A). Furthermore, the TOM complex as analyzed by BN-PAGE was also detected in normal levels (supplementary material Fig. S8B). Next, in vitro import assays were performed with mitochondria depleted for Mim2. Importantly, whereas the insertion of the MIM substrate Ugo1 into these organelles was compromised, no import defects were observed for the TOM substrates pSu9-DHFR and porin (supplementary material Fig. S8C). Taken together the results suggest that the absence of Mim2 causes two effects: a specific reduction in membrane integration of some outer membrane helical proteins and subsequently a global import defect due to altered stability of the TOM complex.

Mim2 is directly involved in the import of Ugo1

Finally, we asked whether Mim2 actually participates in interactions with substrate proteins. To that end, we analyzed import reactions of newly synthesized [³⁵S]Ugo1 by BN-PAGE in combination with an antibody-shift assay. Mitochondria were isolated from wild-type and *mim2Δ* cells transformed with an empty plasmid and a plasmid encoding Mim2-HA, respectively. After import of Ugo1, mitochondria were lysed in digitonin,

Fig. 6. Deletion of *MIM2* leads to various import defects and impaired assembly of the TOM complex. (A) Whole-cell lysates of wild-type cells and those lacking Mim1, Mim2 or both proteins were analyzed by SDS-PAGE and immunodecoration with the indicated antibodies. The precursor of the mitochondrial matrix protein Hep1 is indicated by an arrowhead. (B) Mitochondria isolated from a wild-type or *mim2Δ* strain were incubated with the indicated radiolabeled precursor proteins for the indicated time periods. At the end of the import reactions samples were treated as described below, analyzed by SDS-PAGE and autoradiography, and bands corresponding to imported material were quantified. Samples containing radiolabeled Ugo1 were trypsinized in order to generate a specific 23 kDa fragment (f) (see Papic et al., 2011). After import of Fzo1, carbonate extraction was performed and the membranous fraction was analyzed; when pSu9-DHFR was imported, the mature protein (m) was quantified. After import of porin and AAC mitochondria were treated with PK and the protected molecules were quantified. The intensity of bands representing imported material into wild-type mitochondria for the longest time period was set as 100%. (p) precursor form of pSu9-DHFR and full-length Ugo1. A representative experiment of three independent repeats is presented. (C) Radiolabeled precursor of Tom40 was imported into mitochondria that had been isolated from *mim2Δ* or the corresponding wild-type strain. After import, the mitochondria were solubilized with digitonin and analyzed by BN-PAGE and autoradiography. The two assembly intermediates of Tom40 (I, II) and the assembled TOM core complex (TOM) are indicated.

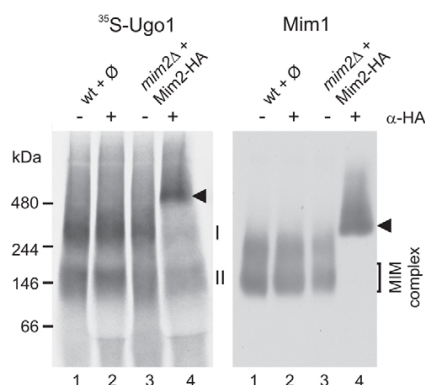


Fig. 7. Mim2 is directly involved in Ugo1 import. Mitochondria isolated from a wild-type strain containing the empty plasmid (Ø) and from a *mim2Δ* strain overexpressing Mim2–HA were incubated with radiolabeled precursor of Ugo1. After the import reactions mitochondria were solubilized in digitonin; the lysate was cleared by centrifugation and then incubated with or without an antibody against the HA-tag (α-HA). Samples were analyzed by BN-PAGE, autoradiography (left panel) and then immunodecoration with an antibody against Mim1 (right panel). Mim2-containing complexes that were shifted by the antibody are indicated by an arrowhead.

halved and an antibody specific for the HA-tag was added to one portion. Strikingly, addition of the antibody resulted in a shift of the radioactive signal of [³⁵S]Ugo1 to higher molecular weights only if mitochondria harboring Mim2–HA were used (Fig. 7, left panel, arrowhead). Thus, Mim2 interacts with substrate proteins. A similar shift was observed for the Mim1 signal (Fig. 7, right panel) suggesting that both Mim1 and Mim2 are subunits of the functional substrate-binding MIM complex.

Taken together, this study reveals that the integral MOM protein Mim2 is a novel component of the MIM complex that mediates the import of integral MOM helical proteins.

Discussion

In this work we report on the identification of Mim2 as a novel protein with a crucial function in the biogenesis of mitochondria. Mim2 is located in the MOM, exposing its N-terminus to the cytosol and the C-terminus to the IMS. The protein shares this topology with its binding partner Mim1 and it also shows functional similarity to the latter protein. Altered mitochondrial morphology, reduced growth, lower steady-state levels of several mitochondrial components as well as compromised assembly of TOM complex are consequences of both *MIM2* and *MIM1* deletion. Mim1, Tom20 and the multispan proteins of the MOM seem to be the main substrates that are affected by the absence of Mim2. We propose that hampered biogenesis in the absence of Mim2 results in reduced steady-state amounts and assembly of different proteins in *mim2Δ* cells that in turn cause the other observed phenotypes in these cells. For example, the altered morphology of mitochondria in *mim1Δ* and *mim2Δ* cells can be explained by the lower levels of their substrate proteins Fzo1 and Ugo1. The latter two proteins mediate mitochondrial fusion and thus their reduced levels interfere with the balance between fusion and fission of the organelles.

Strikingly, the steady-state level of Mim1 is severely reduced in mitochondria lacking Mim2. This finding might suggest that the

observed effects in *mim2Δ* cells are solely due to the loss of Mim1. Yet several observations are in contrast to this scenario. First, the growth phenotype of *mim1Δ* cells can be partially rescued by the overexpression of Mim2. Therefore additional copies of Mim2 can, to a certain extent, reduce the requirement for Mim1. Second, overexpression of Mim1 in a *mim2Δ* strain does not improve the growth retardation but rather has even somewhat negative effect on growth. These observations suggest a unique function of Mim2 and might indicate that in the absence of Mim2 some unassembled Mim1 molecules exert a dominant-negative effect by competing with the function of the MIM complex. Third, our pull-down experiments and native electrophoresis assays demonstrate that both proteins are present in a stable functional complex that interacts with substrate proteins.

Our results shed new light on the stoichiometry of the MIM complex as they show that reduced levels of Mim1 or its overexpression have a minor effect on complex size. Thus it seems that the actual complex of around 200 kDa contains a rather fixed number of copies of Mim1 and Mim2. In the absence of Mim1 we could not observe a Mim2-containing sub-complex suggesting that Mim1 is a crucial component for the formation of the MIM complex. In contrast, a Mim1-containing complex was formed even in the absence of Mim2 suggesting that the latter protein is not absolutely essential for complex formation. Naturally, we cannot exclude the possibility that additional, yet to be identified, proteins are further components of the MIM complex. Future efforts to functionally reconstitute the complex from isolated subunits can provide an answer to this open question. Taken together, the identification and characterization of Mim2 get us one step ahead in solving the riddle of import of outer membrane proteins, yet the elucidation of the precise composition of the MIM complex and its molecular mode of action has to be the next venture.

Materials and Methods

SILAC-based immunoprecipitation

Mim1Δ (YPH499 background) cells expressing plasmid encoding either native Mim1 or GFP-Mim1 were grown in synthetic media containing either ¹⁵N₂-¹³C₆ lysine (heavy) or (light) lysine (Ong et al., 2002). Cells were harvested in mid-exponential phase and mitochondria were isolated after enzymatic spheroplastation, using an abridged protocol. EDTA was omitted from all buffers. Mitochondria were lysed in 1% digitonin, 10% (v/v) glycerol, 150 mM NaCl, 50 mM MOPS/KOH, pH 7.4, containing complete protease inhibitor cocktail (Roche). Samples were clarified by centrifugation and incubated with GFP-binder beads (gta100, Chromotek). Beads were isolated, washed and pooled according to forward (Mim1 light and GFP-Mim1 heavy) and reverse (Mim1 heavy and GFP-Mim1 light) experiments. Proteins were eluted with 4% SDS, 100 mM Tris–HCl pH 8.0, 0.1 M DTT and subjected to filter aided sample preparation method and digestion with endoproteinase (Wiśniewski et al., 2009).

Mass spectrometry and data analysis

Peptides were separated by nLC at 4 h gradient length without prior fractionation, electrosprayed online and analyzed with LTQ-Orbitrap-XL or Orbitrap-Velos mass spectrometers using collision-induced dissociation or higher-energy collisional dissociation fragmentation, respectively (Olsen et al., 2005; Olsen et al., 2009). Data analysis was performed using the MaxQuant software environment (Cox and Mann, 2008) version 1.0.13.9. Searches of generated peak lists were carried out with Mascot (Perkins et al., 1999) against the translation of all 6809 gene models from the Saccharomyces Genome Database (release date 12 December 2007) and 175 frequently observed contaminants. Identifications were accepted at a false discovery rate of 1% both at the peptide and protein level using a decoy database strategy with reversed protein sequences (Elias and Gygi, 2007).

Yeast strains and growth conditions

Standard genetic techniques were used for growth and manipulation of yeast strains. Unless otherwise stated, the wild-type strain W303 was used. The *mim1Δ/mim2Δ* double-deletion strain was obtained by mating of the single deletion strains followed by tetrad dissection. Transformation of yeast was carried out according to the

lithium-acetate method. For drop-dilution assays, yeast cells were grown in synthetic medium to an OD₆₀₀ of 1.0, diluted in fivefold increment, and then 5 µl of each dilution were spotted onto solid media and growth was monitored for few days.

Recombinant DNA techniques

To express Mim1 or Mim2 in yeast cells with or without a C-terminal HA-tag, the ORF of *MIM1* or *MIM2* (systematic name *YHR099W-A*) was amplified by PCR with or without its stop codon using yeast genomic DNA as template. Primers used contained *EcoRI* and *HindIII* restriction sites which were used to introduce the amplified fragment into the expression vector pYX142 which contains the HA-tag sequence. Constructs were verified by sequencing. For expression of Mim1 with a C-terminal His₇-tag, the plasmid pRS426-TPIpro-Mim1-His₇ was used (Popov-Celeketić et al., 2008).

Yeast genes were deleted by a PCR-based approach using the HIS3 marker amplified from pFA6a-His3MX6 plasmid (Wach et al., 1997) or the kanamycin resistance cassette amplified from pFA6a-kanMX4 plasmid (Wach et al., 1994). For the deletion of *MIM1* the primers KSD311 (5'-AGAAACATCACCCTTCT-TACGAAACTGCCACAAGACAGAAATCGTACGTCGAGGTCGAC-3') and KSD 312 (5'-GTGTGTGTATTTATTTATGTAGTTGCTAATGCTTTGGTGAT-CGTATCGATGAATTCGAGCTCG-3') were used, for *MIM2* KSD099f (5'-CCCAGCACCACAGACATCACTGCAGCAGCAACAATACTAGAACCGT-ACGCTGCAGGTCGAC-3') and KSD099r (5'-TTATCTGTTATAACTGCTA-TATGCGGATACATAAACAACAACATCGATGAATTCGAGCTCG-3'). Deletion of genes was confirmed by screening-PCR. Haploid deletions strains were obtained by tetrad dissection.

A yeast strain harboring Mim2 under the control of an inducible promoter was obtained by transforming the pYX113-GAL1pro-*MIM2*-HA vector into *mim2Δ* strain. To construct this plasmid the *MIM2* ORF without the stop codon was subcloned from pYX142-*MIM2*-HA. For expression of GFP-Mim2 the ORF of *MIM2* was cloned into pYX132-Nterm-GFP using *BamHI* and *HindIII* sites. The pYX132-Nterm-GFP plasmid contains the coding sequence for GFP without a stop codon cloned between *EcoRI* and *BamHI* sites.

Biochemical procedures

Mitochondria were isolated from yeast cells by differential centrifugation as previously described (Daum et al., 1982). Subcellular fractionation was performed according to published procedures (Walther et al., 2009). Import experiments with radiolabeled precursor proteins and isolated mitochondria were performed in an import buffer containing 250 mM sucrose, 0.25 mg/ml BSA, 80 mM KCl, 5 mM MgCl₂, 10 mM MOPS-KOH, 2 mM NADH, 2 mM ATP, pH 7.2. Radiolabeled precursor proteins were synthesized in rabbit reticulocyte lysate in the presence of [³⁵S]methionine. Import assays for the mitochondrial precursor proteins pSu9-DHFR, AAC, Porin, and Ugo1 were performed as described before (Papic et al., 2011). For swelling experiments, isolated mitochondria were incubated with a hypotonic buffer (20 mM HEPES, pH 7.2) for 30 min on ice. In the carbonate extraction reaction mitochondria were dissolved in 0.1 M Na₂CO₃. After 30 min on ice, samples were centrifuged (75,000 g, 60 min, 2°C) and pellet and supernatant were analyzed.

For pull-down experiments, mitochondria from the *mim1Δ/mim2Δ* yeast strain expressing Mim2-HA and Mim1-His₇ or the *mim2Δ* strain expressing Mim2-HA were used. After lysis in digitonin buffer (0.5% digitonin, 20 mM Tris-HCl, 50 mM NaCl, 10% glycerol, 1 mM PMSF, pH 7.4) and clarifying spin (20,000 g, 20 min, 2°C) supernatants were incubated for 1 h at 2°C with Ni-NTA agarose beads (NEB) that were pre-equilibrated in digitonin-buffer. After washing twice, bound material was analyzed by SDS-PAGE and immunodecoration.

Co-immunoprecipitation experiments were performed using isolated wild-type mitochondria and mitochondria isolated from a strain expressing Mim2-HA. After binding of the HA-antibody to Protein G Sepharose beads these were incubated with cleared lysate of the mitochondria in digitonin buffer (1% digitonin, 20 mM Tris-HCl, 50 mM NaCl, 10% glycerol, 1 mM PMSF, pH 7.4). After several washes, bound proteins were analyzed by SDS-PAGE and immunodecoration.

Protein samples were analyzed by SDS-PAGE and blotting to nitrocellulose membranes followed by visualization through autoradiography. Alternatively, incubation with antibodies was carried out according to standard procedures and visualization was performed via the ECL method. Intensity of the observed bands was quantified with the AIDA software (Raytest). Unless stated otherwise, each presented experiment represents at least three independent repetitions.

Blue native PAGE

Mitochondria were lysed in 40 µl TX-100 or digitonin buffer (0.5% TX-100 or 1-1.5% digitonin, 20 mM Tris-HCl, 0.1 mM EDTA, 50 mM NaCl, 10% glycerol, 1 mM PMSF, pH 7.4). After incubation for 15 min at 4°C and a clarifying spin (30,000 g, 15 min, 2°C), 5 µl sample buffer (5% [w/v] Coomassie Brilliant Blue G-250, 100 mM Bis-Tris, 500 mM 6-aminocaproic acid, pH 7.0) were added, and the mixture was analyzed by electrophoresis in a 6 to 13% gradient blue native gel (Schägger et al., 1994). Gels were blotted to polyvinylidene fluoride membranes and proteins were further analyzed by autoradiography or immunodecoration. For

antibody shift, the antibody was added to the cleared mitochondrial lysate and the samples were incubated 30 min on ice prior to the addition of the sample buffer.

Fluorescence microscopy

For visualization of mitochondria, cells were transformed with a yeast expression vector harboring the mitochondrial presequence of subunit 9 of the F₀-ATPase of *N. crassa* fused to GFP, pVT100U-mtGFP (Westermann and Neupert, 2000). Microscopy images were acquired with an Axioskop20 fluorescence microscope equipped with an Axiocam MRm camera using the 43 Cy3 filter set and the AxioVision software (Zeiss).

Acknowledgements

We thank K. Rehn and E. Kracker for technical support, F. Essmann for helpful discussions and critically reading the manuscript, and J. Müller (IFIB, Tübingen, Germany) and A. Barna (IFIB, Tübingen, Germany) for providing plasmids.

Funding

This work was supported by the Deutsche Forschungsgemeinschaft [grant number RA 1048/4-1 to D.R.], and a postdoctoral fellowship from the Carl Zeiss Stiftung (K.S.D.).

Supplementary material available online at

<http://jcs.biologists.org/lookup/suppl/doi:10.1242/jcs.103804/-/DC1>

References

- Ahting, U., Waizenegger, T., Neupert, W. and Rapaport, D. (2005). Signal-anchored proteins follow a unique insertion pathway into the outer membrane of mitochondria. *J. Biol. Chem.* **280**, 48-53.
- Altmann, K. and Westermann, B. (2005). Role of essential genes in mitochondrial morphogenesis in *Saccharomyces cerevisiae*. *Mol. Biol. Cell* **16**, 5410-5417.
- Becker, T., Pfannschmidt, S., Guiard, B., Stojanovski, D., Milenkovic, D., Kutik, S., Pfanner, N., Meisinger, C. and Wiedemann, N. (2008). Biogenesis of the mitochondrial TOM complex: Mim1 promotes insertion and assembly of signal-anchored receptors. *J. Biol. Chem.* **283**, 120-127.
- Becker, T., Guiard, B., Thornton, N., Zufall, N., Stroud, D. A., Wiedemann, N. and Pfanner, N. (2010). Assembly of the mitochondrial protein import channel: role of Tom5 in two-stage interaction of Tom40 with the SAM complex. *Mol. Biol. Cell* **21**, 3106-3113.
- Becker, T., Wenz, L. S., Krüger, V., Lehmann, W., Müller, J. M., Goroncy, L., Zufall, N., Lithgow, T., Guiard, B., Chacinska, A. et al. (2011). The mitochondrial import protein Mim1 promotes biogenesis of multispanning outer membrane proteins. *J. Cell Biol.* **194**, 387-395.
- Burri, L., Vascotto, K., Gentle, I. E., Chan, N. C., Beilharz, T., Stapleton, D. I., Ramage, L. and Lithgow, T. (2006). Integral membrane proteins in the mitochondrial outer membrane of *Saccharomyces cerevisiae*. *FEBS J.* **273**, 1507-1515.
- Chacinska, A., Koehler, C. M., Milenkovic, D., Lithgow, T. and Pfanner, N. (2009). Importing mitochondrial proteins: machineries and mechanisms. *Cell* **138**, 628-644.
- Cox, J. and Mann, M. (2008). MaxQuant enables high peptide identification rates, individualized p.p.b.-range mass accuracies and proteome-wide protein quantification. *Nat. Biotechnol.* **26**, 1367-1372.
- Daum, G., Gasser, S. M. and Schatz, G. (1982). Import of proteins into mitochondria. Energy-dependent, two-step processing of the intermembrane space enzyme cytochrome b2 by isolated yeast mitochondria. *J. Biol. Chem.* **257**, 13075-13080.
- Dimmer, K. S. and Rapaport, D. (2010). The enigmatic role of Mim1 in mitochondrial biogenesis. *Eur. J. Cell Biol.* **89**, 212-215.
- Dukanovic, J. and Rapaport, D. (2011). Multiple pathways in the integration of proteins into the mitochondrial outer membrane. *Biochim. Biophys. Acta* **1808**, 971-980.
- Elias, J. E. and Gygi, S. P. (2007). Target-decoy search strategy for increased confidence in large-scale protein identifications by mass spectrometry. *Nat. Methods* **4**, 207-214.
- Endo, T. and Yamano, K. (2009). Multiple pathways for mitochondrial protein traffic. *Biol. Chem.* **390**, 723-730.
- Hubner, N. C., Bird, A. W., Cox, J., Spletstoeser, B., Bandilla, P., Poser, I., Hyman, A. and Mann, M. (2010). Quantitative proteomics combined with BAC TransgeneOmics reveals in vivo protein interactions. *J. Cell Biol.* **189**, 739-754.
- Hulett, J. M., Lueder, F., Chan, N. C., Perry, A. J., Wolynec, P., Likić, V. A., Gooley, P. R. and Lithgow, T. (2008). The transmembrane segment of Tom20 is recognized by Mim1 for docking to the mitochondrial TOM complex. *J. Mol. Biol.* **376**, 694-704.
- Ishikawa, D., Yamamoto, H., Tamura, Y., Moritoh, K. and Endo, T. (2004). Two novel proteins in the mitochondrial outer membrane mediate beta-barrel protein assembly. *J. Cell Biol.* **166**, 621-627.
- Kastenmayer, J. P., Ni, L., Chu, A., Kitchen, L. E., Au, W. C., Yang, H., Carter, C. D., Wheeler, D., Davis, R. W., Boeke, J. D. et al. (2006). Functional genomics of

- genes with small open reading frames (sORFs) in *S. cerevisiae*. *Genome Res.* **16**, 365-373.
- Kemper, C., Habib, S. J., Engl, G., Heckmeyer, P., Dimmer, K. S. and Rapaport, D. (2008). Integration of tail-anchored proteins into the mitochondrial outer membrane does not require any known import components. *J. Cell Sci.* **121**, 1990-1998.
- Lueder, F. and Lithgow, T. (2009). The three domains of the mitochondrial outer membrane protein Mim1 have discrete functions in assembly of the TOM complex. *FEBS Lett.* **583**, 1475-1480.
- Meineke, B., Engl, G., Kemper, C., Vasiljev-Neumeyer, A., Paulitschke, H. and Rapaport, D. (2008). The outer membrane form of the mitochondrial protein Mcl1 follows a TOM-independent membrane insertion pathway. *FEBS Lett.* **582**, 855-860.
- Mnaimneh, S., Davierwala, A. P., Haynes, J., Moffat, J., Peng, W. T., Zhang, W., Yang, X., Pootoolal, J., Chua, G., Lopez, A. et al. (2004). Exploration of essential gene functions via titratable promoter alleles. *Cell* **118**, 31-44.
- Neupert, W. and Herrmann, J. M. (2007). Translocation of proteins into mitochondria. *Annu. Rev. Biochem.* **76**, 723-749.
- Olsen, J. V., de Godoy, L. M., Li, G., Macek, B., Mortensen, P., Pesch, R., Makarov, A., Lange, O., Horning, S. and Mann, M. (2005). Parts per million mass accuracy on an Orbitrap mass spectrometer via lock mass injection into a C-trap. *Mol. Cell. Proteomics* **4**, 2010-2021.
- Olsen, J. V., Nielsen, M. L., Damoc, N. E., Griep-Raming, J., Moehring, T., Makarov, A., Schwartz, J., Horning, S. and Mann, M. (2009). Characterization of the Velos, an enhanced LTQ orbitrap, for proteomics. *Mol. Cell. Proteomics* **8**, S40-S41.
- Ong, S. E., Blagoev, B., Kratchmarova, I., Kristensen, D. B., Steen, H., Pandey, A. and Mann, M. (2002). Stable isotope labeling by amino acids in cell culture, SILAC, as a simple and accurate approach to expression proteomics. *Mol. Cell. Proteomics* **1**, 376-386.
- Otera, H., Taira, Y., Horie, C., Suzuki, Y., Suzuki, H., Setoguchi, K., Kato, H., Oka, T. and Mihara, K. (2007). A novel insertion pathway of mitochondrial outer membrane proteins with multiple transmembrane segments. *J. Cell Biol.* **179**, 1355-1363.
- Papic, D., Krumpe, K., Dukanovic, J., Dimmer, K. S. and Rapaport, D. (2011). Multispan mitochondrial outer membrane protein Ugo1 follows a unique Mim1-dependent import pathway. *J. Cell Biol.* **194**, 397-405.
- Perkins, D. N., Pappin, D. J., Creasy, D. M. and Cottrell, J. S. (1999). Probability-based protein identification by searching sequence databases using mass spectrometry data. *Electrophoresis* **20**, 3551-3567.
- Popov-Celeketić, J., Waizenegger, T. and Rapaport, D. (2008). Mim1 functions in an oligomeric form to facilitate the integration of Tom20 into the mitochondrial outer membrane. *J. Mol. Biol.* **376**, 671-680.
- Rojo, M., Legros, F., Chateau, D. and Lombès, A. (2002). Membrane topology and mitochondrial targeting of mitofusins, ubiquitous mammalian homologs of the transmembrane GTPase Fzo. *J. Cell Sci.* **115**, 1663-1674.
- Schägger, H., Cramer, W. A. and von Jagow, G. (1994). Analysis of molecular masses and oligomeric states of protein complexes by blue native electrophoresis and isolation of membrane protein complexes by two-dimensional native electrophoresis. *Anal. Biochem.* **217**, 220-230.
- Schmitt, S., Prokisch, H., Schlunck, T., Camp, D. G., 2nd, Ahting, U., Waizenegger, T., Scharfe, C., Meitinger, T., Imhof, A., Neupert, W. et al. (2006). Proteome analysis of mitochondrial outer membrane from *Neurospora crassa*. *Proteomics* **6**, 72-80.
- Selbach, M. and Mann, M. (2006). Protein interaction screening by quantitative immunoprecipitation combined with knockdown (QUICK). *Nat. Methods* **3**, 981-983.
- Setoguchi, K., Otera, H. and Mihara, K. (2006). Cytosolic factor- and TOM-independent import of C-tail-anchored mitochondrial outer membrane proteins. *EMBO J.* **25**, 5635-5647.
- Thornton, N., Stroud, D. A., Milenkovic, D., Guiard, B., Pfanner, N. and Becker, T. (2010). Two modular forms of the mitochondrial sorting and assembly machinery are involved in biogenesis of alpha-helical outer membrane proteins. *J. Mol. Biol.* **396**, 540-549.
- Vermeylen, M., Eberl, H. C., Matarese, F., Marks, H., Denissov, S., Butter, F., Lee, K. K., Olsen, J. V., Hyman, A. A., Stunnenberg, H. G. et al. (2010). Quantitative interaction proteomics and genome-wide profiling of epigenetic histone marks and their readers. *Cell* **142**, 967-980.
- Wach, A., Brachat, A., Pöhlmann, R. and Philippsen, P. (1994). New heterologous modules for classical or PCR-based gene disruptions in *Saccharomyces cerevisiae*. *Yeast* **10**, 1793-1808.
- Wach, A., Brachat, A., Alberti-Segui, C., Rebischung, C. and Philippsen, P. (1997). Heterologous HIS3 marker and GFP reporter modules for PCR-targeting in *Saccharomyces cerevisiae*. *Yeast* **13**, 1065-1075.
- Waizenegger, T., Stan, T., Neupert, W. and Rapaport, D. (2003). Signal-anchor domains of proteins of the outer membrane of mitochondria: structural and functional characteristics. *J. Biol. Chem.* **278**, 42064-42071.
- Waizenegger, T., Schmitt, S., Zivkovic, J., Neupert, W. and Rapaport, D. (2005). Mim1, a protein required for the assembly of the TOM complex of mitochondria. *EMBO Rep.* **6**, 57-62.
- Walther, D. M. and Rapaport, D. (2009). Biogenesis of mitochondrial outer membrane proteins. *Biochim. Biophys. Acta* **1793**, 42-51.
- Walther, D. M., Papic, D., Bos, M. P., Tommassen, J. and Rapaport, D. (2009). Signals in bacterial beta-barrel proteins are functional in eukaryotic cells for targeting to and assembly in mitochondria. *Proc. Natl. Acad. Sci. USA* **106**, 2531-2536.
- Walther, T. C. and Mann, M. (2010). Mass spectrometry-based proteomics in cell biology. *J. Cell Biol.* **190**, 491-500.
- Wattenberg, B. and Lithgow, T. (2001). Targeting of C-terminal (tail)-anchored proteins: understanding how cytoplasmic activities are anchored to intracellular membranes. *Traffic* **2**, 66-71.
- Westermann, B. and Neupert, W. (2000). Mitochondria-targeted green fluorescent proteins: convenient tools for the study of organelle biogenesis in *Saccharomyces cerevisiae*. *Yeast* **16**, 1421-1427.
- Wiśniewski, J. R., Zougman, A., Nagaraj, N. and Mann, M. (2009). Universal sample preparation method for proteome analysis. *Nat. Methods* **6**, 359-362.
- Zahedi, R. P., Sickmann, A., Boehm, A. M., Winkler, C., Zufall, N., Schönfisch, B., Guiard, B., Pfanner, N. and Meisinger, C. (2006). Proteomic analysis of the yeast mitochondrial outer membrane reveals accumulation of a subclass of preproteins. *Mol. Biol. Cell* **17**, 1436-1450.

3 Discussion and Outlook

3.1 The Proteome of Aging

3.1.1 Studying Aging by Quantitative Proteomics

The causes of numerous human diseases are well understood at the molecular level, owing to revolutionary advances in the biomedical sciences. In this respect, aging is a notable exception. Hence, its mechanism has been referred to as “one of the great unsolved mysteries of biology” [2]. A general consensus exists as to the fact that senescence is associated with a broad range of cellular deteriorations. However, it is difficult to discriminate between effects that are causative of and those merely associated with aging since reliable experimental evidence is often lacking. During the past two decades, it has become evident that longevity is regulated by specific cellular signaling pathways. Nonetheless, it remains largely obscure how the transcription factors acting downstream of these signaling cascades achieve lifespan extension.

Aging has been studied in different laboratory model systems all of which have distinct advantages and disadvantages. The nematode *C. elegans* with its short lifespan and easy maintenance is ideally suited for forward and reverse genetic screens to identify modulators of longevity. After their initial discovery, new longevity candidate genes can immediately be validated within weeks. This led to the establishment of several important paradigms in aging research which were later shown to be conserved in mammals. Adult nematodes exclusively contain postmitotic somatic cells and thus cannot serve as a model for a variety of biological processes important in mammalian aging, such as telomere shortening or stem cell aging.

Studying the impact of specific genes on longevity in mice is considerably more difficult. Besides the effort to generate transgenic animals, subsequent studies for lifespan determination are costly and take several years. However, aging-related physiological and biochemical changes can be analyzed with a broad range of assays and results are likely to be more relevant to human health.

Since the introduction of microarrays, researchers have attempted to define how aging and lifespan-modulating signaling pathways affect gene expression. Relatively large

sets of genes involved in multiple biochemical processes were identified, but the overlap between individual studies was often low. This, for example, holds true for reports of age-related transcriptional changes in mouse brain [140, 171, 183, 221] or *C. elegans* [30, 101]. Similarly, little overlap was found between individual reports addressing the transcriptional response of DAF-16, the transcription factor responsible for lifespan extension via the IIS pathway [202, 218].

A major limitation of transcriptomics approaches is the fact that posttranscriptional regulatory mechanisms may influence the steady state concentrations and activities of proteins. An emerging body of evidence suggests that aging affects the integrity of the proteostasis network, and it is likely that processes like translation efficiency, folding and degradation play an even more important role in this field of research. MS based proteomics has only very recently enabled the analysis of complex protein mixtures to a depth of several thousands of proteins. Moreover, the concept of SILAC labeling has been extended to a wide range of multicellular model organisms. We have made use of these technological advances to address aging in two commonly used model organisms. The studies presented in this thesis address proteome changes in both mice and *C. elegans* in a comparable experimental setup and therefore provide insight into how well aging is conserved in evolution.

3.1.2 The Proteome of Mice, but Not of Worms Is Conserved during Aging

The most striking difference between mice and worms is the sheer extent of proteome remodeling during aging. While pronounced protein abundance changes are observed in *C. elegans*, tight homeostasis is maintained in mouse tissue (Figure 3.1.1). Although the two species differ substantially in lifespan, the comparison was done between similar time points with respect to biological age. Animals were considered young adults soon after entering the reproductive phase whereas old animals were defined as an age at which less than 50% of the initial population remained alive. At first sight, the discrepancy between worm and mouse could be attributed to the fact that all cells in adult nematodes are post-mitotic. However, if proteome maintenance in mammals was predominantly achieved by mitotic cell replacement, the degree of proteome conservation should have differed according to the mitotic index of individual mouse tissues. Instead, protein levels were found to be equally well preserved across a variety of tissues during aging. Both brain and heart muscle are known to have very low rates of cell division and are thus considered post-mitotic but showed similarly low shifts in protein expression as kidney, a tissue with a higher rate of cell division [72].

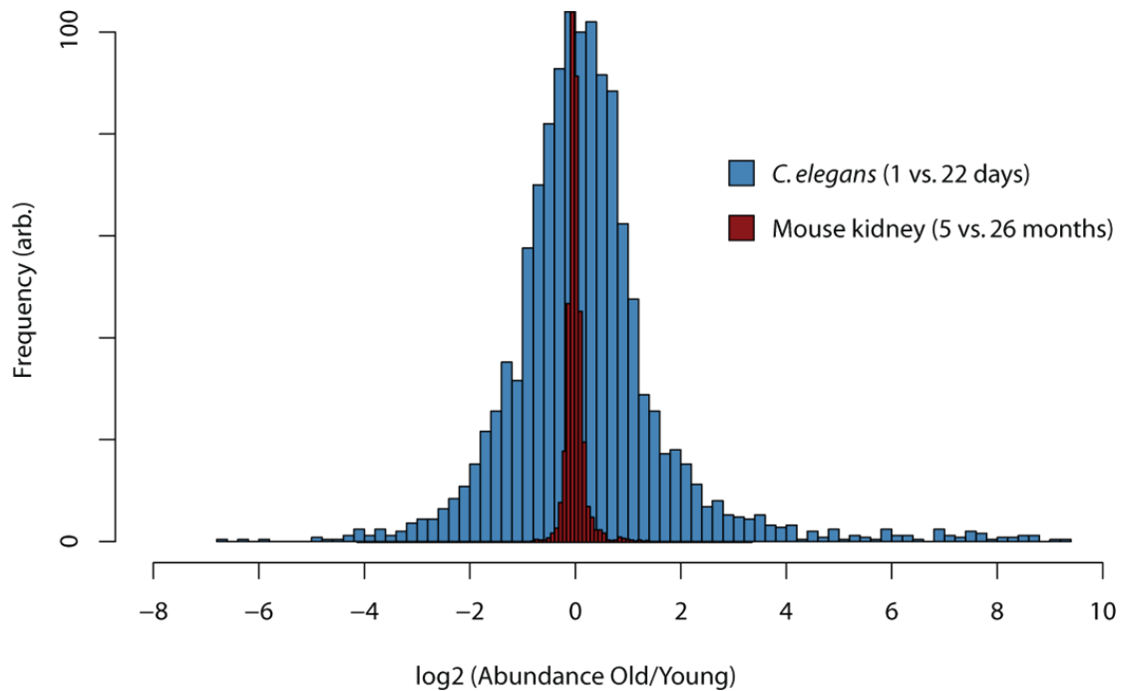


Figure 3.1.1: Proteome changes during aging in *C. elegans* and mice. Logarithmic abundance differences detected between the proteomes of young and old animals were calculated and plotted as histograms.

Recent data from us and other groups suggest that an age-dependent proteostasis decline is conserved in metazoan evolution. For example, we and others have demonstrated a pronounced accumulation of misfolded protein deposits in nematodes [57, 253]. In humans, aging is the highest risk factor for the onset of several neurodegenerative diseases related to an accumulation of misfolded proteins, including Alzheimer's, Parkinson's and Huntington's disease. This indicates that selective pressure has optimized proteome maintenance to ensure minimal proteotoxic stress and thereby the highest level of fitness before and during the reproductive phase. Both in worms and in mice, this selective pressure is abolished after approximately one third of the maximum lifespan under laboratory conditions [118, 190] when fertility is compromised due to oocyte quality decline [189]. In line with this notion, we show that aging in *C. elegans* results in a successive proteome remodeling which is most pronounced immediately after the cessation of the reproductive phase. Moreover, proteins with an abundance increase were generally more prone to become insoluble at a later time point in life. Finally, depleting some of the most aggregation-prone proteins significantly extended lifespan. Therefore, it is conceivable that age related proteostasis decline and

the resulting deleterious proteome imbalance is at least one limiting factor to the post-reproductive lifespan in worms.

Surprisingly, although proteostasis decline itself is conserved from worm to mouse, aging appears to result in much lower proteome imbalance in mice compared to *C. elegans*. The complexity of the two organisms, however, differs greatly. In contrast to mammals, nematodes possess a simple anatomy with rudimentary organs. Although formal evidence is lacking, it is tempting to speculate that the requirements for a tight proteome maintenance have drastically increased during evolution. Even a relatively subtle degree of proteome imbalance in any essential organ could result in death mammalian organisms whereas nematodes might tolerate much more extensive deregulation in protein expression. One could therefore state that mammals have become “addicted” to highly efficient proteostasis during evolution.

3.1.3 Outlook and Future Directions

The work presented here only offers a snapshot of how aging affects the proteome in metazoans. The fact that this process is not well conserved between two organisms which are far apart in the tree of life raises the question whether more closely related species share a more similar degree of proteome maintenance. An obvious first step towards addressing this question would be the analysis of additional organisms within the same orders of the organisms used in this thesis, Rhabditida or rodents, respectively. For example, the effect of aging on the nematode *C. briggsae* and additional species closely related to *C. elegans* could be studied using a similar experimental setup based on SILAC quantification. Similarly, isogenic young and aged rats could be obtained. However, due to a lack of an available SILAC labeled reference material, quantification would have to be achieved either by a super-SILAC or chemical labeling strategy, because label-free approaches would not be accurate enough for the expected low abundance changes. These datasets would allow to answer the question whether either of the two analyzed organisms represents an exceptional case in terms protein maintenance during senescence. In a next step, proteomics could be employed to investigate the aging process of additional model organisms such as the fruit fly *Drosophila melanogaster* or the zebrafish *Danio rerio*, both of which can be subjected to SILAC labeling. These data would provide valuable insights as to when in evolution the requirement for highly efficient proteostasis arose.

So far, we have primarily investigated protein abundance changes during aging. Established enrichment methods for peptides carrying post-translational modifications, especially phosphorylation, acetylation and ubiquitination could be applied to study

how these modifications are affected by senescence in mammalian tissues. While altered phosphorylation patterns could reveal deregulation of specific kinases or phosphatases, increased abundance of ubiquitinated proteins may point at deficiencies in protein degradation. Moreover, the implication of the deacetylase family of sirtuins, most prominently SIRT3, in age-related pathologies such as cancer, heart failure and neurodegenerative diseases [112, 301] suggest that acetylation plays a major role in the aging process. Knockout mice of the mitochondrial sirtuins, SIRT3 and SIRT5, have been generated [184], both of which displayed specific metabolic changes ranging from fatty acid metabolism to respiration and reactive oxygen species defense [301]. Large scale acetylome mapping of these strains would strongly contribute to our understanding how protein acetylation regulates metabolism and how it is affected by aging. Finally, the accumulation of oxidated amino acid side chains has been suggested to be a major cause of cellular decay. However, convincing data as to the extent of these modifications in aged tissues is lacking. Thus, oxidative modifications could be a promising target for MS-based proteomics. A major technical challenge is the fact that peptides are subjected to relatively harsh conditions during sample preparation and analysis procedure and are therefore prone to oxidative *in vitro* modifications. Protocols aimed at quantifying such modifications would either have to employ chemical derivatization strategies or perform all preparation in an inert gas environment to exclude reactions with ambient air oxygen. To increase sensitivity, enrichment strategies via modification specific antibodies would further have to be considered. An encouraging example that the analysis of oxidative modifications by MS-based proteomics is feasible has been provided by a recent report in which methionine oxidations were successfully quantified [98].

The fact that misfolded protein aggregates accumulate during aging has recently been established in flies and worms [57, 61, 253]. Although the overall composition of the proteome remains virtually unchanged in various mouse tissues, it is conceivable that aging may also reduce the solubility of a subset of the proteome and thereby interfere with its function. Hence, a low stringency isolation procedure for insoluble proteins in mammalian tissues, similar to the protocol developed for *C. elegans*, should be established. Proteomic analysis of these fractions would clarify whether aggregates other than amyloid precursors drive the progression of senescence, as our data suggests for nematodes.

Collectively, the advances in MS-based proteomics have the potential to provide researchers with data allowing to test several opposing aging theories critically and advance our understanding of the aging process at the molecular level.

3.2 Mitochondrial Organellar Proteomics

Studying the composition and function of protein complexes in mitochondrial membranes is challenging and requires tailor made protocols. For example, several detergents have been established which allow gentle membrane lysis while maintaining the integrity of large protein complexes. By this means, these complexes become accessible to analysis by protocols such as blue native electrophoresis (BNGE) or immunoprecipitation.

In the first publication, we employed digitonin lysis to screen for novel interactors of the MOM protein Mim1, using an affinity-tagged variant of the protein [65]. The experiment was performed as a crossover SILAC experiment to distinguish between interactors and background binders. In contrast to immunoprecipitation experiments with soluble proteins, the resulting dataset showed a large number of proteins which were significantly enriched in the pulldown over the control. Virtually all of these were known to reside in the MOM but were unlikely to be genuine Mim1 interactors. This finding suggests that the lysis protocol did not yield complete solubilization but rather dissociated membranes into patches, which were subsequently purified during the immunoprecipitation experiment. Since the complex was unlikely to withstand more stringent lysis or washing procedures, a second data filtering step based on label free quantification was applied, assuming a higher recovery for direct interactors due to a closer proximity to the bait protein. This approach proved to be successful and lead to the identification of Mim2, a novel subunit of the MIM complex.

So far, our approach is limited to subunits with high copy numbers within complexes and might not be suitable to detect substoichiometric binders. To that end, it would be advantageous to include an orthogonal second purification step. For example, SILAC labeled cells expressing human influenza hemagglutinin (HA) epitope-tagged variants of membrane embedded bait proteins, or unlabeled control cells, could be subjected to mitochondrial isolation followed by detergent solubilization. After elution with high concentrations of HA peptides under native conditions, isolated complexes could be subjected to blue native gel electrophoresis to separate different complex isoforms and remove contaminating proteins. SILAC quantification would allow to exclude contaminants that are introduced through non-specific binding to either tube walls or resin. Once the subunits of a particular complex are established, subsequent experiments with spiked-in SILAC labeled protein epitope signature tag (PrEST) constructs [313] could be performed to reveal their precise stoichiometry. This approach would also be suitable to analyze established complexes in more detail.

Of note, the observed specific enrichment of contaminating proteins in our pulldown

experiment may provide an explanation for incorrectly identified interactors of mitochondrial membrane proteins in the literature. For example, the protein Mdm10 was previously suggested to be a subunit of the TOB/SAM complex. The authors used a similar solubilization protocol as in our case. However, only qualitative MS analysis or antibody-based Western detection of the purified complex members was performed [203]. The presence of this protein in the TOB/SAM complex remains controversial [303].

In a further study, also part of this thesis, an entirely different experimental strategy lead to the discovery of the MICOS, the complex responsible for CS formation [119]. Instead of dissolving membranes with the help of detergents, mild sonication was applied to shear the organelles into vesicles. These vesicles were subjected to density gradient centrifugation and quantified in different fractions via a spike-in SILAC standard. This powerful concept of PCP has previously been applied to assign proteins to specific organelles. However, it has not previously been applied to resolve suborganellar structures. Besides the discovery of MICOS, our dataset contains a rich resource allowing to discriminate between proteins residing in or being associated with either of the two mitochondrial membranes as well as contaminants from other organelles. Moreover, fine structures in the abundance profiles of particular proteins even allowed to predict substoichiometrical interactions between MIM and MOM proteins. Our adaptation of the PCP method could therefore be applied in the future to address biological questions in which submitochondrial localization plays a role. Furthermore, physical contacts between different organelles could be established in this fashion. Collectively, novel biochemical approaches, combined with high resolution-MS, will enable researchers to dissect numerous mitochondrial processes at much greater detail.

Abbreviations

3D	three-dimensional
AC	alternating current
APEX	absolute protein expression profiling
ATP	Adenosine-5'-triphosphate
CID	collision induced decay
CJ	cristae junction
CS	mitochondrial contact site
daf	dauer formation
DBE	<i>daf-16</i> family member binding element
DC	direct current
DDL	<i>daf-16</i> dependent longevity
DHIC	DDL-1 containing HSF-1 inhibitory complex
emPAI	exponentially modified protein abundance index
ESI	electrospray ionization
ETD	electron transfer dissociation
FT	Fourier transformation
GFP	green fluorescent protein
GO	gene ontology
HCD	higher energy collisional dissociation
HSE	heat shock response element
HSF	heat shock factor
iBAQ	intensity based absolute quantification
ICAT	isotope-coded affinity tag
ICR	ion cyclotron resonance
IGF	insulin-like growth factor
IGF-IR	insulin-like growth factor 1 receptor
IMS	mitochondrial intermembrane space
IR	insulin receptor
IRR	insulin receptor-related receptor
iTRAQ	isobaric tags for relative and absolute quantitation

JNK	Jun N-terminal kinase
LOPIT	localization of organelle proteins by isotope tagging
LTQ	linear trap quadrupole
MALDI	matrix-assisted laser desorption/ionization
MICOS	mitochondrial contact site
MIM	mitochondrial inner membrane
MOM	mitochondrial outer membrane
MS	mass spectrometry
MS/MS	tandem mass spectrometry
mtDNA	mitochondrial DNA
NADH	nicotinamide adenine dinucleotide
NADPH	nicotinamide adenine dinucleotide phosphate
ORF	open reading frame
PAI	protein abundance index
PCP	protein correlation profiling
PMF	post-mitochondrial fraction
RF	radio frequency
RNAi	RNA interference
ROS	reactive oxygen species
SILAC	stable isotope labeling by amino acids in cell culture
SIR	silent information regulator
TOF	time of flight mass analyzer
TOR	target of rapamycin
wt	wild type
XIC	extracted ion current
YFP	yellow fluorescent protein

References

- [1] D. Accili and K. C. Arden. FoxOs at the crossroads of cellular metabolism, differentiation, and transformation. *Cell*, 117(4):421–426, May 2004.
- [2] D. Ackerman and D. Gems. The mystery of *C. elegans* aging: an emerging role for fat. Distant parallels between *C. elegans* aging and metabolic syndrome? *Bioessays*, 34(6):466–471, Jun 2012.
- [3] R. Aebersold and M. Mann. Mass spectrometry-based proteomics. *Nature*, 422(6928):198–207, Mar 13 2003.
- [4] S. Agarwal and R. S. Sohal. DNA oxidative damage and life expectancy in houseflies. *Proc Natl Acad Sci U S A*, 91(25):12332–5, Dec 6 1994.
- [5] L. Aitlhadj and S. R. Stürzenbaum. The use of FUdR can cause prolonged longevity in mutant nematodes. *Mech Ageing Dev*, 131(5):364–365, May 2010.
- [6] Z. F. Altun, L. A. Herndon, C. Crocker, R. Lints, and D. H. e. Hall. WormAtlas, 2002-2010.
- [7] J. Amin, J. Anathan, and R. Voellmy. Key Features of Heat-shock Regulatory Elements. *Molecular and Cellular Biology*, 8(9):3761–3769, Sept. 1988.
- [8] J. S. Andersen, C. J. Wilkinson, T. Mayor, P. Mortensen, E. A. Nigg, and M. Mann. Proteomic characterization of the human centrosome by protein correlation profiling. *Nature*, 426(6966):570–4, Dec 4 2003.
- [9] R. S. Annan, M. J. Huddleston, R. Verma, R. J. Deshaies, and S. A. Carr. A multi-dimensional electrospray MS-based approach to phosphopeptide mapping. *Anal Chem*, 73(3):393–404, Feb 2001.
- [10] R. S. Balaban, S. Nemoto, and T. Finkel. Mitochondria, oxidants, and aging. *Cell*, 120(4):483–95, Feb 25 2005.
- [11] W. E. Balch, R. I. Morimoto, A. Dillin, and J. W. Kelly. Adapting proteostasis for disease intervention. *Science*, 319:916–919, 2008.

- [12] M. Bantscheff, M. Schirle, G. Sweetman, J. Rick, and B. Kuster. Quantitative mass spectrometry in proteomics: a critical review. *Anal Bioanal Chem*, 389(4):1017–31, Oct 2007.
- [13] A. Barthel, D. Schmoll, and T. G. Unterman. FoxO proteins in insulin action and metabolism. *Trends Endocrinol Metab*, 16(4):183–189, 2005.
- [14] T. Becker, L.-S. Wenz, V. Krüger, W. Lehmann, J. M. Müller, L. Goroncy, N. Zufall, T. Lithgow, B. Guiard, A. Chacinska, R. Wagner, C. Meisinger, and N. Pfanner. The mitochondrial import protein Mim1 promotes biogenesis of multispanning outer membrane proteins. *J Cell Biol*, 194(3):387–395, Aug 2011.
- [15] I. Ben-Porath and R. A. Weinberg. The signals and pathways activating cellular senescence. *Int J Biochem Cell Biol*, 37(5):961–976, May 2005.
- [16] A. Ben-Zvi, E. A. Miller, and R. I. Morimoto. Collapse of proteostasis represents an early molecular event in *Caenorhabditis elegans* aging. *Proceedings of the National Academy of Sciences of the United States of America*, 106(35):14914–14919, Sept. 2009.
- [17] R. J. Berry and M. E. Jakobson. Life and death in an island population of the house mouse. *Exp Gerontol*, 6(2):187–197, Apr 1971.
- [18] F. Blondeau, B. Ritter, P. D. Allaire, S. Wasiak, M. Girard, N. K. Hussain, A. Angers, V. Legendre-Guillemain, L. Roy, D. Boismenu, R. E. Kearney, A. W. Bell, J. J. M. Bergeron, and P. S. McPherson. Tandem MS analysis of brain clathrin-coated vesicles reveals their critical involvement in synaptic vesicle recycling. *Proc Natl Acad Sci U S A*, 101(11):3833–3838, Mar 2004.
- [19] M. Bluher, B. B. Kahn, and C. R. Kahn. Extended longevity in mice lacking the insulin receptor in adipose tissue. *Science*, 299:572–574, 2003.
- [20] A. G. Bodnar, M. Ouellette, M. Frolkis, S. E. Holt, C. P. Chiu, G. B. Morin, C. B. Harley, J. W. Shay, S. Lichtsteiner, and W. E. Wright. Extension of life-span by introduction of telomerase into normal human cells. *Science*, 279(5349):349–352, Jan 1998.
- [21] P. J. Boersema, T. T. Aye, T. A. B. van Veen, A. J. R. Heck, and S. Mohammed. Triplex protein quantification based on stable isotope labeling by peptide dimethylation applied to cell and tissue lysates. *Proteomics*, 8(22):4624–4632, Nov 2008.

-
- [22] P. V. Bondarenko, D. Chelius, and T. A. Shaler. Identification and relative quantitation of protein mixtures by enzymatic digestion followed by capillary reversed-phase liquid chromatography-tandem mass spectrometry. *Anal Chem*, 74(18):4741–4749, Sep 2002.
- [23] B. P. Braeckman and J. R. Vanfleteren. Genetic control of longevity in *C. elegans*. *Exp Gerontol*, 42(1-2):90–98, 2007.
- [24] A. H. Brand and N. Perrimon. Targeted gene expression as a means of altering cell fates and generating dominant phenotypes. *Development*, 118(2):401–415, Jun 1993.
- [25] S. Brenner. The genetics of *Caenorhabditis elegans*. *Genetics*, 77(1):71–94, May 1974.
- [26] S. Broughton and L. Partridge. Insulin/IGF-like signalling, the central nervous system and aging. *Biochemical Journal*, 418:1–12, Feb 15 2009.
- [27] H. M. Brown-Borg, K. E. Borg, C. J. Meliska, and A. Bartke. Dwarf mice and the ageing process. *Nature*, 384(6604):33–33, 1996.
- [28] A. Brunet, A. Bonni, M. J. Zigmond, M. Z. Lin, P. Juo, L. S. Hu, M. J. Anderson, K. C. Arden, J. Blenis, and M. E. Greenberg. Akt promotes cell survival by phosphorylating and inhibiting a Forkhead transcription factor. *Cell*, 96(6):857–868, Mar 1999.
- [29] A. Brunet, L. B. Sweeney, J. F. Sturgill, K. F. Chua, P. L. Greer, Y. Lin, H. Tran, S. E. Ross, R. Mostoslavsky, H. Y. Cohen, L. S. Hu, H.-L. Cheng, M. P. Jedrychowski, S. P. Gygi, D. A. Sinclair, F. W. Alt, and M. E. Greenberg. Stress-dependent regulation of FOXO transcription factors by the SIRT1 deacetylase. *Science*, 303(5666):2011–2015, Mar 2004.
- [30] Y. V. Budovskaya, K. Wu, L. K. Southworth, M. Jiang, P. Tedesco, T. E. Johnson, and S. K. Kim. An *elt-3/elt-5/elt-6* GATA transcription circuit guides aging in *C. elegans*. *Cell*, 134(2):291–303, Jul 25 2008.
- [31] *C. elegans* Sequencing Consortium. Genome sequence of the nematode *C. elegans*: a platform for investigating biology. *Science*, 282(5396):2012–2018, Dec 1998.
- [32] D. Callahan. Europe and the United States: contrast and convergence. *J Med Philos*, 33(3):280–93, Jun 2008.

- [33] S. E. Calvo and V. K. Mootha. The mitochondrial proteome and human disease. *Annu Rev Genomics Hum Genet*, 11:25–44, Sep 2010.
- [34] J. Campisi. Senescent cells, tumor suppression, and organismal aging: good citizens, bad neighbors. *Cell*, 120(4):513–522, Feb 2005.
- [35] J. Campisi and F. d’Adda di Fagagna. Cellular senescence: when bad things happen to good cells. *Nat Rev Mol Cell Biol*, 8(9):729–740, Sep 2007.
- [36] A. Canela, J. Martín-Caballero, J. M. Flores, and M. A. Blasco. Constitutive expression of tert in thymocytes leads to increased incidence and dissemination of T-cell lymphoma in Lck-Tert mice. *Mol Cell Biol*, 24(10):4275–4293, May 2004.
- [37] E. Chang and C. B. Harley. Telomere length and replicative aging in human vascular tissues. *Proc Natl Acad Sci U S A*, 92(24):11190–11194, Nov 1995.
- [38] C. Chen, J. Jack, and R. S. Garofalo. The Drosophila insulin receptor is required for normal growth. *Endocrinology*, 137(3):846–56, March 1 1996.
- [39] W.-C. Chiang, T.-T. Ching, H. Lee, C. Mousigian, and A.-L. Hsu. HSF-1 Regulators DDL-1/2 Link Insulin-like Signaling to Heat-Shock Responses and Modulation of Longevity. *Cell*, 148(1):322–334, 2012.
- [40] C. Choudhary, C. Kumar, F. Gnäd, M. L. Nielsen, M. Rehman, T. C. Walther, J. V. Olsen, and M. Mann. Lysine acetylation targets protein complexes and co-regulates major cellular functions. *Science*, 325(5942):834–840, Aug 2009.
- [41] D. J. Clancy, D. Gems, L. G. Harshman, S. Oldham, H. Stocker, E. Hafen, S. J. Leivers, and L. Partridge. Extension of Life-Span by Loss of CHICO, a Drosophila Insulin Receptor Substrate Protein. *Science*, 292(5514):104–106, April 6 2001.
- [42] J. Clos, J. T. Westwood, P. B. Becker, S. Wilson, K. Lambert, and C. Wu. Molecular cloning and expression of a hexameric Drosophila heat shock factor subject to negative regulation. *Cell*, 63(5):1085–1097, 1990.
- [43] E. Cohen, J. Bieschke, R. M. Perciavalle, J. W. Kelly, and A. Dillin. Opposing activities protect against age-onset proteotoxicity. *Science*, 313:1604–1610, 2006.
- [44] E. Cohen and A. Dillin. The insulin paradox: aging, proteotoxicity and neurodegeneration. *Nature Reviews Neuroscience*, 9(10):759–767, Oct 2008.

-
- [45] J. Colinge and K. L. Bennett. Introduction to computational proteomics. *PLoS Comput Biol*, 3(7):e114, Jul 2007.
- [46] M. Collado, M. A. Blasco, and M. Serrano. Cellular senescence in cancer and aging. *Cell*, 130(2):223–233, Jul 2007.
- [47] T. P. Conrads, K. Alving, T. D. Veenstra, M. E. Belov, G. A. Anderson, D. J. Anderson, M. S. Lipton, L. Pasa-Toli, H. R. Udseth, W. B. Chrisler, B. D. Thrall, and R. D. Smith. Quantitative analysis of bacterial and mammalian proteomes using a combination of cysteine affinity tags and ¹⁵N-metabolic labeling. *Anal Chem*, 73(9):2132–2139, May 2001.
- [48] D. A. Cottrell, E. L. Blakely, M. A. Johnson, P. G. Ince, G. M. Borthwick, and D. M. Turnbull. Cytochrome c oxidase deficient cells accumulate in the hippocampus and choroid plexus with age. *Neurobiol Aging*, 22(2):265–72, Mar-Apr 2001.
- [49] J. Cox and M. Mann. Quantitative, high-resolution proteomics for data-driven systems biology. *Annu Rev Biochem*, 80:273–299, Jun 2011.
- [50] J. Cox, I. Matic, M. Hilger, N. Nagaraj, M. Selbach, J. V. Olsen, and M. Mann. A practical guide to the MaxQuant computational platform for SILAC-based quantitative proteomics. *Nature Protocols*, 4(5):698–705, 2009.
- [51] J. Cox, A. Michalski, and M. Mann. Software Lock Mass by Two-Dimensional Minimization of Peptide Mass Errors. *Journal of the American Society for Mass Spectrometry*, 22(8):1373–1380, Aug 2011.
- [52] J. Cox, N. Neuhauser, A. Michalski, R. A. Scheltema, J. V. Olsen, and M. Mann. Andromeda: A Peptide Search Engine Integrated into the MaxQuant Environment. *Journal of Proteome Research*, 10(4):1794–1805, Apr 2011.
- [53] A. M. Cuervo and J. F. Dice. Age-related decline in chaperone-mediated autophagy. *Journal of Biological Chemistry*, 275(40):31505–31513, Oct 6 2000.
- [54] C. Cunningham, Jr, G. L. Glish, and D. J. Burinsky. High amplitude short time excitation: a method to form and detect low mass product ions in a quadrupole ion trap mass spectrometer. *J Am Soc Mass Spectrom*, 17(1):81–84, Jan 2006.
- [55] S. Cvejic, Z. Zhu, S. J. Felice, Y. Berman, and X.-Y. Huang. The endogenous ligand Stunted of the GPCR Methuselah extends lifespan in *Drosophila*. *Nat Cell Biol*, 6(6):540–546, Jun 2004.

- [56] H. Daitoku, M. Hatta, H. Matsuzaki, S. Aratani, T. Ohshima, M. Miyagishi, T. Nakajima, and A. Fukamizu. Silent information regulator 2 potentiates Foxo1-mediated transcription through its deacetylase activity. *Proceedings of the National Academy of Sciences of the United States of America*, 101(27):10042–10047, July 6 2004.
- [57] D. C. David, N. Ollikainen, J. C. Trinidad, M. P. Cary, A. L. Burlingame, and C. Kenyon. Widespread Protein Aggregation as an Inherent Part of Aging in *C. elegans*. *Plos Biology*, 8(8), Aug 2010.
- [58] S. W. Davies, M. Turmaine, B. A. Cozens, M. DiFiglia, A. H. Sharp, C. A. Ross, E. Scherzinger, E. E. Wanker, L. Mangiarini, and G. P. Bates. Formation of neuronal intranuclear inclusions underlies the neurological dysfunction in mice transgenic for the HD mutation. *Cell*, 90(3):537–548, Aug. 1997.
- [59] L. M. F. de Godoy, J. V. Olsen, J. Cox, M. L. Nielsen, N. C. Hubner, F. Frohlich, T. C. Walther, and M. Mann. Comprehensive mass-spectrometry-based proteome quantification of haploid versus diploid yeast. *Nature*, 455(7217):1251–U60, 2008.
- [60] L. M. F. de Godoy, J. V. Olsen, G. A. de Souza, G. Li, P. Mortensen, and M. Mann. Status of complete proteome analysis by mass spectrometry: SILAC labeled yeast as a model system. *Genome Biol*, 7(6):R50, 2006.
- [61] F. Demontis and N. Perrimon. FOXO/4E-BP Signaling in *Drosophila* Muscles Regulates Organism-wide Proteostasis during Aging. *Cell*, 143(5):813–825, Nov. 2010.
- [62] J. Dengjel, L. Jakobsen, and J. S. Andersen. Organelle proteomics by label-free and SILAC-based protein correlation profiling. *Methods Mol Biol*, 658:255–265, 2010.
- [63] I. E. Deyev, F. Sohet, K. P. Vassilenko, O. V. Serova, N. V. Popova, S. A. Zozulya, E. B. Burova, P. Houillier, D. I. Rzhovsky, A. A. Berchatova, A. N. Murashev, A. O. Chugunov, R. G. Efremov, N. N. Nikolsky, E. Bertelli, D. Eladari, and A. G. Petrenko. Insulin receptor-related receptor as an extracellular alkali sensor. *Cell Metab*, 13(6):679–689, Jun 2011.
- [64] G. Dietzl, D. Chen, F. Schnorrer, K.-C. Su, Y. Barinova, M. Fellner, B. Gasser, K. Kinsey, S. Oppel, S. Scheiblauer, A. Couto, V. Marra, K. Keleman, and B. J. Dickson. A genome-wide transgenic RNAi library for conditional gene inactivation in *Drosophila*. *Nature*, 448(7150):151–156, Jul 2007.

-
- [65] K. S. Dimmer, D. Papic, B. Schumann, D. Sperl, K. Krumpe, D. M. Walther, and D. Rapaport. A crucial role of Mim2 in the biogenesis of mitochondrial outer membrane proteins. *J Cell Sci*, Mar 2012.
- [66] G. P. Dimri, X. Lee, G. Basile, M. Acosta, G. Scott, C. Roskelley, E. E. Medrano, M. Linskens, I. Rubelj, and O. Pereira-Smith. A biomarker that identifies senescent human cells in culture and in aging skin in vivo. *Proc Natl Acad Sci U S A*, 92(20):9363–9367, Sep 1995.
- [67] M.-Q. Dong, J. D. Venable, N. Au, T. Xu, S. K. Park, D. Cociorva, J. R. Johnson, A. Dillin, and I. Yates, John R. Quantitative mass spectrometry identifies insulin signaling targets in *C. elegans*. *Science*, 317(5838):660–663, Aug 3 2007.
- [68] D. J. Douglas, A. J. Frank, and D. Mao. Linear ion traps in mass spectrometry. *Mass Spectrom Rev*, 24(1):1–29, 2005.
- [69] P. M. Douglas and A. Dillin. Protein homeostasis and aging in neurodegeneration. *Journal of Cell Biology*, 190(5):719–729, Sep 6 2010.
- [70] E. Dufour and N. G. Larsson. Understanding aging: revealing order out of chaos. *Biochim Biophys Acta*, 1658(1-2):122–32, Jul 23 2004.
- [71] T. P. J. Dunkley, R. Watson, J. L. Griffin, P. Dupree, and K. S. Lilley. Localization of organelle proteins by isotope tagging (LOPIT). *Mol Cell Proteomics*, 3(11):1128–1134, Nov 2004.
- [72] J. L. Edwards and R. E. Klein. Cell renewal in adult mouse tissues. *Am J Pathol*, 38:437–453, Apr 1961.
- [73] J. E. Elias and S. P. Gygi. Target-decoy search strategy for increased confidence in large-scale protein identifications by mass spectrometry. *Nature Methods*, 4(3):207–214, Mar 2007.
- [74] M. Elstner, C. Andreoli, U. Ahting, I. Tetko, T. Klopstock, T. Meitinger, and H. Prokisch. MitoP2: an integrative tool for the analysis of the mitochondrial proteome. *Mol Biotechnol*, 40(3):306–315, Nov 2008.
- [75] J. R. Engen, E. M. Bradbury, and X. Chen. Using stable-isotope-labeled proteins for hydrogen exchange studies in complex mixtures. *Anal Chem*, 74(7):1680–1686, Apr 2002.

- [76] M. A. Essers, S. Weijzen, A. M. de Vries-Smits, I. Saarloos, N. D. de Ruiter, J. L. Bos, and B. M. Burgering. FOXO transcription factor activation by oxidative stress mediated by the small GTPase Ral and JNK. *Embo J*, 23(24):4802–12, Dec 8 2004.
- [77] P. Fabrizio, C. Gattazzo, L. Battistella, M. Wei, C. Cheng, K. McGrew, and V. D. Longo. Sir2 blocks extreme life-span extension. *Cell*, 123(4):655–667, Nov 2005.
- [78] P. Fabrizio and V. D. Longo. The chronological life span of *Saccharomyces cerevisiae*. *Aging Cell*, 2(2):73–81, Apr 2003.
- [79] J. B. Fenn, M. Mann, C. K. Meng, S. F. Wong, and C. M. Whitehouse. Electrospray ionization for mass spectrometry of large biomolecules. *Science*, 246(4926):64–71, Oct 1989.
- [80] M. Fernandez, H. Xiao, and J. T. Lis. Fine-structure Analyses of the *Drosophila* and *Saccharomyces* Heat-shock Factor - Heat-shock Element Interactions. *Nucleic Acids Research*, 22(2):167–173, Jan. 1994.
- [81] R. Fernandez, D. Tabarini, N. Azpiazu, M. Frasch, and J. Schlessinger. The *Drosophila* insulin receptor homolog: a gene essential for embryonic development encodes two receptor isoforms with different signaling potential. *Embo J*, 14(14):3373–84, Jul 17 1995.
- [82] K. Flurkey, J. Papaconstantinou, R. A. Miller, and D. E. Harrison. Lifespan extension and delayed immune and collagen aging in mutant mice with defects in growth hormone production. *Proc Natl Acad Sci U S A*, 98(12):6736–41, Jun 5 2001.
- [83] F. Forner, E. A. Arriaga, and M. Mann. Mild protease treatment as a small-scale biochemical method for mitochondria purification and proteomic mapping of cytoplasm-exposed mitochondrial proteins. *Journal of Proteome Research*, 5(12):3277–3287, 2006.
- [84] F. Forner, L. J. Foster, S. Campanaro, G. Valle, and M. Mann. Quantitative proteomic comparison of rat mitochondria from muscle, heart, and liver. *Mol Cell Proteomics*, 5(4):608–19, Apr 2006.
- [85] F. Forner, C. Kumar, C. A. Luber, T. Fromme, M. Klingenspor, and M. Mann. Proteome differences between brown and white fat mitochondria reveal specialized metabolic functions. *Cell Metab*, 10(4):324–335, Oct 2009.

-
- [86] L. Foster, C. De Hoog, X. Xie, V. Mootha, and M. Mann. A mammalian organelle map by protein correlation profiling. *Molecular & Cellular Proteomics*, 4(8):S5–S5, Aug 2005.
- [87] L. J. Foster, A. Rudich, I. Talior, N. Patel, X. D. Huang, L. M. Furtado, P. J. Bilan, M. Mann, and A. Klip. Insulin-dependent interactions of proteins with GLUT4 revealed through stable isotope labeling by amino acids in cell culture (SILAC). *Journal of Proteome Research*, 5(1):64–75, 2006.
- [88] J. Fredens, K. Engholm-Keller, A. Giessing, D. Pultz, M. R. Larsen, P. Hojrup, J. Moller-Jensen, and N. J. Faergeman. Quantitative proteomics by amino acid labeling in *C. elegans*. *Nature Methods*, 8(10):845–U109, Oct 2011.
- [89] D. B. Friedman and T. E. Johnson. A mutation in the age-1 gene in *Caenorhabditis elegans* lengthens life and reduces hermaphrodite fertility. *Genetics*, 118(1):75–86, Jan 1988.
- [90] D. B. Friedman and T. E. Johnson. Three mutants that extend both mean and maximum life span of the nematode, *Caenorhabditis elegans*, define the age-1 gene. *J Gerontol*, 43(4):B102–B109, Jul 1988.
- [91] T. Furuyama, T. Nakazawa, I. Nakano, and N. Mori. Identification of the differential distribution patterns of mRNAs and consensus binding sequences for mouse DAF-16 homologues. *Biochemical Journal*, 349:629–634, July 2000.
- [92] D. Garigan, A.-L. Hsu, A. G. Fraser, R. S. Kamath, J. Ahringer, and C. Kenyon. Genetic Analysis of Tissue Aging in *Caenorhabditis elegans*: A Role for Heat-Shock Factor and Bacterial Proliferation. *Genetics*, 161(3):1101–1112, July 1, 2002 2002.
- [93] D. Gaston, A. D. Tsaousis, and A. J. Roger. Predicting proteomes of mitochondria and related organelles from genomic and expressed sequence tag data. *Methods Enzymol*, 457:21–47, 2009.
- [94] C. L. Gatlin, G. R. Kleemann, L. G. Hays, A. J. Link, and J. Yates, 3rd. Protein identification at the low femtomole level from silver-stained gels using a new frit-less electrospray interface for liquid chromatography-microspray and nanospray mass spectrometry. *Anal Biochem*, 263(1):93–101, Oct 1998.
- [95] T. Geiger, J. Cox, P. Ostasiewicz, J. R. Wisniewski, and M. Mann. Super-SILAC mix for quantitative proteomics of human tumor tissue. *Nat Methods*, 7(5):383–385, May 2010.

- [96] M. L. Genova, B. Ventura, G. Giuliano, C. Bovina, G. Formiggini, G. Parenti Castelli, and G. Lenaz. The site of production of superoxide radical in mitochondrial Complex I is not a bound ubisemiquinone but presumably iron-sulfur cluster N2. *FEBS Lett*, 505(3):364–8, Sep 21 2001.
- [97] R. C. Gentleman, V. J. Carey, D. M. Bates, B. Bolstad, M. Dettling, S. Dudoit, B. Ellis, L. Gautier, Y. Ge, J. Gentry, K. Hornik, T. Hothorn, W. Huber, S. Iacus, R. Irizarry, F. Leisch, C. Li, M. Maechler, A. J. Rossini, G. Sawitzki, C. Smith, G. Smyth, L. Tierney, J. Y. H. Yang, and J. Zhang. Bioconductor: open software development for computational biology and bioinformatics. *Genome Biol*, 5(10):R80, 2004.
- [98] B. Ghesquière, V. Jonckheere, N. Colaert, J. Van Durme, E. Timmerman, M. Goethals, J. Schymkowitz, F. Rousseau, J. Vandekerckhove, and K. Gevaert. Redox proteomics of protein-bound methionine oxidation. *Mol Cell Proteomics*, 10(5):M110.006866, May 2011.
- [99] T. Gidalevitz, A. Ben-Zvi, K. H. Ho, H. R. Brignull, and R. I. Morimoto. Progressive disruption of cellular protein folding in models of polyglutamine diseases. *Science*, 311:1471–1474, 2006.
- [100] A. Gilchrist, C. E. Au, J. Hiding, A. W. Bell, J. Fernandez-Rodriguez, S. Lesimple, H. Nagaya, L. Roy, S. J. C. Gosline, M. Hallett, J. Paiement, R. E. Kearney, T. Nilsson, and J. J. M. Bergeron. Quantitative proteomics analysis of the secretory pathway. *Cell*, 127(6):1265–1281, Dec 2006.
- [101] T. R. Golden, A. Hubbard, C. Dando, M. A. Herren, and S. Melov. Age-related behaviors have distinct transcriptional profiles in *Caenorhabditis elegans*. *Aging Cell*, 7(6):850–865, Dec 2008.
- [102] T. R. Golden and S. Melov. Microarray analysis of gene expression with age in individual nematodes. *Aging Cell*, 3(3):111–124, Jun 2004.
- [103] E. Gonzalez-Suarez, E. Samper, A. Ramirez, J. M. Flores, J. Martin-Caballero, J. L. Jorcano, and M. A. Blasco. Increased epidermal tumors and increased skin wound healing in transgenic mice overexpressing the catalytic subunit of telomerase, mTERT, in basal keratinocytes. *Embo J*, 20(11):2619–30, Jun 1 2001.
- [104] S. Gottlieb and G. Ruvkun. daf-2, daf-16 and daf-23: genetically interacting genes controlling Dauer formation in *Caenorhabditis elegans*. *Genetics*, 137(1):107–20, May 1994.

-
- [105] J. W. Gouw, B. B. J. Tops, P. Mortensen, A. J. R. Heck, and J. Krijgsveld. Optimizing identification and quantitation of ^{15}N -labeled proteins in comparative proteomics. *Anal Chem*, 80(20):7796–7803, Oct 2008.
- [106] E. L. Greer and A. Brunet. FOXO transcription factors at the interface between longevity and tumor suppression. *Oncogene*, 24(50):7410–7425, Nov 2005.
- [107] S. Gu, S. Pan, E. M. Bradbury, and X. Chen. Use of deuterium-labeled lysine for efficient protein identification and peptide de novo sequencing. *Anal Chem*, 74(22):5774–5785, Nov 2002.
- [108] R. Gupta, P. Kasturi, A. Bracher, C. Loew, M. Zheng, A. Villella, D. Garza, F. U. Hartl, and S. Raychaudhuri. Firefly luciferase mutants as sensors of proteome stress. *Nature Methods*, 8(10):879–U155, Oct 2011.
- [109] S. P. Gygi, B. Rist, S. A. Gerber, F. Turecek, M. H. Gelb, and R. Aebersold. Quantitative analysis of complex protein mixtures using isotope-coded affinity tags. *Nat Biotechnol*, 17(10):994–9, Oct 1999.
- [110] C. R. Hackenbrock. Chemical and physical fixation of isolated mitochondria in low-energy and high-energy states. *Proc Natl Acad Sci U S A*, 61(2):598–605, Oct 1968.
- [111] J. W. Hager. A new linear ion trap mass spectrometer. *Rapid Communications in Mass Spectrometry*, 16(6):512–526, 2002.
- [112] M. C. Haigis and L. P. Guarente. Mammalian sirtuins—emerging roles in physiology, aging, and calorie restriction. *Genes Dev*, 20(21):2913–21, Nov 1 2006.
- [113] J. Halaschek-Wiener. Analysis of long-lived *C. elegans* *daf-2* mutants using serial analysis of gene expression. *Genome Res.*, 15:603–615, 2005.
- [114] D. M. Hall, T. D. Oberley, P. M. Moseley, G. R. Buettner, L. W. Oberley, R. Weindruch, and K. C. Kregel. Caloric restriction improves thermotolerance and reduces hyperthermia-induced cellular damage in old rats. *Faseb Journal*, 14(1):78–86, Jan. 2000.
- [115] X. Han, A. Aslanian, and J. R. Yates, 3rd. Mass spectrometry for proteomics. *Curr Opin Chem Biol*, 12(5):483–490, Oct 2008.
- [116] C. B. Harley, A. B. Futcher, and C. W. Greider. Telomeres shorten during ageing of human fibroblasts. *Nature*, 345(6274):458–60, May 31 1990.

References

- [117] D. Harman. Aging: a theory based on free radical and radiation chemistry. *J Gerontol*, 11(3):298–300, Jul 1956.
- [118] S. M. Harman and G. B. Talbert. The effect of maternal age on ovulation, corpora lutea of pregnancy, and implantation failure in mice. *J Reprod Fertil*, 23(1):33–39, Oct 1970.
- [119] M. Harner, C. Korner, D. Walther, D. Mokranjac, J. Kaesmacher, U. Welsch, J. Griffith, M. Mann, F. Reggiori, and W. Neupert. The mitochondrial contact site complex, a determinant of mitochondrial architecture. *Embo J*, 30(21):4356–70, Nov 2 2011.
- [120] D. E. Harrison, R. Strong, Z. D. Sharp, J. F. Nelson, C. M. Astle, K. Flurkey, N. L. Nadon, J. E. Wilkinson, K. Frenkel, C. S. Carter, M. Pahor, M. A. Javors, E. Fernandez, and R. A. Miller. Rapamycin fed late in life extends lifespan in genetically heterogeneous mice. *Nature*, 460(7253):392–395, Jul 2009.
- [121] N. D. Hastie, M. Dempster, M. G. Dunlop, A. M. Thompson, D. K. Green, and R. C. Allshire. Telomere reduction in human colorectal carcinoma and with ageing. *Nature*, 346(6287):866–8, Aug 30 1990.
- [122] L. Hayflick. The Limited in Vitro Lifetime of Human Diploid Cell Strains. *Exp Cell Res*, 37:614–36, Mar 1965.
- [123] S. T. Henderson and T. E. Johnson. daf-16 integrates developmental and environmental inputs to mediate aging in the nematode *Caenorhabditis elegans*. *Current Biology*, 11(24):1975–1980, Dec 11 2001.
- [124] L. A. Herndon, P. J. Schmeissner, J. M. Dudaronek, P. A. Brown, K. M. Listner, Y. Sakano, M. C. Paupard, D. H. Hall, and M. Driscoll. Stochastic and genetic factors influence tissue-specific decline in ageing *C. elegans*. *Nature*, 419(6909):808–814, Oct. 2002.
- [125] D. Herranz and M. Serrano. SIRT1: recent lessons from mouse models. *Nat Rev Cancer*, 10(12):819–823, Dec 2010.
- [126] M. Hertweck, C. Goebel, and R. Baumeister. *C. elegans* SGK-1 Is the Critical Component in the Akt/PKB Kinase Complex to Control Stress Response and Life Span. *Developmental Cell*, 6(4):577 – 588, 2004.

-
- [127] A. R. Heydari, B. Wu, C., R. Takahashi, R. Strong, and A. Richardson. Expression of Heat-shock Protein 70 Is Altered By Age and Diet At the Level of Transcription. *Molecular and Cellular Biology*, 13(5):2909–2918, May 1993.
- [128] I. Hirayama, H. Tamemoto, H. Yokota, S. K. Kubo, J. Wang, H. Kuwano, Y. Nagamachi, T. Takeuchi, and T. Izumi. Insulin receptor-related receptor is expressed in pancreatic beta-cells and stimulates tyrosine phosphorylation of insulin receptor substrate-1 and -2. *Diabetes*, 48(6):1237–1244, Jun 1999.
- [129] M. Holzenberger, J. Dupont, B. Ducos, P. Leneuve, A. G  lo  n, P. Even, P. Cervera, and Y. Le Bouc. IGF-1 receptor regulates lifespan and resistance to oxidative stress in mice. *Nature*, 421:182–187, 2003.
- [130] A.-L. Hsu, C. T. Murphy, and C. Kenyon. Regulation of Aging and Age-Related Disease by DAF-16 and Heat-Shock Factor. *Science*, 300(5622):1142–1145, May 16 2003.
- [131] J.-L. Hsu, S.-Y. Huang, N.-H. Chow, and S.-H. Chen. Stable-isotope dimethyl labeling for quantitative proteomics. *Anal Chem*, 75(24):6843–6852, Dec 2003.
- [132] Q. Hu, R. J. Noll, H. Li, A. Makarov, M. Hardman, and R. Graham Cooks. The Orbitrap: a new mass spectrometer. *J Mass Spectrom*, 40(4):430–443, Apr 2005.
- [133] Y. Ishihama, Y. Oda, T. Tabata, T. Sato, T. Nagasu, J. Rappsilber, and M. Mann. Exponentially modified protein abundance index (emPAI) for estimation of absolute protein amount in proteomics by the number of sequenced peptides per protein. *Mol Cell Proteomics*, 4(9):1265–1272, Sep 2005.
- [134] Y. Ishihama, J. Rappsilber, and M. Mann. Modular stop and go extraction tips with stacked disks for parallel and multidimensional peptide fractionation in proteomics. *Journal of Proteome Research*, 5(4):988–994, 2006.
- [135] D. Ishikawa, H. Yamamoto, Y. Tamura, K. Moritoh, and T. Endo. Two novel proteins in the mitochondrial outer membrane mediate beta-barrel protein assembly. *J Cell Biol*, 166(5):621–627, Aug 2004.
- [136] V. Janzen, R. Forkert, H. E. Fleming, Y. Saito, M. T. Waring, D. M. Dombkowski, T. Cheng, R. A. DePinho, N. E. Sharpless, and D. T. Scadden. Stem-cell ageing modified by the cyclin-dependent kinase inhibitor p16INK4a. *Nature*, 443(7110):421–426, Sep 2006.

- [137] J. C. Jeyapalan, M. Ferreira, J. M. Sedivy, and U. Herbig. Accumulation of senescent cells in mitotic tissue of aging primates. *Mech Ageing Dev*, 128(1):36–44, Jan 2007.
- [138] L. Ji, A. Ebata, D. Yuqing, G. Rizki, T. Iwata, and S. S. Lee. Caenorhabditis elegans HCF-1 Functions in Longevity Maintenance as a DAF-16 Regulator. *Plos Biology*, 6(9):e233, 2008.
- [139] K. Jia, D. Chen, and D. L. Riddle. The TOR pathway interacts with the insulin signaling pathway to regulate C. elegans larval development, metabolism and life span. *Development*, 131(16):3897–3906, Aug 2004.
- [140] C. H. Jiang, J. Z. Tsien, P. G. Schultz, and Y. Hu. The effects of aging on gene expression in the hypothalamus and cortex of mice. *Proceedings of the National Academy of Sciences of the United States of America*, 98(4):1930–1934, February 13 2001.
- [141] J. C. Jiang, E. Jaruga, M. V. Repnevskaya, and S. M. Jazwinski. An intervention resembling caloric restriction prolongs life span and retards aging in yeast. *FASEB J*, 14(14):2135–2137, Nov 2000.
- [142] T. E. Johnson and W. B. Wood. Genetic analysis of life-span in Caenorhabditis elegans. *Proc Natl Acad Sci U S A*, 79(21):6603–6607, Nov 1982.
- [143] K. R. Jonscher and J. Yates, 3rd. The quadrupole ion trap mass spectrometer – a small solution to a big challenge. *Anal Biochem*, 244(1):1–15, Jan 1997.
- [144] M. Kaeberlein, M. McVey, and L. Guarente. The SIR2/3/4 complex and SIR2 alone promote longevity in Saccharomyces cerevisiae by two different mechanisms. *Genes Dev*, 13(19):2570–80, Oct 1 1999.
- [145] M. Kaeberlein, R. W. Powers, 3rd, K. K. Steffen, E. A. Westman, D. Hu, N. Dang, E. O. Kerr, K. T. Kirkland, S. Fields, and B. K. Kennedy. Regulation of yeast replicative life span by TOR and Sch9 in response to nutrients. *Science*, 310(5751):1193–1196, Nov 2005.
- [146] R. S. Kamath, A. G. Fraser, Y. Dong, G. Poulin, R. Durbin, M. Gotta, A. Kanapin, N. Le Bot, S. Moreno, M. Sohrmann, D. P. Welchman, P. Zipperlen, and J. Ahringer. Systematic functional analysis of the Caenorhabditis elegans genome using RNAi. *Nature*, 421(6920):231–237, Jan 2003.

-
- [147] P. Kapahi, B. M. Zid, T. Harper, D. Koslover, V. Sapin, and S. Benzer. Regulation of lifespan in *Drosophila* by modulation of genes in the TOR signaling pathway. *Curr Biol*, 14(10):885–890, May 2004.
- [148] M. Karas and F. Hillenkamp. Laser desorption ionization of proteins with molecular masses exceeding 10,000 daltons. *Anal Chem*, 60(20):2299–2301, Oct 1988.
- [149] B. K. Kennedy, N. Austriaco, Jr, J. Zhang, and L. Guarente. Mutation in the silencing gene SIR4 can delay aging in *S. cerevisiae*. *Cell*, 80(3):485–496, Feb 1995.
- [150] C. Kenyon, J. Chang, E. Gensch, A. Rudner, and R. Tabtiang. A *C. elegans* mutant that lives twice as long as wild type. *Nature*, 366:461–464, 1993.
- [151] E. A. Kikis, T. Gidalevitz, and R. I. Morimoto. Protein homeostasis in models of aging and age-related conformational disease. *Adv Exp Med Biol*, 694:138–159, 2010.
- [152] K. D. Kimura, H. A. Tissenbaum, Y. Liu, and G. Ruvkun. *daf-2*, an insulin receptor-like gene that regulates longevity and diapause in *Caenorhabditis elegans*. *Science*, 277:942–946, 1997.
- [153] K. H. Kingdon. A method for the neutralization of electron space charge by positive ionization at very low gas pressures. *Physical Review*, 21(4):408–418, Apr. 1923.
- [154] R. E. Kingston, T. J. Schuetz, and Z. Larin. Heat-inducible Human Factor That Binds To A Human Hsp70 Promoter. *Molecular and Cellular Biology*, 7(4):1530–1534, Apr. 1987.
- [155] D. M. Kirby and D. R. Thorburn. Approaches to finding the molecular basis of mitochondrial oxidative phosphorylation disorders. *Twin Res Hum Genet*, 11(4):395–411, Aug 2008.
- [156] T. B. L. Kirkwood. Understanding the odd science of aging. *Cell*, 120(4):437–447, Feb 2005.
- [157] T. Kislinger, B. Cox, A. Kannan, C. Chung, P. Hu, A. Ignatchenko, M. S. Scott, A. O. Gramolini, Q. Morris, M. T. Hallett, J. Rossant, T. R. Hughes, B. Frey, and A. Emili. Global survey of organ and organelle protein expression in mouse: combined proteomic and transcriptomic profiling. *Cell*, 125(1):173–186, Apr 2006.

- [158] M. R. Klass. Aging in the nematode *Caenorhabditis elegans*: major biological and environmental factors influencing life span. *Mech. Ageing Dev.*, 6:413–429, 1977.
- [159] M. R. Klass. A method for the isolation of longevity mutants in the nematode *Caenorhabditis elegans* and initial results. *Mech Ageing Dev*, 22(3-4):279–286, 1983.
- [160] J. Krijgsveld, R. F. Ketting, T. Mahmoudi, J. Johansen, M. Artal-Sanz, C. P. Verrijzer, R. H. A. Plasterk, and A. J. R. Heck. Metabolic labeling of *C. elegans* and *D. melanogaster* for quantitative proteomics. *Nature Biotechnology*, 21(8):927–931, Aug 2003.
- [161] J. Krishnamurthy, M. R. Ramsey, K. L. Ligon, C. Torrice, A. Koh, S. Bonner-Weir, and N. E. Sharpless. p16INK4a induces an age-dependent decline in islet regenerative potential. *Nature*, 443(7110):453–457, Sep 2006.
- [162] J. Krishnamurthy, C. Torrice, M. R. Ramsey, G. I. Kovalev, K. Al-Regaiey, L. Su, and N. E. Sharpless. Ink4a/Arf expression is a biomarker of aging. *J Clin Invest*, 114(9):1299–1307, Nov 2004.
- [163] M. Kruger, M. Moser, S. Ussar, I. Thievensen, C. A. Luber, F. Forner, S. Schmidt, S. Zanivan, R. Fassler, and M. Mann. SILAC mouse for quantitative proteomics uncovers kindlin-3 as an essential factor for red blood cell function. *Cell*, 134(2):353–64, Jul 25 2008.
- [164] A. Kumar, S. Agarwal, J. A. Heyman, S. Matson, M. Heidtman, S. Piccirillo, L. Umansky, A. Drawid, R. Jansen, Y. Liu, K.-H. Cheung, P. Miller, M. Gerstein, G. S. Roeder, and M. Snyder. Subcellular localization of the yeast proteome. *Genes Dev*, 16(6):707–719, Mar 2002.
- [165] E.-S. Kwon, S. D. Narasimhan, K. Yen, and H. A. Tissenbaum. A new DAF-16 isoform regulates longevity. *Nature*, 466(7305):498–502, 2010.
- [166] J. N. Landis and C. T. Murphy. Integration of diverse inputs in the regulation of *Caenorhabditis elegans* DAF-16/FOXO. *Dev Dyn*, 239(5):1405–1412, May 2010.
- [167] M. Larance, A. P. Bailly, E. Pourkarimi, R. T. Hay, G. Buchanan, S. Coulthurst, D. P. Xirodimas, A. Gartner, and A. I. Lamond. Stable-isotope labeling with amino acids in nematodes. *Nature Methods*, 8(10):849–U114, Oct 2011.

-
- [168] P. L. Larsen, P. S. Albert, and D. L. Riddle. Genes that regulate both development and longevity in *Caenorhabditis elegans*. *Genetics*, 139:1567–1583, 1995.
- [169] E. Lasonder, Y. Ishihama, J. S. Andersen, A. M. W. Vermunt, A. Pain, R. W. Sauerwein, W. M. C. Eling, N. Hall, A. P. Waters, H. G. Stunnenberg, and M. Mann. Analysis of the *Plasmodium falciparum* proteome by high-accuracy mass spectrometry. *Nature*, 419(6906):537–542, Oct 2002.
- [170] C. K. Lee, R. G. Klopp, R. Weindruch, and T. A. Prolla. Gene expression profile of aging and its retardation by caloric restriction. *Science*, 285(5432):1390–1393, Aug. 1999.
- [171] C.-K. Lee, R. Weindruch, and T. A. Prolla. Gene-expression profile of the ageing brain in mice. *Nat Genet*, 25(3):294–297, 2000.
- [172] R. Y. Lee, J. Hench, and G. Ruvkun. Regulation of *C. elegans* DAF-16 and its human ortholog FKHL1 by the *daf-2* insulin-like signaling pathway. *Curr. Biol.*, 11:1950–1957, 2001.
- [173] S. S. Lee. A systematic RNAi screen identifies a critical role for mitochondria in *C. elegans* longevity. *Nature Genet.*, 33:40–48, 2003.
- [174] M. K. Lehtinen, Z. Yuan, P. R. Boag, Y. Yang, J. Villen, E. B. E. Becker, S. DiBacco, N. de la Iglesia, S. Gygi, T. K. Blackwell, and A. Bonni. A Conserved MST-FOXO Signaling Pathway Mediates Oxidative-Stress Responses and Extends Life Span. *Cell*, 125(5):987–1001, 2006.
- [175] A. M. Leroi, A. Bartke, G. De Benedictis, C. Franceschi, A. Gartner, E. S. Gonos, E. Gonos, M. E. Fedei, M. E. Feder, T. Kivisild, S. Lee, N. Kartaf-Ozer, N. Kartal-Ozer, M. Schumacher, E. Sikora, E. Slagboom, M. Tatar, A. I. Yashin, J. Vijg, and B. Zwaan. What evidence is there for the existence of individual genes with antagonistic pleiotropic effects? *Mech Ageing Dev*, 126(3):421–429, Mar 2005.
- [176] S. M. Li, C. M. Armstrong, N. Bertin, H. Ge, S. Milstein, M. Boxem, P. O. Vidalain, J. D. J. Han, A. Chesneau, T. Hao, D. S. Goldberg, N. Li, M. Martinez, J. F. Rual, P. Lamesch, L. Xu, M. Tewari, S. L. Wong, L. V. Zhang, G. F. Berriz, L. Jacotot, P. Vaglio, J. Reboul, T. Hirozane-Kishikawa, Q. R. Li, H. W. Gabel, A. Elewa, B. Baumgartner, D. J. Rose, H. Y. Yu, S. Bosak, R. Sequerra, A. Fraser, S. E. Mango, W. M. Saxton, S. Strome, S. van den Heuvel, F. Piano, J. Vandenhaute, C. Sardet, M. Gerstein, L. Doucette-Stamm, K. C. Gunsalus, J. W. Harper, M. E. Cusick, F. P.

- Roth, D. E. Hill, and M. Vidal. A map of the interactome network of the metazoan *C. elegans*. *Science*, 303(5657):540–543, Jan. 2004.
- [177] K. Lin, J. B. Dorman, A. Rodan, and C. Kenyon. *daf-16*: An HNF-3/forkhead family member that can function to double the life-span of *Caenorhabditis elegans*. *Science*, 278(5341):1319–1322, Nov 14 1997.
- [178] K. Lin, H. Hsin, N. Libina, and C. Kenyon. Regulation of the *Caenorhabditis elegans* longevity protein DAF-16 by insulin/IGF-1 and germline signaling. *Nat Genet*, 28(2):139–145, 2001.
- [179] S. J. Lin, M. Kaeberlein, A. A. Andalis, L. A. Sturtz, P. A. Defossez, V. C. Culotta, G. R. Fink, and L. Guarente. Calorie restriction extends *Saccharomyces cerevisiae* lifespan by increasing respiration. *Nature*, 418(6895):344–8, Jul 18 2002.
- [180] Y. J. Lin, L. Seroude, and S. Benzer. Extended life-span and stress resistance in the *Drosophila* mutant *methuselah*. *Science*, 282(5390):943–946, Oct 1998.
- [181] H. Liu, R. G. Sadygov, and J. R. Yates, 3rd. A model for random sampling and estimation of relative protein abundance in shotgun proteomics. *Anal Chem*, 76(14):4193–4201, Jul 2004.
- [182] Y. Liu, G. Fiskum, and D. Schubert. Generation of reactive oxygen species by the mitochondrial electron transport chain. *J Neurochem*, 80(5):780–7, Mar 2002.
- [183] P. M. Loerch, T. Lu, K. A. Dakin, J. M. Vann, A. Isaacs, C. Geula, J. Wang, Y. Pan, D. H. Gabuzda, C. Li, T. A. Prolla, and B. A. Yankner. Evolution of the aging brain transcriptome and synaptic regulation. *PLoS One*, 3(10):e3329, 2008.
- [184] D. B. Lombard, F. W. Alt, H.-L. Cheng, J. Bunkenborg, R. S. Streeper, R. Mostoslavsky, J. Kim, G. Yancopoulos, D. Valenzuela, A. Murphy, Y. Yang, Y. Chen, M. D. Hirschey, R. T. Bronson, M. Haigis, L. P. Guarente, R. V. Farese, Jr, S. Weissman, E. Verdin, and B. Schwer. Mammalian Sir2 homolog SIRT3 regulates global mitochondrial lysine acetylation. *Mol Cell Biol*, 27(24):8807–8814, Dec 2007.
- [185] M. F. Lopez, B. S. Kristal, E. Chernokalskaya, A. Lazarev, A. I. Shestopalov, A. Bogdanova, and M. Robinson. High-throughput profiling of the mitochondrial proteome using affinity fractionation and automation. *Electrophoresis*, 21(16):3427–3440, Oct 2000.

-
- [186] P. Lu, C. Vogel, R. Wang, X. Yao, and E. M. Marcotte. Absolute protein expression profiling estimates the relative contributions of transcriptional and translational regulation. *Nat Biotechnol*, 25(1):117–124, Jan 2007.
- [187] C. A. Lubner, J. Cox, H. Lauterbach, B. Fancke, M. Selbach, J. Tschopp, S. Akira, M. Wiegand, H. Hochrein, M. O’Keeffe, and M. Mann. Quantitative proteomics reveals subset-specific viral recognition in dendritic cells. *Immunity*, 32(2):279–289, Feb 2010.
- [188] J. Lund, P. Tedesco, K. Duke, J. Wang, S. K. Kim, and T. E. Johnson. Transcriptional profile of aging in *C. elegans*. *Current Biology*, 12(18):1566–1573, Sep 17 2002.
- [189] S. Luo and C. T. Murphy. *Caenorhabditis elegans* reproductive aging: Regulation and underlying mechanisms. *Genesis*, 49(2):53–65, Feb 2011.
- [190] S. Luo, W. M. Shaw, J. Ashraf, and C. T. Murphy. TGF-beta Sma/Mab signaling mutations uncouple reproductive aging from somatic aging. *PLoS Genet*, 5(12):e1000789, Dec 2009.
- [191] U. Mählknecht and B. Zschoernig. Involvement of sirtuins in life-span and aging related diseases. *Adv Exp Med Biol*, 739:252–261, 2012.
- [192] A. Makarov. Electrostatic axially harmonic orbital trapping: a high-performance technique of mass analysis. *Anal Chem*, 72(6):1156–1162, Mar 2000.
- [193] A. Makarov, E. Denisov, A. Kholomeev, W. Balschun, O. Lange, K. Strupat, and S. Horning. Performance evaluation of a hybrid linear ion trap/orbitrap mass spectrometer. *Anal Chem*, 78(7):2113–20, Apr 1 2006.
- [194] A. Makarov, E. Denisov, and O. Lange. Performance evaluation of a high-field Orbitrap mass analyzer. *J Am Soc Mass Spectrom*, 20(8):1391–1396, Aug 2009.
- [195] E. Maklashina and B. A. Ackrell. Is defective electron transport at the hub of aging? *Aging Cell*, 3(1):21–7, Feb 2004.
- [196] L. Mao, I. Römer, G. Nebrich, O. Klein, A. Koppelstätter, S. C. Hin, D. Hartl, and C. Zabel. Aging in mouse brain is a cell/tissue-level phenomenon exacerbated by proteasome loss. *J Proteome Res*, 9(7):3551–3560, Jul 2010.
- [197] S. K. Mathi, J. Chan, and V. M. Watt. Insulin receptor-related receptor messenger ribonucleic acid: quantitative distribution and localization to subpopulations of epithelial cells in stomach and kidney. *Endocrinology*, 136(9):4125–4132, Sep 1995.

- [198] V. Mayya, K. Rezaul, Y.-S. Cong, and D. Han. Systematic comparison of a two-dimensional ion trap and a three-dimensional ion trap mass spectrometer in proteomics. *Mol Cell Proteomics*, 4(2):214–223, Feb 2005.
- [199] C. M. McCay, M. F. Crowell, and L. A. Maynard. The effect of retarded growth upon the length of life span and upon the ultimate body size. 1935. *Nutrition*, 5:155–171, 1989.
- [200] D. B. McClatchy, M.-Q. Dong, C. C. Wu, J. D. Venable, and J. R. Yates, 3rd. ¹⁵N metabolic labeling of mammalian tissue with slow protein turnover. *J Proteome Res*, 6(5):2005–2010, May 2007.
- [201] J. M. McCord and I. Fridovich. Superoxide Dismutase An Enzymic Function For Erythrocuprein (hemocuprein). *Journal of Biological Chemistry*, 244(22):6049, 1969.
- [202] J. McElwee, K. Bubb, and J. H. Thomas. Transcriptional outputs of the *Caenorhabditis elegans* forkhead protein DAF-16. *Aging Cell*, 2:111–121, 2003.
- [203] C. Meisinger, M. Rissler, A. Chacinska, L. K. S. Szklarz, D. Milenkovic, V. Kozjak, B. Schönfisch, C. Lohaus, H. E. Meyer, M. P. Yaffe, B. Guiard, N. Wiedemann, and N. Pfanner. The mitochondrial morphology protein Mdm10 functions in assembly of the preprotein translocase of the outer membrane. *Dev Cell*, 7(1):61–71, Jul 2004.
- [204] A. Michalski, E. Damoc, J.-P. Hauschild, O. Lange, A. Wieghaus, A. Makarov, N. Nagaraj, J. Cox, M. Mann, and S. Horning. Mass spectrometry-based proteomics using Q Exactive, a high-performance benchtop quadrupole Orbitrap mass spectrometer. *Mol Cell Proteomics*, 10(9):M111.011015, Sep 2011.
- [205] A. Michalski, E. Damoc, O. Lange, E. Denisov, D. Nolting, M. Müller, R. Viner, J. Schwartz, P. Remes, M. Belford, J.-J. Dunyach, J. Cox, S. Horning, M. Mann, and A. Makarov. Ultra high resolution linear ion trap Orbitrap mass spectrometer (Orbitrap Elite) facilitates top down LC MS/MS and versatile peptide fragmentation modes. *Mol Cell Proteomics*, 11(3):O111.013698, Mar 2012.
- [206] J. Miquel, P. R. Lundgren, K. G. Bensch, and H. Atlan. Effects of temperature on the life span, vitality and fine structure of *Drosophila melanogaster*. *Mech Ageing Dev*, 5(5):347–70, Sep-Oct 1976.
- [207] S. Mnaimneh, A. P. Davierwala, J. Haynes, J. Moffat, W.-T. Peng, W. Zhang, X. Yang, J. Pootoolal, G. Chua, A. Lopez, M. Trocheset, D. Morse, N. J. Krogan, S. L. Hiley, Z. Li, Q. Morris, J. Grigull, N. Mitsakakis, C. J. Roberts, J. F.

- Greenblatt, C. Boone, C. A. Kaiser, B. J. Andrews, and T. R. Hughes. Exploration of essential gene functions via titratable promoter alleles. *Cell*, 118(1):31–44, Jul 2004.
- [208] A. V. Molofsky, S. G. Slutsky, N. M. Joseph, S. He, R. Pardal, J. Krishnamurthy, N. E. Sharpless, and S. J. Morrison. Increasing p16INK4a expression decreases forebrain progenitors and neurogenesis during ageing. *Nature*, 443(7110):448–452, Sep 2006.
- [209] V. K. Mootha, J. Bunkenborg, J. V. Olsen, M. Hjerrild, J. R. Wisniewski, E. Stahl, M. S. Bolouri, H. N. Ray, S. Sihag, M. Kamal, N. Patterson, E. S. Lander, and M. Mann. Integrated analysis of protein composition, tissue diversity, and gene regulation in mouse mitochondria. *Cell*, 115(5):629–640, Nov 2003.
- [210] R. I. Morimoto. Proteotoxic stress and inducible chaperone networks in neurodegenerative disease and aging. *Genes & Development*, 22(11):1427–1438, June 2008.
- [211] J. F. Morley, H. R. Brignull, J. J. Weyers, and R. I. Morimoto. The threshold for polyglutamine-expansion protein aggregation and cellular toxicity is dynamic and influenced by aging in *Caenorhabditis elegans*. *Proceedings of the National Academy of Sciences of the United States of America*, 99(16):10417–10422, Aug 6 2002.
- [212] J. F. Morley and R. I. Morimoto. Regulation of longevity in *Caenorhabditis elegans* by heat shock factor and molecular chaperones. *Mol. Biol. Cell*, 15:657–664, 2004.
- [213] J. Z. Morris, H. A. Tissenbaum, and G. Ruvkun. A phosphatidylinositol-3-OH kinase family member regulating longevity and diapause in *Caenorhabditis elegans*. *Nature*, 382:536–539, 1996.
- [214] R. K. Mortimer and J. R. Johnston. Life span of individual yeast cells. *Nature*, 183(4677):1751–1752, Jun 1959.
- [215] M. C. Motta, N. Divecha, M. Lemieux, C. Kamel, D. Chen, W. Gu, Y. Bultsma, M. McBurney, and L. Guarente. Mammalian SIRT1 represses forkhead transcription factors. *Cell*, 116(4):551–63, Feb 20 2004.
- [216] A. Mukhopadhyay and H. A. Tissenbaum. Reproduction and longevity: secrets revealed by *C. elegans*. *Trends Cell Biol*, 17(2):65–71, Feb 2007.

- [217] J. Muller-Hocker. Cytochrome-c-oxidase deficient cardiomyocytes in the human heart—an age-related phenomenon. A histochemical ultracytochemical study. *Am J Pathol*, 134(5):1167–73, May 1989.
- [218] C. T. Murphy, S. A. McCarroll, C. I. Bargmann, A. Fraser, R. S. Kamath, J. Ahringer, H. Li, and C. Kenyon. Genes that act downstream of DAF-16 to influence the lifespan of *Caenorhabditis elegans*. *Nature*, 424(6946):277–284, Jul 17 2003.
- [219] N. Nagaraj, R. C. J. D’Souza, J. Cox, J. V. Olsen, and M. Mann. Feasibility of large-scale phosphoproteomics with higher energy collisional dissociation fragmentation. *J Proteome Res*, 9(12):6786–6794, Dec 2010.
- [220] E. A. A. Nollen, S. M. Garcia, G. van Haften, S. Kim, A. Chavez, R. I. Morimoto, and R. H. A. Plasterk. Genome-wide RNA interference screen identifies previously undescribed regulators of polyglutamine aggregation. *Proc Natl Acad Sci U S A*, 101(17):6403–6408, Apr 2004.
- [221] P. Oberdoerffer, S. Michan, M. McVay, R. Mostoslavsky, J. Vann, S. K. Park, A. Hartlerode, J. Stegmuller, A. Hafner, P. Loerch, S. M. Wright, K. D. Mills, A. Bonni, B. A. Yankner, R. Scully, T. A. Prolla, F. W. Alt, and D. A. Sinclair. SIRT1 redistribution on chromatin promotes genomic stability but alters gene expression during aging. *Cell*, 135(5):907–18, Nov 28 2008.
- [222] Y. Oda, K. Huang, F. R. Cross, D. Cowburn, and B. T. Chait. Accurate quantitation of protein expression and site-specific phosphorylation. *Proc Natl Acad Sci U S A*, 96(12):6591–6596, Jun 1999.
- [223] J. Oeppen and J. W. Vaupel. Demography: Broken limits to life expectancy. *Science*, 296(5570):1029–31, May 10 2002.
- [224] S. Ogg, S. Paradis, S. Gottlieb, G. I. Patterson, L. Lee, H. A. Tissenbaum, and G. Ruvkun. The Forkhead transcription factor DAF-16 transduces insulin-like metabolic and longevity signals in *C. elegans*. *Nature*, 389(6654):994–999, Oct 30 1997.
- [225] S. Ogg and G. Ruvkun. The *C. elegans* PTEN homolog, DAF-18, acts in the insulin receptor-like metabolic signaling pathway. *Mol. Cell*, 2:887–893, 1998.
- [226] S. W. Oh. Identification of direct DAF-16 targets controlling longevity, metabolism and diapause by chromatin immunoprecipitation. *Nature Genet.*, 38:251–257, 2006.

- [227] N. Ohtani, D. J. Mann, and E. Hara. Cellular senescence: its role in tumor suppression and aging. *Cancer Sci*, 100(5):792–797, May 2009.
- [228] W. M. Old, K. Meyer-Arendt, L. Aveline-Wolf, K. G. Pierce, A. Mendoza, J. R. Sevinisky, K. A. Resing, and N. G. Ahn. Comparison of label-free methods for quantifying human proteins by shotgun proteomics. *Mol Cell Proteomics*, 4(10):1487–1502, Oct 2005.
- [229] J. V. Olsen, L. M. F. de Godoy, G. Q. Li, B. Macek, P. Mortensen, R. Pesch, A. Makarov, O. Lange, S. Horning, and M. Mann. Parts per million mass accuracy on an orbitrap mass spectrometer via lock mass injection into a C-trap. *Molecular & Cellular Proteomics*, 4(12):2010–2021, Dec 2005.
- [230] J. V. Olsen, B. Macek, O. Lange, A. Makarov, S. Horning, and M. Mann. Higher-energy C-trap dissociation for peptide modification analysis. *Nat Methods*, 4(9):709–712, Sep 2007.
- [231] J. V. Olsen, J. C. Schwartz, J. Griep-Raming, M. L. Nielsen, E. Damoc, E. Denisov, O. Lange, P. Remes, D. Taylor, M. Splendore, E. R. Wouters, M. Senko, A. Makarov, M. Mann, and S. Horning. A dual pressure linear ion trap Orbitrap instrument with very high sequencing speed. *Mol Cell Proteomics*, 8(12):2759–2769, Dec 2009.
- [232] H. Olzscha, S. M. Schermann, A. C. Woerner, S. Pinkert, M. H. Hecht, G. G. Tartaglia, M. Vendruscolo, M. Hayer-Hartl, F. U. Hartl, and R. M. Vabulas. Amyloid-like aggregates sequester numerous metastable proteins with essential cellular functions. *Cell*, 144(1):67–78, Jan 2011.
- [233] S. E. Ong, B. Blagoev, I. Kratchmarova, D. B. Kristensen, H. Steen, A. Pandey, and M. Mann. Stable isotope labeling by amino acids in cell culture, SILAC, as a simple and accurate approach to expression proteomics. *Mol Cell Proteomics*, 1(5):376–86, May 2002.
- [234] W. C. Orr, R. J. Mockett, J. J. Benes, and R. S. Sohal. Effects of overexpression of copper-zinc and manganese superoxide dismutases, catalase, and thioredoxin reductase genes on longevity in *Drosophila melanogaster*. *J Biol Chem*, 278(29):26418–22, Jul 18 2003.
- [235] W. C. Orr and R. S. Sohal. Extension of life-span by overexpression of superoxide dismutase and catalase in *Drosophila melanogaster*. *Science*, 263(5150):1128–30, Feb 25 1994.

- [236] A. B. Paaby and P. S. Schmidt. Dissecting the genetics of longevity in *Drosophila melanogaster*. *Fly (Austin)*, 3(1):29–38, 2009.
- [237] L. Packer and K. Fuehr. Low oxygen concentration extends the lifespan of cultured human diploid cells. *Nature*, 267(5610):423–5, Jun 2 1977.
- [238] D. J. Pagliarini, S. E. Calvo, B. Chang, S. A. Sheth, S. B. Vafai, S.-E. Ong, G. A. Walford, C. Sugiana, A. Boneh, W. K. Chen, D. E. Hill, M. Vidal, J. G. Evans, D. R. Thorburn, S. A. Carr, and V. K. Mootha. A mitochondrial protein compendium elucidates complex I disease biology. *Cell*, 134(1):112–123, Jul 2008.
- [239] D. Papic, K. Krumpe, J. Dukanovic, K. S. Dimmer, and D. Rapaport. Multispan mitochondrial outer membrane protein Ugo1 follows a unique Mim1-dependent import pathway. *J Cell Biol*, 194(3):397–405, Aug 2011.
- [240] S. Paradis and G. Ruvkun. *Caenorhabditis elegans* Akt/PKB transduces insulin receptor-like signals from AGE-1 PI3 kinase to the DAF-16 transcription factor. *Genes Dev.*, 12:2488–2498, 1998.
- [241] O. Perisic, H. Xiao, and J. T. Lis. Stable binding of *Drosophila* heat shock factor to head-to-head and tail-to-tail repeats of a conserved 5 bp recognition unit. *Cell*, 59(5):797–806, Dec 1989.
- [242] D. N. Perkins, D. J. Pappin, D. M. Creasy, and J. S. Cottrell. Probability-based protein identification by searching sequence databases using mass spectrometry data. *Electrophoresis*, 20(18):3551–67, Dec 1999.
- [243] A. Pierce, R. D. Unwin, C. A. Evans, S. Griffiths, L. Carney, L. Zhang, E. Jaworska, C.-F. Lee, D. Blinco, M. J. Okoniewski, C. J. Miller, D. A. Bitton, E. Spooncer, and A. D. Whetton. Eight-channel iTRAQ enables comparison of the activity of six leukemogenic tyrosine kinases. *Mol Cell Proteomics*, 7(5):853–863, May 2008.
- [244] L. Pirkkala, P. Nykanen, and L. Sistonen. Roles of the heat shock transcription factors in regulation of the heat shock response and beyond. *Faseb J*, 15(7):1118–31, May 2001.
- [245] J. Popov-Celeketi, T. Waizenegger, and D. Rapaport. Mim1 functions in an oligomeric form to facilitate the integration of Tom20 into the mitochondrial outer membrane. *J Mol Biol*, 376(3):671–680, Feb 2008.

- [246] R. W. Powers, 3rd, M. Kaeberlein, S. D. Caldwell, B. K. Kennedy, and S. Fields. Extension of chronological life span in yeast by decreased TOR pathway signaling. *Genes Dev*, 20(2):174–184, Jan 2006.
- [247] J. S. Price, J. G. Waters, C. Darrah, C. Pennington, D. R. Edwards, S. T. Donell, and I. M. Clark. The role of chondrocyte senescence in osteoarthritis. *Aging Cell*, 1(1):57–65, Oct 2002.
- [248] T. Rabilloud, S. Kieffer, V. Procaccio, M. Louwagie, P. L. Courchesne, S. D. Patterson, P. Martinez, J. Garin, and J. Lunardi. Two-dimensional electrophoresis of human placental mitochondria and protein identification by mass spectrometry: toward a human mitochondrial proteome. *Electrophoresis*, 19(6):1006–1014, May 1998.
- [249] R. Rabl, V. Soubannier, R. Scholz, F. Vogel, N. Mendl, A. Vasiljev-Neumeyer, C. Körner, R. Jagasia, T. Keil, W. Baumeister, M. Cyrklaff, W. Neupert, and A. S. Reichert. Formation of cristae and crista junctions in mitochondria depends on antagonism between Fcj1 and Su e/g. *J Cell Biol*, 185(6):1047–1063, Jun 2009.
- [250] M. Raices, H. Maruyama, A. Dillin, and J. Karlseder. Uncoupling of longevity and telomere length in *C. elegans*. *PLoS Genet*, 1(3):e30, Sep 2005.
- [251] J. Rappsilber, U. Ryder, A. I. Lamond, and M. Mann. Large-scale proteomic analysis of the human spliceosome. *Genome Res*, 12(8):1231–1245, Aug 2002.
- [252] J. Reinders and A. Sickmann. Modificomics: posttranslational modifications beyond protein phosphorylation and glycosylation. *Biomol Eng*, 24(2):169–77, Jun 2007.
- [253] P. Reis-Rodrigues, G. Czerwieniec, T. W. Peters, U. S. Evani, S. Alavez, E. A. Gaman, M. Vantipalli, S. D. Mooney, B. W. Gibson, G. J. Lithgow, and R. E. Hughes. Proteomic analysis of age-dependent changes in protein solubility identifies genes that modulate lifespan. *Aging Cell*, 11(1):120–127, Feb 2012.
- [254] G. Reverter-Branchat, E. Cabiscol, J. Tamarit, and J. Ros. Oxidative damage to specific proteins in replicative and chronological-aged *Saccharomyces cerevisiae*: common targets and prevention by calorie restriction. *J Biol Chem*, 279(30):31983–31989, Jul 2004.
- [255] C. Richter, J. W. Park, and B. N. Ames. Normal oxidative damage to mitochondrial and nuclear DNA is extensive. *Proc Natl Acad Sci U S A*, 85(17):6465–7, Sep 1988.

- [256] D. L. Riddle, M. M. Swanson, and P. S. Albert. Interacting genes in nematode dauer larva formation. *Nature*, 290(5808):668–71, Apr 23 1981.
- [257] J. Rinehart, Y. D. Maksimova, J. E. Tanis, K. L. Stone, C. A. Hodson, J. Zhang, M. Risinger, W. Pan, D. Wu, C. M. Colangelo, B. Forbush, C. H. Joiner, E. E. Gulcicek, P. G. Gallagher, and R. P. Lifton. Sites of regulated phosphorylation that control K-Cl cotransporter activity. *Cell*, 138(3):525–536, Aug 2009.
- [258] P. L. Ross, Y. N. Huang, J. N. Marchese, B. Williamson, K. Parker, S. Hattan, N. Khainovski, S. Pillai, S. Dey, S. Daniels, S. Purkayastha, P. Juhasz, S. Martin, M. Bartlett-Jones, F. He, A. Jacobson, and D. J. Pappin. Multiplexed protein quantitation in *Saccharomyces cerevisiae* using amine-reactive isobaric tagging reagents. *Mol Cell Proteomics*, 3(12):1154–69, Dec 2004.
- [259] P. G. Sadowski, T. P. J. Dunkley, I. P. Shadforth, P. Dupree, C. Bessant, J. L. Griffin, and K. S. Lilley. Quantitative proteomic approach to study subcellular localization of membrane proteins. *Nat Protoc*, 1(4):1778–1789, 2006.
- [260] K. D. Sarge, S. P. Murphy, and R. I. Morimoto. Activation of heat shock gene transcription by heat shock factor 1 involves oligomerization, acquisition of DNA-binding activity, and nuclear localization and can occur in the absence of stress. *Mol. Cell. Biol.*, 13:1392–1407, 1993.
- [261] S. H. Satyal, D. Y. Chen, S. G. Fox, J. M. Kramer, and R. I. Morimoto. Negative regulation of the heat shock transcriptional response by HSBP1. *Genes & Development*, 12(13):1962–1974, July 1998.
- [262] M. M. Savitski, M. L. Nielsen, and R. A. Zubarev. ModifiComb, a new proteomic tool for mapping substoichiometric post-translational modifications, finding novel types of modifications, and fingerprinting complex protein mixtures. *Mol Cell Proteomics*, 5(5):935–48, May 2006.
- [263] B. Schwanhäusser, D. Busse, N. Li, G. Dittmar, J. Schuchhardt, J. Wolf, W. Chen, and M. Selbach. Global quantification of mammalian gene expression control. *Nature*, 473(7347):337–342, May 2011.
- [264] J. C. Schwartz, M. W. Senko, and J. E. P. Syka. A two-dimensional quadrupole ion trap mass spectrometer. *J Am Soc Mass Spectrom*, 13(6):659–669, Jun 2002.
- [265] M. Scigelova, M. Hornshaw, A. Giannakopoulos, and A. Makarov. Fourier transform mass spectrometry. *Mol Cell Proteomics*, 10(7):M111.009431, Jul 2011.

-
- [266] M. Scigelova and A. Makarov. Orbitrap mass analyzer—overview and applications in proteomics. *Proteomics*, 6 Suppl 2:16–21, Sep 2006.
- [267] M. Scigelova and A. Makarov. Advances in bioanalytical LC-MS using the Orbitrap mass analyzer. *Bioanalysis*, 1(4):741–754, Jul 2009.
- [268] T. Shibatani, M. Nazir, and W. F. Ward. Alteration of rat liver 20S proteasome activities by age and food restriction. *Journals of Gerontology Series a-Biological Sciences and Medical Sciences*, 51(5):B316–B322, Sep 1996.
- [269] P. Shier and V. M. Watt. Primary structure of a putative receptor for a ligand of the insulin family. *J Biol Chem*, 264(25):14605–14608, Sep 1989.
- [270] M. K. Shigenaga, T. M. Hagen, and B. N. Ames. Oxidative damage and mitochondrial decay in aging. *Proc Natl Acad Sci U S A*, 91(23):10771–8, Nov 8 1994.
- [271] A. C. Smith and A. J. Robinson. MitoMiner, an integrated database for the storage and analysis of mitochondrial proteomics data. *Mol Cell Proteomics*, 8(6):1324–1337, Jun 2009.
- [272] H. Steen, B. Kuster, M. Fernandez, A. Pandey, and M. Mann. Tyrosine phosphorylation mapping of the epidermal growth factor receptor signaling pathway. *J Biol Chem*, 277(2):1031–1039, Jan 2002.
- [273] H. Steen and M. Mann. The ABC’s (and XYZ’s) of peptide sequencing. *Nat Rev Mol Cell Biol*, 5(9):699–711, Sep 2004.
- [274] Y. Suh. Functionally significant insulin-like growth factor I receptor mutations in centenarians. *Proc. Natl Acad. Sci. USA*, 105:3438–3442, 2008.
- [275] M. D. Sury, J.-X. Chen, and M. Selbach. The SILAC Fly Allows for Accurate Protein Quantification in Vivo. *Molecular & Cellular Proteomics*, 9(10):2173–2183, Oct 2010.
- [276] J. E. P. Syka, J. A. Marto, D. L. Bai, S. Horning, M. W. Senko, J. C. Schwartz, B. Ueberheide, B. Garcia, S. Busby, T. Muratore, J. Shabanowitz, and D. F. Hunt. Novel linear quadrupole ion trap/FT mass spectrometer: performance characterization and use in the comparative analysis of histone H3 post-translational modifications. *J Proteome Res*, 3(3):621–626, 2004.
- [277] A. Taguchi, L. M. Wartschow, and M. F. White. Brain IRS2 signaling coordinates life span and nutrient homeostasis. *Science*, 317:369–372, 2007.

- [278] D. J. L. Tan, H. Dvinge, A. Christoforou, P. Bertone, A. Martinez Arias, and K. S. Lilley. Mapping organelle proteins and protein complexes in *Drosophila melanogaster*. *J Proteome Res*, 8(6):2667–2678, Jun 2009.
- [279] M. Tatar, A. Kopelman, D. Epstein, M. Tu, C. Yin, and R. Garofalo. A mutant *Drosophila* insulin receptor homolog that extends life-span and impairs neuroendocrine function. *Science*, 292:107–110, 2001.
- [280] R. C. Taylor and A. Dillin. Aging as an Event of Proteostasis Collapse. *Cold Spring Harbor Perspectives in Biology*, 3(5), May 2011.
- [281] Thermo Fisher Scientific. LTQ Orbitrap Biotech Operations - Training Course Manual.
- [282] A. Thompson, J. Schäfer, K. Kuhn, S. Kienle, J. Schwarz, G. Schmidt, T. Neumann, R. Johnstone, A. K. A. Mohammed, and C. Hamon. Tandem mass tags: a novel quantification strategy for comparative analysis of complex protein mixtures by MS/MS. *Anal Chem*, 75(8):1895–1904, Apr 2003.
- [283] H. A. Tissenbaum and L. Guarente. Increased dosage of a sir-2 gene extends lifespan in *Caenorhabditis elegans*. *Nature*, 410:227–230, 2001.
- [284] A. Tomas-Loba, I. Flores, P. J. Fernandez-Marcos, M. L. Cayuela, A. Maraver, A. Tejera, C. Borrás, A. Matheu, P. Klatt, J. M. Flores, J. Vina, M. Serrano, and M. A. Blasco. Telomerase reverse transcriptase delays aging in cancer-resistant mice. *Cell*, 135(4):609–22, Nov 14 2008.
- [285] A. Tonoki, E. Kuranaga, T. Tomioka, J. Hamazaki, S. Murata, K. Tanaka, and M. Miura. Genetic Evidence Linking Age-Dependent Attenuation of the 26S Proteasome with the Aging Process. *Molecular and Cellular Biology*, 29(4):1095–1106, Feb 15 2009.
- [286] D. Torosier, W. C. Orr, and R. S. Sohal. Carbonylation of mitochondrial proteins in *Drosophila melanogaster* during aging. *Biochem Biophys Res Commun*, 363(2):418–24, Nov 16 2007.
- [287] J. Tower. Transgenic methods for increasing *Drosophila* life span. *Mech Ageing Dev*, 118(1-2):1–14, Sep 2000.
- [288] A. Trifunovic, A. Wredenberg, M. Falkenberg, J. N. Spelbrink, A. T. Rovio, C. E. Bruder, Y. M. Bohlooly, S. Gidlof, A. Oldfors, R. Wibom, J. Tornell, H. T. Jacobs,

- and N. G. Larsson. Premature ageing in mice expressing defective mitochondrial DNA polymerase. *Nature*, 429(6990):417–23, May 27 2004.
- [289] J. F. Turrens, A. Alexandre, and A. L. Lehninger. Ubisemiquinone is the electron donor for superoxide formation by complex III of heart mitochondria. *Arch Biochem Biophys*, 237(2):408–14, Mar 1985.
- [290] A. Turturro, W. W. Witt, S. Lewis, B. S. Hass, R. D. Lipman, and R. W. Hart. Growth curves and survival characteristics of the animals used in the Biomarkers of Aging Program. *J Gerontol A Biol Sci Med Sci*, 54(11):B492–501, Nov 1999.
- [291] S. D. Tyner, S. Venkatachalam, J. Choi, S. Jones, N. Ghebranious, H. Igelmann, X. Lu, G. Soron, B. Cooper, C. Brayton, S. H. Park, T. Thompson, G. Karsenty, A. Bradley, and L. A. Donehower. p53 mutant mice that display early ageing-associated phenotypes. *Nature*, 415(6867):45–53, Jan 2002.
- [292] M. Uhlen, P. Oksvold, L. Fagerberg, E. Lundberg, K. Jonasson, M. Forsberg, M. Zwahlen, C. Kampf, K. Wester, S. Hober, H. Wernerus, L. Björling, and F. Ponten. Towards a knowledge-based Human Protein Atlas. *Nat Biotechnol*, 28(12):1248–1250, Dec 2010.
- [293] M. Uhlen, E. Björling, C. Agaton, C. A.-K. Szigarto, B. Amini, E. Andersen, A.-C. Andersson, P. Angelidou, A. Asplund, C. Asplund, L. Berglund, K. Bergström, H. Brumer, D. Cerjan, M. Ekström, A. Elobeid, C. Eriksson, L. Fagerberg, R. Falk, J. Fall, M. Forsberg, M. G. Björklund, K. Gumbel, A. Halimi, I. Hallin, C. Hamsten, M. Hansson, M. Hedhammar, G. Hercules, C. Kampf, K. Larsson, M. Lindskog, W. Lodewyckx, J. Lund, J. Lundeberg, K. Magnusson, E. Malm, P. Nilsson, J. Odling, P. Oksvold, I. Olsson, E. Oster, J. Ottosson, L. Paavilainen, A. Persson, R. Rimini, J. Rockberg, M. Runeson, A. Sivertsson, A. Sköllerö, J. Steen, M. Stenvall, F. Sterky, S. Strömberg, M. Sundberg, H. Tegel, S. Tourle, E. Wahlund, A. Waldén, J. Wan, H. Wernérus, J. Westberg, K. Wester, U. Wrethagen, L. L. Xu, S. Hober, and F. Pontén. A human protein atlas for normal and cancer tissues based on antibody proteomics. *Mol Cell Proteomics*, 4(12):1920–1932, Dec 2005.
- [294] A. Ullrich, J. R. Bell, E. Y. Chen, R. Herrera, L. M. Petruzzelli, T. J. Dull, A. Gray, L. Coussens, Y. C. Liao, and M. Tsubokawa. Human insulin receptor and its relationship to the tyrosine kinase family of oncogenes. *Nature*, 313(6005):756–761, 1985.

- [295] A. Ullrich, A. Gray, A. W. Tam, T. Yang-Feng, M. Tsubokawa, C. Collins, W. Henzel, T. Le Bon, S. Kathuria, and E. Chen. Insulin-like growth factor I receptor primary structure: comparison with insulin receptor suggests structural determinants that define functional specificity. *EMBO J*, 5(10):2503–2512, Oct 1986.
- [296] A. van der Horst and B. M. T. Burgering. Stressing the role of FoxO proteins in lifespan and disease. *Nat Rev Mol Cell Biol*, 8(6):440–450, Jun 2007.
- [297] E. Vasile, Y. Tomita, L. F. Brown, O. Kocher, and H. F. Dvorak. Differential expression of thymosin beta-10 by early passage and senescent vascular endothelium is modulated by VPF/VEGF: evidence for senescent endothelial cells in vivo at sites of atherosclerosis. *FASEB J*, 15(2):458–466, Feb 2001.
- [298] M. Vermulst, J. H. Bielas, G. C. Kujoth, W. C. Ladiges, P. S. Rabinovitch, T. A. Prolla, and L. A. Loeb. Mitochondrial point mutations do not limit the natural lifespan of mice. *Nat Genet*, 39(4):540–543, Apr 2007.
- [299] M. Viswanathan and L. Guarente. Regulation of *Caenorhabditis elegans* lifespan by sir-2.1 transgenes. *Nature*, 477(7365):E1–E2, Sept. 2011.
- [300] J. J. Vowels and J. H. Thomas. Genetic analysis of chemosensory control of dauer formation in *Caenorhabditis elegans*. *Genetics*, 130(1):105–23, Jan 1992.
- [301] G. R. Wagner and R. M. Payne. Mitochondrial acetylation and diseases of aging. *J Aging Res*, 2011:234875, 2011.
- [302] T. Waizenegger, S. Schmitt, J. Zivkovic, W. Neupert, and D. Rapaport. Mim1, a protein required for the assembly of the TOM complex of mitochondria. *EMBO Rep*, 6(1):57–62, Jan 2005.
- [303] D. M. Walther and D. Rapaport. Biogenesis of mitochondrial outer membrane proteins. *Biochim Biophys Acta*, 1793(1):42–51, Jan 2009.
- [304] J. M. Warrick, H. L. Paulson, G. L. Gray-Board, Q. T. Bui, K. H. Fischbeck, R. N. Pittman, and N. M. Bonini. Expanded polyglutamine protein forms nuclear inclusions and causes neural degeneration in *Drosophila*. *Cell*, 93(6):939–949, June 1998.
- [305] G. C. Williams. Pleiotropy, Natural Selection, and the Evolution of Senescence. *Evolution*, 11(4):398–411, Dec. 1957.

- [306] E. A. Winzeler, D. D. Shoemaker, A. Astromoff, H. Liang, K. Anderson, B. Andre, R. Bangham, R. Benito, J. D. Boeke, H. Bussey, A. M. Chu, C. Connelly, K. Davis, F. Dietrich, S. W. Dow, M. El Bakkoury, F. Foury, S. H. Friend, E. Gentalen, G. Giaever, J. H. Hegemann, T. Jones, M. Laub, H. Liao, N. Liebundguth, D. J. Lockhart, A. Lucau-Danila, M. Lussier, N. M'Rabet, P. Menard, M. Mittmann, C. Pai, C. Rebischung, J. L. Revuelta, L. Riles, C. J. Roberts, P. Ross-MacDonald, B. Scherens, M. Snyder, S. Sookhai-Mahadeo, R. K. Storms, S. Véronneau, M. Voet, G. Volckaert, T. R. Ward, R. Wysocki, G. S. Yen, K. Yu, K. Zimmermann, P. Philippsen, M. Johnston, and R. W. Davis. Functional characterization of the *S. cerevisiae* genome by gene deletion and parallel analysis. *Science*, 285(5429):901–906, Aug 1999.
- [307] S. Wolff, H. Ma, D. Burch, G. A. Maciel, T. Hunter, and A. Dillin. SMK-1, an Essential Regulator of DAF-16-Mediated Longevity. *Cell*, 124(5):1039–1053, 2006.
- [308] C. Wu. Activating Protein Factor Binds In vitro To Upstream Control Sequences In Heat-shock Gene Chromatin. *Nature*, 311(5981):81–84, 1984.
- [309] H. Xiao and J. T. Lis. Germline Transformation Used To Define Key Features of Heat-shock Response Elements. *Science*, 239(4844):1139–1142, Mar. 1988.
- [310] Y. H. Yang, H. Y. Hou, E. M. Haller, S. V. Nicosia, and W. L. Bai. Suppression of FOXO1 activity by FHL2 through SIRT1-mediated deacetylation. *Embo Journal*, 24(5):1021–1032, Mar. 2005.
- [311] J. Yates, 3rd, J. K. Eng, A. L. McCormack, and D. Schieltz. Method to correlate tandem mass spectra of modified peptides to amino acid sequences in the protein database. *Anal Chem*, 67(8):1426–1436, Apr 1995.
- [312] R. P. Zahedi, A. Sickmann, A. M. Boehm, C. Winkler, N. Zufall, B. Schönfisch, B. Guiard, N. Pfanner, and C. Meisinger. Proteomic analysis of the yeast mitochondrial outer membrane reveals accumulation of a subclass of preproteins. *Mol Biol Cell*, 17(3):1436–1450, Mar 2006.
- [313] M. Zeiler, W. L. Straube, E. Lundberg, M. Uhlen, and M. Mann. A Protein Epitope Signature Tag (PrEST) library allows SILAC-based absolute quantification and multiplexed determination of protein copy numbers in cell lines. *Mol Cell Proteomics*, 11(3):O111.009613, Mar 2012.

Curriculum Vitae

Personal details

Name	Dirk Martin Walther
Date of birth	December 11, 1981
Place of birth	Heidelberg, Germany
Nationality	German

Education

August 2008 - Present	PhD studies Prof. Dr. Matthias Mann Max-Planck-Institute of Biochemistry, Martinsried, Germany
October 2002 - February 2008	Studies in Biochemistry University of Tübingen, Germany Graduated with Diploma

Scientific Publications

Dimmer, K.S., Papic, D., Schumann, B., Sperl, D., Krumpe, K., **Walther, D.M.**, and Rapaport, D. (2012). A crucial role of Mim2 in the biogenesis of mitochondrial outer membrane proteins. *J Cell Sci* 125(Pt 14), 3464-73.

Harner, M., Korner, C., **Walther, D. M.**, Mokranjac, D., Kaesmacher, J., Welsch, U., Griffith, J., Mann, M., Reggiori, F., and Neupert, W. (2011). The mitochondrial contact site complex, a determinant of mitochondrial architecture. *Embo J* 30, 4356-4370.

Walther, D.M., and Mann, M. (2011). Accurate quantification of more than 4000 mouse tissue proteins reveals minimal proteome changes during aging. *Mol Cell Proteomics* 10, M110 004523.

Walther, D.M., Bos, M.P., Rapaport, D., and Tommassen, J. (2010). The mitochondrial porin, VDAC, has retained the ability to be assembled in the bacterial outer membrane. *Mol Biol Evol* 27, 887-895.

Walther, D.M., Papic, D., Bos, M.P., Tommassen, J., and Rapaport, D. (2009). Signals in bacterial beta-barrel proteins are functional in eukaryotic cells for targeting to and assembly in mitochondria. *Proc Natl Acad Sci U S A* 106, 2531-2536.

Walther, D.M., and Rapaport, D. (2009). Biogenesis of mitochondrial outer membrane proteins. *Biochim Biophys Acta* 1793, 42-51.

Walther, D.M., Rapaport, D., and Tommassen, J. (2009). Biogenesis of beta-barrel membrane proteins in bacteria and eukaryotes: evolutionary conservation and divergence. *Cell Mol Life Sci.* 66, 2789-2804.